THE
PHYSICAL REVIEW

A journal of experimental and theoretical physics established by E. L. Nichols in 1893

SECOND SERIES, VOL. 78, No. 4 MAY 15, 1950

New Isotopes of Neptunium*

L. B. MAGNUSSON,† S. G. THOMPSON, AND G. T. SEABORG
Radiation Laboratory and Department of Chemistry, University of California, Berkeley, California

(Received February 7, 1950)

Evidence is presented for three new, light neptunium isotopes formed by deuteron bombardments of U^{233}, U^{235}, and U^{238}. The isotope Np^{231} has a half-life of 50±3 min. and emits alpha-particles of 6.28-Mev energy; the proportion of decay by electron-capture has not been determined. The isotope Np^{233} decays predominantly by electron-capture with a 35±3-min. half-life; it has an alpha-decay half-life roughly determined to be *ca.* 10 yr. corresponding to a K/α-branching ratio of 1.5×10^5 and the alpha-particles have an energy of 5.53 Mev. A 13±3-min. period with electromagnetic radiation, indicating orbital electron-capture, is attributed to Np^{232}. Approximate cross sections for formation of various neptunium isotopes by deuterons of energy from 15 to 100 Mev have been determined. The cross sections are low, of the order of 10^{-26} cm², possibly because most of the excited nuclei undergo fission.

1. INTRODUCTION

A NEW field, that of the synthetic transuranium elements, was opened with the discovery in 1940 of an isotope of neptunium, element 93, by McMillan and Abelson.[1,2] Concurrently with investigations of other transuranium isotopes, a rapid advance in knowledge of the nuclear properties of neptunium isotopes was made during the next several years. By 1945 six neptunium isotopes of mass numbers 234–239 inclusive were known and well characterized.

A prerequisite to research in the transuranium field was the determination of some of the chemical properties of neptunium so that it could be separated from other elements, particularly its neighbors, uranium and plutonium. On the basis of the chemical properties, Seaborg, McMillan, Wahl, and Kennedy[3,4] were thus enabled to identify as a new neptunium isotope, a two-day negative beta-particle emitter formed in the deuteron bombardment of uranium. The assignment of this isotope as Np^{238} was proved by the use of separated isotopes and yield considerations.[5]

A very long-lived, alpha-particle emitting neptunium isotope was found a year later.[6] This was Np^{237}, formed by the β^--decay of U^{237}. The isotope Np^{237} may be produced in macro-amounts in uranium piles by the $(n, 2n)$ reaction on U^{238} and hence is the most important isotope for chemical studies of the element.[7–10] The possibilities for identifying new neptunium isotopes as the result of irradiating natural uranium were virtually exhausted at this point since the 16-Mev deuterons of the 60-in. Berkeley cyclotron were not energetic enough to remove more than three neutrons in a (d, xn) type reaction on U^{238}. Deuteron bombardment of U^{235} was expected to produce light neptunium iso-

* This paper is based on work done under the auspices of the AEC.

† Now at Argonne National Laboratory, Chicago, Illinois.

[1] E. M. McMillan, Phys. Rev. **55**, 510 (1939).

[2] E. M. McMillan and P. H. Abelson, Phys. Rev. **57**, 1185 (1940).

[3] Seaborg, McMillan, Wahl, and Kennedy, Phys. Rev. **69**, 366 (1946); *The Transuranium Elements: Research Papers* (McGraw-Hill Book Company, Inc., New York, 1949), Paper No. 1.1, National Nuclear Energy Series, Plutonium Project Record Vol. 14B.

[4] Seaborg, Wahl, and Kennedy, Phys. Rev. **69**, 367 (1946); National Nuclear Energy Series, Plutonium Project Record Vol. 14B, Paper No. 1.4.

[5] Kennedy, Perlman, Segrè, and Wahl, National Nuclear Energy Series, Plutonium Project Record Vol. 14B, Paper No. 1.9.

[6] A. C. Wahl and G. T. Seaborg, Phys. Rev. **73**, 940 (1948); National Nuclear Energy Series, Plutonium Project Record Vol. 14B, Paper No. 1.5.

[7] L. B. Magnusson and T. J. LaChapelle, J. Am. Chem. Soc. **70**, 3534 (1948); National Nuclear Energy Series, Plutonium Project Record Vol. 14B, Paper No. 1.7.

[8] Hindman, Magnusson, and LaChapelle, J. Am. Chem. Soc. **71**, 687 (1949); National Nuclear Energy Series, Plutonium Project Record Vol. 14B, Paper Nos. 15.1, 15.2, 15.3, 15.4, 15.6, 15.8, 15.11.

[9] S. Fried and N. Davidson, J. Am. Chem. Soc. **70**, 3539 (1948); National Nuclear Energy Series, Plutonium Project Record Vol. 14B, Paper No. 15.5.

[10] J. J. Katz and D. M. Gruen, J. Am. Chem. Soc. **71**, 2106 (1949).

topes, but the small abundance of U^{235} (less than one percent) in natural uranium complicated any identification of the products over the background activity of the heavier neptunium isotopes produced from U^{238}.

Milligram quantities of both U^{233} and U^{235} became available for cyclotron bombardment in 1944. James, Florin, Hopkins, and Ghiorso[11] identified Np^{236}, Np^{235}, and Np^{234} as products of deuteron bombardments of U^{235}. The isotope Np^{234} was also made by deuteron bombardment[12] of U^{233}. The radioactive properties of these neptunium isotopes were summarized in a recent review.[13]

At the beginning (June, 1948) of the research reported in this paper, trends in stability with mass number were clearly apparent. Neptunium, of course, exhibits the general instability characteristic of elements of odd Z, in this case only one isotope, Np^{237}, being stable toward both electron-capture and β^--decay. Neptunium isotopes with mass numbers above 237 are β^--unstable, and those with mass numbers below 236 are unstable toward electron-capture. The observed mode of decay of Np^{236} is by β^--emission but decay by electron-capture is undoubtedly also possible. The data on these isotopes, however, reveal little about the effect of mass number on the energies (and half-lives) for decay by alpha-particle emission. Alpha-particles had been observed only from two isotopes of neptunium. The Np^{237} emits alpha-particles of 4.77-Mev energy and James[14] has found that Np^{235} has an alpha-branching decay of about *ca.* 0.005 percent emitting alpha-particles of 5.06 Mev. Much work in this laboratory has been directed toward the correlation of the systematics known to exist for the alpha-decay energies and half-lives for heavy elements.[15] It was hoped that new light neptunium isotopes could be produced which might decay by alpha-particle emission and thereby yield data for extension of the alpha-particle energy, half-life, and mass number relations for this region, and this hope was realized in that some such data were obtained for the isotopes Np^{231} and Np^{233}.

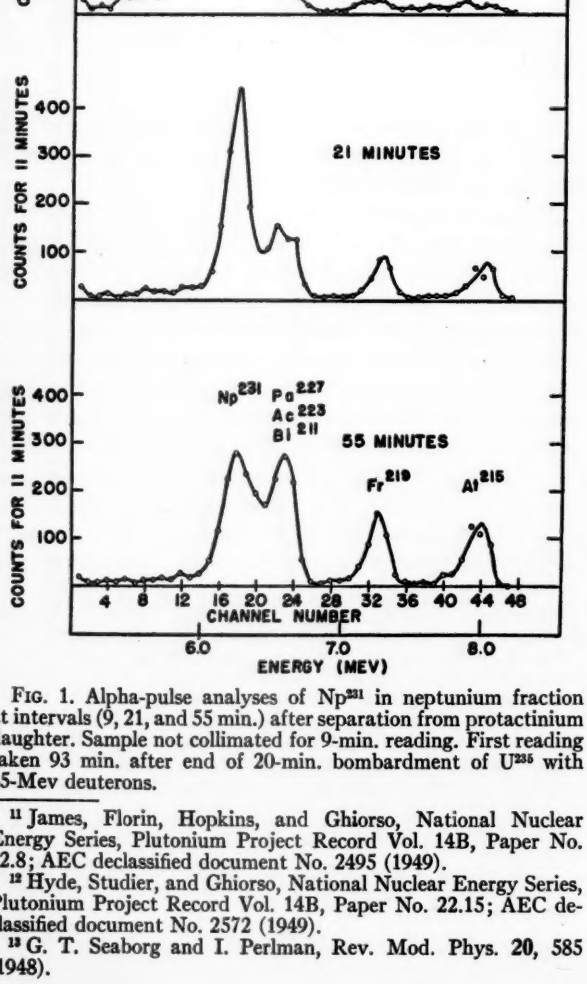

FIG. 1. Alpha-pulse analyses of Np^{231} in neptunium fraction at intervals (9, 21, and 55 min.) after separation from protactinium daughter. Sample not collimated for 9-min. reading. First reading taken 93 min. after end of 20-min. bombardment of U^{235} with 45-Mev deuterons.

The isotopes Np^{232} and Np^{233} probably had been produced in the 22-Mev deuteron bombardment of U^{233} but had not been identified.[12] The half-lives were thought to be too short for detection or possibly so close to those of Np^{236}, Np^{238}, or Np^{239} as to escape resolution.

This paper will report results obtained from deuteron bombardments at energies ranging from 15–100 Mev of U^{233}, U^{235}, and U^{238} using the 60- and 184-in. Berkeley cyclotrons. Data have been obtained for the identification of three new isotopes, Np^{233}, Np^{232}, and Np^{231}. Relative yields for a number of neptunium isotopes have been determined in many of the bombardments.

2. THE ISOTOPE Np^{231}

A process for extracting radioactively pure neptunium within an hour or two after the end of bombardment was devised (see Section 5, procedures B1 to B3) and applied to a series of 100-Mev deuteron (184-in. cyclotron) bombardments of natural uranium (metal). The neptunium fractions from these bombardments contained a new alpha-activity. Alpha-pulse analyses[16] at intervals revealed the growth of an alpha-decay series which was recognized as the collateral series of short-lived alpha-emitters[17] following the alpha-decay of Pa^{227}. The following series was indicated:

$$Np^{231} \xrightarrow{\alpha} Pa^{227} \xrightarrow{\alpha} Ac^{223} \xrightarrow{\alpha} Fr^{219} \xrightarrow{\alpha} At^{215} \xrightarrow{\alpha} Bi^{211} \xrightarrow{\alpha} Tl^{207} \xrightarrow{\beta^-} Pb^{207}.$$

[11] James, Florin, Hopkins, and Ghiorso, National Nuclear Energy Series, Plutonium Project Record Vol. 14B, Paper No. 22.8; AEC declassified document No. 2495 (1949).

[12] Hyde, Studier, and Ghiorso, National Nuclear Energy Series, Plutonium Project Record Vol. 14B, Paper No. 22.15; AEC declassified document No. 2572 (1949).

[13] G. T. Seaborg and I. Perlman, Rev. Mod. Phys. **20**, 585 (1948).

[14] R. A. James (unpublished data).

[15] Perlman, Ghiorso, and Seaborg, Phys. Rev. **74**, 1730 (1948); **75**, 1096 (1949); **77**, 26 (1950).

[16] Ghiorso, Jaffey, Robinson, and Weissbourd, National Nuclear Energy Series, Plutonium Project Record Vol. 14B, Paper No. 17.3.

[17] Meinke, Ghiorso, and Seaborg, Phys. Rev. **74**, 695 (1948).

The parent-daughter relationship of Np^{231} and Pa^{227} was confirmed by repeated chemical separations of protactinium from the neptunium and measurement of the 38-min. decay of Pa^{227} in the protactinium fraction.

The electron and electromagnetic radiation in the neptunium fraction seemed to be largely from the known neptunium isotopes of mass number greater than 233. There was so much electron activity and electromagnetic radiation from the heavier neptunium isotopes that the ionization interfered with the alpha-particle energy determinations of Np^{231} using the differential pulse analyzer. The relatively small numbers of alpha-particle counts from Np^{231} also suggested that the yield of the $(d, 9n)$ reaction from U^{238} was very low. Increasing the energy of the deuterons did not seem to improve the relative yield of Np^{231}.

Bombardments of U^{235} with deuterons of energies varying between 45 and 100 Mev gave improved yields of Np^{231} by the $(d, 6n)$ reaction. Figure 1 shows alpha-pulse analysis data for one of the neptunium fractions from these bombardments at intervals corresponding to 9, 21, and 55 min. after separation from protactinium. A ring collimator was placed over the sample for the 21- and 55-min. readings to give sharper definition of the peaks by eliminating degraded alpha-particles scattered from the sample plate. The growth of Pa^{227} and its daughters to equilibrium with the Np^{231} is clearly apparent. Separate peaks for Pa^{227}, Ac^{223}, and Bi^{211} are not observed since the energies are about equal and the instrument was set at a low resolving power to bring the entire series within the register range. Figure 2 shows the best energy resolution obtained for Np^{231}, Pa^{227}, Ac^{223}, and Bi^{211}. The Fr^{219} and At^{215} are beyond the range covered by the instrument in this run. The Np^{231} for this measurement was produced by the $(d, 4n)$ reaction with 45-Mev deuterons on U^{233}. The energies of the alpha-particles from Pa^{227} and Ac^{223} are known to be 6.46 and 6.64 Mev, respectively.[17] From these data the energy of the alpha-particle from Np^{231} is 6.28 Mev.

The measurement of the half-life of Np^{231} was complicated by the presence of its alpha-decay daughters. The resolution of the alpha-pulse analyzer usually proved to be too low to permit following the decay of the Np^{231} peak directly in the presence of near equilibrium amounts of the daughters. The most reliable values of the half-life were obtained from pulse analysis of aliquots of an Np^{231} solution freshly purified from Pa^{227} and daughters. The aliquot size was determined by pulse analysis for Np^{237} tracer used in all runs. Figure 3 shows plots of the decay of the alpha-activity of Np^{231}. Curves A and B are plots of the activity of Np^{231} relative to the tracer Np^{237}, and curve D is obtained from data on the decay of Np^{231} measured in the presence of its daughter by a series of pulse analyses which had unusually good resolution (as in Fig. 2). The slope of the lines is a measure of the Np^{231} half-life, the absolute values of the ratios having no significance. Included in the figure is an observed rate of decrease in recoil Pa^{227} activity from an Np^{231} sample (curve C). In this determination the Pa^{227} atoms recoiling from the alpha-decay of Np^{231}, mounted on a platinum counting plate, were caught on a second plate charged to a negative potential with respect to the first; the plates containing the recoil atoms were subsequently pulse-analyzed for Pa^{227} and daughters. The results all indicate that the half-life of Np^{231} is *ca.* 50 min.

The isotope Np^{231} is undoubtedly unstable toward electron-capture and a consideration of the alpha-systematics[15] indicates that it is probably this process

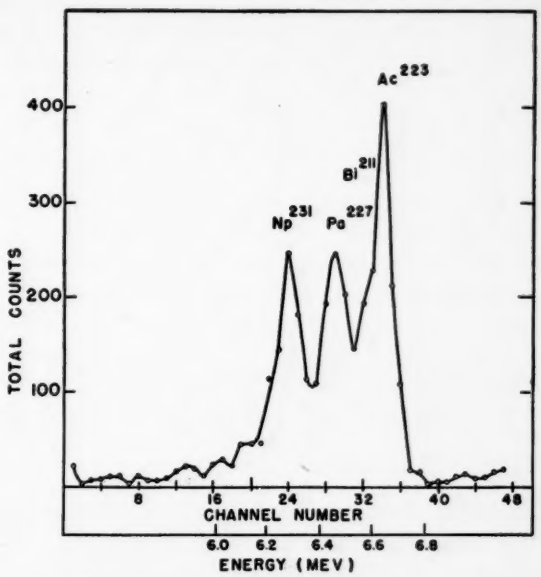

FIG. 2. Energy determination of the alpha-particle from Np^{231} (6.28 Mev) by pulse analysis. 10-min. count taken 95 min. after separation from Pa^{227} daughter and 175 min. after end of 45-min. bombardment of U^{233} with 45-Mev deuterons.

which controls the rate of decay. The electromagnetic radiations characteristic of this process were not resolvable in these experiments from the radiations resulting from the decay of the heavier neptunium isotopes. The electron-capture decay daughter of Np^{231} is U^{231}, which also decays by electron-capture with a four-day half-life. The determination of the percentage of Np^{231} which decays by electron-capture by measurement of the number of U^{231} daughter atoms is very insensitive for several reasons: namely, (1) the low Geiger tube counting efficiency for x-rays, (2) the factor of 100 in the ratio of the half-lives, and (3) as will be seen later, the low yields of Np^{231}. Uranium was separated from a neptunium fraction after complete decay of the Np^{231}, but the Geiger counter activity in the uranium fraction was only slightly above counter background and was not positively identified as U^{231}. The poor sensitivity of the method allows us to place only an upper limit of 10^3 on the ratio of electron-capture to alpha-emission from these data. From an estimate of the upper limit to the amount of x-radiation from Np^{231}

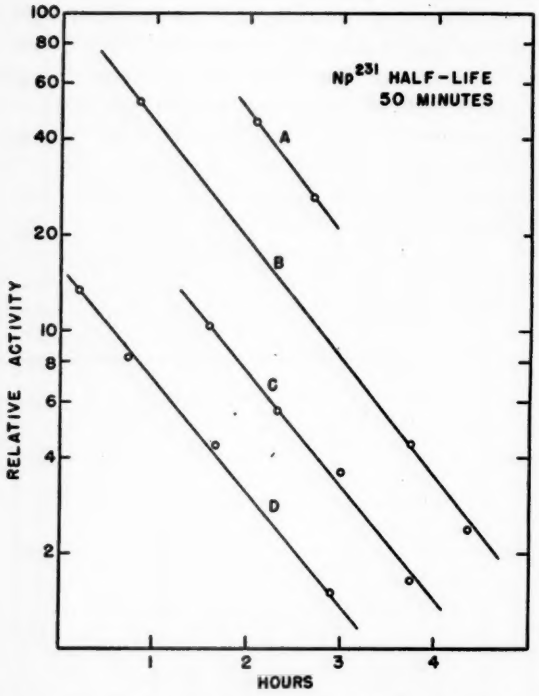

FIG. 3. Decay of the alpha-activity of Np^{231}. Curves A and B from pulse analysis of Np^{231} freshly separated from Pa^{227} and daughters. Curve C represents decaying yield of daughter Pa^{227} recoil atoms from Np^{231}. Curve D from pulse analysis of Np^{231} in presence of daughters.

which would have escaped detection, the upper limit for this ratio may be lowered to *ca.* 10^2.

3. THE ISOTOPE Np^{233}

Although the 50-min. period of electromagnetic activity expected for Np^{231} was not resolved from the decay curves, x-rays of 35-min. half-life were consistently observed in the neptunium fractions from bombardments of U^{233} and U^{235} with 45- to 100-Mev deuterons in the 184-in. cyclotron. That this activity was due to a neptunium isotope was verified by the fact that it followed precisely the same chemistry as Np^{237} tracer in separations using a chemical procedure specific for neptunium (see Section 5, procedures B1 to B3). After complete decay of the 35-min. neptunium activity, a uranium fraction containing U^{233} as a tracer was separated from this neptunium fraction in order to detect the uranium daughter produced by the electron-capture process. The amount of uranium daughter to be expected was roughly calculable by assuming that one *L* x-ray was emitted per neptunium disintegration, and that the *L* x-rays were counted with an efficiency of two percent in the argon-filled Geiger counter tube. The uranium fraction was examined in the differential pulse analyzer, and no daughter alpha-activity was observed. If the parent were Np^{232}, about three alpha-counts per minute of U^{232} should have been found; but if the parent were Np^{233}, the daughter activity should not be detectable since U^{233} has too long a half-life. The limit of detection was about 0.1 count per minute. A preliminary assignment of the 35-min. activity was therefore made to Np^{233}.

A bombardment of U^{233} with 15-Mev deuterons in the 60-in. cyclotron also yielded the 35-min. period. A different method of purification was used (see Section 5, procedures B2, B4, and B5) providing additional chemical evidence that the short-lived activity was a neptunium isotope. Since no Np^{231} was formed in this bombardment, isotopes of mass number less than 232 were ruled out. The neptunium isotopes which could be formed from the U^{233} were limited to the products of the (d, n), $(d, 2n)$, and $(d, 3n)$ reactions. The (d, n) reaction product is the 4.4-day Np^{234}, and since the 35-min. activity did not decay to U^{232} in the previous experiments, it is assigned to Np^{233}.

The radiations were characterized by beryllium, aluminum, and lead absorption measurements with argon- and xenon-filled Geiger tubes. All counts were corrected for the long-lived neptunium background and were corrected for decay to an arbitrary standard time. The Np^{233} absorption curves are given in Figs. 4 and 5. Although more than one sample was used to obtain these curves, the data were normalized through use of the Np^{237} tracer contents of the samples so that the figures represent equal amounts of Np^{233}. From the fact that electromagnetic radiations cause more ionization in xenon than in argon and hence are counted more efficiently, it is evident that the absorption data reveal the x-radiation characteristic of an electron-capture process. Comparison of the curves obtained with the argon- and xenon-filled counter tubes shows the presence of soft electrons which are absorbed by 100 mg/cm² of beryllium (maximum energy *ca.* 300 kev). The apparent component of 2 g/cm² beryllium half-thickness is a composite of the *K* and *L* x-rays. The composite x-radiation was counted more efficiently in the xenon-filled tube than in the argon-filled tube by a factor of five. The magnitudes of the counting rates observed through the aluminum and lead absorbers prove the electromagnetic nature of the radiations and indicate roughly the range of energies and relative abundance of the x-rays. The average half-thickness in lead for the 94–114-kev uranium *K* x-rays is 125 mg/cm². The lead absorption curves have slopes of *ca.* 230 mg/cm² indicating the presence of gamma-radiation in addition to the *K* x-rays. Gamma-radiations in these samples were not resolved in detail and will be discussed further in the section on Np^{232}. The observed electrons of 300-kev maximum energy suggest the presence of gamma-rays with some internal conversion. It is likewise likely from the lead absorption data that some gamma-radiation of energy not more than 400 kev is associated with Np^{233}. The average half-thickness in aluminum for the 13–20-kev uranium *L* x-rays is 130 mg/cm² and the aluminum absorption curves indicate the presence of x-rays of this energy over the background of *K* x-ray and gamma-radiations. The absolute counting

efficiencies for electromagnetic radiations of these energies are not well known but have been calculated to be of the order of one percent, in Geiger counter tubes containing 10 cm of argon.[14]

The absence of Np^{231} alpha-particles in the pure neptunium fraction from the low energy (15-Mev) deuteron bombardment of U^{233} permitted a sensitive detection of other short-lived neptunium alpha-activity. Figure 6 is a series of three of the alpha-pulse analyses. A small short-lived peak corresponding to an alpha-particle energy of 5.53 Mev was present, and its decay was followed by summing the counting rates recorded at this energy. The decay of counts per minute recorded under this peak is given in Fig. 7. A plot of the data following subtraction of background yielded a half-life of *ca.* 35 min. No other short-lived alpha-activity of this energy is known, so, in view of the correspondence in half-life with that observed for the radiations detected with the Geiger counter, the alpha-particles are assigned to Np^{233}. The ratio of alpha-disintegrations per minute to Geiger counts per minute (argon tube, 1.5 g/cm² Be absorber) for Np^{233} was 1.8×10^{-2}. With the assumption of one L x-ray per disintegration, an Auger coefficient of 0.5 for the L x-rays, and a counting efficiency of one percent, the partial half-life of Np^{233} for alpha-particle emission is calculated to be *ca.* 10 yr. corresponding to a K/α-branching ratio of 1.5×10^{5}. These data on the alpha-radioactivity are in good agreement with the systematics.[15]

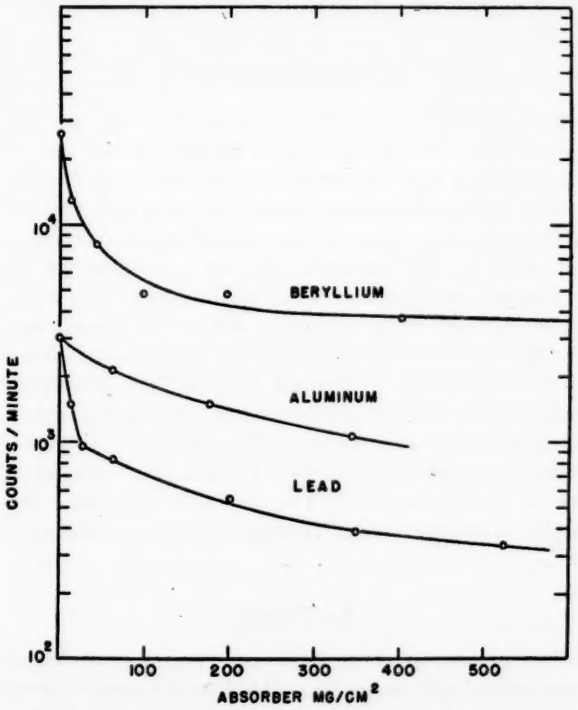

FIG. 4. Absorption of Np^{233} radiations measured with argon-filled Geiger tube. See Section 5 for placement of sample and absorbers. Data for aluminum and lead curves taken with 1.5 g/cm² beryllium next to tube window. All absorption data corrected to 90 min. after end of 30-min. bombardment of U^{233} with 15-Mev deuterons.

4. THE ISOTOPE Np^{232}

Some of the early decay curves, particularly those involving the decay of electromagnetic radiation, on the samples containing Np^{233} indicated that another period was present with half-life less than 35 min. This period was believed to be that of Np^{232}, since decay measurements on neptunium fractions from a number of bombardments in which Np^{232} was undoubtedly produced had virtually eliminated the possibility of a longer half-life for the isotope. Identification of these short-lived neptunium isotopes has been difficult since the chemical purification necessary prior to radiation measurements has required an hour or more. A better counting ratio of Np^{232} to Np^{233} was sought by shortening still further the chemical purification of the neptunium produced in another short bombardment of U^{233} in the 60-in. cyclotron. The first count of the neptunium fraction was taken 45 min. after bombardment. The decay of x-ray activity was followed with a xenon-filled Geiger tube using as alternate absorbers (a) 1.5 g/cm² of beryllium and (b) 1.5 g/cm² beryllium plus 155 mg/cm² of lead. Figure 8 gives the actual counting rates of this larger sample, although a smaller aliquot was used for the first three hours of counting. The short-lived decay can be resolved only on the basis of two activities and the half-life values, 35 min. (Np^{233}) and 13 min., give the best fit to the data.

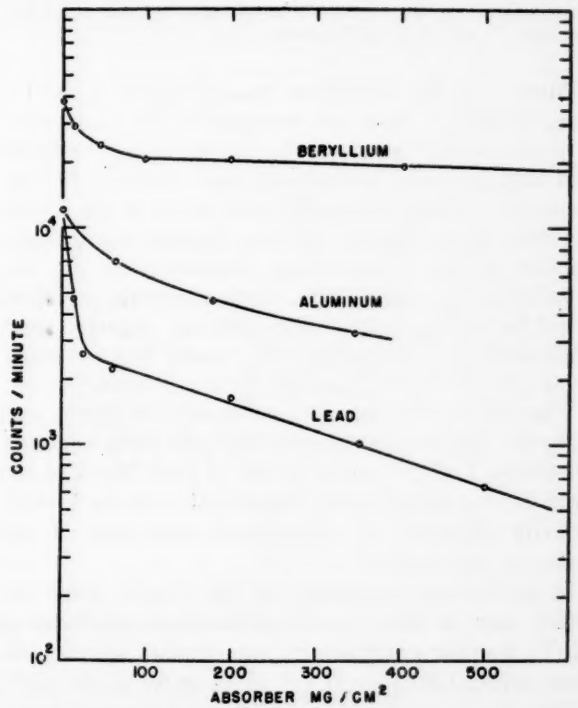

FIG. 5. Absorption of Np^{233} radiations measured with xenon-filled Geiger tube. Same conditions and amount of Np^{233} as for Fig. 4.

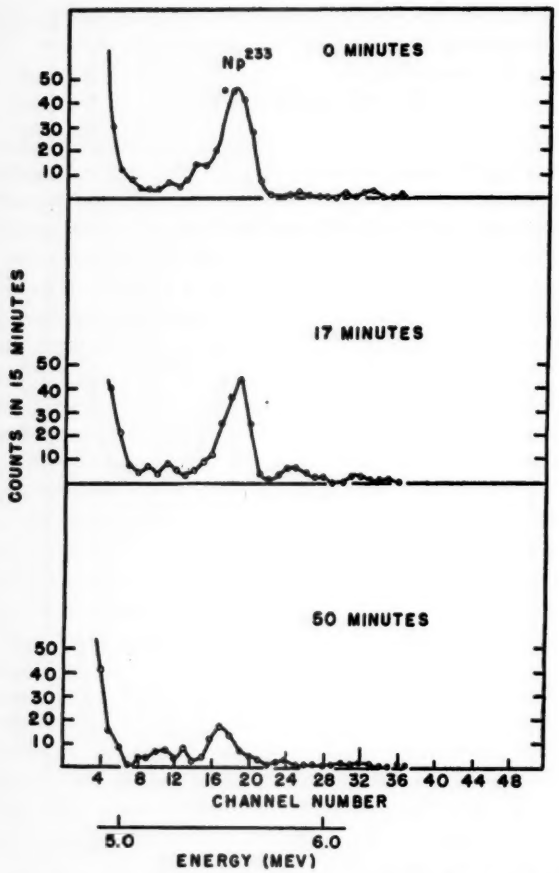

FIG. 6. Pulse analyses of alpha-particles from Np^{233} (5.53 Mev.). First measurement begun 64 min. after end of 30-min. bombardment of U^{233} with 15-Mev deuterons.

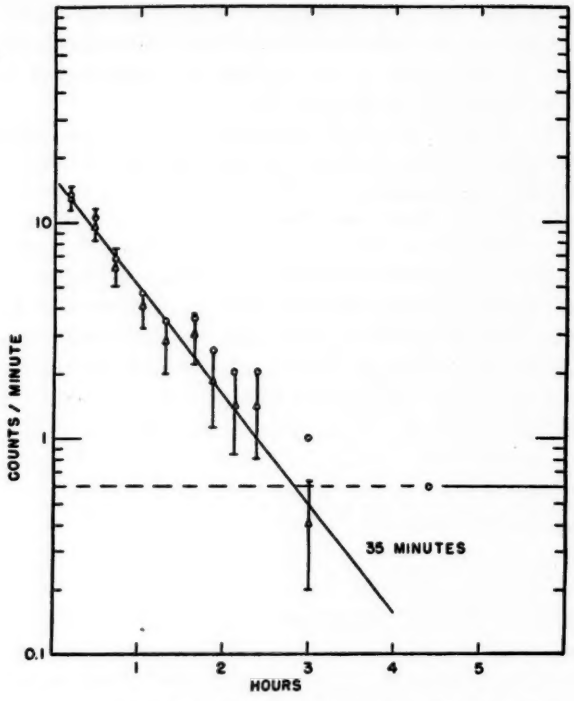

FIG. 7. Decay of Np^{233} alpha-activity. Sums of counting rates over channels 13–20 of a 48-channel pulse analyzer. Zero time is 60 min. after end of 30-min. bombardment of U^{233} with 15-Mev deuterons.

More extensive absorption measurements of the 13-min. radiations were not attempted. The close similarity to the Np^{233} x-rays in the absorption by beryllium and lead, however, leaves little doubt that the 13-min. radiations include x-rays. Measurements of the counting rates of the samples with no absorber using a thin window Geiger counter tube demonstrated the impossibility that the 13-min. electromagnetic radiation could be coming from a beta-emitting impurity since there were approximately ten to twenty times as many x-ray quanta of 13–20-kev energy as electrons.

The decay of hard electromagnetic radiation was followed with another xenon-filled tube using alternate absorbers, 1 g/cm² and 11 g/cm² of lead. Much of the hard gamma-radiation was associated with the 13-min. activity although an unequivocal resolution of the data was not possible.

A preliminary assignment of the 13-min. x-ray activity may be made to the electron-capture decay of Np^{232}. Further confirmatory experiments should produce detectable yields of U^{232} as daughter of the Np^{232}.

No alpha-particle radioactivity was observed in agreement with the systematics[15] which would predict that the degree of alpha-branching should be smaller than could be detected in experiments of the present sensitivity.

5. EXPERIMENTAL

The chemical properties of neptunium are not discussed here. The information available at the time of this research may be found in the National Nuclear Energy Series, Plutonium Project Record Vol. 14B and in the references given in the Introduction. The essential need in this research was for a process for the separation and purification of neptunium which would be much more rapid than any devised hitherto, since the objective was the identification of isotopes believed to be short-lived. This need was fulfilled largely by modification of the mechanics of previously known chemical separation processes. The most rapid isolations from the target required only 45 min., but some sacrifice in purity resulted. The methods described here required, on the average, from an hour to an hour and a half.

A. Targets

The targets in every case were uranium. A known amount of Np^{237} tracer was added to the target solvent for later measurement of aliquots and chemical yield. The Np^{231} was first found in 184-in. cyclotron bombardments of one-gram amounts of natural uranium metal. The best solvent found for quick dissolution of uranium metal targets was hot 10*M* hydrochloric acid

containing a trace of Fe(III). The resulting U(IV) solution was oxidized to U(VI) with an excess of liquid bromine.

The targets for the bombardments of U^{235} in the 184-in. cyclotron were 100-mg amounts of U_3O_8 sealed in thin-walled Pyrex tubes. After bombardment the tube was dropped into a centrifuge tube containing solvent and crushed with a glass rod. Hot 8*M* nitric acid with a trace of Fe(III) was a rapid solvent for the uranium oxide. The 45-Mev bombardments of U^{238} and U^{233} also employed oxides held in Pyrex tubes. The bombardments of U^{233} in the 60-in. cyclotron were made using milligram amounts of UO_3 prepared by drying uranyl nitrate solution in platinum interceptor boats or troughs.

The bombardment energy in the 184-in. cyclotron was varied by adjusting the distance of the target probe from the center of the cyclotron.

B. Neptunium Separations

Neptunium was isolated from all other radioactive species by combinations of co-precipitation and solvent extraction techniques. The procedures may be outlined as follows.

1. Lanthanum Fluoride

A few mg of MnO_2 is precipitated from the 1*N* HNO_3 solution of uranyl nitrate by adding a solution of $KMnO_4$ followed by enough $NaNO_2$ solution to reduce all the permanganate. The $KMnO_4$ ensures that all the uranium is U(VI) and the MnO_2 is an effective decontaminant, particularly for protactinium, usually present in large yield. The MnO_2 precipitate is discarded. The nitrite reduces Np(VI) to Np(V). A milligram or less of La(III) is added followed by the addition of HF to precipitate LaF_3 which carries the neptunium. The uranium remains in the supernatant solution. The LaF_3

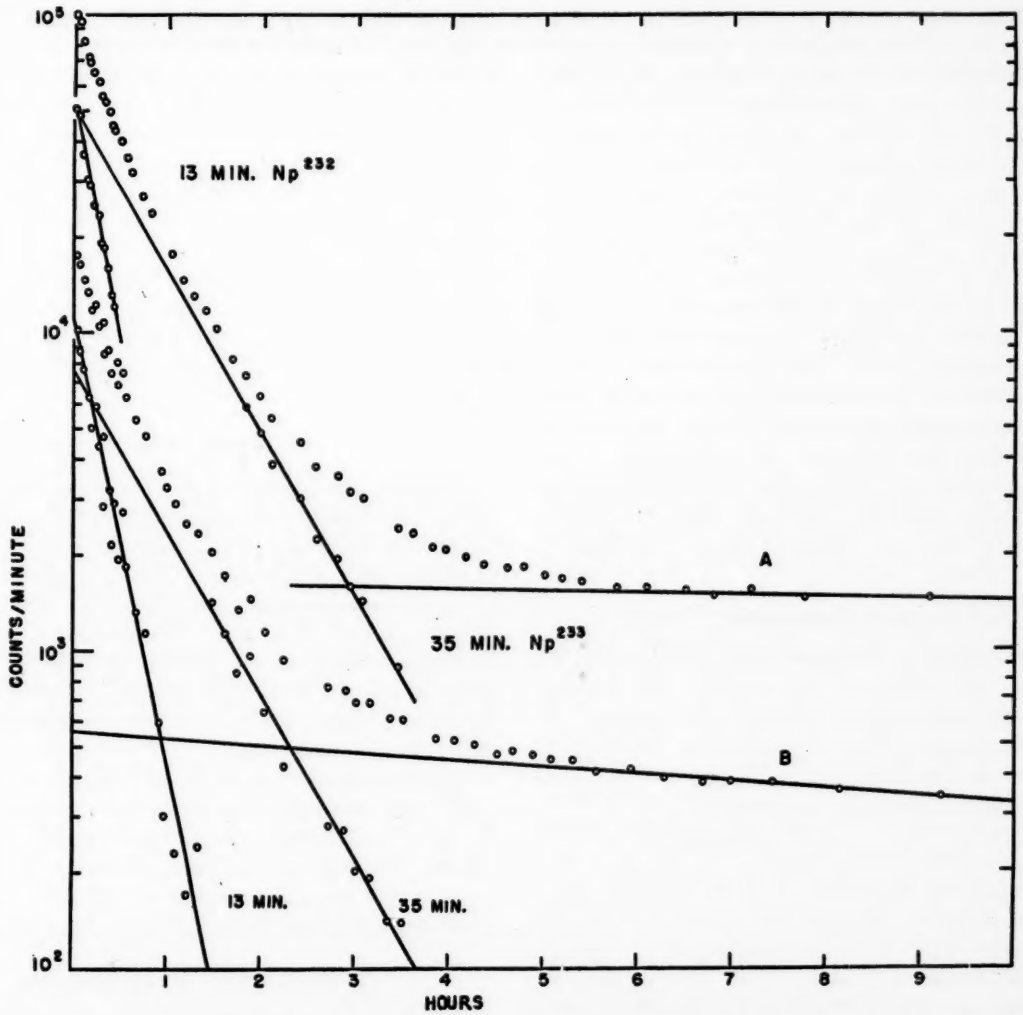

FIG. 8. Decay of electromagnetic radiations in neptunium fraction from 15-min. bombardment of U^{233} with *ca.* 17-Mev deuterons. Zero time is 45 min. after end of bombardment. Curve A with 1.5 g/cm² beryllium absorber between sample and counting tube window. Curve B with 1.5 g/cm² beryllium absorber plus 155 mg/cm² lead absorber over sample.

precipitate is metathesized to $La(OH)_3$ by heating and stirring with concentrated KOH solution. The $La(OH)_3$ is dissolved in HNO_3 and the solution is diluted with H_2SO_4 to give a solution of approximate composition: 1*M* H_2SO_4, 1*M* HNO_3. The solution is made about 0.1*M* in $NaBrO_3$, heated, and LaF_3 is precipitated and separated following the addition of HF to a concentration of about 0.1*M*. The supernatant containing Np(VI) is then diluted a factor of five by the addition of excess SO_2 solution so that all bromate is reduced to bromide. More La(III) is added and precipitated as LaF_3, which carries the neptunium as Np(IV), from a solution which has been made 1–3*M* in HF.

2. *Ether Extraction*

The LaF_3 is dissolved with hot, saturated $Al(NO_3)_3$ as the result of the formation of a soluble complex ion containing aluminum and fluoride, the solution is diluted and made 1*M* in HNO_3 and 0.1*M* in $NaBrO_3$, and heated 2–3 min. to oxidize the neptunium. Solid NH_4NO_3 is added to make its concentration 10*M* in the solution and the neptunium is extracted from the solution with twice its volume of diethyl ether. (The ether used for this extraction must be free from reducing impurities, e.g., alcohols and aldehydes. Effective purification is attained by shaking it with $K_2Cr_2O_7$—1*M* H_2SO_4 solution followed by distilled water washes.) The ether extract of neptunium is washed once with 10*M* NH_4NO_3 solution, and may then be poured or pipetted onto platinum counting plates. The combined lanthanum fluoride plus ether extraction procedures could be carried out within a time of one hour, and yielded neptunium fractions pure with respect to alpha-activity. These fractions were usually also sufficiently pure for the measurements with Geiger counters. As confirmation of the purity, it was customary to put the neptunium through another extraction into an organic solvent involving the formation of a chelate complex with thenoyl trifluoroacetone, described as follows.

3. *Thenoyl Trifluoroacetone (TTA)*

The neptunium is extracted from its ether solution into water containing a little $NaNO_2$ and La(III). Lanthanum hydroxide is precipitated carrying the neptunium and separating it from nitrate. The $La(OH)_3$ is dissolved in 5*M* HCl, 0.1*M* KI, and 0.05*M* $N_2H_4 \cdot 2HCl$ solution, followed by heating 1–2 min. at 90°C. The solution is diluted to 0.5*M* HCl and heated for a minute again to reduce free iodine. This reduction treatment produces Np(IV) which is then extracted into a benzene solution of thenoyl trifluoroacetone. In this procedure the 0.5*M* HCl solution of Np(IV) is agitated 20–30 min. with a 0.3*M* solution of TTA in benzene. The benzene solution is placed on a platinum counting plate and evaporated by heating the plate with an induction coil. The neptunium chelate compound is volatile and a large percentage is lost if the benzene solution is simply dried and heated strongly. It was found that a small amount of trichloroacetic acid placed on the plate before adding the benzene solution effectively prevented volatilization of the neptunium during drying and ignition. When the TTA extraction procedure is employed, an additional 45-min. time is required.

4. *Zirconium Phosphate*

Zirconium phosphate may be used as a carrier for Np(IV) in an oxidation cycle procedure analogous in principle to the lanthanum fluoride method. The uranium target solvent was 6*M* HNO_3, 10^{-3}*M* Ce(IV), 0.02*M* Zr(IV) with added Np^{237} tracer. The target solution is adjusted to 3*M* in HNO_3 and is made 0.02*M* in $NaBrO_3$. The solution is heated one minute to oxidize neptunium to Np(VI). The solution is made 0.5*M* in H_3PO_4 and is heated a minute to coagulate the zirconium phosphate precipitate which does not carry the Np(VI). The supernatant solution containing Np(VI) is reduced with excess $N_2H_4 \cdot H_2SO_4$ to destroy bromate and is then made 0.01*M* in $N_2H_4 \cdot H_2SO_4$ and 0.005*M* in Fe(II) to reduce neptunium to Np(IV). This reduction is very rapid. About 1 mg of Zr(IV) per ml of solution is added and the solution is heated and stirred. Zirconium phosphate precipitates carrying Np(IV) and the precipitate is washed with 3*M* HNO_3—0.5*M* H_3PO_4 solution. Uranium remains in the supernatant solution. About 0.1 mg La(III) as a nitrate solution is slurred with the zirconium phosphate (about 1 mg) and the zirconium is dissolved by forming a complex ion with fluoride by the addition of a 1*M* HF, 1*M* HNO_3 solution. A precipitate of LaF_3 remains, bearing the neptunium.

5. *Resin Column*

A column containing the ion exchange resin, Dowex-50, has been used for the separation of trace amounts of neptunium from uranium. Neptunium as Np(V) is adsorbed[18] on a small amount of resin from a solution of low acid concentration and placed at the top of a column packed with resin and containing 13*M* HCl. The neptunium is eluted rapidly by passing 13*M* HCl through the column. The samples for counting are prepared by placing the elutriant dropwise directly on platinum counting plates.

The absorption and alpha-particle data given for Np^{233} were obtained from neptunium samples purified by the zirconium phosphate, ether extraction, and resin column procedures in that order. The data for Np^{232} were obtained by counting aliquots of the LaF_3 precipitate after employing the zirconium phosphate procedure.

C. Radioactive Measurements

Samples for radioactive assay were mounted on platinum plates of 2-mil thickness. A uniform geomet-

[18] James, Orth, and Street (unpublished work).

rical arrangement was used for all Geiger counter activity measurements. Since the principal objective of this work was measurement of electromagnetic radiations, no large general lead housing was used around the Geiger tube and sample. As a shield against general background radiation, a small lead shield was placed directly around the brass, bell-type Geiger tube. This arrangement was used to minimize spurious counting rates caused by the scattering of primary and secondary radiations around the absorbers. The sample plate was supported on a flat aluminum holder in a Lucite stand below the mica window of the counter tube. The distance from sample to counter window was 2.1 cm for all measurements. The mica windows for all the tubes used were near 3 mg/cm² in thickness. The Geiger tubes were filled to 10 cm mercury pressure of argon or xenon with 1 cm pressure of ethanol.

A value of 8.5 percent for the fraction of the radiation which entered the counter from the sample at the 2.1-cm distance was determined by counting the β^--particles from Pa^{234} (UX_2) in equilibrium with a known weight of U^{238} (as UO_2) mounted between cellophane sheets in the same position. The Th^{234} (UX_1) β^--particles were eliminated by a thin aluminum absorber (30 mg/cm²).

Beryllium absorbers were used to determine the relative amounts of electron and electromagnetic radiation. The absorbers were placed in the top shelf of the Lucite stand, giving a distance of 0.4 cm between the top surface of the absorber and the counter window. The absorptions of the electromagnetic radiations in aluminum and lead were measured with the aluminum or lead absorbers resting over the sample plate holder and with a large beryllium absorber in the top shelf.

Alpha-particle activity was assayed in "50 percent geometry" argon-filled ionization chambers. The determination of alpha-particle energies and analysis of mixtures of alpha-emitting isotopes were made in a 48-channel ionization pulse analyzer[16] in which the energy range covered by the 48 channels could be varied.

6. CROSS SECTIONS

In the course of the search for radiations from light neptunium isotopes, measurements of the intensities of the radiations from previously known isotopes were also obtained. From these measurements and the times and intensities of bombardment, it is possible to calculate the atom yields and cross sections for formation. However, only in the 60-in. cyclotron bombardments of U^{233} was the absolute beam intensity known to any accuracy.

TABLE I. U^{233} cross sections (unit 10^{-24} cm²).

	Deuteron energy (Mev) 15	50
Np^{234}	$1(10^{-2})$	$2(10^{-2})$
Np^{233}	$8(10^{-3})$	$8(10^{-3})$
Np^{232}	$2(10^{-2})$	—
Np^{231}	0	$<2(10^{-3})$

Nevertheless, very rough values for the cross sections have been calculated for the 184-in. cyclotron bombardments under the assumption of a deuteron beam of about 2 μa/cm². In view of the uncertainty in the beam intensities, the values determined for a given cross section in two different bombardments cannot be expected to agree better than within a factor of about three. The relative cross sections determined for the various isotopes produced in any given bombardment, however, should be nearly as accurate as the decay schemes, half-lives, and counting efficiencies are known. Aside from the uncertainty introduced by these factors, the reliability of the determinations depends on the accuracy of counting and decay resolution.

The atom yields of Np^{236} were calculated from the measured alpha-activity of the daughter, Pu^{236}, and the yields of Np^{238} from the observed Np^{238} β^--particle activity. Gross assumptions are required for the calculation of the atom yields of the electron-capturing isotopes. The number of L x-rays associated with each isotope was measured approximately; and the atom yields were calculated with the assumptions that one L x-ray is emitted per disintegration, that the counting efficiency in the argon tube is one percent, and that the Auger coefficient for the L x-rays is 0.5. Upper limits for the cross sections for the formation of Np^{231} were calculated on the basis that the ratio electron-capture/alpha-emission is 100. No 50-min. x-ray activity corresponding to the electron-capture decay of Np^{231} could be resolved from decay curves, and an upper limit of 100 for the electron-capture/alpha-emission ratio was derived from the observed x-ray activity of Np^{233} samples containing known amounts of Np^{231} alpha-activity and an estimated limit of detection for the Np^{231} x-radiations. Tables I–III list the very approximate cross sections in units of 10^{-24} cm². Blanks in the tables signify that insufficient data for the calculation were obtained in the experiments.

These cross sections are to be regarded as a by-

TABLE II. U^{235} cross sections (unit 10^{-24} cm²).

	Deuteron energy (Mev) 45	70	100
Np^{236}	$2(10^{-3})$	$2(10^{-3})$	$2(10^{-3})$
Np^{235}	$2(10^{-2})$	$2(10^{-3})$	$8(10^{-3})$
Np^{234}	$1(10^{-2})$	$8(10^{-3})$	$8(10^{-3})$
Np^{232}	$4(10^{-3})$	—	—
Np^{231}	$<4(10^{-4})$	$<6(10^{-4})$	$<6(10^{-4})$

TABLE III. U^{238} cross sections (unit 10^{-24} cm²).

	Deuteron energy (Mev) 45	120
Np^{238}	$6(10^{-3})$	—
Np^{236}	$3(10^{-3})$	$6(10^{-3})$
Np^{235}	$8(10^{-3})$	$2(10^{-2})$
Np^{234}	$8(10^{-3})$	—
Np^{233}	$<4(10^{-4})$	—
Np^{231}	0	$<4(10^{-5})$

product of the present investigation and are useful chiefly for the practical purposes of indicating the intensity of radioactivity which may be produced for each of the isotopes under the conditions outlined in this paper. The nature of such targets, namely small amounts of powdered material, and the conditions of the bombardments were not such as to lead to sufficiently accurate cross sections to enable safe deductions to be made in regard to the mechanism of these relatively high energy nuclear reactions involving heavy nuclei.

However, it can be seen that the cross sections for the (d, n), $(d, 2n)$, $(d, 3n)$, $(d, 4n)$, etc., reactions on uranium in this energy range are substantially smaller than for the same reactions on non-fissioning nuclei. Apparently, a predominant fraction of the excited intermediate nuclei undergo the fission reaction. Consideration of the results suggest that the total cross section for the formation of neptunium isotopes by (d, xn) reactions does not change greatly over the energy range investigated, which suggests that increased excitation does not markedly increase fission and competing reaction yields at the expense of (d, xn) reaction yields.

It may be noticed that the reactions involving the emission of only a small number of neutrons, such as the (d, n) and $(d, 2n)$ reactions, do not drop off very much in yield even at relatively high deuteron energies. This indicates that reactions involving only small energy transfers[19] from the high energy bombarding particles are important here as has been found also to be the case for reactions with lighter nuclei. It may also be noticed that the lightest isotope, Np^{231}, is not formed in yields as high as the other isotopes at any deuteron energy, which perhaps indicates an increasing relative yield of the fission reaction with decreasing mass of the intermediate excited neptunium nuclei, as might be expected from the simple Bohr-Wheeler picture of the fission process.

ACKNOWLEDGMENTS

We are indebted to Albert Ghiorso for cooperation in the measurements of alpha-particle activities with the pulse analyzer.

We thank Professors J. G. Hamilton, T. M. Putnam, and B. Rossi, and the crew of the 60-in. Crocker Laboratory cyclotron, and Dr. D. C. Sewell, J. T. Vale, and their associates of the 184-in. cyclotron for assistance in the bombardments.

[19] R. Serber, Phys. Rev. 72, 1114 (1947).

PHYSICAL REVIEW VOLUME 78, NUMBER 4 MAY 15, 1950

Nuclear Mass Determinations from Nuclear Q-Values

A. TOLLESTRUP, W. A. FOWLER, AND C. C. LAURITSEN
Kellogg Radiation Laboratory, California Institute of Technology, Pasadena California

(Received January 31, 1950)

Consistent values of the masses of the light nuclei have been calculated from the best measurements of Q-values for several nuclear reactions, and from mass spectrographic measurements. Tables are given of the Q-values and of the calculated mass values.

1. INTRODUCTION

THE Q-values for several reactions involving light nuclei have been recently measured with probable errors of 20 kev or less. In general these measurements have been made possible through the employment of high resolution electrostatic or magnetic analyzers for determining the energy of the particles involved in the reaction. These new data are sufficient to determine the nuclear masses relative to H^1 through B^{10}, independently of mass spectroscopic data. Unfortunately sufficient data are not yet available to base the masses upon O^{16} and consequently the mass spectroscopic value for H^1 is used. Furthermore some uncertainty still exists in the mass of He^4 and subsequent nuclei as discussed below.

The mass values of H^1, D^2, C^{12} and N^{14} were calculated from the mass spectroscopic doublets $2H-D$, CH^4-O, CH^2-N^{14}, and $3D-C_4$. In view of the discrepancies recently found in the early values of $2H-D$, it was decided to use Nier's[1] recent values for the first three doublets combined with the results of Bainbridge[2] for the last doublet.* Nier's value for $2H-D$ combined with Bell and Elliott's[3] new value for $H^1(n, \gamma)D$ leads to an $n-H^1$ difference of 788 kev compared to 782 ± 1 kev as determined at Los Alamos from threshold measurements on $T^3(p, n)He^3$ combined with the decay energy of tritium. The nuclear data have been combined with the mass spectroscopic values of C^{12} and N^{14} to yield the masses of N^{13}, C^{13}, and C^{14}.

Table I lists all the accurately determined Q-values considered in this note. The $Li^7(p, \alpha)He^4$ value is not new but was included in order to determine the mass of the α-particle and hence it influences all subsequent

[1] T. R. Roberts and A. O. C. Nier, Phys. Rev. 77, 746(A) (1950).
[2] K. T. Bainbridge, NRC Nuclear Science Series No. 1.
* It is emphasized that a future change in the mass spectroscopic value of H^1 will change the masses for D^2 to B^{10} inclusive by the same amount.
[3] R. E. Bell and R. G. Elliott (private communication).

TABLE I. Table of accurate Q-values.

Reaction	Q-measured	Adopted value of Q Mev	mMU*	Reference
$H^1(n, \gamma)D^2$	2.230 ±0.007	2.230	2.395	Bell and Elliott (priv. comm.).
$D^2(\gamma, n)H^1$	−2.186 ±0.004	−2.230	−2.395	NRC Nuclear Science Series No. 1.
$D^2(d, p)T^3$	4.036 ±0.022	4.032	4.330	Phys. Rev. **75**, 1947 (1949).
$D^2(d, n)He^3$	3.265 ±0.018	3.268	3.510	Phys. Rev. **75**, 1947 (1949).
$T^3(\beta^-)He^3$	0.0189±0.0005 0.0180±0.0186	0.0185	0.0199	Phys. Rev. **75**, 984 (1949). Phys. Rev. **76**, 853 (1949).
$T^3(p, n)He^3$	−0.7637±0.001	−0.7637	−0.8202	Phys. Rev. **76**, 325 (1949).
$He^3(n, p)T^3$	0.764 ±0.010 0.766 ±0.010	0.7637	0.8202	Phys. Rev. **75**, 1110 (1949). Phys. Rev. **77**, 641 (1950).
$Li^6(n, \alpha)T^3$	4.56 ±0.08** 4.92 ±0.03**	4.785	5.139	Phys. Rev. **75**, 782 (1949). Phys. Rev. **75**, 782 (1949).
$Li^6(p, \alpha)He^3$	4.017 ±0.022	4.021	4.319	Phys. Rev. **76**, 428 (1949).
$Li^6(d, p)Li^7$	5.006 ±0.016	5.012	5.383	Phys. Rev. **76**, 1766 (1949).
$Li^6(d, \alpha)He^4$	22.20 ±0.04	(22.292)	(23.942)	Phys. Rev. **56**, 548 (1939).
$Li^7(d, p)Le^8$	−0.193	−0.193	−0.207	Phys. Rev. **76**, 1766 (1949).
$Li^7(p, \alpha)He^4$	17.28 ±0.03	17.280	18.559	Phys. Rev. **56**, 548 (1939).
$Li^7(p, n)Be^7$	−1.6456 −1.6449±0.0016	−1.6453	−1.767	Phys. Rev. **75**, 246 (1949). Phys. Rev. **76**, 502 (1949).
$Be^8(\alpha)He^4$	0.089 ±0.005	0.089	0.0956	Phys. Rev. **76**, 428 (1949).
$Be^9(\gamma, n)Be^8$	$-\frac{2.230}{1.338}=-1.667$	−1.671	−1.795	Phys. Rev. **74**, 1225(A) (1949).
$Be^9(p, n)B^9$	−1.851 ±0.006 −1.8519±0.002	−1.8514	−1.9884	Phys. Rev. **65**, 33 (1944). Phys. Rev. **77**, 752(A) (1950).
$Be^9(p, d)Be^8$	0.558 ±0.003	0.559	0.600	Phys. Rev. **76**, 428 (1949).
$Be^9(p, \alpha)Li^6$	2.121 ±0.012	2.125	2.282	Phys. Rev. **76**, 428 (1949).
$Be^9(d, p)Be^{10}$	4.576 ±0.012	4.568	4.906	Phys. Rev. **76**, 1547 (1949).
$Be^9(d, \alpha)Li^7$	7.145 ±0.024	7.137	7.665	Phys. Rev. **76**, 1547 (1949).
$Be^{10}(\beta^-)B^{10}$	0.566 ±0.010	0.560	0.601	Phys. Rev. **76**, 183A (1949).
$B^{10}(p, \alpha)Be^7$	1.146 ±0.005	1.146	1.231	Phys. Rev. **76**, 587A (1949).
$B^{10}(n, \alpha)Li^7$	2.785 ±0.025	2.791	2.998	Phys. Rev. **74**, 1259A(1949).
$B^{11}(p, n)C^{11}$	−2.762 ±0.002	−2.762	−2.966	Phys. Rev. **77**, 752(A) (1950).
$C^{11}(\beta^+)B^{11}$	0.981 ±0.005	0.958	1.029	Proc. Roy. Soc. **A177**, 357 (1940-1941).
$C^{12}(d, p)C^{13}$	2.729 ±0.009	2.726	2.928	Phys. Rev. **76**, 1543 (1949).
$C^{12}(d, n)N^{13}$	−0.281 ±0.003	−0.279	−0.300	Phys. Rev. **75**, 1398 (1949).
$C^{13}(p, n)N^{13}$	−3.003 ±0.003	−3.005	−3.227	Phys. Rev. **77**, 752(A) (1950).
$C^{14}(p, n)N^{14}$	−0.620 ±0.009	−0.626	−0.672	Phys. Rev. **75**, 1 (1949).
$C^{14}(\beta^-)N^{14}$	0.156 ±0.001	0.156	0.168	NRC Nuclear Science Series No. 5.
$N^{13}(\beta^+)C^{13}$	2.222 ±0.003	2.223	2.387	NRC Nuclear Science Series No. 5.
$N^{14}(n, p)C^{14}$	0.616 ±0.010 0.630 ±0.006	0.626	0.672	Phys. Rev. **75**, 1110 (1949). Phys. Rev. **77**, 641 (1950).
$O^{16}(d, p)O^{17}$	1.925 ±0.009	1.925	2.067	Phys. Rev. **76**, 1543 (1949).
$O^{18}(p, n)F^{18}$	−2.455 ±0.002	−2.455	−2.637	Phys. Rev. **77**, 752(A) (1950).
$F^{19}(p, \alpha)O^{16}$	8.113 ±0.030	8.113	8.713	Phys. Rev. **78**, 88(A) (1950).

* 1 mMU = 0.9311 Mev.
** When corrected for the new range-energy relation [W. P. Jesse and J. Sadaushis, Phys. Rev. **78**, 1 (1950)], these results are close to the adopted value.

masses. The range of the α-particles from this reaction nearly coincides with the range of those from ThC′ and hence the measurement was considered to be more accurate than that of $Li^6(d, \alpha)He^4$ which if accurately known could also be used to determine the α-particle mass.

Among the data listed, there are eight independent cycles which determine the $n-H^1$ difference, the values ranging from 776±9 to 789±6 kev. The weighted mean of 782±1 kev is determined almost entirely by the Los Alamos data. Using this value the Q-values in each case were adjusted to be consistent with this difference. The adjustments made were weighted according to the experimental errors given and in no case did the change exceed 7 kev with the single exception of Townsend's value for $C^{11}(\beta^+)B^{11}$. Since the value of the $B^{11}(p, n)C^{11}$ threshold is very accurately known, the whole discrepancy of 23 kev in this case was ascribed to the

TABLE II. Table of atomic masses.

	From mass spectroscopic data	From nuclear data	Bethe	Δ (mMU)
n^1		1. 008 977	1. 008 930	+0.047
H^1	1. 008 137 4	*	1. 008 123	+0.014
D^2	2. 014 726	2. 014 719	2. 014 708	+0.011
T^3		3. 016 971	3. 017 02	−0.05
He^3		3. 016 951	3. 017 00	−0.05
He^4		4. 003 910	4. 003 90	+0.01
Li^6		6. 017 043	6. 016 97	+0.07
Li^7		7. 018 242	7. 018 22	+0.02
Li^8		8. 025 031	8. 025 02	+0.01
Be^7		7. 019 169	7. 019 16	+0.01
Be^8		8. 007 916	8. 007 85	+0.06
Be^9		9. 015 098	9. 015 03	+0.07
Be^{10}		10. 016 774	10. 016 77	0
B^9		9. 016 246	9. 016 20	+0.05
B^{10}		10. 016 173	10. 016 18	−0.01
C^{12}	12. 003 900	*	12. 003 82	+0.08
C^{13}		13. 007 554	13. 007 51	+0.04
C^{14}		14. 007 733	14. 007 67	+0.06
N^{13}		13. 009 941	13. 009 88	−0.04
N^{14}	14. 007 565	*	14. 007 51	+0.05
O^{17}		17. 004 515	17. 004 50	+0.02
F^{19}		19. 004 486	19. 004 50	−0.01

* Mass spectroscopic values used here.

$C^{11}(\beta^+)B^{11}$ determination. It was found that Townsend's measurement of $N^{13}(\beta^+)C^{13}$ was also some 20 kev different from two other precise measurements which agreed with each other. (See NRC Nuclear Science Series No. 5.) Consequently we have not included his results in adjusting the Q-values.

Finally, all other independent cycles among the reactions listed were considered. There are seven of these, and the Q-values in each case were adjusted in relation to the experimental errors to satisfy the cycles; in no case did this adjustment require a change of more than 9 kev, nor were any of the experimental errors exceeded. These *adopted* Q-values are listed in column 3 of Table I together with the reference. The values are given in Mev and in milli-mass units based upon 1 mMU=0.9311 Mev. These Q-values were then combined with the mass spectroscopic value for H^1 to yield the masses which are listed in Table II, while the mass spectroscopic data for C^{12}, N^{14} were also used to yield the masses of N^{13}, C^{13}, C^{14}. For comparison the values given in *Elementary Nuclear Physics* by H. A. Bethe are also listed together with the differences.

It is evident from the above that the reactions $Li^6(d, \alpha)$ and $Li^7(p, \alpha)$ should be accurately determined in a high resolution spectrograph in order to fix the α-particle mass. This would make the nuclear data satisfactory up to B^{10}. The H^1, D^2, C^{12}, O^{16} system is one of the basic mass spectroscopic cycles, and should be checked by nuclear methods. As mentioned earlier, the H^1 to D^2 part of this cycle now agrees with nuclear data, and the remaining two intervals D^2 to C^{12} and C^{12} to O^{16} offer two remaining checks on these data. C^{12} can be obtained from existing data if the two reactions, $B^{10}(d, p)B^{11}$ ($Q\sim 9$ Mev) and $C^{13}(d, \alpha)B^{11}$, ($Q\sim 5$ Mev), are determined accurately. Furthermore, the series $O^{16}(d, \alpha)N^{14}$ ($Q\sim 3$ Mev), $N^{14}(n, \alpha)B^{11}$ ($Q\sim -0.3$ Mev) and $B^{10}(d, p)B^{11}$ would connect B^{10} directly with O^{16}, but has the disadvantage of involving a neutron induced reaction with a negative Q. While the internal consistency of the nuclear data seems very good, a compounding of errors is certainly possible and comparisons with the mass spectroscopic values are very desirable.

Numerical Evaluation of the Fermi Beta-Distribution Function*

I. FEISTER
National Bureau of Standards, Washington, D. C.
(Received December 12, 1949)

In making a Fermi-Kurie plot of a β-spectrum various approximations have been used to evaluate $f(Z, \eta)$. It is probable, however, that none of these approximations is completely adequate for all values of Z and η. Hence an accurate computation and tabulation of this important function is now in preparation. Three approximations for $f(Z, \eta)$ are compared with some representative values of $f(Z, \eta)$ that have been computed for the proposed table, and the accuracy and range of validity of these approximations are indicated.

I. INTRODUCTION

IN comparing an observed beta-momentum distribution with that predicted by the Fermi theory for "allowed" beta-transitions, it is customary to plot $[N(H\rho)/f(Z, \eta)]^{\frac{1}{2}}$ against the electron energy E, where $N(H\rho)$ is the number of β-particles emitted per unit momentum interval; $f(Z, \eta)$ is the Fermi distribution function; Z is the charge of residual nucleus; and $\eta = H\rho/1704$ is the momentum of β-rays emitted in units of m_0c. In making such a plot it is evidently desirable that the accuracy with which the theoretical function $f(Z, \eta)$ is computed be equal to or better than the experimental accuracy of $N(H\rho)$.

Since the direct evaluation of $f(Z, \eta)$ is difficult and tedious, various approximations have been used for this purpose. However, there is insufficient information in the literature about the relative accuracy and range of validity of these approximations. Three frequently used approximations for $f(Z, \eta)$ are here compared and their range of validity indicated.

II. APPROXIMATIONS FOR THE FERMI FUNCTION

The "Fermi distribution function" or "transition probability function" is

$$f(Z, \eta) = \eta^2 F(Z, \eta), \tag{1}$$

where $F(Z, \eta)$, the "Coulomb correction factor," is caused by the effect of nuclear attraction upon the emitted β-distribution. The function $f(Z, \eta)$ was given by Fermi in his original paper.[1] If we omit momentum-independent factors, which do not affect the shape of the Fermi-Kurie (FK) plot, this function is:

$$f(Z, \eta) = \eta^{2+2S} e^{\pi y} |\Gamma(1+S+iy)|^2, \tag{2}$$

where

$$S = (1-\gamma^2)^{\frac{1}{2}} - 1$$

$$\gamma = \begin{cases} +Z\alpha = +Z/137 \text{ for } \beta^- \text{-emission} \\ -Z\alpha = -Z/137 \text{ for } \beta^+ \text{-emission} \end{cases}$$

$$y = \gamma \frac{(1+\eta^2)^{\frac{1}{2}}}{\eta}$$

Γ = Γ-function.

Since the direct evaluation of (2) by means of a series expansion of the Γ-function is inconvenient, various approximations have been utilized for this purpose. In his original paper[1] Fermi used the following approximation for $Z = 82.2$

$$f(82.2, \eta) \approx 4.5\eta + 1.6\eta^2. \tag{3}$$

This expression, however, has very limited applicability.

Later Kurie, Richardson, and Paxton[2] gave the "non-relativistic approximation"

$$f(Z, \eta) \approx \eta^2 \frac{2\pi y}{1-e^{-2\pi y}} \equiv f_N(Z, \eta) \tag{4}$$

which they estimated could be used for all light elements up to about Cu, $Z = 29$ (provided η is not $\gg 1$). Thus this expression also has quite limited applicability.

A more generally useful approximation has been given by Bethe and Bacher[3] and put in the following convenient form by Longmire and Brown[4]

$$f(Z, \eta) \approx f_N(Z, \eta) \eta^{2S} (y^2 + \tfrac{1}{4})^S \tag{5}$$

which can be written[5]

$$f(Z, \eta) \approx f_N(Z, \eta) \left[\frac{(1+\eta^2)(1+4\gamma^2)-1}{4}\right]^S. \tag{6}$$

According to Longmire and Brown, this approximation seemed to be accurate to about one percent for values of Z up to 84.

Nordheim and Yost[6] have given the following approximation for the complex Γ-function in (2):

$$|\Gamma(1+S+iy)|^2 \approx \frac{2\pi |y| (1-2S)}{|e^{\pi y} - e^{-\pi y}|}. \tag{7}$$

Substituting this expression in (2) we obtain

$$f(Z, \eta) \approx f_N(Z, \eta)(1-2S)\eta^{2S}. \tag{8}$$

* Assisted by the AEC.
[1] E. Fermi, Zeits. f. Physik 88, 172 (1934).
[2] Kurie, Richardson, and Paxton, Phys. Rev. 49, 368 (1936).
[3] H. A. Bethe and R. F. Bacher, Rev. Mod. Phys. 8, 194 (1936).
[4] C. Longmire and H. Brown, Phys. Rev. 75, 267 (1949).
[5] In obtaining (6) from (5) the factor $(1/4)^S$ in (6) was apparently inadvertently omitted by Longmire and Brown.
[6] L. W. Nordheim and F. L. Yost, Phys. Rev. 51, 942 (1937).

TABLE I. Comparison of non-relativistic, Bethe and Bacher, and Nordheim and Yost approximations for $f(Z, \eta)$ with accurate values of $f(Z, \eta)$ for β^--emission computed by NBS Computation Laboratory.

Z	η	Kinetic energy (Mev)	Accurate relativistic $f(Z, \eta)$	Non-relativistic approximation for $f(Z, \eta)$	% Error	Bethe and Bacher approximation for $f(Z, \eta)$	% Error	Nordheim and Yost approximation for $f(Z, \eta)$	% Error
0	0.6	0.085	0.360						
	1	0.212	1.000						
	2	0.632	4.000						
	3	1.105	9.000						
	4	1.597	16.000						
	5	2.094	25.000						
10	0.6	0.085	0.547	0.544	−0.55*	0.547	0*	0.549	+0.37*
	1	0.212	1.363	1.359	−0.29	1.364	+0.07	1.366	+0.22
	2	0.632	5.109	5.114	+0.10	5.114	+0.10*	5.121	+0.23
	3	1.105	11.318	11.36	+0.33	11.33	+0.09	11.35	+0.30
	4	1.597	19.992	20.07	+0.41	20.00	+0.05	20.04	+0.25
	5	2.094	31.128	31.29	+0.51*	31.14	+0.03	31.19	+0.19*
20	0.6	0.085	0.788	0.772	−2.03*	0.789	+0.13	0.797	+1.14*
	1	0.212	1.806	1.784	−1.22	1.808	+0.11*	1.822	+0.89*
	2	0.632	6.377	6.399	+0.35	6.392	+0.24*	6.438	+0.96
	3	1.105	13.880	14.04	+1.13	13.91	+0.22	14.01	+0.94
	4	1.597	24.304	24.74	+1.79	24.35	+0.21	24.54	+0.99
	5	2.094	37.633	38.49	+2.29*	37.71	+0.21	37.98	+0.93
30	0.6	0.085	1.081	1.034	−4.35*	1.082	+0.09*	1.111	+2.78*
	1	0.212	2.324	2.270	−2.32	2.329	+0.22	2.380	+2.41
	2	0.632	7.773	7.835	+0.80	7.792	+0.24	7.945	+2.21
	3	1.105	16.590	17.05	+2.77	16.64	+0.30	16.95	+2.17
	4	1.597	28.732	29.94	+4.21	28.81	+0.28	29.35	+2.16
	5	2.094	44.155	46.51	+5.32*	44.29	+0.31*	45.10	+2.13*
40	0.6	0.085	1.417	1.321	−6.77*	1.415	−0.14*	1.501	+5.93*
	1	0.212	2.910	2.803	−3.68	2.911	+0.03	3.047	+4.71
	2	0.632	9.249	9.414	+1.78	9.269	+0.22	9.629	+4.11
	3	1.105	19.316	20.34	+5.32	19.36	+0.21	20.10	+4.04
	4	1.597	33.005	35.64	+7.97	33.10	+0.27	34.32	+3.97*
	5	2.094	50.229	55.28	+10.1*	50.37	+0.28*	52.23	+3.98
50	0.6	0.085	1.785	1.624	−9.02*	1.777	−0.45*	1.981	+11.0*
	1	0.212	3.543	3.374	−4.77	3.530	−0.37	3.840	+8.38
	2	0.632	10.736	11.11	+3.47	10.72	−0.19	11.49	+6.98
	3	1.105	21.880	23.88	+9.16	21.87	−0.05	23.34	+6.67
	4	1.597	36.790	41.75	+13.5	36.77	−0.05	39.24	+6.66
	5	2.094	55.318	64.71	+17.0*	55.31	−0.02*	58.97	+6.60*
60	0.6	0.085	2.170	1.935	−10.8*	2.152	−0.83	2.579	+18.8*
	1	0.212	4.197	3.972	−5.36	4.158	−0.93*	4.774	+13.7
	2	0.632	12.143	12.90	+6.26	12.05	−0.74	13.48	+11.0
	3	1.105	24.078	27.62	+14.7	23.91	−0.71	26.59	+10.4
	4	1.597	39.721	48.20	+21.4	39.45	−0.68	43.80	+10.3
	5	2.094	58.859	74.68	+26.9*	58.49	−0.63*	64.85	+10.2*
70	0.6	0.085	2.556	2.251	−11.9*	2.521	−1.37*	3.327	+30.2*
	1	0.212	4.840	4.589	−5.19	4.759	−1.67	5.878	+21.4
	2	0.632	13.359	14.76	+10.5	13.13	−1.72*	15.56	+16.5
	3	1.105	25.682	31.52	+22.7	25.25	−1.67	29.67	+15.5
	4	1.597	41.429	54.96	+32.7	40.74	−1.67	47.73	+15.2
	5	2.094	60.328	85.06	+50.0*	59.31	−1.69	69.33	+14.9*
80	0.6	0.085	2.925	2.569	−12.2*	2.872	−1.81*	4.286	+46.5*
	1	0.212	5.429	5.217	−3.90	5.285	−2.58	7.181	+32.3
	2	0.632	14.264	16.68	+17.0	13.84	−2.95	17.68	+23.9
	3	1.105	26.468	35.54	+34.3	25.65	−3.10	32.33	+22.2
	4	1.597	41.587	61.93	+48.9	40.30	−3.10	50.55	+21.5
	5	2.094	59.312	95.81	+61.5*	57.47	−3.10*	71.95	+21.3*
90	0.6	0.085	3.257	2.889	−11.3*	3.181	−2.33*	5.544	+70.2*
	1	0.212	5.919	5.853	−1.12	5.702	−3.67	8.733	+47.5
	2	0.632	14.730	18.64	+26.5	14.05	−4.62	19.78	+34.3
	3	1.105	26.234	39.67	+51.2	24.97	−4.80	34.45	+31.3
	4	1.597	39.955	69.05	+72.8	38.00	−4.90	52.03	+30.2
	5	2.094	55.588	106.8	+92.1*	52.83	−4.97*	72.17	+29.8*

* Asterisks indicate lowest and highest percent error in each group of six values.

In addition to the expressions for $f(Z, \eta)$ given above, various other approximations have been used which will not be discussed here. As pointed out by Longmire and Brown,[4] however, there is apparently no uniform practice for the evaluation of this function. In most cases the approximation used and the accuracy of the evaluation is not specifically stated, so that there may be some doubt as to whether the method used to calculate $f(Z, \eta)$ has been sufficiently accurate in all such cases.

For the reasons indicated the writer felt that a table of accurately computed Fermi functions was very much needed, and the Computation Laboratory of the National Bureau of Standards is now working on such a table. It is planned to compute $f(Z, \eta)$ for both negatrons and positrons; for all values of Z from 1 to 100; and for values of η from 0.050 to 7.00 (0.67 kev to 3100 kev) at sufficiently close intervals that any other values desired may ordinarily be obtained by direct interpolation from the table. The accuracy of the calculations will in most cases greatly exceed the best experimental accuracy with which β-distributions can now be determined.

III. COMPARISON OF THREE APPROXIMATIONS FOR $f(Z, n)$

The computations, while not yet complete, have proceeded to the point where the validity of the approximations for $f(Z, \eta)$ noted above can be determined at selected points. In Table I some representative values of $f(Z, \eta)$ for β^--emission obtained by the non-relativistic approximation (4), the Bethe and Bacher approximation (6),[7] and the Nordheim and Yost approximation (8) are compared with the corresponding accurate values computed directly from (2) by the NBS Computation Laboratory.

A constant percentage error in $f(Z, \eta)$ with respect to η would not affect the shape of an FK plot. Hence for the purpose of making such a plot, the factor to be considered in the "percent error" columns in Table I is the *variation* in the percentage error rather than the percentage error itself. As an aid in doing this, the lowest and highest percent errors for each Z listed are indicated with an asterisk.

We see from Table I that the non-relativistic approximation (4) becomes increasingly poor with higher Z and higher η. If we set $\sim$1 percent as a desirable limit for the variation of percentage error in $f(Z, \eta)$, then this approximation is good only for Z up to about 10 for values of η between 0.6 and 5 ($\sim$100–2100 kev).

The Bethe and Bacher approximation is much better, remaining within $\sim$1 percent of the accurate values for Z up to about 60. Moreover, Table I indicates that the percentage error in this approximation varies only slightly with η. Thus the linearity and end point of an FK plot would not be affected appreciably by the use of this approximation for values of Z up to about 80, the criterion used here being that the variation in percentage error is within $\sim$1 percent for $\eta = 0.6$ to 5.

The Nordheim and Yost approximation (8) is much better than the non-relativistic approximation, but is not as good as the Bethe and Bacher approximation. The percentage error in this approximation increases with Z, remaining within $\sim$1 percent of the true values only for Z up to about 20. However, for the purpose of making an FK plot of a β-spectrum the table indicates that (8) may be used for values of Z up to about 35, using the same criterion as before.

The table of Fermi functions, when completed, will in most cases make unnecessary the use of an approximation for the numerical evaluation of $f(Z, \eta)$.[8]

The author wishes to acknowledge the assistance of Dr. L. F. Curtiss in initiating the Fermi function computation project.

[7] Using the expression given by Longmire and Brown (see reference 4) for the Coulomb correction factor $F(Z, \eta)$, with the correction previously noted.

[8] It is expected that the computations for this table will be completed by the end of 1949.

Recoil Coincidence-Absorption Measurement of Neutron Spectra from the Reactions $A^{40}(d, n)$ and $N^{15}(d, n)$*

DONALD C. WORTH†
Sloane Physics Laboratory, Yale University,‡ New Haven, Connecticut

A counter method offering a more convenient and flexible measurement of neutron energy in the medium to high energy range is further described. Experimental results obtained by the application of this method to the reactions $A^{40}(d, n)$ and $N^{15}(d, n)$ are given.

For the argon reaction, Q-values of 5.97, 4.63, 2.87, and 1.57 Mev were observed. The $K^{41}-A^{40}$ mass difference was thus observed to be 0.99936 ± 0.00027 MU.

For the nitrogen reaction, Q-values of 10.9, 4.8, 1.6, and 0.2 Mev were observed, the last value being in some doubt.

I. INTRODUCTION

THE results described in this paper were obtained using a recoil coincidence absorption technique, previously outlined,[1] in which the extrapolated ranges of recoil protons were measured. The recoils originate from the impingement of neutrons upon the hydrogen filling of the first of two proportional counters in coincidence. The two counters were separated so that variable amounts of absorption may be inserted for the purpose of determining the ranges of various proton groups. The use of coincidence counting insures that the recoils originate inside the first counter, and in addition greatly reduces the background counting rate.

This coincidence-absorption approach was undertaken because of the greater ease of collecting data as compared with the photographic emulsion and cloud-chamber measurements of neutron energy, and also because of the desirability of comparing the resolution with that of these methods. It was not believed that the coincidence-absorption technique was capable of greater accuracy than the cloud chamber of photographic emulsion approach at *medium* energies, but rather that it would be more flexible and much more rapid in the study of *high* energies and might prove to have inherently as good resolution in this energy region.

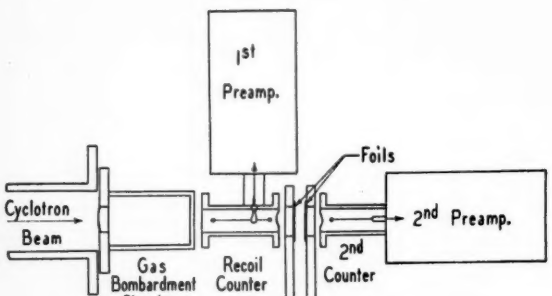

FIG. 1. Schematic diagram of the arrangement of counters, bombardment chamber, and foil changer.

II. THE EQUIPMENT

The physical arrangement of the counters, foil changer and target is shown in Fig. 1. The gas bombardment chamber may be seen just beyond the cyclotron vacuum gate port, and is shown in detail in Fig. 2. The chamber is offset so as most effectively to intercept the beam. Unfortunately aluminum foil could not be used since it gives a relatively large neutron yield and some low neutron-yield substance such as gold was required. This posed the additional problem of measuring the absorption inserted in the path of the beam, but by means of range data taken with an evacuated Faraday cage, this foil was determined to be 3.29 cm air equivalent. Thus the foil lowered the extrapolated energy of the transmitted beam from 3.92 Mev to 3.20 Mev. The foil required a double supporting grid over the bombarded area of slightly more than an inch. As an added precaution, a piece of gold foil (9 cm air equivalent) was fastened to the inside end of the chamber to prevent any yield from the brass at this solid angle-favored position. Actually, for the low bombarding energy used this was not necessary. The distance from the center of the grid to the end of the chamber was 6.5 cm.

With regard to the counters, the first (recoil source) was 8 cm long, was filled with hydrogen at a pressure of about 30 cm Hg, and was operated at a potential of about 1500 volts. The second was filled with hydrogen at 15 cm pressure, operated at about 1100 volts, and

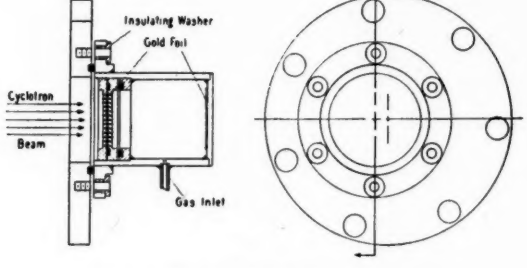

FIG. 2. Gas bombardment chamber.

* Part of a dissertation presented to the faculty of the Graduate School of Yale University in candidacy for the degree of Doctor of Philosophy.
† AEC Fellow (1948–1949).
‡ Assisted by the joint program of the ONR and the AEC.
[1] D. C. Worth, Phys. Rev. 75, 903 (1949).

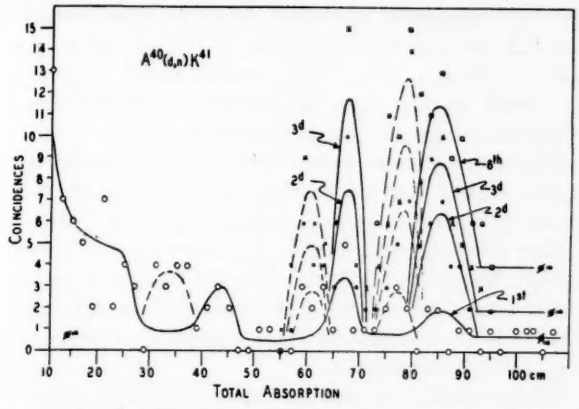

FIG. 3. Complete proton recoil spectrum from the bombardment A^{40} by 3.2-Mev deuterons. Numbers refer to successive runs on the long range groups.

had an average effective counter depth of 1.5 cm. Both counters had 0.005-in. tungsten center wires and 1-inch brass cathodes, with the center wire of each kept at a high potential above ground. (D.c. blocking condensers served to introduce the count pulses to the preamplifiers.) The reason for using hydrogen in the second counter was to reduce the number of elastic recoil counts by reason of the smaller scattering cross section over that of a conventional filling, e.g., argon. As shown in the original sketch, there was for some time a foil at the cyclotron end of the first counter in order to obtain test coincidences; but it later developed that extraneous groups were observed because of recoils from grease layers outside this foil. The two counters were so spaced that the air gap between the foils was 1.9 cm, while the separation between the end of bombardment chamber and the inside front of the first counter was 7 mm.

The remainder of the counting equipment has been outlined previously. Of prime importance to this experiment is the coincidence circuit, particularly the feature of adjustable counting levels by means of a diode discriminator, since the proper setting of counting levels is necessary in order to obtain meaningful data. In general, the higher the background level (due to accidental coincidences between the two channels), the less "peaked" is the counting. However, the background must not be so high as to worsen the relative statistics between true counts and accidentals. For "peaked" operation, the first channel counting rate was some three times that in the second—group structure would be seen even more clearly with a higher degree of peaking (higher bias, smaller counting rate) in the second channel, but this would impair the statistics even further. In the present work the largest beam current that could reliably be obtained from the cyclotron was 0.5 μa (and sometimes less) so that this put a limitation on both the peaking and the statistics. The usual resolution time employed in the coincidence circuit was 2.5×10^{-7} sec.

TABLE I. Observed extrapolated group ranges and corresponding energies for the $A^{40}(d,n)K^{41}$ reaction.

Observed extrap. range	Corrected extrap. range	Extrap. recoil energy
29 cm	29.5 cm	4.74 Mev
46	47.3	6.06
71	73.5	7.82
94	97.8	9.15

Normalization of the observed coincidence counting rate by means either of the first channel counting rate or of the integrated beam current is satisfactory. The data presented here involved the use of the beam current integrator.

As may be seen from the various dimensions given, the geometry was hardly ideal and is difficult to evaluate. This condition was imposed by the small beam currents available. The spread in recoil energy allowed over the average angular aperture from scatterer to second counter (half-angle of 10° 17′) is 3.2 percent and this uncertainty predominates over errors arising from beam inhomogeneity as well as range and angle straggling.

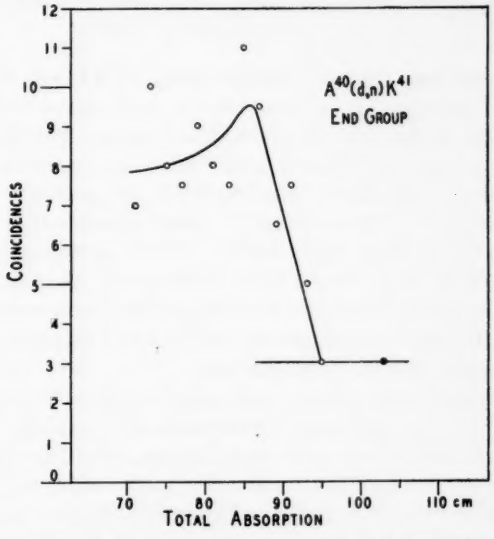

FIG. 4. Unpeaked curve of the end group yield from argon.

III. EXPERIMENTAL RESULTS

A. Bombardment of Argon

In this experiment, tank argon was bombarded by 3.2-Mev deuterons. The principal reason for the choice

TABLE II. Summary of Q-values and excitations observed in the $A^{40}(d,n)K^{41}$ reaction.

Level	Q-value (Mev)	Total excitation (Mev)	Level spacing (Mev)
Ground	5.97±0.25	0	
			1.34
1st excited	4.63±0.20	1.34±0.15	
			1.76
2nd excited	2.87	3.10	
			1.30
3rd excited	1.57	4.40	

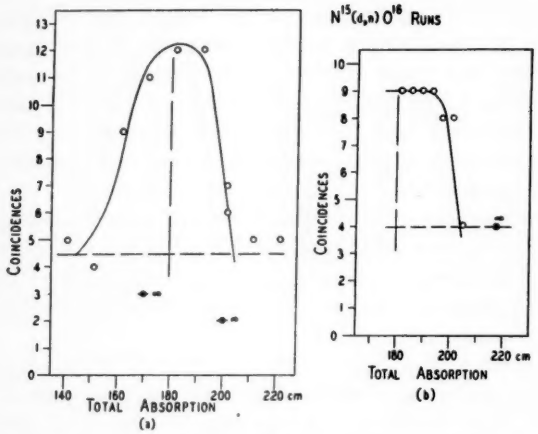

FIG. 5. Long range recoil yield from the bombardment of N^{15} by 3.2-Mev deuterons. Curve (*a*) is peaked, curve (*b*) unpeaked.

of argon was that the energy levels of K^{41} are of interest because of recent work in this region of the periodic table. The (*d*, *n*) reaction has not previously been reported. Furthermore, Sailor had noticed an unusually high background yield in his proton study of deuteron-bombarded argon,[2] and it was felt that this indicated a fairly high neutron yield, particularly in view of the high atomic number involved. As it turned out, however, most of this high yield was associated with the short range groups and the outer range groups were much smaller in magnitude.

Despite this relatively high neutron yield, the various factors which militate against coincidence yield (low beam intensity, successive solid angles, small scattering efficiency, and peaking) reduced it to the order of a few counts per minute. In order to obtain any accuracy in the results, long counting periods were necessary. In fact, it was most convenient to make a series of four-minute-count runs, adding the statistics for each absorption point so that the last two groups observed might be seen to emerge progressively from background. Actually, this is a rigorous test, since if the counts observed as a slight peak in one run were of spurious origin, subsequent runs would show a cancellation of this peak. A plot of the original survey run and the successive long range runs is shown in Fig. 3, and an unpeaked curve of the end group is shown in Fig. 4.

In Fig. 3, the dotted groups represent those which are believed to originate from external grease layers, as mentioned above. This conclusion has been reached by noting a constant range difference from each of the real groups, this difference corresponding to the absorption of the entrance foil. Note that the agreement in the extrapolated range of the end group in the peaked and unpeaked runs is satisfactory.

A rather thick target (4 cm air equivalent) was used because of yield considerations. The basic absorption was 11.3 cm, of which 9.5 cm was aluminum, 0.7 cm was the maximum absorption in the recoil counter, and 0.2 cm was the absorption in the second counter corresponding to the correct counter depth (argon gas was used in this counter at this particular time). Observed ranges are listed in Table I.

Substituting these values of the extrapolated recoil energy (hence that of incident neutrons) in the well-known *Q*-equation, one obtains the results of Table II.

Only one determination of any energy level of K^{41} previously reported.[3] Bleuler *et al.* found from their studies of the beta-decay of A^{41} that the excitation of the first level in K^{41} is 1.37 Mev, a value in good agreement with the above determination.

These results indicate the mass difference $K^{41}-A^{40}$ to be 0.99936 ± 0.00027 MU in agreement, just within the experimental error, with the value 0.99976 ± 0.00020 MU predicted from the best values for the $K^{41}-A^{41}$ and $A^{41}-A^{40}$ mass differences.[4]

B. Bombardment of N^{15}

At the time that this work was undertaken, no report of such studies had been published. Recently the results of photographic emulsion study of this reaction have been reported.[5]

Ammonia gas, enriched to 61.5 percent in N^{15}, was formed from enriched ammonium nitrate[6] by mixing the nitrate with concentrated sodium hydroxide solution in an evacuated generating system.[7] The gas was then water dried by passing it through pulverized potassium hydroxide, and condensed in a Toepler pump

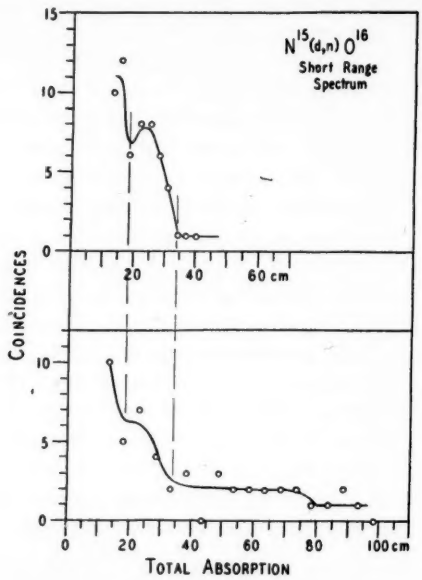

FIG. 6. Short range recoil yield from N^{15}.

[2] V. L. Sailor, Phys. Rev. **75**, 1836 (1949).

[3] Bleuler, Bollman, and Zunti, Helv. Phys. Acta **19**, 419 (1946).

[4] I am indebted to V. L. Sailor for these values derived from his studies of this section of the periodic table.

[5] E. L. Hudspeth and C. P. Swann, Phys. Rev. **76**, 464 (1949).

[6] Obtained from Eastman Kodak Company, Rochester, New York.

[7] Built jointly by L. D. Wyly and the author.

TABLE III. Observed extrapolated group ranges and corresponding energies for the $N^{15}(d, n)O^{16}$ reaction.

Observed extrap. range	Corrected extrap. range	Extrap. recoil energy
19 cm	19.0 cm	3.58 Mev
33	33.5	4.96
78	80.7	8.20
204	216	14.2

filling system by the use of liquid aid. The final target was about 3.5-cm air equivalent thickness, and the rest of the arrangement was the same as for the argon bombardment.

The long range end group is shown in Fig. 5 (curve *a*), while an unpeaked curve is shown in Fig. 5 (curve *b*). The latter plot is the sum of two successive runs. Note that these plots cover the absorption region beyond 140 cm air equivalent. Figure 6 shows two runs (taken a month apart) on the short range region from 13 cm to 98 cm. The unplotted region from 100 cm to 140 cm exhibited no counts above background. The uncorrected extrapolated ranges that seem to be indicated are: 19, 33, 78, and 204 cm. The corrected ranges and recoil energies are given in Table III.

On the assumption all the groups are due to the $N^{15}(d, n)$ reaction, the Q-values found are given in Table IV.

The 33-cm group cannot be due to deuterium contamination, and does not seem to be due to $N^{14}(d, n)$. This level may be the one recently suggested by Hudspeth and Swann;[5] the 19-cm group represents a possible unreported level. Note that the observed excitation of the first level is in agreement with the value determined by $F^{19}(p, \alpha)$ observation.[8]

Fairly conservative experimental errors are assigned to these Q-values because of the rather poor statistics and the indeterminancy of geometric corrections. Particularly in the case of the long range group there is a question about the reliability of present range-energy data.

IV. COMMENTS ON THE METHOD

The results obtained are gratifying, considering the early stage of development of this technique, and seem to indicate the value of its further exploitation. As employed, the method allowed data to be gathered in a few hours. When the second counter is at low bias, there is no impairment of the statistics with increasing neutron energies such as is caused in other methods by a decreasing angular aperture in which the longer recoil tracks must end. There is a worsening of the statistics due to the decreasing neutron-proton scattering cross section, but this is common to all recoil methods. The flexibility of the technique may be seen in that the particular arrangement allowed observation of neutron energies from 1.5 Mev to nearly 15 Mev. End group yield can be increased at the expense of excited state resolution by using high gas pressure or a polystyrene radiator in the first counter.

Of course, there are various factors which make application of this technique difficult. Foremost among these is the very low scattering efficiency compatible with low recoil absorption by the scattering medium. (Here the counting rate was lowered by a factor of 10^5 below that of charged particle counting due to the necessity of using the intermediate elastic collision process.) In order to have good geometry and to overcome the impairment of the statistics just mentioned, it is necessary to have a fairly intense ion beam. Furthermore, faster counters and coincidence circuit would help to reduce the relative number of accidental coincidences, and thus improve the statistics by allowing higher counting rates.

The author is happy to express his gratitude to Professor E. C. Pollard, who suggested this problem, for his helpful advice and encouragement.

The author is also thankful for the AEC fellowship grant which made this work possible.

TABLE IV. Summary of Q-values and excitations observed in the $N^{15}(d, n)O^{16}$ reaction.

	Q-value (Mev)	Total excitation (Mev)	Level spacing (Mev)
Ground	10.9±0.5	0	
			6.1
1st excited	4.8±0.3	6.1±0.3	
			3.2
2nd excited	1.55	9.3	
			1.4
3rd excited	0.19	10.7	

[8] Lauritsen, Lauritsen, and Fowler, Phys. Rev. 59, 241 (1941).

Non-Adiabatic Meson Theory of Nuclear Forces

S. M. DANCOFF
Physics Department, University of Illinois, Urbana, Illinois
(Received January 20, 1950)

Two nucleon forces are studied using a technique with which a detailed account of the nucleon recoil during meson emission and absorption may be given. The nucleon motion is treated relativistically. The method is applied to the neutral scalar meson field. It is concluded that the conventional static approximation gives results for this case which are not misleading. It is pointed out that the concept of potential energy is not always applicable in such problems, its validity depending not so much on the "separation" of the nucleons as on the character of the wave function for the state of the system concerned.

I. INTRODUCTION

CALCULATIONS of the two nucleon forces to be expected on the basis of meson theory have generally included the following assumptions:

(1) It is permissible to calculate the potential energy of the two nucleons due to the exchange of mesons; the motion of the two nucleons in this potential is then to be worked out as a second step (adiabatic approximation).

(2) Relativistic effects in the motion of the nucleons may be neglected.[1]

However, considerable doubt has been expressed as to the validity of both of these assumptions and it appears reasonable to ask to what extent the well-known objectionable features of the resulting theory can be modified in a calculation of a more general nature.

The present formalism permits a direct computation of the binding energy of a two nucleon system without the introduction of the concept of potential energy. The nucleons are considered to obey the Dirac equation.

The formalism is roughly equivalent to a weak coupling theory. It is developed for the case of a neutral scalar meson field with scalar coupling. A lowest state of finite binding is obtained, together with spin dependent terms not unlike those that may operate in the deuteron. Quantitative agreement is not obtained.

II. NEUTRAL SCALAR THEORY

The Hamiltonian density is

$$H=\Psi_P^*H_P\Psi_P+\Psi_N^*H_N\Psi_N+\psi(-\Delta+\mu^2)\psi +g(\Psi_P^*\beta\Psi_P+\Psi_N^*\beta\Psi_N)\psi. \quad (1)$$

Here Ψ_P and Ψ_N are the four-component wave field operators of two independent nucleon fields, labeled P and N; H_P and H_N are the corresponding Hamiltonian operators for free nucleons. ψ is the wave field operator of the meson field whose quanta have mass μ; β is the conventional Dirac matrix, and g is the coupling parameter. We also use $\hbar=c=1$; we will introduce $\omega_k=(\mu^2+k^2)^{\frac{1}{2}}$ and $E_P=(M^2+P^2)^{\frac{1}{2}}$, where ω_k is the energy of a meson of momentum k and E_P is the energy of a nucleon of momentum P.

In the adiabatic approximation, $\Psi_P^*\beta\Psi_P$ is replaced by $\delta(\mathbf{r}-\mathbf{r}_P)$; the other terms in H are treated accordingly. The last term is treated as a perturbation and its second-order effect is calculated in a system which in zero order has nucleons at $\mathbf{r}_P$ and $\mathbf{r}_N$ and no mesons. The meson operator is

$$\psi(\mathbf{r})=\sum_{\mathbf{k}}(2L^3\omega_k)^{-\frac{1}{2}}(A_{\mathbf{k}}e^{i\mathbf{k}\cdot\mathbf{r}}+A_{\mathbf{k}}^*e^{-i\mathbf{k}\cdot\mathbf{r}}). \quad (2)$$

The summation is over the eigenvectors of momentum in a cube of side L. $A_{\mathbf{k}}$ and $A_{\mathbf{k}}^*$ are annihilation and creation operators, respectively. The result is the "Yukawa potential"

$$\Delta E^{(2)}=-\frac{g^2}{4\pi}\frac{e^{-\mu R}}{R}, \quad \text{with } R=|\mathbf{r}_P-\mathbf{r}_N|. \quad (3)$$

With $\mu\sim 300$ electron masses and $(g^2/4\pi)\sim 0.3$ this has about the right range and depth to account for the binding of the deuteron in its triplet state. There is no explanation, however, of the triplet-singlet splitting.

We modify the attack in the following way. We take for the wave functional of the composite system

$$\Psi=\sum_{\mathbf{PNk}ij}[a_{\mathbf{PN}}^{ij}\{\mathbf{P}^i\mathbf{N}^j\}+b_{\mathbf{PNk}}^{ij}\{\mathbf{P}^i\mathbf{N}^j\mathbf{k}\}]. \quad (4)$$

The brace $\{\mathbf{P}^i\mathbf{N}^j\}$ is the functional representing the presence of a nucleon with momentum $\mathbf{P}$ in spin state i and a second with momentum $\mathbf{N}$ in spin state j. The second brace represents a state in which, in addition, a meson of momentum $\mathbf{k}$ is present. The coefficients a and b with their indices are the probability amplitudes for these particular configurations in the composite system. If it were legitimate to neglect the possibility that two or more mesons were ever present we would have

$$\sum_{\mathbf{PNk}ij}[|a_{\mathbf{PN}}^{ij}|^2+|b_{\mathbf{PNk}}^{ij}|^2]=1. \quad (5)$$

We will in fact make this assumption. This is slightly less restrictive than the weak coupling approximation because we do not assume that the b's are small com-

[1] Investigations by L. Van Hove, Phys. Rev. **75**, 1519 (1949), G. Araki, Phys. Rev. **75**, 1101 (1949), and K. M. Watson and J. V. Lepore, Phys. Rev. **76**, 1157 (1949) have dealt with the influence of the relativistic nucleon properties on the two nucleon interactions. In these researches the adiabatic approximation is made or implied.

pared to the a's. Further, we do not assume that the various a's are given by some zero-order distribution; instead the a's and b's are now co-determined by the equations of motion. The convergence of the approximation method is to be tested by making a second calculation in which terms in (4) are included which allow for the presence of two mesons.

If now $\mathbf{H}$ is the space integral of H above, we write

$$\mathbf{H}\Psi=E\Psi, \tag{6}$$

where E is the energy of the system. We get

$$\sum_{(\mathbf{PN}ij)} a^{ij}_{\mathbf{PN}}(E_P+E_N)\{\mathbf{P}^i\mathbf{N}^j\}$$

$$+\sum_{(\mathbf{PN}ij\mathbf{k})} b^{ij}_{\mathbf{PNk}}(E_P+E_N+\omega_k)\{\mathbf{P}^i\mathbf{N}^j\mathbf{k}\}$$

$$+\sum_{(\mathbf{PN}\,\mathbf{P}_1\mathbf{N}_1ijrs)} a^{ij}_{\mathbf{PN}}(\mathbf{P}_1{}^r\mathbf{N}_1{}^s\mathbf{k}|\mathbf{H}_1|\mathbf{P}^i\mathbf{N}^j)\{\mathbf{P}_1{}^r\mathbf{N}_1{}^s\mathbf{k}\}$$

$$+\sum_{(\mathbf{PN}\,\mathbf{P}_1\mathbf{N}_1ijrs\mathbf{k})} b^{ij}_{\mathbf{PNk}}(\mathbf{P}_1{}^r\mathbf{N}_1{}^s|\mathbf{H}_1|\mathbf{P}^i\mathbf{N}^j\mathbf{k})\{\mathbf{P}_1{}^r\mathbf{N}_1{}^s\}$$

$$=E\sum_{(\mathbf{PN}ij\mathbf{k})}[a^{ij}_{\mathbf{PN}}\{\mathbf{P}^i\mathbf{N}^j\}+b^{ij}_{\mathbf{PNk}}\{\mathbf{P}^i\mathbf{N}^j\mathbf{k}\}]. \tag{7}$$

Here $\mathbf{H}_1$ is the third, or interaction term in $\mathbf{H}$. It appears above in various matrix elements for transitions from an initial state, specified on the right, to a final state specified on the left.

By taking scalar products with appropriate functionals we get the pair of coupled equations

$$a^{rs}_{\mathbf{PN}}(E-E_P-E_N)=\sum_{(\mathbf{P}_1\mathbf{N}_1ij\mathbf{k})} b^{i\ j}_{\mathbf{P}_1\mathbf{N}_1\mathbf{k}}(\mathbf{P}^r\mathbf{N}^s|\mathbf{H}_1|\mathbf{P}_1{}^i\mathbf{N}_1{}^j\mathbf{k}),$$

$$b^{i\ j}_{\mathbf{P}_1\mathbf{N}_1\mathbf{k}}(E-E_{P_1}-E_{N_1}-\omega_k)=\sum_{(\mathbf{P}_2\mathbf{N}_2\alpha\beta)} a^{\alpha\ \beta}_{\mathbf{P}_2\mathbf{N}_2}(\mathbf{P}_1{}^i\mathbf{N}_1{}^j\mathbf{k}|\mathbf{H}_1|\mathbf{P}_2{}^\alpha\mathbf{N}_2{}^\beta). \tag{8}$$

The b^j's may be eliminated to get what amounts to an integral equation for the a's. In doing this we use the following substitutions:

(a) The matrix element of $\mathbf{H}_1$ may be written as $g(2L^3\omega_k)^{-\frac{1}{2}}\times$(δ function of momentum variables)$\times$⟨spin matrix elements⟩.

(b) We choose to calculate in the center of mass system. That is, we set

$$a^{rs}_{\mathbf{PN}}=a^{rs}_{\mathbf{P}}\delta(\mathbf{P}+\mathbf{N}).$$

We now get

$$a^{rs}_{\mathbf{P}}=\frac{1}{E-2E_P}\sum_{(\mathbf{k}ij)}\frac{g^2}{\omega_kL^3}\times\frac{a^{ij}_{\mathbf{P}-\mathbf{k}}\langle\mathbf{P}^r|\beta_P|\mathbf{P}-\mathbf{k}^i\rangle\langle\mathbf{P}^s|\beta_N|\mathbf{P}-\mathbf{k}^j\rangle}{E-E_{\mathbf{P}-\mathbf{k}}-E_P-\omega_k}. \tag{9}$$

The sum on the right has had deleted from it terms which correspond to the emission of a meson followed by its absorption by the *same* nucleon. Such a term is associated with the self-energy of a single nucleon. To exclude such processes from our calculation of the interaction between two nucleons will lead to no error if we calculate only to order g^2. However, higher order corrections to the interaction energy would have to include an effect of the self-energy; that is, the self-energies of interacting nucleons are somewhat different than the corresponding quantities for well-separated nucleons. This effect is the analog of the Lamb shift in the hydrogen spectrum.

The sum on the spin indices i and j goes over the values 1 and 2 only, corresponding to positive energy states. Processes in which nucleon pairs appear can make no contribution to the interaction to order g^2. This was in fact anticipated by the form chosen for (4).

The evaluation of the spin sum gives

$$\langle\mathbf{B}^i|\beta|\mathbf{A}^j\rangle=\frac{1}{D_AD_B}\left[1-\frac{\mathbf{A}\cdot\mathbf{B}}{(E_A+M)(E_B+M)}+\frac{i\boldsymbol{\sigma}^{ij}\cdot(\mathbf{A}\times\mathbf{B})}{(E_A+M)(E_B+M)}\right], \tag{10}$$

where $D_A=[2E_A/(M+E_A)]^{\frac{1}{2}}$ and $\boldsymbol{\sigma}^{ij}$ is the indicated component of the Pauli spin matrix vector. We substitute the above, at the same time suppressing the superscripts on the $a_{\mathbf{P}}{}^{ij}$ coefficients, hence treating these coefficients as products of two two-component matrices. We get

$$a_{\mathbf{P}}=\frac{1}{E-2E_P}\sum_k\frac{g^2}{\omega_kL^3}\frac{1}{D_P{}^2D^2{}_{\mathbf{P}-\mathbf{k}}}\frac{1}{E-E_P-E_{\mathbf{P}-\mathbf{k}}-\omega_k}\times\left[1-\frac{\mathbf{P}\cdot(\mathbf{P}-\mathbf{k})+i\boldsymbol{\sigma}_P\cdot(\mathbf{P}-\mathbf{k})\times\mathbf{P}}{(E_P+M)(E_{\mathbf{P}-\mathbf{k}}+M)}\right]\times\left[1-\frac{\mathbf{P}\cdot(\mathbf{P}-\mathbf{k})+i\boldsymbol{\sigma}_N\cdot(\mathbf{P}-\mathbf{k})\times\mathbf{P}}{(E_P+M)(E_{\mathbf{P}-\mathbf{k}}+M)}\right]a_{\mathbf{P}-\mathbf{k}}. \tag{11}$$

It is instructive to note at this point that the adiabatic approximation discussed earlier is equivalent to the non-relativistic approximation applied to (11). If, throughout, we neglect P and k compared to M, and if we set $E_P=M+P^2/2M$ and $E=2M-\kappa^2$, where κ^2 is the binding energy of the system, then

$$a_{\mathbf{P}}=\frac{M}{P^2+\kappa^2}\sum\frac{g^2}{L^3\omega_k{}^2}a_{\mathbf{P}-\mathbf{k}}, \tag{12}$$

there being no coupling between different spin states. The transition to continuous k values is obtained by replacing the summation by $(L^3/8\pi^3)$ times the three-dimensional integral.

We introduce the fourier transform of $a_{\mathbf{P}}$:

$$U(\mathbf{S})=\int d^3\mathbf{k}\exp(i\mathbf{k}\cdot\mathbf{S})a_{\mathbf{k}};$$
$$a_{\mathbf{k}}=\frac{1}{8\pi^3}\int d^3\mathbf{S}\exp(-i\mathbf{k}\cdot\mathbf{S})U(\mathbf{S}). \tag{13}$$

Now

$$U(\mathbf{S})=\frac{g^2M}{8\pi^3}\int d^3\mathbf{P}\frac{\exp(i\mathbf{P}\cdot\mathbf{S})}{\kappa^2+P^2}$$
$$\cdot\frac{1}{8\pi^3}\int\int\frac{d^3\mathbf{k}d^3\mathbf{y}}{\omega_k{}^2}U(\mathbf{y})\exp[-i\mathbf{y}\cdot(\mathbf{P}-\mathbf{k})], \tag{14}$$

$$(\kappa^2-\Delta)U(\mathbf{S})=(g^2M/8\pi^3)U(\mathbf{S})\int d^3\mathbf{k}\exp(i\mathbf{k}\cdot\mathbf{S})/\omega_k{}^2$$
$$=g^2MU(\mathbf{S})[\exp(-\mu S)/4\pi S].$$

This is an ordinary differential equation to determine the binding energy, κ^2. It is identical in form with the Schrödinger equation of motion obtained in the second step of the adiabatic approximation, hence the eigenvalue, κ^2, is the same. The function $U(\mathbf{S})$ is not a wave function, however, since its integrated square is less than unity. The bracketed quantity is the "Yukawa potential" which we see has at least the formal properties of a potential in a conventional Schrödinger equation. If κ^2 is regarded as given, then this equation fixes the value of $(g^2/4\pi)\sim0.3$, as discussed earlier.

Next we improve the approximation by keeping $\mathbf{k}$ to all powers and in addition keeping the first power of $(\mathbf{P}/M)$. It is convenient also to use the total spin angular momentum

$$\boldsymbol{\sigma}=(\boldsymbol{\sigma}_P+\boldsymbol{\sigma}_N)/2, \tag{15}$$

whose z projection can have the values $(1, 0, -1)$. Now

$$a_{\mathbf{P}}=\frac{-M}{\kappa^2+P^2}\cdot\frac{g^2}{8\pi^3}\int\frac{d^3\mathbf{k}}{\omega_kD_k{}^2(M-E_k-\omega_k)}$$
$$\times\left[1+\frac{\mathbf{P}\cdot\mathbf{k}+i\boldsymbol{\sigma}\cdot\mathbf{k}\times\mathbf{P}}{M(M+E_k)}\right]a_{\mathbf{P}-\mathbf{k}}. \tag{16}$$

The term $\mathbf{P}\cdot\mathbf{k}$ in the bracket is a relativistic correction to the non-spin dependent interaction and we strike it out; the term involving $\boldsymbol{\sigma}$ is the interesting one. Following the procedure of (13) to (14), we find

$$(\kappa^2-\Delta)U(\mathbf{S})=-\frac{Mg^2}{8\pi^3}\int\frac{d^3\mathbf{k}\exp(i\mathbf{k}\cdot\mathbf{S})}{\omega_kD_k{}^2(M-E_k-\omega_k)}$$
$$\times\left[1-\frac{\boldsymbol{\sigma}\cdot\mathbf{k}\times\mathbf{grad}}{M(M+E_k)}\right]U(\mathbf{S}). \tag{17}$$

The integral involving the 1 in the bracket is negligibly different from the right side of (14). We equate it simply to $g^2MU(\mathbf{S})e^{-\mu S}/4\pi S$. The second term can be written as

$$-(g^2/2M)\boldsymbol{\sigma}\cdot\mathbf{grad}F(S)\times[-i\,\mathbf{grad}U(\mathbf{S})], \tag{18}$$

where

$$F(S)=\frac{M}{8\pi^3}\int\frac{d^3\mathbf{k}\exp(i\mathbf{k}\cdot\mathbf{S})}{E_k\omega_k(\omega_k+E_k-M)}. \tag{19}$$

Now if we set $\mathbf{grad}F(S)=(\mathbf{S}/S)F'(S)$ and define an operator $\mathbf{L}=-i\mathbf{S}\times\mathbf{grad}$, then the second term of (17) becomes

$$-(g^2/2M)[F'(S)/S](\boldsymbol{\sigma}\cdot\mathbf{L})U(\mathbf{S}). \tag{20}$$

As far as the determination of κ^2 is concerned, this is equivalent to a conventional spin-orbit potential introduced into the adiabatic approximation. In fact (20) is just the Thomas relativistic spin-orbit coupling, associated with the motion of a spinning vector in an accelerated coordinate system. Inglis first suggested in 1936[2] that this coupling, well-known in atoms, applied as well to the motion of nucleons. It was pointed out at the time[2] that such a coupling could be derived purely from arguments of covariance if the nucleon could be regarded as moving in an assigned potential field. The above derivation of (20) may be regarded as a generalization of this proof to the case where the internucleon interactions are determined by the exchange of scalar mesons.

In the limit $M\to\infty$, $F(S)$ becomes simply the Yukawa potential, $[e^{-\mu S}/4\pi S]$. In this limit the equivalent potential (20) exhibits a $1/S^3$ singularity. Its ratio to the leading term is of order $(MS)^{-2}$. Now the lowest eigenfunction, $U_0(S)$, of (17) in the absence of the spin-orbit term, has the shape of the usual deuteron wave function as derived from the adiabatic approximation. Its range or width is of the order of twenty times larger than M^{-1}. Consequently if the term (20) is treated as a perturbation it is evident that its effect on the system in displacing and splitting energy levels will be small. This term will act only on states having non zero spin angular momentum and orbital angular momentum. Consequently, thinking of it as a perturbation, its observable effects in the two nucleon system are small. These considerations are essentially unchanged if one uses the exact form of $F(S)$, namely (19), which is less singular at $S=0$ than S^{-1}. In fact, it is $F'(S)$ which exhibits the singularity S^{-1}, but the deviation of $F(S)$ from the Yukawa potential occurs only in a very small region which is negligible for the above arguments.

Returning briefly to (16), we remark that if we improved the approximation further by keeping terms in (11) bilinear in the nucleon spins, we would obtain terms in the equivalent potential identifiable with the spin-spin interaction and also the "tensor force." However, this part of the potential would bear to the leading

[2] D. R. Inglis, Phys. Rev. **50**, 783 (1936).

term a ratio $(MS)^{-4}$ and would, therefore, produce effects (quadrupole moment, singlet-triplet splitting) which would be quite negligible.

Now the singularity S^{-3} of the approximate expression for $[F'(S)/S]$ suggests the question of whether the system might tend to collapse to a very small radius to take advantage of this large potential energy which can be attractive in at least some states. Of course, the probability for this catastrophe seems to be reduced by the fact that the exact expression for $F(S)$ is less singular than the approximate one. But this consideration is actually beside the point. If trial functions $U(S)$ are being studied whose radius is of order M^{-1} or less, then it is no longer valid to neglect higher powers of $\mathbf{P}/M$ as we did in deriving (16). This neglect is in fact equivalent to the assumption that $U(\mathbf{S})$ has only Fourier components of momentum small compared to M. Now if we cannot make this neglect then we also cannot derive the Schrödinger Eq. (17) and we cannot speak about a potential energy, even an equivalent one.

What we must now consider is whether the eigenfunction corresponding to the lowest eigenvalue of (11) is characterized by strong high Fourier components $(P>M)$. What we will do is assume a trial function which does have this character ("narrow"), calculate the trial eigenvalue from (11) using a variational procedure and compare this with the eigenvalue obtained from (14) for the "wide" function.

Rather than minimize the energy, E, it is equivalent and more convenient to minimize the coupling constant. We have

$$\left(\frac{g^2}{8\pi^3}\right)=\int d^3\mathbf{P}a_{\mathbf{P}}{}^2(E-2E_P)\div\Big[\int\int d^3\mathbf{P}d^3\mathbf{k}a_{\mathbf{P}} \times\frac{1}{D_P{}^2D_k{}^2\omega_{\mathbf{k}-\mathbf{P}}}\cdot\frac{1}{E-E_P-E_k-\omega_{\mathbf{k}-\mathbf{P}}} \cdot\left\{1-\frac{\mathbf{P}\cdot\mathbf{k}+i\boldsymbol{\sigma}_P\cdot\mathbf{k}\times\mathbf{P}}{(E_P+M)(E_k+M)}\right\} \cdot\left\{1-\frac{\mathbf{P}\cdot\mathbf{k}+i\boldsymbol{\sigma}_N\cdot\mathbf{k}\times\mathbf{P}}{(E_P+M)(E_k+M)}\right\}a_k\Big]. \quad (21)$$

For a trial function we select

$$a_k=Ce^{-k\rho} \quad (22)$$

whose Fourier transform is

$$U(S)=\frac{(8\pi C/\rho)}{(S^2+\rho^2)^2}. \quad (23)$$

The spin variables associated with a_k need not be exhibited if by the expressions $\boldsymbol{\sigma}_P$, $\boldsymbol{\sigma}_N$, etc. we now mean the matrix elements of these operators between initial and final spin states.

We assume $\rho\ll M^{-1}$, and correspondingly that the significant values of k in (22) run to magnitudes much greater than M. Under these conditions (21) can be simplified to the form

$$\left(\frac{g^2}{8\pi^3}\right)=\int d^3\mathbf{P}\cdot a_{\mathbf{P}}{}^2(+2P) \div\Big[\int\int d^3\mathbf{P}d^3\mathbf{k}\frac{a_P}{4|\mathbf{k}-\mathbf{P}|}\cdot\frac{1}{P+k+|\mathbf{P}-\mathbf{k}|} \cdot\left(1-\frac{\mathbf{P}\cdot\mathbf{k}}{Pk}+i\frac{\boldsymbol{\sigma}_P\cdot\mathbf{k}\times\mathbf{P}}{Pk}\right) \times\left(1-\frac{\mathbf{P}\cdot\mathbf{k}}{Pk}+i\frac{\boldsymbol{\sigma}_N\cdot\mathbf{k}\times\mathbf{P}}{Pk}\right)a_k\Big]. \quad (24)$$

Both numerator and denominator can be evaluated analytically. For the denominator the substitutions $y=P+k$, $x=P-k$, $\Delta=|\mathbf{P}-\mathbf{k}|$ are convenient. The result is

$$\frac{g^2}{8\pi^3}=\frac{3\pi C^2/\rho^4}{[(2\pi^2C^2)/3\rho^4][1+\boldsymbol{\sigma}_P\cdot\boldsymbol{\sigma}_N(4\ln 2-3)]} =\frac{9}{2\pi}[1-0.23\boldsymbol{\sigma}_P\cdot\boldsymbol{\sigma}_N]^{-1}. \quad (25)$$

$\boldsymbol{\sigma}_P\cdot\boldsymbol{\sigma}_N$ is $+1$ for a triplet state, -3 for a singlet. In any case the value of $g^2/4\pi$ is greater than 16.6, in contrast to its value of 0.3 as obtained for the "wide" trial function. It is, therefore, evident that there will be no collapse of the two nucleon system and that the distribution a_k will be essentially identical with that given by the eigenfunction of Schrödinger's equation for the Yukawa potential.

Of course the trial "narrow" function (22) is specialized in belonging to an S state. If, however, we had used a trial function corresponding to higher angular momentum, but again with a width much less than M^{-1}, we would have found trial eigenvalues of the order of (25), and therefore much higher than the one given by the "wide" function.

We conclude that when relativistic effects are taken into account in the neutral scalar theory the relation between binding energy and coupling constant is the same as in the adiabatic approximation. Further there is only an extremely small splitting between a "singlet" and a "triplet" state.

It is clear that relativistic effects will be considerably more important in theories such as the pseudoscalar or vector, where spin-dependent interactions occur in the leading order of the non-relativistic approximation. The application of the above methods to such theories is being studied.

Some New Mass Comparisons Involving Si, Fe, Ni, Cu, Zn, W, and Pt*

HENRY E. DUCKWORTH, HOWARD A. JOHNSON, RICHARD S. PRESTON, AND RICHARD F. WOODCOCK
Scott Laboratory, Wesleyan University, Middletown, Connecticut

(Received January 30, 1950)

A number of mass comparisons have been made using a large Dempster-type mass spectrograph with a spark source. Packing fraction differences have been obtained for the doublets $Si^{28}-Fe^{56}$, $Si^{29}-Ni^{58}$, $Si^{30}-Ni^{60}$, $W^{183}-Ni^{61}$, $W^{186}-Ni^{62}$, $Pt^{192}-Zn^{64}$, $Pt^{195}-Cu^{65}$, $Pt^{198}-Zn^{66}$.

1. INTRODUCTION

THE divergence of the masses of atoms from whole numbers first suggested by Aston[1] in 1923, and first measured by Costa[2] in 1925, has become increasingly important with the growth of nuclear physics. The interest in this subject led in the middle 1930's to the construction of double-focusing mass spectrographs by Dempster,[3] Bainbridge and Jordan,[4] and Mattauch.[5] These instruments of high resolving power were used to measure isotopic masses precisely, the divergence from integral values being expressed usually in terms of a packing fraction.[6] As a result of these measurements, Aston's original packing fraction curve,[7] drawn in 1927, was superseded by Dempster's more accurate one in 1938.[8]

Recent mass measurements suggest that there are large fluctuations in the packing fraction curve,[9] and also indicate that the minimum, which occurs in the neighborhood of mass 60, is lower than given by Dempster's curve.[9–12] However, there have been several inconsistencies among recent measurements, and these two features have yet to be unequivocably demonstrated. Also, there is the recent suggestion by Feenberg[13] that a plateau in the packing fraction curve may exist in the region $108 \leqslant A \leqslant 124$. It is hoped that the present measurements, and others in progress, will help to establish the true shape and position of the curve.

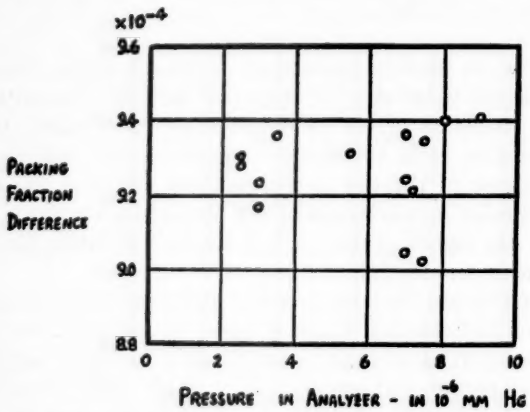

FIG. 1. Values of the $Pt^{195}-Cu^{65}$ packing fraction difference plotted against the pressure in the analyzing section of the mass spectrograph.

2. APPARATUS

The measurements reported in this paper have been made using the method devised by Dempster.[14] In this method, a double-focusing mass spectrograph, equipped with a "hot-spark" ion source, is used to photograph doublets consisting of almost coincident singly and multiply charged ions. The electrodes between which the spark occurs consist, wholly or in part, of the elements desired in the comparison. Thus, for example, Dempster has photographed the doublet formed by singly charged Cu^{65} and triply charged Pt^{195} and, from measurements thereon, has calculated the packing fraction difference (Δf) between these two nuclides. For this comparison, one electrode was a copper-beryllium alloy and the other a platinum-iridium alloy.

The mass spectrograph used in the present work, a large Dempster-type instrument, has recently been constructed at Wesleyan University.[15] Its resolution, with a principal slit of 0.001", is 7000 which is sufficient to resolve completely a large number of interesting doublets.

3. SECURING MATCHED DOUBLET LINES

It is difficult to make reliable measurements of a doublet spacing if the two lines are not fairly well matched in intensity. If the two lines of the doublet are being photographed simultaneously, as has been the usual practice, the electrodes between which the spark occurs and which vaporize to form the positive ion beam must contain the desired nuclides in appropriate proportions. These electrodes are often hard to prepare, especially if one is dealing with two elements whose

* This paper is based on work done at Wesleyan University under Contract AT(30-1)-451 with the Atomic Energy Commission.

[1] F. W. Aston, Phil. Mag. 45, 941 (1923).
[2] J. L. Costa, Ann. de physique 4, 425 (1925).
[3] A. J. Dempster, Proc. Am. Phil. Soc. 75, 755 (1935).
[4] K. T. Bainbridge and E. B. Jordan, Phys. Rev. 50, 282 (1936).
[5] Josef Mattauch, Phys. Rev. 50, 617 (1936).
[6] The term "packing fraction," introduced by Aston, is defined as $f=(A-I)/I$, where A is the mass of the atom in question, and I is the nearest integer.
[7] F. W. Aston, *Mass Spectra and Isotopes* (Edward Arnold and Company, London, England, 1942), p. 81.
[8] A. J. Dempster, Phys. Rev. 53, 869 (1938).
[9] K. Ogata, Phys. Rev. 75, 200 (1949).
[10] H. E. Duckworth, Phys. Rev. 62, 19 (1942).
[11] A. J. Dempster, Phys. Rev. 74, 1225 (1948).
[12] A. E. Shaw, Phys. Rev. 75, 1011 (1949).
[13] E. Feenberg, Rev. Mod. Phys. 19, 239 (1947).
[14] A. J. Dempster, Phys. Rev. 53, 64 (1938).
[15] H. E. Duckworth, Rev. Sci. Inst. 21, 54 (1950).

boiling points are widely different. As an example of this sort, suppose one is attempting to photograph the doublet consisting of singly charged Zn^{66} and triply charged Pt^{198}. One cannot simply make an alloy of these two elements. If one uses platinum as one electrode and an alloy of zinc as the other, the zinc alloy, generally possessing a low boiling point, vaporizes rapidly and appears to limit the temperature of the spark, with the result that few platinum ions are created. Furthermore, some of the vaporized zinc will condense on the platinum, thereby protecting it still further. It is sometimes possible to salvage from such an unsuccessful experiment, platinum electrodes which have been contaminated by zinc to just the proper degree that when a spark occurs between two of them the zinc and platinum ions are released in the desired ratio for a limited period of time. In more favorable comparisons, where the temperature of the spark is hot enough to vaporize both electrodes readily, there is still the general problem of fabricating electrodes of the desired composition.

An alternative method, which avoids these difficulties, is to photograph the two lines in a doublet consecutively. This requires an arrangement for changing electrodes so that the line intensities may be matched by running the spark between different pairs of electrodes for different times. In this way the $Zn^{66}-Pt^{198}$ doublet mentioned above has been photographed by using one brass and one platinum electrode for the first minute, two platinum electrodes for the following fifteen minutes, and brass and platinum electrodes again for the final minute. Of course, such a method can only be used if the fields of the mass spectrograph are very constant. By bracketing the Pt−Pt spark with two brass-Pt sparks, it was hoped to detect any change in the fields during the exposure, by a broadening of the zinc lines. It has been discovered that this test for constancy is not sensitive enough when the field changes are very small. Consequently, accurate absolute measurements have not been made on doublets photographed in this manner. However, useful comparative measurements which have been made will be described later in this paper in the nickel-tungsten and zinc-platinum comparisons. Except for these, the present measurements have been made from doublets photographed simultaneously in the conventional manner. When the necessary field stabilities have been achieved, the consecutive method should greatly simplify the problem of securing matched doublet lines.

TABLE I. Packing fraction of Fe^{56}.

	Doublet	Packing Fraction
Present work	$Si^{28}-Fe^{56}$	-8.52 ± 0.05
A. J. Dempster*	$N^{14}-Fe^{56}$	$-7.1\ \pm0.4$
K. Ogata**	$C_4{}^{13}H_8{}^{1}-Fe^{56}$	-8.32 ± 0.05

* See reference 14.
** See reference 9.

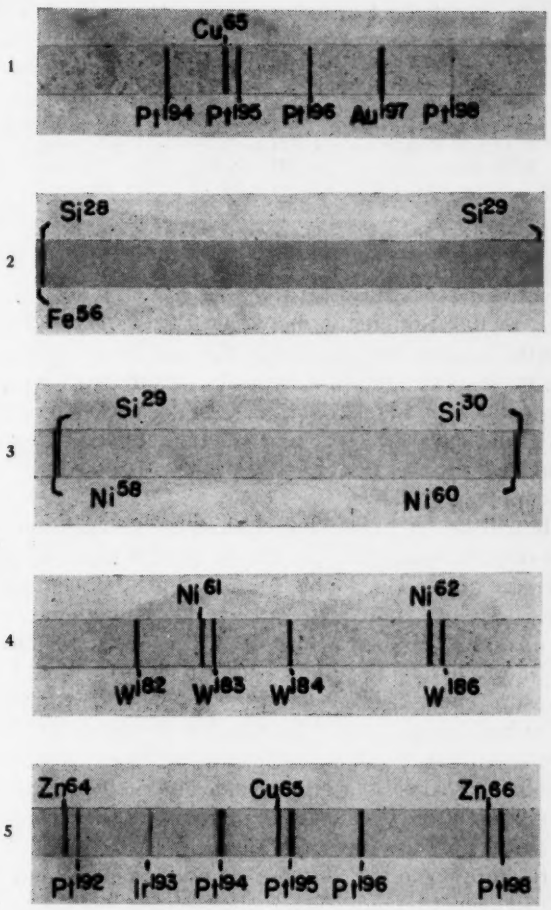

FIG. 2. Spectrum 1: A typical $Cu^{65}-Pt^{195}$ doublet used in studying the effect of pressure on doublet spacing. Spectrum 2: A typical $Si^{29}-Fe^{56}$ doublet used in the silicon-iron comparison. Spectrum 3: Representative $Si^{29}-Ni^{58}$ and $Si^{30}-Ni^{60}$ doublets used in the silicon-nickel comparison. Spectrum 4: Sample $Ni^{61}-W^{183}$ and $Ni^{62}-W^{186}$ doublets. Spectrum 5: Representative $Zn^{64}-Pt^{192}$, $Cu^{65}-Pt^{195}$, and $Zn^{66}-Pt^{198}$ doublets used in the zinc-platinum comparison. Magnification 8×.

4. $Cu^{65}-Pt^{195}$ COMPARISON AND THE EFFECT OF PRESSURE ON THE DOUBLET SPACING

Dempster and Shaw have recently observed[16] that the spacing of doublets consisting of triply charged samarium atoms and hydrocarbons of the corresponding mass is dependent upon the pressure in their mass spectrograph. This effect is attributed to a differential slowing down of the ions by residual gas.

The $Cu^{65}-Pt^{195}$ doublet has been used to study this effect in the Wesleyan mass spectrograph. With a spark between a platinum electrode and a gold electrode containing two percent copper, doublets at mass 65 formed by singly charged Cu^{65} and triply charged Pt^{195} were photographed with exposure times ranging from three to ten minutes. Exposures were taken at various pressures in the range 2.5×10^{-6} to 9×10^{-6} mm Hg. The results of this experiment are shown in Fig. 1, where the pack-

[16] A. J. Dempster and A. E. Shaw, Phys. Rev. 77, 746 (1950).

TABLE II. Packing fraction of Ni^{58}.

	Doublet	Packing Fraction
Present work	$Si^{29}-Ni^{58}$	-8.09 ± 0.05
Aston*		$-8.5\ \pm0.35$
T. Okuda *et al.***	$C_4^{12}H_{10}-Ni^{58}$	-6.97 ± 0.07
A. E. Shaw†	$C_2^{12}H_5-Ni^{58}$	-8.29 ± 0.07

* F. W. Aston, *Mass Spectra and Isotopes* (Edward Arnold and Company, London, England, 1942), p. 151.
** See reference 21.
† See reference 12.

TABLE III. Packing fraction of Ni^{60}.

	Doublet	Packing Fraction
Present work	$Si^{30}-Ni^{60}$	-8.54 ± 0.02
T. Okuda *et al.**	$C_5^{12}-Ni^{60}$	-8.37 ± 0.06
A. E. Shaw†	$C_5^{12}-Ni^{60}$	-8.69 ± 0.08

* See reference 21.
† See reference 12.

ing fraction difference between Pt^{195} and Cu^{65} is plotted against the pressure in the analyzing region of the mass spectrograph. A typical exposure is shown in spectrum 1 of Fig. 2. The mass scale needed for the computation of the packing fraction differences was provided by the $Pt^{194}-Pt^{195}$ spacing, assumed to be integral.

It will be seen from Fig. 1 that the dependence of the doublet spacing on the gas pressure is small in this pressure range. The doublets used in the other comparisons described in this paper have been photographed at pressures less than 5×10^{-6} and it has been assumed, on the basis of the results with $Cu^{65}-Pt^{195}$, that the pressure effects are negligible. The pressure readings have been made with a Distillation Products VG–1A ionization gauge calibrated for air. Since much of the residual gas comes from the silicone used in the diffusion pumps and from vacuum wax, there is some uncertainty as to the absolute pressure values.

In addition to the fourteen exposures represented in Fig. 1, nineteen additional photographs of the $Cu^{65}-Pt^{195}$ doublets have been taken without noting the corresponding pressures. It is known, however, that the pressures were less than 6×10^{-6} mm. The mean packing fraction difference for these latter nineteen exposures[17] is 9.20 ± 0.02, compared with a mean of 9.26 ± 0.02 for the former eleven. The average of the 33 exposures is 9.23 ± 0.015. The extreme values for the entire group are 9.03 and 9.42. This doublet had been studied with the Wesleyan mass spectrograph a few months ago. At that time measurements on six exposures[18] inferior to the present ones gave $\Delta f=9.26\pm0.06$. Dempster[14] obtained for this doublet $\Delta f=8.93\pm0.1$.

The errors included in the present measurements are probable errors in all cases, based on the internal consistency of the data. No attempt has been made to allow for possible systematic error or to allow a comfortable margin of safety.

5. SILICON-IRON COMPARISON

With a spark between a silicon electrode and an electrode of stainless steel containing 10 percent nickel, close doublets were photographed at mass 28, formed by singly charged Si^{28} and doubly charged Fe^{56}. Exposure times ranged from 30 to 40 seconds. A typical photograph, shown in spectrum 2 of Fig. 2 is seen to be poorly matched in intensity. However, measurements of five such exposures were quite consistent and yielded an average packing fraction difference of 3.32 ± 0.02. The $Si^{28}-Si^{29}$ separation, assumed to be integral, served as the mass scale. Mattauch and Flammersfeld[19] have recently given the packing fraction of Si^{28} as -5.20 ± 0.04, based on both mass spectrographic and disintegration evidence. This value combined with the present packing fraction difference, gives the packing fraction of Fe^{56} as -8.52 ± 0.05. In Table I this value is compared to previously measured values.

6. SILICON-NICKEL COMPARISON

Using the same electrodes as in the Si—Fe comparison, $Si^{29}-Ni^{58}$ and $Si^{30}-Ni^{60}$ doublets were photographed at masses 29 and 30, with exposure times ranging from 3 to 5 minutes. A typical photograph of these close doublets is shown in spectrum 3 of Fig. 2. From five photographs of the $Si^{29}-Ni^{58}$ doublet, the packing fraction difference is $\Delta f=3.07\pm0.02$, while from eight photographs of the $Si^{30}-Ni^{60}$ doublet $\Delta f=2.90\pm0.01$. The $Si^{28}-Si^{29}$ and $Si^{29}-Si^{30}$ separations provided suitable mass scales. Mattauch and Flammersfeld list the packing fractions of Si^{29} and Si^{30} as -5.02 ± 0.04 and -5.64 ± 0.02, respectively. The present results, combined with these, give values of -8.09 ± 0.05 for Ni^{58} and -8.54 ± 0.02 for Ni^{60}. A comparison between the present values for Ni^{58} and Ni^{60} and those obtained elsewhere is given in Tables II and III.

7. NICKEL-TUNGSTEN COMPARISON

When a tungsten electrode was used with the stainless steel electrode mentioned above, $W^{183}-Ni^{61}$ and $W^{186}-Ni^{62}$ doublets were formed at mass numbers 61 and 62. The doublets shown in spectrum 4 of Fig. 2, were photographed with an exposure time of 15 minutes. The $W^{182}-W^{183}$ and $W^{184}-W^{186}$ separations were used as mass scales. From three such $W^{183}-Ni^{61}$ exposures, $\Delta f=8.49\pm0.02$, while from four $W^{186}-Ni^{62}$ exposures, $\Delta f=9.03\pm0.02$.

These doublets were first photographed consecutively, using the scheme described above. Although only those

[17] Throughout the paper the factor $\times10^{-4}$ will be understood and not written in expressing the numerical value of the packing fraction.
[18] H. E. Duckworth, Phys. Rev. 76, 690 (1949).
[19] J. Mattauch and A. Flammersfeld, "Isotopic Report—1948," Verlag d. Zeits. f. Natur., Tübingen, Germany, 1949. Professor K. T. Bainbridge has kindly communicated the Mattauch and Flammersfeld values to the authors.

photographs whose constituent lines appeared to be sharp were selected for measurement, the values of Δf obtained therefrom scattered widely. For example, the four best $W^{183}-Ni^{61}$ exposures gave Δf values ranging from 8.41 to 9.03, compared to a spread of 8.46 to 8.53 for the three best simultaneous exposures. However, although the nickel and tungsten lines were not photographed simultaneously in these earlier plates, the Ni^{61} and Ni^{62} lines *were*, as were those for W^{183} and W^{186}. Thus, it was possible to compute the *difference* between the Δf's for the two doublets. This difference was found on the four best exposures to be 0.52 ± 0.07, in splendid agreement with the value of 0.54 ± 0.03 (9.03 −8.49) obtained from the simultaneous photographs.

8. ZINC-PLATINUM COMPARISON

It was hoped to photograph both the $Zn^{64}-Pt^{192}$ and $Zn^{66}-Pt^{198}$ doublets. Some of the difficulties encountered have been described above, and the exposure time for consecutive photographing of the $Zn^{66}-Pt^{198}$ doublet has been given. Use of the brass as a source of zinc resulted in the appearance of the $Cu^{65}-Pt^{195}$ doublet, the copper lines being photographed simultaneously with the zinc. Thus, although no absolute measurements could be made from these plates, it was possible, as in the case of the Ni−W comparison, to obtain the difference in Δf's between the $Zn^{66}-Pt^{198}$ and $Cu^{65}-Pt^{195}$ doublets. This difference is found on 25 photographs to be 0.20 ± 0.03, and when combined with the present results for the Cu−Pt doublet gives for $Pt^{198}-Zn^{66}$ the value $\Delta f=9.43\pm0.04$. In the course of other work zinc-contaminated platinum electrodes were used, and two fair simultaneous photographs of the $Zn^{66}-Pt^{198}$ doublet were taken. The packing fraction differences measured from these are 9.58 and 9.64.

To photograph the $Zn^{64}-Pt^{192}$ doublet a brass and a platinum electrode were used for the first 20 seconds, two platinum electrodes were used for the following hour, and brass and platinum electrodes used for an additional 20 seconds. A typical exposure is shown in spectrum 5 of Fig. 2. On five exposures the difference between the $Pt^{192}-Zn^{64}$ and $Pt^{195}-Cu^{65}$ packing fraction differences is found to be 0.01 ± 0.02. This leads to a value for the $Pt^{192}-Zn^{64}$ separation of $\Delta f=9.24\pm0.03$. The five consecutive exposures yield values between 9.20 and 9.53, with a mean of 9.40 ± 0.04.

For these Zn−Pt comparisons the $Pt^{192}-Pt^{194}$ and $Pt^{196}-Pt^{198}$ spacings served as mass scales.

9. MASSES OF THE ISOBARS Zn^{64} AND Ni^{64}

Professor Dempster[20] has recently measured the mass of Zn^{64}, obtaining a packing fraction of −7.68, using the $O^{16}-Zn^{64}$ doublet. K. Ogata,[9] using the $C_5{}^{12}H_4{}^{1}-Zn^{64}$ doublet has obtained a value of -7.24 ± 0.10. Shaw,[12] in measuring the mass of the isobar, Ni^{64}, using the $C_4{}^{12}C^{13}H_3-Ni^{64}$ doublet, has found $f=-8.62\pm0.08$, while T. Okuda *et al.*,[21] using the $C_5{}^{12}H_4-Ni^{64}$ doublet, have obtained -8.22 ± 0.09. These results suggest that the packing fraction of Ni^{64} is about one unit smaller than Zn^{64}.

Three poor $O^{16}-Zn^{64}$ doublets have been photographed in this laboratory and give packing fractions for Zn^{64} of −8.00, −7.85 and −7.98. These doublets are poor in the respect that the Zn lines were faint; $Zn^{64}-Zn^{66}$ served as the mass scale. It is planned to improve these doublets, but it is interesting to note that these preliminary attempts suggest a lower packing fraction than either Dempster or Ogata found. Some other local work bears on the mass difference between these isobars. The $Ni^{64}-Pt^{192}$ doublet was photographed consecutively before the limitations of that method were fully realized. The measurements are thought to be reliable enough to indicate that Δf for the $Ni^{64}-Pt^{192}$ doublet is not much different than for the $Zn^{64}-Pt^{192}$ doublet. They are probably within 0.25 of one another.

It is pertinent to note, as Flügge and Mattauch[22] have pointed out, that there are disintegration data available which may be used to check the $Zn^{64}-Ni^{64}$ mass difference. Cu^{64} emits electrons to from Zn^{64} and, at the same time, emits positrons to form Ni^{64}. Since both these activities have the same half-life, they are assumed to start from the same state of Cu^{64}. Assuming the negatron and positron energies to be 0.571 Mev and 0.657 Mev respectively, as given by Cook and Langer,[23] one can compute the packing fraction of Ni^{64} to be 0.19 smaller than that of Zn^{64}. It is hoped that it may soon be possible to reconcile mass spectrographic values with this accurately determined mass difference.

It is most desirable that further disintegration experiments be done in the Ni−Cu−Zn region with a view to determining accurate mass differences between adjacent or nearly adjacent isotopes and elements. Such fine structure data would be invaluable as a check on certain mass spectrographic conclusions, viz. the $Ni^{64}-Zn^{64}$ case, and would provide additional springboards for mass comparisons involving singly and multiply charged ions.

10. DISCUSSION OF RESULTS

It is gratifying to note that the present packing fractions for Ni^{58} and Ni^{60} of -8.09 ± 0.05 and -8.54 ± 0.02 are in substantial agreement with Shaw's recent values of -8.29 ± 0.07 and -8.69 ± 0.08. It is, perhaps, significant that they are not as low. This agreement, plus the present value of -8.52 ± 0.05 for Fe^{56}, supports the view that the minimum in the packing fraction curve has a value of approximately −8.5, or possibly lower. This lowering of the minimum results, through the Ni−W, Cu−Pt and Zn−Pt comparisons, in a lowering and steepening of the upper end of the curve in the W−Pt region. This steepening may be inter-

[20] A. J. Dempster, Phys. Rev. **74**, 1225 (1948).

[21] Okuda, Ogata, Kuroda, Sima, and Shindo, Phys. Rev. **59**, 104 (1941).

[22] S. Flügge and J. Mattauch, Physik. Zeits. **44**, 181 (1943).

[23] C. S. Cook and L. M. Langer, Phys. Rev. **73**, 601 (1948).

preted as supporting Feenberg's suggestion that the plateau which Dempster had drawn in the region 180–210 should be shifted to the region 108–124.

A detailed discussion of the effect on the packing fraction curve of the present measurements and others in progress will be given in a later paper.

The authors wish to express thanks to Mr. Clifford Gieselbreth for help in constructing electrodes and to Mrs. Mary Woodcock for preparing the figures for this paper. They also appreciate Professor Stearns' generosity in allowing them the use of the Astronomy Department's comparator.

PHYSICAL REVIEW VOLUME 78, NUMBER 4 MAY 15, 1950

Spectroscopic Isotope Shift and Nuclear Polarization*

G. BREIT, G. B. ARFKEN, AND W. W. CLENDENIN
Yale University, New Haven, Connecticut

(Received January 30, 1950)

Staggering of term values of odd isotopes with respect to those of the even ones is discussed. The validity of the static picture of nuclei as applied to their interaction with electrons is examined. It is found that the partial excitation of nuclei by atomic electrons results in polarization effects which lower the energy by amounts comparable to the observed irregularities and staggering. Correlations of observed shifts with the formation of stable shells are also discussed in a tentative way.

NOTATION

Ψ = wave function of nucleus and atomic electrons or electron.
N_i = nuclear functions; N_0 = nuclear ground state; N_1 = nuclear perturbing state.
$H=H^N+H^e+H'$ = Hamiltonian of the whole system.
E_i^N = energy of nuclear level.
E = total energy.
$E_i=E-E_i^N$.
$(\mathbf{r}, \mathbf{s})\cdots$ Cartesian and spin coordinates of electrons taken collectively.
φ_i defined by $\Psi=\Sigma_i N_i\varphi_i(\mathbf{r}, \mathbf{s})$.
$\psi=\varphi_0$, $\varphi=\varphi_1$, $H_{ij}'=(N_i, H'N_j)$.
Operators: $H_0=H^e+H_{00}'$, $H_1=H^e+H_{11}'$.
(f, g) = radial functions for ψ.
(f_φ, g_φ) = radial functions for φ.
$G=rg$, $G_\varphi=rg_\varphi$, $\chi=\begin{pmatrix}G\\G_\varphi\end{pmatrix}$.
$-U$ = potential energy of electron inside the nucleus (approximated by a constant).
$\hat{E}_0=E_0+U$, $\hat{E}_1=E_1+U$; a = nuclear radius.
$y=f/g$, y_φ/g_φ.
$V=H_{01}'$ (approximated by a constant).
θ defined by $-2V/[(E_0-E_1)^2+4V^2]^{\frac{1}{2}}=\sin\theta$.
k_1, k_2 = the two possible values of $2\pi\times$wave number for χ inside nucleus; values of k_1, k_2 are obtainable from Eq. (3.6).
$z_1=k_1a$.
$z_2=k_2a$.
ξ_1, ξ_2 are defined by Eq. (3.2).
$a'=amc/\hbar$, $\gamma=Ze^2/\hbar c$.
$\rho=(1-\gamma^2)^{\frac{1}{2}}$.
$\Delta(\delta y)\equiv y_{a+\delta a}(a+\delta a)-y_a(a+\delta a)$.
A = mass number.
$\delta_e E$ = change in the electron's energy $\delta_e E$ caused by $A\to A+\delta A$.
$s=\delta_e E/\delta U$.
$\mathfrak{M}$ defined by Eq. (6.5).
κ_0 defined by Eq. (6.7); κ_0 = value of k_1 for $V=0$.
κ defined by Eq. (7).
n = principal quantum number.
δ = quantum defect.
F = relativistic correction factor for electron density at nucleus.
$\mathfrak{R}$ = ratio of electron density at nucleus to that for a free electron.
p = momentum of electron in units mc.
$C(E)$ coefficient of lowest power of r in formula for linear density of s electron for unit linear density at $r=\infty$.
$S(r)$ = wave function of s nucleon in ground state.
z_N = charge of nuclear particle interacting with electron.

* Assisted by the joint program of the ONR and AEC.

I. INTRODUCTION

IT is usually supposed that the hyperfine structure of spectroscopic terms can be understood sufficiently well by considering only the static features of the nucleus. A marked exception has been pointed out by A. Bohr who found that the deuteron has to be considered in terms of its constituent parts rather than as a static system. Conditions in the deuteron are somewhat exceptional because the whole nuclear charge is carried by the proton, while in heavier nuclei the charge on any one of the nuclear protons is a small fraction of the whole. The centering of the electronic wave function on a proton is not likely to be as important in these cases. It appears, nevertheless, that the static picture is not necessarily a good one and may be inadequate in discussions of isotopic displacements of spectroscopic terms. In the usual theory[1] of these displacements the change in nuclear radius which is held responsible for the effect is only a small fraction ($\sim$1/600) of the whole radius. The change in potential energy between the electron and the nucleus is correspondingly small in comparison with the whole deviation from Coulomb energy which is expected from customary nuclear models. It would not be too surprising, therefore, if other effects than changes in the nuclear radius were found to be important. One such effect has been suggested by Brix and Kopfermann[2] in connection with

[1] G. Racah, Nature **129**, 723 (1932); J. E. Rosenthal and G. Breit, Phys. Rev. **41**, 459 (1932); G. Breit, Phys. Rev. **42**, 348 (1932).
[2] P. Brix and H. Kopfermann, Zeits. f. Physik **126**, 344 (1949).

anomalies in the isotopic displacements for Sm and Nd. Kopfermann's suggestion that these anomalies are caused by the deviation of the nuclear charge distribution from spherical symmetry is not literally tenable in the form stated by him because nuclei of spin O must have spherical symmetry. The essential idea is applicable, however, because the value zero for the total angular momentum can be secured by having the wave function in the form of a linear combination of space coordinate and spin functions none of which correspond to zero angular momentum. The charge distribution could be reasonably supposed to be determined by the space coordinate factors and the deviation from spherical symmetry which corresponds to these is independent of the magnetic quantum numbers. Thus, *e.g.*,

$$\psi = 3^{-\frac{1}{2}}(u_1 S_{-1} - u_0 S_0 + u_{-1} S_1)$$

with u_1, u_0, u_{-1} and S_1, S_0, S_{-1} standing for space coordinate and spin functions of angular momentum 1 with magnetic quantum numbers 1, 0, -1, respectively, is a wave function for a state of resultant angular momentum zero. The charge density is obtainable from

$$|u_1|^2 + |u_0|^2 + |u_{-1}|^2,$$

which is spherically symmetric. The charge density for a spinless state described by one of the u_m can have a quadrupole moment, however, and the mean electrostatic energy of the electron can be affected by a deviation from spherical symmetry of the charge distribution of the states u_1, u_0, u_{-1}. In order that this revision of Kopfermann's attempt to correlate anomalies in the isotopic shift with quadrupole moments be applicable to nuclei of zero total angular momentum, it is necessary to suppose that the coupling of the space coordinate functions to the sum of the spins does not affect the charge distribution. This is true for the wave function as it is written above. It will be remembered, however, that such a wave function is modified by spin-orbit and spin-orbit-spin (tensor) forces which are often supposed to be large in nuclei.[3] A dilemma seems to present itself at this point: One must either discard the view that large spin-orbit interactions are responsible for shell structure or else one must consider the connection between the isotope displacement and the occurrence of quadrupole moments as accidental for nuclei of zero spin. It is not clear, however, that the conditions of nuclear structure which are favorable for a large quadrupole moment are necessarily dissociated from irregularities in the average electrostatic energy of the electron which may exist quite apart from the direct geometrical effects on charge distribution associated with the existence of a quadrupole moment. Kopfermann's assumption of equal progressions in total volume of nuclei independently of their shape is an appealingly simple one. It cannot be considered, however, to be a necessary consequence of nuclear theory. Other possible sources of irregularities in the isotopic shift deserve consideration as well, therefore.

Another interpretation of Kopfermann's viewpoint brought out in a discussion by Dr. A. Bohr is that the nucleus has an intrinsic angular momentum and quadrupole moment with respect to an axis definable by internal coordinates and that the condition of zero spin arises from a factor in the wave function containing the polar coordinate angles of the spin axis. But also on this view Kopfermann's explanation implies an absence of dynamic interaction between the rotation of the spin axis and the internal coordinates, in addition to the constant volume assumption. While these hypotheses have plausibility their validity appears to require justification.

The isotopic shift of heavy elements shows a striking difference between even and odd isotopes of elements with even Z. The odd isotopes behave as though their volume were anomalously small in the language of the volume effect explanation. An increase in nuclear volume amounts to a decrease of the attraction between the electron and the nucleus and the staggered position of the term values of the odd isotopes suggests that there might be some specific source of attraction between an electron and the nucleus of an odd isotope. It will be recalled here that the direction of the effect is such as though for the odd isotopes the nuclear radius were somewhat smaller than would be expected from the observed term values of the even ones. On a naive view the smaller stability of odd isotopes suggests an abnormally large nuclear radius, in accordance with the virial theorem. It is perhaps conceivable that an odd neutron dangles more or less on the outside of the nucleus without affecting the proton charge distribution to a large degree. Such an explanation appears a forced one, however, because the question arises as to why a pair of neutrons should not behave similarly to a single one. It appears natural to investigate the order of magnitude of polarization effects of a nucleus by atomic electrons because such effects should lower the energy and because the observed density of nuclear levels for odd isotopes is usually larger for odd isotopes than for even ones.[4,5] It is found in the estimates presented that the polarization effects can conceivably be large enough to have an influence on the phenomenon and may possibly be one of the main contributing factors.

II. GENERAL EXPANSION

The wave function Ψ will be expanded in terms of products of a normal orthogonal complete set of nuclear functions N_i. The coefficients of the N_i are functions of

[3] M. G. Mayer, Phys. Rev. **74**, 235 (1948).

[4] A. C. G. Mitchell (private communication); also Kern, Mitchell, and Zaffarano, Phys. Rev. **76**, 94 (1949); Brolley, Sampson, and Mitchell, Phys. Rev. **76**, 624 (1949); Mitchell, Mei, Maienschein, and Peacock, Phys. Rev. **76**, 1450 (1949), and other papers.

[5] Pollard, Sailor, and Wylie, Phys. Rev. **75**, 725 (1949); Davison, Buchanan, and Pollard, Phys. Rev. **76**, 890 (1949); L. D. Wylie, Phys. Rev. **76**, 316 (1949); R. J. Creagan, Phys. Rev. **76**, 1769 (1949), and other papers.

the electronic coordinates. These functions are denoted here by φ_i. The expansion is

$$\Psi=\Sigma_i N_i\varphi_i(\mathbf{r}, \mathbf{s}), \tag{1}$$

where r, s denote the Cartesian and spin coordinates of the electrons. The Hamiltonian is represented as

$$H=H^N+H^e+H', \tag{1.1}$$

where superscipts N, e refer, respectively, to the nucleus and electron. The operator H^N contains no electronic coordinates and spins. Similarly H^e is free of nuclear quantities. The total energy of the system is denoted by E so that

$$(H-E)\Psi=0. \tag{1.2}$$

The functions N_i satisfy the orthogonality relations

$$(N_i, N_j)=\delta_{ij}. \tag{1.3}$$

The eigenvalues of H^N corresponding to the N_i will be designated by E_i^N so that

$$(H^N-E_i^N)N_i=0. \tag{1.4}$$

The E_i^N will be referred to as the energy values of nuclear levels i. As in all perturbation calculations the spectrum of the unperturbed problem is affected by the choice of the complete set of functions in terms of which the expansion is made. The energies E_i^N thus depend on the choice of the operator H^N. This arbitrariness may be supposed to be not very serious, however, in the present problem because the forces exerted on a nuclear particle by the electrons are not as effective as those originating in other nuclear particles. The operator H^N may include, for instance, some of the electrostatic potential produced by the electrons in the nucleus. It will be seen, however, that the calculation as carried out below will bring in such effects of its own accord so that the results are largely independent of additions to H^N and corresponding subtractions from H' or H^e.

Substitution of the form of Ψ given by Eq. (1) into the complete wave equation gives

$$(H^e-E_i)\varphi_i+\Sigma_j H_{ij}'\varphi_j=0, \tag{1.5}$$

where

$$E_i=E-E_i^N \tag{1.6}$$

is the energy left over for the electrons when the nucleus is in the state i. Here

$$H_{ij}'=(N_i, H'N_j)_N \tag{1.7}$$

with the understanding that

$$(\ )_N$$

designates a scalar product in the space of nuclear variables only, i.e., with the convention of treating the electron variables as fixed parameters. The H_{ij}' are functions of the electronic variables. They have the significance of matrix elements of H' for a dynamic consideration of the nuclear system and a static consideration of the electrons. Equation (1.5) gives in a sense the reaction of the nuclear system on the electronic one. If the non-diagonal H_{ij}' could be neglected one would have only the correction terms $-H_{ii}'$ to the E_i which correspond to a picture of the nucleus in which its effect on the electrons is describable by a static field. In fact for this approximation

$$(H^e+H_{ii}'-E_i)\varphi_i=0, \tag{1.8}$$

so that for each i there is an effective Hamiltonian H^e+H_{ii}' which determines E_i, φ_i. The energy of the system is in this approximation

$$E=E_i^N+E_i=(\varphi_i N_i, H\varphi_i N_i)/(\varphi_i N_i, \varphi_i N_i), \tag{1.9}$$

as is readily verified from the previous formulas. This energy is independent of the breakup of H into H^N, H', H^e except insofar as this breakup affects the wave function $\varphi_i N_i$. Since the right side of Eq. (1.9) is the expectation value of H, it is approximately independent of the choice of $\varphi_i N_i$ in accordance with the Ritz variational principle. The errors in the energy E involve the errors in the wave function only quadratically. The approximation of Eq. (1.8) gives in a sense a static picture of the action of the nucleus on the electrons, for it corresponds to the elimination of an explicit consideration of internal nuclear coordinates and a picture of an effective Hamiltonian H^e+H' containing electronic coordinates only. From a calculational viewpoint the present paper is concerned with estimates of some of the inaccuracies resulting from the application of Eq. (1.8).

The effect of the non-diagonal terms in Eq. (1.5) can be taken into account with sufficient accuracy by a perturbation calculation which is practically identical with the standard second-order calculation of the energy. This fact will be first established by an examination of a special case for which an explicit solution can be worked out.

III. TWO NUCLEAR LEVELS; ONE ELECTRON

In the present section the influence of only one excited nuclear level will be considered. The consideration of the electronic system will be simplified also by taking into account only one electron and bringing in, therefore, some contributions to the energy which have to be modified so as to be in agreement with the exclusion principle. The state N_0 will denote the nuclear ground state, N_1 the perturbing state. The corresponding functions φ_0, φ_1 will be now called ψ, φ. The coupled equations are

$$H_0\psi+H_{01}'\varphi=E_0\psi, \quad H_{10}'\psi+H_1\varphi=E_1\varphi, \tag{2}$$

where

$$H_0=H^e+H_{00}', \quad H_1=H^e+H_{11}'. \tag{2.1}$$

The functions ψ, φ are four-component functions for Dirac's electron. In order to simplify calculation it will be assumed that: (a) H_{01}' does not operate on the

electronic spin coordinates which is the case for electrostatic interactions, (b) inside the nucleus H_0 is of the form of Dirac's electron Hamiltonian with a constant potential energy, (c) it is sufficiently accurate to replace H_{01}' and H_{10}' by a real constant V through the nuclear interior and zero outside the nucleus. The calculation will be carried through as though $H_0=H_1$. The latter simplification does not restrict the range of applicability of the results because the difference between H_1 and H_0 is equivalent according to (b) to a difference between E_1 and E_0.

The radial wave functions for ψ will be designated by f, g in the customary manner [see Eqs. (12.3a)] and those for φ by f_φ, g_φ.

In terms of the abbreviations

$$G=rg, \quad G_\varphi=rg_\varphi, \quad \chi=\begin{pmatrix} G \\ G_\varphi \end{pmatrix} \tag{2.2}$$

there results the convenient equation

$$\frac{d^2\chi}{dr^2}+\frac{1}{c^2\hbar^2}\begin{pmatrix} \hat{E}_0^2-m^2c^4+V^2, & -(\hat{E}_0+\hat{E}_1)V \\ -(\hat{E}_0+\hat{E}_1)V, & \hat{E}_1^2-m^2c^4+V^2 \end{pmatrix}\chi=0, \tag{2.3}$$

where

$$\hat{E}_0=E_0+U, \quad \hat{E}_1=E_1+U. \tag{2.4}$$

Here U is the negative of the potential energy between the electron and the nucleus. The nuclear radius is denoted by a. As an approximation U is taken to be zero for $r>a$. For $r<a$ it will be approximated by

$$U\cong Ze^2/a. \tag{2.5}$$

By straightforward calculation it is found that the region $0<r<a$ gives the following connection between

$$y=f/g, \tag{2.6}$$

and

$$y_\varphi=f_\varphi/g_\varphi, \tag{2.7}$$

$$y=(\alpha+\beta y_\varphi)/(\gamma+\delta y_\varphi), \tag{3}$$

where

$$\begin{aligned} \alpha&=-(\hbar c/a)\eta_1\eta_2, \\ \beta&=\eta'(a_{11}'\mathbf{c}+a_{12}'\mathbf{s})+\eta''a_{11}', \\ \gamma&=\eta'(-a_{21}'\mathbf{s}+a_{22}'\mathbf{c})-\eta''a_{22}', \\ \delta&=(a/\hbar c)(a_{11}'a_{22}'-a_{12}'^2). \end{aligned} \tag{3.1}$$

Here

$$\eta_i=\xi_i-1, \quad \xi_i=k_ia\cot(k_ia), \quad (i=1,2) \tag{3.2}$$

$$\eta'=(\eta_1-\eta_2)/2, \quad \eta''=(\eta_1+\eta_2)/2, \tag{3.3}$$

$$a_{11}'=\hat{E}_1+mc^2, \quad a_{22}'=\hat{E}_0+mc^2, \quad a_{12}'=a_{21}'=V, \tag{3.4}$$

$$\begin{aligned} \mathbf{s}&=\sin\theta=-2V/[(E_0-E_1)^2+4V^2]^{\frac{1}{2}}, \\ \mathbf{c}&=\cos\theta=(E_0-E_1)/[(E_0-E_1)^2+4V^2]^{\frac{1}{2}}, \end{aligned} \tag{3.5}$$

$$k_1^2=c_{11}+c_{12}\tan(\theta/2), \quad k_2^2=c_{22}-c_{12}\tan(\theta/2); \tag{3.6}$$

with

$$\begin{aligned} c_{11}&=(\hat{E}_0^2-m^2c^4+V^2)/(c^2\hbar^2), \\ c_{22}&=(\hat{E}_1^2-m^2c^4+V^2)/(c^2\hbar^2), \\ c_{12}&=c_{21}=-V(\hat{E}_0+\hat{E}_1)/(c^2\hbar^2), \end{aligned} \tag{3.7}$$

where the c_{ij} are the elements of the matrix occurring in Eq. (2.3).

By means of the equations listed, one can obtain y at $r=a$ in terms of y_φ at the same point. On the other hand, the boundary condition at $r=\infty$ when applied to g, f and g_φ, f_φ determines y and y_φ at $r=a$ for an assumed E. With these values of y and y_φ, Eq. (3) determines the energy.[6] A complete solution along these lines is not necessary, however, because the variation of y_φ with E is important on a much coarser scale than that within which there is any question as to the value of E. The value of y_φ is essentially determined by the nuclear excitation energy $E_1^N-E_0^N$ and the change in y caused by V can be used to estimate the energy change by comparison with the corresponding change for the central field problem.

Expanding in V^2 and retaining only terms of first power in V^2 one has the approximation

$$\begin{aligned} y\cong(\hbar c/a)(\zeta_1/a_{22}')\{1+(\delta\xi_1/\zeta_1)+\zeta'\delta_1/(\zeta_1a_{11}') \\ +V^2/(a_{11}'a_{22}')+(\hbar c/a)[\zeta'\zeta_2\delta_1/(\zeta_1a_{11}') \\ -\zeta'\delta_2/a_{22}'+V^2\zeta_2/(a_{11}'a_{22}')]/D\}, \end{aligned} \tag{4}$$

where

$$D=a_{11}'y_\varphi-(\hbar c/b)\zeta_2, \tag{4.1}$$

and

$$\zeta_i=(\eta_i)_{V=0}, \quad \zeta'=(\eta')_{V=0}, \quad (i=1,2) \tag{4.2}$$

$$\delta_i=-2V^2(\hat{E}_{i-1}+mc^2)/(E_0-E_1)^2. \tag{4.3}$$

The quantities

$$\delta\xi_1=[\cot z_1-(z_1/\sin^2z_1)]z_1V^2\hat{E}_0/[(\hat{E}_0^2-m^2c^4)(\hat{E}_0-\hat{E}_1)], \tag{4.4}$$

$$\delta\xi_2=[\cot z_2-(z_2/\sin^2z_2)]z_2V^2\hat{E}_1/[(\hat{E}_1^2-m^2c^4)(\hat{E}_1-\hat{E}_0)], \tag{4.5}$$

are the first-order changes in ξ_1, ξ_2. Here the $z_i=k_ia$, with k_i taken for $V=0$. It was found that Eq. (4) is a sufficiently good approximation to Eq. (3) and that effects of higher powers of V^2 are, therefore, not serious.

Substitution of numbers gives

$$y\cong-0.205[1+0.00012V^2-0.0016V^2/(1+4.98y_\varphi)], \tag{4.6}$$

where V is expressed in mc^2 and the following values of parameters have been used

$$a=1.5\times(208)^{\frac{1}{3}}\times10^{-13}\text{ cm}, \quad U=82e^2/a=26.0mc^2, \quad E_0=mc^2, \quad E_1=mc^2/2.$$

These values of the parameters are intended to represent conditions for Pb^{208}.

The change in y caused by V may be compared with that produced by cutting off the Coulomb potential at $r=a$. The cut-off will be supposed to be made in such a way as to replace the Coulomb energy in $0<r<a$ by the constant value $-Ze^2/a$. One finds for the cut-off

[6] G. Breit and G. E. Brown, Phys. Rev. **76**, 1307 (1949).

field

$$[y(a)]_{\text{cut-off}}=-(\gamma/3)-\gamma^2(2+\gamma/a')a'/45+\cdots, \quad a'=amc/\hbar, \quad \gamma=Ze^2/\hbar c. \tag{5}$$

For the solution of the Dirac equation in a Coulomb field one has, on the other hand,

$$[y(a)]_{\text{Coulomb}}=-[\gamma/(1+\rho)]\times\{1+2\gamma a'/[(2\rho+1)(\rho+1)]+\cdots\}, \quad \rho=(1-\gamma^2)^{\frac{1}{2}}. \tag{5.1}$$

For the values of the parameters employed in Eq. (4.6) these formulas give -0.334 as the value of $y(a)$ for the straight cut-off field and -0.204 for the unmodified Coulomb case. The change caused by the cut-off is $0.334-0.204=0.130$.

It is not fair to use this change as a criterion of sensitivity of energy to changes in y because the experimental energy shift, on the nuclear volume change picture, is more closely related to changes in y produced by changing the nuclear radius. The value of y at the increased nuclear radius $a+\delta a$ undergoes the change

$$\Delta(\delta y)\equiv y_{a+\delta a}(a+\delta a)-y_a(a+\delta a)\cong[-(2\gamma a'/15)+1]\gamma(\delta a'/3a')\cong\gamma\delta a'/3a', \tag{5.2}$$

in accordance with Eqs. (5), (5.1). For $Z=82$ this formula gives

$$\Delta(\delta y)\cong 0.199\delta a/a. \tag{5.3}$$

If the nuclear volume is supposed to be proportional to the mass number A then $\delta a/a=\delta A/3A$ and for a change of A from 207 to 208 one obtains

$$\Delta(\delta y)\cong 0.00032. \tag{5.4}$$

If, instead, one employed the number 0.130, obtained by direct application of Eq. (5.1), one could estimate $\Delta(\delta y)$ as $0.130/624=0.00021$, which agrees approximately with Eq. (5.4) but underestimates the effect. The crudeness of the latter estimate is caused by the change in the shape of the electronic wave function inside the nucleus which is produced by the cut-off. For $E_1=0.5$ with a Coulomb field in $a<r<\infty$ the value of y_φ may be estimated approximately to be -2. Using this value and requiring that the effect of V^2 in Eq. (4.6) be equal to one-half of the amount in Eq. (5.4) one obtains for V the value $1.6\ mc^2$. The sign of the change in y produced by either sign of V is positive while the cut-off of the Coulomb potential increases y as in Eq. (3.4). The effect under discussion is seen to oppose the nuclear volume effect, in accordance with expectation.

If instead of $y_\varphi=-2$ one had used a value corresponding approximately to the vanishing of the denominator in Eq. (4.6) one would have obtained a much smaller value of V. Such a value of y_φ corresponds to a stationary state of the electron in the condition described by the wave function φ. Thus, for example, the straight cut-off gives according to Eq. (5.1) the value -0.204 which makes the denominator very small and this value would have to be reproduced by the branch of the wave function which is regular at $r=\infty$ if the level is a stationary one. Such a condition corresponds to a resonance of the nuclear excitation energy with a jump of the electron to a lower energy level. It would be incorrect to make use of it because nuclear levels have larger spacings than those between optical energy levels while the x-ray levels are occupied, so that transitions into them cannot take place. The unoccupied shells which are left in the building up of the periodic system do not have the azimuthal quantum number $L=0$ or 1. Transitions to the unoccupied levels may be assumed to be improbable, because the wave functions do not penetrate to the nucleus. The value $y_\varphi=-2$ is very different from those corresponding to approximate resonance and the effect computed above is, therefore, not especially concerned with forbidden transitions to occupied electron states. In order to have greater certainty concerning this point calculations by the standard second-order perturbation formula have been carried out and the results are presented in Section IV. The application of the second-order perturbation method for approximate calculation is justifiable because the approximate Eq. (4) agrees with Eq. (3) reasonably up to $V=10\ mc^2$.

The estimates made in the present section do not take into account the fact that negative energy states of the electron are occupied. This is clear from the fact that there is in principle no difference between the occupied atomic electron shells and the occupied negative energy states. While of little value for direct quantitative application they are included in this paper because they indicate the approximate validity of the second-order perturbation theory and also because their approximate agreement with other estimates is an indication that the effect of pair theory is not too pronounced.

IV. SECOND-ORDER PERTURBATION ENERGY

The second-order energy will be first estimated in a model which neglects the Coulomb interaction outside the nucleus. The crude character of this procedure is partly offset by calculating the volume effect for the same model and expressing the answer in terms of the ratio of the two effects. The normalization factor of the initial electronic state cancels out as a result. The object of this calculation is more that of locating the energy region which contributes principally to the effect rather than of obtaining a precise number for the effective value of V.

The ratio of the second-order perturbation energy $E^{(2)}$ to the change in the electron's energy $\delta_c E$ caused by a fractional increase $\delta A/3A$ in nuclear radius can be expressed in the following form:

$$\frac{E^{(2)}}{\delta_c E}=-\frac{V^2}{\pi}\frac{3A}{\delta A}\frac{a}{Ze^2s}\int\frac{N^2|\mathfrak{M}(E)|^2}{E_1-E}dk, \tag{6}$$

where

$$s=\delta_c E/\delta U=\int_0^a (f_0^2+g_0^2)r^2dr, \tag{6.1}$$

with f_0, g_0 denoting the radial functions for the ground state. The normalization convention regarding integration over angles is such that

$$\int_0^\infty (f_0^2+g_0^2)r^2dr=1. \tag{6.2}$$

The remaining undefined symbols in Eq. (6) will now be explained. The change in energy $\delta_c E$ is supposed to be produced by a change δU in U through the distance a and the value

$$\delta U=(Ze^2/a)(\delta a/a) \tag{6.3}$$

is used with

$$\delta a/a=\delta A/3A. \tag{6.4}$$

These relations give the first-order change in energy for a straight horizontal cut-off of the Coulomb potential. At this point there is an apparent inconsistency in the model because the effect of the Coulomb potential is omitted for the wave functions. The inconsistency does not involve anything more than the approximation of substituting wave functions outside the nucleus for $Z=0$ for those with the true Z, affecting somewhat the relative weights of different parts of the continuum.

The matrix element $\mathfrak{M}$ for the continuum is defined by

$$VNN_0\mathfrak{M}=\int_0^a (ff_0+gg_0)Vr^2dr, \tag{6.5}$$

where the normalization constants N, N_0 are introduced by

$$\begin{gathered}(rg_0)=N_0\sin\kappa_0 r, \quad (r<a),\\ \langle r^2(f^2+g^2)\rangle_{Av}=1,\\ (rg)=N\sin\kappa r, \quad (r<a).\end{gathered} \tag{6.6}$$

The values of the quantities are obtainable from:

$$s=a/2-s_0c_0/2k_0+(\hbar^2c^2/a)[\kappa_0 a s_0c_0/2-s_0^2+(\kappa_0 a)^2/2]/(\hat{E}_0+mc^2)^2, \tag{6.7}$$

$$\kappa_0=[(E_0+U)^2-m^2c^4]^{\frac{1}{2}}/\hbar c, \quad s_0=\sin(\kappa_0 a), \quad c_0=\cos(\kappa_0 a),$$
$$1/N^2=[E/(E+mc^2)](1+C^2)\sin^2(\kappa a), \tag{7}$$

$$\kappa=[(E+U)^2-m^2c^4]^{\frac{1}{2}}/\hbar c, \tag{7.1}$$

$$C=\left[\frac{(\hat{E}-mc^2)(E+mc^2)}{(\hat{E}+mc^2)(E-mc^2)}\right]^{\frac{1}{2}}\left[\cot\kappa a-\frac{1}{\kappa a}\right]+\frac{1}{\kappa a}, \tag{7.2}$$

$$\hat{E}=E+U,$$

$$\mathfrak{M}(E)=\frac{\hbar^2c^2/a}{(\hat{E}+mc^2)(\hat{E}_0+mc^2)}\times\left[\frac{\hat{E}+mc^2}{E-E_0}(\kappa_0 a)sc_0+\frac{\hat{E}_0+mc^2}{E_0-E}(\kappa a)s_0c-ss_0\right], \tag{7.3}$$

$$s=\sin(\kappa a), \quad c=\cos(\kappa a). \tag{7.4}$$

Computation for $E_0=mc^2$, $E_1=mc^2/2$ and otherwise for the same values of the parameters as in Section III yields for V the approximate value 1.7 mc^2 if it is desired that the effect of V be $\frac{1}{2}$ of the absolute value of the volume effect. The contributions from $E>180\ mc^2$ have been neglected and the number is, therefore, an overestimate for V. Only the contributions to the integral arising from the continuum have been taken into account so that the exclusion principle does not affect this part of $E^{(2)}$. Most of the effect comes from high excitation energies of about 50 mc^2.

This fact would seem to indicate that the energy change is not sensitive to the position of perturbing nuclear levels of moderate excitation energy. Calculations described in Section V show, however, that the model used underestimates the importance of the smaller electron excitations.

V. EFFECT OF COULOMB FIELD

The effect of the Coulomb field at electron distances $r>a$ has not been considered so far. This produces an increase in the contribution to $E^{(2)}$ from the region of excited electron states close to ionization. The situation can be understood qualitatively in terms of discrete states just below ionization. For a screened nuclear field, with effective internal and external charges Z, Z_0 the non-relativistic electron density for s states at $r=0$ is

$$\psi^2(0)=ZZ_0^2/[\pi a_H^3(n-\delta)^3]$$

where a_H is the Bohr radius and δ the quantum defect, which is assumed to be independent of the principal quantum number n. The spacing between adjacent levels is

$$\Delta E=Z_0^2e^2/[a_H(n-\delta)^3].$$

The density at the nucleus per unit energy range of electron states is, therefore,

$$\psi^2(0)/\Delta E=(Z/a_H)(m/\pi\hbar^2). \tag{8}$$

On the other hand, in the absence of the Coulomb field, the corresponding quantity for states having momentum p is

$$pEdE/(2\pi^2c^2\hbar^3), \tag{8.1}$$

relativistically. Formula (8) underestimates the density, being non-relativistic. The appropriate correction factor taking account of relativistic effects will be called F. The ratio of the Coulombian density to that for a free electron will be called $\mathfrak{R}$ so that according to Eqs. (8), (8.1)

$$\mathfrak{R}=2\pi F(\hbar/p)(Z/a_H). \tag{8.2}$$

For small values of p this ratio increases. Allowing F to have the value 2 the value of $\mathfrak{R}$ following from the above estimate for $p=mc/2$, $Z=80$ is $\cong 20$. An omission of the effect of the large concentration of electron density per unit energy range is seen to underestimate the influence of the low excitation states of the electron

and to give an underestimate of the effect of low nuclear excitations in comparison with the high ones.

The effect of the Coulomb field is calculated here relativistically but with the omission of effects of deviations from the Coulomb law at small distances. Arguments can be produced to indicate that the latter effect is not serious up to $E=10$ or 20. The calculation as made applies to a model which precludes the possibility of an isotopic nuclear volume effect due to static causes but allows for nuclear polarization effects. The solution of Dirac's radial equations along standard lines due to Dirac,[7] Gordon,[8] and Darwin[9] and the application of standard relations of these solutions to Whittaker's confluent hypergeometric function gives for small values of r

$$(rf)^2+(rg)^2=C(E)r^{2\rho}, \tag{9}$$

where γ and ρ are given by Eqs. (5), (5.1), and

$$C(E)=(2p)^{2\rho}[1+(\rho/E)]\,|\,\Gamma(\rho+i\sigma)/\Gamma(2\rho+1)\,|^2e^{\pi\sigma} \tag{9.1}$$

with

$$\sigma=E\gamma/p, \tag{9.2}$$

$$p=(E^2-1)^{\frac{1}{2}}. \tag{9.3}$$

The normalization is such as to give unit average linear density for large r, i.e., such that $\langle(rf)^2+(rg)^2\rangle=1$. The unit of energy is here mc^2 and that of length is $\hbar/mc$. The momentum in units mc is designated by p. Higher powers of r are omitted in Eq. (9). The expression on the right of Eq. (9.1) has been obtained by an independent calculation along the lines mentioned. It can also be obtained from Eq. (40) in Fermi's classic paper[10] on β-ray theory, which makes use of Hulme's work[11] on Dirac's equation. In comparing Eq. (9) with Fermi's result, account must be taken of the following circumstances: (a) Fermi's problem includes the consideration of both spin directions while in the present work only one spin direction enters; for this reason a factor $\frac{1}{2}$ must be applied to Fermi's expression in the comparison; (b) in β-ray theory the emission of electrons in $p_{\frac{1}{2}}$ states has to be considered while in the present problem only $s_{\frac{1}{2}}$ states perturb the initial state. The effect of the latter circumstance is to bring in a factor $2E/(E+\rho)$ to be applied to $C(E)$. The origin of this factor is as follows. From the symmetry properties of Dirac's radial equations one finds that a change of f into g, g into $-f$, E into $-E$ and r into $-r$ changes the equations for $s_{\frac{1}{2}}$ into those for $p_{\frac{1}{2}}$. Since the argument of the hypergeometric functions is $2(1-E^2)^{\frac{1}{2}}r$, a change of the sign of r is equivalent to changing the sign of p and leaving r unchanged. The quantity σ is thus unchanged and the factor $1+\rho/E$ is replaced by $1-\rho/E$ for $p_{\frac{1}{2}}$ states. Summation over $s_{\frac{1}{2}}$ and $p_{\frac{1}{2}}$ states replaces, therefore, $1+\rho/E$ by 2 and this replacement is equivalent to multiplication by $2E/(E+\rho)$. Finally there is a factor 4π to be applied to the right of Eq. (9) because in the present calculation $\langle(rf)^2+(rg)^2\rangle=1$ while in Fermi's the corresponding average is 4π. Since it is possible to derive Eq. (9) in this way, further details concerning mathematical relations need not be gone into.

For the same convention concerning normalization one can compare Eq. (9) with the corresponding expression in the absence of the Coulomb field. The ratio of the two is

$$\mathfrak{R}=\frac{(E+\rho)(2p)^{2\rho}}{(E+1)(E^2-1)}\left|\frac{\Gamma(\rho+i\sigma)}{\Gamma(2\rho+1)}\right|^2e^{\pi\sigma}r^{2\rho-2} \tag{9.4}$$

for the case of small distances, keeping only the first non-vanishing power of r. The elements of special interest have values of Z approximately equal to 80 so that $\gamma=0.6$, $\rho=0.8$ may be used. For large E the complex Γ-function approaches $\Gamma\,(0.8+0.6i)$, for small p the σ becomes infinite. It is found by numerical trial that for the crude object in hand one obtains a satisfactory representation of $|\,\Gamma(\rho+i\sigma)\,|^2$ by means of Stirling's formula so that

$$C(E)\cong 2^{2\rho+1}\pi\gamma^{2\rho-1}(E+\rho)E^{2\rho-2}\times[\Gamma(2\rho+1)]^{-2}p/[1-\exp(-2\pi\sigma)] \tag{9.5}$$

and

$$\mathfrak{R}=[E/(E+1)]p^{-2}r^{2\rho-2}C(E). \tag{9.6}$$

Since p enters as p in Eq. (9.5) and as p^{-1} in $\mathfrak{R}$ the quantities $C(E)$ and $\mathfrak{R}$ vanish and become infinite, respectively, at low electron energies. The infinity of $\mathfrak{R}$ at $E=1$ enhances the importance of low electron excitations and is in agreement with the estimates at the beginning of Section V. Employing the schematic representation of the interaction of the electron with the nucleus by means of a constant V, and approximating the wave function for the normal state of the electron by the term in the first non-vanishing power of r, one has

$$f_0=-N_0[(1-\rho)/(1+\rho)]^{\frac{1}{2}}r^{\rho-1},\quad g_0=N_0r^{\rho-1}, \tag{9.7}$$

$$E^{(2)}=-(2/\pi)N_0{}^2V^2(1+\rho)^{-1}[a^{2\rho+1}/(2\rho+1)]^2\times\int C(E)\,|\,E_1-E\,|^{-1}dE, \tag{9.8}$$

where N_0 is a normalizing factor for the bound state which will be eliminated by comparison with the volume effect on the isotope shift. The latter will be approximated by the value of the first-order perturbation energy caused by cutting down the negative of the Coulomb energy from the value γ/r to the constant value γ/a within $0<r<a$ and changing the nuclear radius from a to $[1+(1/3A)]a$ for isotopes with mass numbers A, $A+1$. The distortion of the wave function by the nuclear potential well is neglected in the present

[7] P. A. M. Dirac, Proc. Roy. Soc. **A117**, 610 (1928).
[8] W. Gordon, Zeits. f. Physik **48**, 11 (1928).
[9] C. G. Darwin, Proc. Roy. Soc. **A118**, 654 (1928).
[10] E. Fermi, Zeits. f. Physik **88**, 161 (1934). Equation (9.1) may also be derived from the normalized wave functions of M. E. Rose, Phys. Rev. **51**, 484 (1937).
[11] H. R. Hulme, Proc. Roy. Soc. **A133**, 381 (1931).

qualitative considerations. The resultant change in E is called $\delta_c E$. One finds

$$\delta_c E=[2\gamma N_0^2/a(1+\rho)][a^{2\rho+1}/(2\rho+1)](\delta a/a) \quad (9.9)$$

and hence

$$E^{(2)}/\delta_c E\cong-(aV^2/\pi\gamma)(3A/\delta A)[a^{2\rho+1}/(2\rho+1)] \times\int C(E)|E_1-E|^{-1}dp. \quad (10)$$

For $\gamma=0.6$, $\rho=0.8$, $r\hbar/mc=1.5A^{\frac{1}{3}}\ 10^{-13}$ cm, $r=1/43.5$ substitution gives in round numbers

$$E^{(2)}/\delta_c E\cong-(V^2/6200)\int C(E)|E_1-E|^{-1}dp \quad (10.1)$$

and for small p

$$(V^2/6200)C(E)\cong(V^2/910)(E+0.8)E^{-0.4}p/[1-\exp(-3.8E/p)]. \quad (10.2)$$

The bracket with the exponential has a value close to unity. The approximations of Eq. (10.2) yield a simple estimate of contributions to the right side of Eq. (10) from the region $1<E<10$. The region from $E=1$ to $E=2$ contributes

$$\sim(V^2/910)\{2+(E_1+0.8)\ln[(2-E_1)/(1-E_1)]\},$$

and for E between 2 and 10 with $E_1\cong1$ the contribution is $\sim V^2/29$. If $E_1\cong0.9$ then the contribution from $E=1$ to $E=2$ is $\sim V^2/150$. For $E>10$ the parameter $2pr$ which is the argument of the hypergeometric function becomes too large to make the omission of all but the first term in the hypergeometric series a crude approximation. According to these numbers a single nuclear level with an excitation energy between 0 and $\sim$200 kev would cause, on account of contributions from $E=2$ to $E=10$ alone, a value of $|E^{(2)}/\delta_c E|=\frac{1}{2}$ if one takes $|V|=(28/2)^{\frac{1}{2}}=3.8$.

The values of $\mathfrak{R}$ which follow from Eqs. (9.4), (9.6) are about 25 for $E=2$, 10 for $E=10$. For higher E the expression for $\mathfrak{R}$ is only applicable to conditions at smaller distances than the nuclear radius $r=a$. It is nevertheless of interest that even for $E=50$ the formulas give $\mathfrak{R}\cong5$.

VI. MONOPOLE EFFECT

The interaction of the electron with the nucleus has been represented in Eq. (2) by H_{0i}' which has been replaced schematically by the constant value V through the nuclear interior. Estimates of V^2 have been obtained above by comparison with experiment. The values obtained will now be compared with expectation. In making the comparison the experimental indication of the largeness of effects for $s_{\frac{1}{2}}$ and $p_{\frac{1}{2}}$ will be used as a guide. The Coulomb interaction between an electron and a nuclear proton can be considered as being expanded into spherical harmonics in the usual manner,

$$e^2/|\mathbf{r}-\mathbf{r}_P|=(e^2/r_>)[1+(r_</r_>)P_1(\cos\Theta)+\cdots],$$

where

$$(r_<, r_>)=(r, r_P), \quad (r_P>r)$$
$$=(r_P, r), \quad (r>r_P).$$

The first term in this expansion will be referred to as the monopole term. It can give transitions between an $s_{\frac{1}{2}}$ atomic state of the electron and the continuum of $s_{\frac{1}{2}}$ states; it also gives transitions between $p_{\frac{1}{2}}$ and $p_{\frac{1}{2}}$ states. Both of these types of transitions are of immediate interest because the experimental evidence appears to be pointing to the proportionality of the isotope displacement and the density of the electron probability at the nucleus. The dipole term containing P_1 gives transitions between $s_{\frac{1}{2}}$ and $p_{\frac{1}{2}}$ electronic states and is of interest also. It turns out, however, that the effects of penetration of the electron into the nucleus are not marked for the matrix elements between $s_{\frac{1}{2}}$ and $p_{\frac{1}{2}}$ states on account of a cancellation of effects for the first non-vanishing power of r for the Coulomb field. These effects are not readily distinguishable from those for electron states which do not penetrate to the nucleus and they are very small for the part of the continuum corresponding to ionization. For a Coulomb field the matrix element vanishes with the nuclear radius at ionization. It appears safe to conclude that the $s_{\frac{1}{2}}$, $p_{\frac{1}{2}}$ matrix elements do not have much to do with observed phenomena and that the main effects of interest arise from the monopole term. The effect of the latter depends on whether the nuclear wave function is considered to be an antisymmetrized product of single particle central field functions or a linear combination of such products. Estimates will first be made for wave functions which are antisymmetrized products, i.e., products of two determinants; one for neutrons and one for protons. Since the interaction energy is a sum of operators each of which contains quantities referring to no more than one nucleon, it suffices to consider the excitation of only one proton at a time. The matrix element of the energy is then the same as though the electron were interacting only with that proton. The spherical symmetry of the monopole excludes all transitions involving changes either in the azimuthal or magnetic quantum numbers. Only angular averages of the cross-product proton density enter the result. The calculation is the same in form for the excitation of protons or α-particles since the charge e enters only through the combination $z_N e^2$, where $z_N=1$ for protons or 2 for α-particles.

Interactions of this type are strongly decreased by the orthogonality of wave functions with the same value of the azimuthal quantum number. This orthogonality confines the contributions to the matrix elements to electron positions inside the nucleus. An application of the completeness relation to the sum of squares of matrix elements yields an upper limit on the effective value of this sum. The upper limit appears then in a form containing only the wave function of the ground state. The main result of the transformation is

expressible as

$$\sum_n{}' \left| \int H_{0n}'(r) w(r) dr \right|^2 = \int \left(w - \int w du \right)^2 du, \quad (11)$$

where the accent on the summation sign indicates omission of $n=0$ and

$$du = S^2(r)dr, \quad w(r) = e^2 r^{2\rho} / [2\rho(2\rho+1)], \quad (11.1)$$

while $S(r)/r$ stands for the wave function of the nuclear particle in the ground state. For the lower energies in the continuum the spatial dependence of electronic density can be approximated by $r^{2\rho+2}$. One finds that

$$(V^2)_{\text{eff}} \leqq z_N^2 (e^2/a)^2 / [(4\rho+1)(2\rho+1)^2]. \quad (11.2)$$

The evaluation of the right side was made by approximating S by a constant within the nucleus. This approximation is immaterial in view of the smallness of the whole effect which can be inferred from the fact that the right side of Eq. (11.2) is approximately $z_N^2 (mc^2/17)^2$, for $\rho=0.8$ and $a=1.5\times10^{-13}\, A^{\frac{1}{3}}$ cm. The monopole effect for the antisymmetrized product approximation to the nuclear wave function is seen to be very small unless one allows z_N to have a value of about 17. Such a value is difficult to reconcile with the central field approximation which was the starting point of the present estimate.

Larger values for the expected monopole effect are obtained if one considers the possibility of linear combinations of antisymmetrized products of single particle central field functions. For example, let

$$\begin{aligned} \psi &= c_1(\text{I, II}) + c_2(\text{III, IV}), \\ \psi' &= c_1'(\text{I, II}) + c_2'(\text{III, IV}) \end{aligned} \quad (11.3)$$

stand, respectively, for the ground state and perturbing excited state. The symbol (I, II) represents an antisymmetrized product of two single particle wave functions. The notation is similar for (III, IV), the single particle functions I, II, III, IV are mutually orthogonal and are not necessarily central field functions. For a fixed position of the electron the matrix element of the electron-proton electrostatic energy consists of two parts containing, respectively, $c_1^* c_1'$ and $c_2^* c_2'$ as factors. The orthogonality of ψ to ψ' implies $c_1^* c_1' = -c_2^* c_2'$ and the result is expressible therefore in terms of one of these quantities. As an approximation each of the states I, II, III, IV is regarded as localized in a narrow range of values of r centered in the neighborhood of the four values $r_{\text{I}}, \cdots, r_{\text{IV}}$, respectively. This estimate yields

$$|V| = |c_1^* c_1'| (2\rho)^{-1} (e^2/a) \times [r_{\text{III}}^{2\rho} + r_{\text{IV}}^{2\rho} - r_{\text{I}}^{2\rho} - r_{\text{II}}^{2\rho}] / a^{2\rho} \cdots. \quad (11.4)$$

Here $|c_1^* c_1'|$ can be as large as $\frac{1}{2}$ and favorable conditions for a larger $|V|$ than in the previous estimate are obtained by making r_{III}, r_{IV} large in comparison with r_{I}, r_{II}. For such conditions and for $\rho=0.8$ the value of $|V|$ is approximately

$$|V| \cong 0.62 (e^2/a)(r_P/a)^{2\rho}. \quad (11.5)$$

Here r_P stands for a suitably taken mean of r_{III} and r_{IV}. The value of $|V|$ obtainable in this manner is sensitive to the choice of r_P and a. It appears appropriate, therefore, to consider first the range of possible values for these parameters. The value of $a=1.5\times10^{-13}\, A^{\frac{1}{3}}$ cm represents the effective nuclear radius for the charge as a whole. The value of the numerical constant 1.5 can be varied by interpreting the theory of α-decay in different ways. This uncertainty is not very important for the present purpose since the right side of Eq. (11.5) is mainly sensitive to the ratio r_P/a. The value of a will be therefore taken as given sufficiently well by the value 1.5 for the constant in the formula for a. In order to have a large value for the right side of Eq. (11.5) one needs a large r_P/a. The question arises as to how large r_P can be in comparison with a. It would appear that one could modify the Coulomb barrier of the Gamow, Condon-Gurney theory at the nuclear boundary without serious consequences on the comparison with experiment. A few protons could be pictured as being somewhat outside the sphere $r=a$, therefore. It appears fair to add to a about 2.8×10^{-13} cm, since the range of nuclear forces is of this order of magnitude. On this basis one has for $A=208$ the value $V \cong mc^2/3.3$ which is still too small. If instead of protons one considers α-particles then one obtains an additional factor 2 for V so that $V \cong mc^2/1.6$. Four such perturbing levels are equivalent to a single one with $V \cong mc^2/0.8$, which is sufficient to explain the odd-even isotope staggering effect on the basis of differences in nuclear level systems in a wide energy range ($30\, mc^2$) but not sufficient for an explanation by differences in level systems between 0 and 5 Mev. For the latter one needs an additional factor of roughly 4. To obtain it one could invoke interactions with larger units than an α-particle or else wave functions of the type

$$\begin{aligned} \psi &= c_1(\text{I}_1, \text{II}_1, \text{III}_1, \text{IV}_1) + c_2(\text{I}_2, \text{II}_2, \text{III}_2, \text{IV}_2), \\ \psi' &= c_1'(\text{I}_1, \text{II}_1, \text{III}_1, \text{IV}_1) + c_2'(\text{I}_2, \text{II}_2, \text{III}_2, \text{IV}_2). \end{aligned} \quad (11.6)$$

It is difficult to exclude such possibilities but there appears to be no binding reason for assuming them. The fact that the packing fraction has a minimum for $A\sim50$ —which is smaller than any of the mass numbers for which the isotope effect has been observed—could be used as an argument for considering the temporary existence in the nucleus of groups of particles much greater than an α-particle. The large mass of such groups would interfere with the explanation if it depended on the conditions treated by means of Eqs. (11), (11.2) because in this case the effect is caused only by radial fluctuations of charge. The large mass does not interfere, however, under circumstances discussed by means of wave functions such as in Eq. (11.3) with the understanding that I, II, III, IV now apply to the

larger aggregates. While large factors could arise in such a picture it is not proposed here as more than a speculation. It is nevertheless difficult to exclude the presence of an effect depending on low nuclear excitations.

If the monopole effect were estimated only for initial states describable in the central field approximation, i.e., by determinantal wave functions, an upper bound on the expected shift could be set by means of the following consideration. The initial single particle states can be arranged into two classes according to spin direction. The operation of the exclusion principle can be considered separately for the two classes. For each class there is only one particle in an orbital state. There are no matrix elements of the monopole energy between states with different orbital angular momenta L or different magnetic quantum numbers. The exclusion principle does not interfere, therefore, with the contributions from proton states within an occupied shell. If the shells of nuclear particles are supposed temporarily to correspond to different values of L the summation of the squares of matrix elements can be arranged in independent parts, each part corresponding to one of the initial single particle states. A part of the sum belonging to one of the states does not depend on what other states are occupied initially. The whole sum is, therefore, less than the number of protons times contributions such as considered in Eq. (11). If there are several shells for the same L, the sum is decreased because in Eq. (11) all non-diagonal matrix elements are taken into account while the squares of these elements which correspond to the initial and final states being occupied do not occur in the sum for the antisymmetric five function. One may take, therefore, for $Z=80$, the value $80^{\frac{1}{2}}mc^2/17=mc^2/1.9$ as an upper bound for $|V|$ of the monopole effect if the wave function of the initial state is approximated sufficiently well by a determinant having as elements single particle central field functions. It will be noted that this value of $|V|$ is smaller than that indicated by the staggering of the isotopic shift even if one admits the possibility that excitation to higher nuclear energies ($\sim$20 Mev) might be qualitatively different for even and odd isotopes. It will be seen later that the dipole effect cannot account for an appreciable part of the staggering effect. It appears, therefore, that one could perhaps claim the inadequacy of a central field nuclear model if the staggering effect should not be explicable in some other way than as a polarization effect. In the present state of the subject it cannot be claimed that some other explanation will not prove adequate and the mutual exclusiveness of the two possibilities is mentioned only as a matter of record.

The situation just discussed is not changed materially by taking the square of the wave function S^2 in Eq. (11.4) to have the form $(n+1)r^n a^{-n-1}$ and adjusting n to give a maximum of the effect. This generalization introduces an extra factor

$$(n+1)(2\rho+1)^2(4\rho+1)/[(2\rho+n+1)^2(4\rho+n+1)]$$

on the right side of Eq. (11.2). A straightforward calculation for $Z=80$ gives $n=(-1+5^{\frac{1}{2}})\rho-1=0.005$ which is so close to $n=0$ that the difference caused in the expected effect is negligible. The value of V^2 is readily found to be insensitive to n in the range from -0.5 to 1.0, the effects on the upper bound for V^2 being of the order of 10 percent. While the function S has favorable properties for giving a large effect it is not much more favorable than other possibilities which provide for a large range of variations of charge density within the nucleus.

Since it is unlikely that the conditions for approaching the upper bound are realized in nuclei, the monopole effect may be supposed to give rise to appreciable polarization effects only if the central field picture of the nucleus is inadequate. While it is probable that this is true in some sense it is not clear from the previous discussion that the types of modification made use of in Eqs. (11.3), (11.4) are probable. The main reason for an increase in the expected effect by these modifications is the occurrence of matrix elements which are diagonal in single particle states. Furthermore the wave functions in Eq. (11.3) would not give a large effect if it were not for the assumption that two of the single particle states correspond to locations close to the periphery of the nucleus and two other states to locations in the interior. These assumptions are in a sense artificial and have been made above in order to see under what conditions the polarization effect can become comparable with the experimentally observed irregularities in the isotope shift.

VII. DIPOLE EFFECT

In this section the effects of dipole matrix elements are considered and the contributions to the second-order perturbation energy from different parts of the continuum are estimated. The dipole effect arises from the second term in the expansion of $|\mathbf{r}-\mathbf{r}_P|^{-1}$ in terms of Legendre functions.

The needed expressions may be obtained in the following way. The four-component wave functions for the s and $p_{\frac{1}{2}}$ states with magnetic quantum number m can be conveniently represented as

$$\psi_s{}^m=(4\pi)^{-\frac{1}{2}}\begin{pmatrix} f_s[(\mathbf{r}\sigma)/r]S^m \\ -ig_sS^m \end{pmatrix},$$
$$\psi_p{}^m=(4\pi)^{-\frac{1}{2}}\begin{pmatrix} f_pS^m \\ -i[(\mathbf{r}\sigma)/r]g_pS^m \end{pmatrix}, \tag{12}$$

where S^m is a two component spin function with magnetic quantum number m. This spin function is a one-column matrix with two rows and is treated like the spin functions of a single electron in non-relativistic theory which are usually denoted by α and β.

Since one is interested only in averages over all relative orientations of the angular momentum L of a nuclear particle and the angular momentum vector $\mathbf{j}$ of the electron the detailed consideration of individual matrix elements can be avoided. One finds readily by means of Eq. (12) for the $p_{\frac{1}{2}}$ electron that

$$\Sigma_{\mu'}|(s,\mu|x_i/r^3|p,\mu')|^2=(I_{sp}/3)^2, \tag{12.1}$$

where

$$I_{sp}=\int_0^\infty (f_sf_p+g_sg_p)dr=(r^{-2})_{sp}. \tag{12.1a}$$

The x_i denotes either x, y, or z and r is the usual electron-nucleus distance. The magnetic quantum number in the s state is designated by μ, that in the $p_{\frac{1}{2}}$ state by μ' and the sum over all μ' is taken. It will suffice to know the sums occurring in Eq. (12.1) rather than individual matrix elements.

The interaction energy of a nuclear proton with the electron contains the dipole interaction term

$$(e^2r_</r_>^2)\cos\Theta =(e^2r_</r_>^2)[xx_P+yy_P+zz_P]/(rr_P), \tag{12.2}$$

where $r_<$, $r_>$ stand, respectively, for the smaller and greater of the two distances r, r_P. Arguments similar to those used in demonstrations of spectroscopic stability show that the average over the magnetic quantum number M of the nuclear proton of the expression

$$\Sigma_Q|(L,M;s,\mu|(r_</r_>^2)\cos\Theta|L',M';p,\mu')|^2,$$

where Q stands for L', M', μ' can be expressed as the average over M of

$$\Sigma_R|(s,\mu|x/r^3|p,\mu')|^2|(L,M|x_P|L',M')|^2, \tag{12.2a}$$

where R stands for L', M', μ', x, y, z. Using familiar forms for dipole matrix elements[12] the second part of expression (12.2a) for $L'=L+1$ gives rise to

$$\Sigma_S|(L,M|x_P|L+1,M')|^2 =(L+1)(2L+1)^{-1}|(r_P)_{L,L+1}|^2, \tag{12.2b}$$

where S stands for M', x, y, z and $(r_P)_{L,L+1}$ is the matrix element of the proton distance r_P taken between two states having the same magnetic quantum number but different azimuthal quantum numbers L, $L+1$. Substituting Eqs. (12.1) and (12.2b) into Eq. (12.2a) gives

$$(I_{sp}/3)^2\{(L+1)|(r_P)_{L,L+1}|^2 +L|(r_P)_{L,L-1}|^2\}/(2L+1). \tag{12.2c}$$

The integral over r inside the nucleus is negligible and has been omitted. Employing the completeness relation and assuming the nuclear particle to be at $r_P=a$, the surface of the nucleus, expression (12.2c) becomes

$$(\alpha mc^2aI_{sp}/3)^2. \tag{12.3}$$

[12] B. L. van der Waerden, *Die Gruppentheoretische Methode in der Quantenmechanik* (Verlag Julius Springer, Berlin, 1932), p. 78.

The α enters in converting lengths in Eq. (12.2) to $\hbar/mc$. The quantities f_s, g_s and f_p, g_p are the solutions for $k=-1$, $+1$, respectively, of the radial Dirac equations. The choice of signs is such as to make

$$rf=\varphi_1, \quad rg=\varphi_2, \tag{12.3a}$$

where φ_1, φ_2 are Gordon's[8] radial functions.

As in the monopole case, the square root of this will be equated to a constant nuclear perturbing potential, V, integrated over the nucleus. Solving for V one obtains

$$V=\alpha mc^2aI_{sp}\Big/\left[3\int_0^a (f_sf_s'+g_sg_s')r^2dr\right]\cdots. \tag{12.4}$$

In Eq. (12.4) and the following, the prime is used to indicate functions in the continuum when it is desired to distinguish them from the functions for the bound state. To get the expression for V corresponding to the perturbation of a $p_{\frac{1}{2}}$ electron by the continuum of $s_{\frac{1}{2}}$ states, one need only interchange the subscripts s and p in Eq. (12.4).

The approximation used in the monopole case does not apply in this case because

$$f_s/g_s=-f_p/g_p=-[(1-\rho)/(1+\rho)]^{\frac{1}{2}}, \quad (r=0). \tag{12.5}$$

Hence the coefficient of the first power of r in the integrand $f_sf_p+g_sg_p$ is zero and a more exact treatment is required. For convenience the bound electron is assumed to be described by the wave functions for an electron at ionization. This is justified by the strong localization of the integral at small values of r. The shape of the wave function is insensitive to the energy in this region on account of the dominance of potential energy. The functions are taken to be [13,14] the usual Bessel function expressions at ionization. The normalization factor is taken so that

$$rf=(\pi/2)^{\frac{1}{2}}\gamma J_{2\rho}(2(2\gamma r)^{\frac{1}{2}}). \tag{12.6}$$

To facilitate computation, ρ in this section is taken as 0.75 instead of 0.8. From the form of Eq. (12.4) it is seen that the normalization of the s function is immaterial, the comparison being made with the perturbation by the continuum of s states. The solution of the radial equations obtained by Gordon[8] can be written in the following form for the continuum

$$N_s(f_s+i\xi g_s)=N_p[(\rho-i\sigma)/(1-i\gamma/p)](f_p+i\xi g_p) =r^{\rho-1}e^{-ipr}F(\rho+i\sigma+1,2\rho+1,2ipr), \tag{12.7}$$

$$N_p(f_p-i\xi g_p)=-N_s[(\rho+i\sigma)/(1-i\gamma/p)](f_s-i\xi g_s) =r^{\rho-1}e^{-ipr}F(\rho+i\sigma,2\rho+1,2ipr). \tag{12.8}$$

The quantity ξ indicates $[(E-1)/(E+1)]^{\frac{1}{2}}$. In these formulas the normalization factors for s and p states are not as yet related to each other. Adjusting normalization to give unit linear density at large r, the connections between (f_s, g_s) and (f_p, g_p) available in

[13] G. Breit, Phys. Rev. 38, 463 (1931).
[14] G. Breit and L. A. Wills, Phys. Rev. 44, 470 (1933).

Eqs. (12.7) and (12.8) give

$$f_s=(E^2-\rho^2)^{-\frac{1}{2}}[\gamma f_p+(E-1)g_p], \qquad g_s=(E^2-\rho^2)^{-\frac{1}{2}}[\gamma g_p-(E+1)f_p], \tag{12.9}$$

with the help of

$$(f_s^2+g_p^2)/(f_s^2+g_s^2)=(E-\rho)/(E+\rho), \quad (r=0). \tag{12.9a}$$

It will now be shown that

$$I_{sp}=0, \quad (E_s=E_p). \tag{13}$$

Here it is understood that the Coulomb law holds strictly. One can satisfy $E_s=E_p$ exactly either in the discrete or in the continuum. One has the matrix equation of motion which relates matrix elements of the force and momentum by

$$-(Ze^2\mathbf{r}/r^3)_{nm}=(i/\hbar)(E_n-E_m)\mathbf{p}_{nm}, \tag{13.1}$$

where n, m designate energy states in general. Applying this identity to s and $p_{\frac{1}{2}}$ states one sees that the left side of the preceding equation contains as a factor the quantity I_{sp} while on the right there occurs the product of a vanishing energy difference and a finite matrix element of the momentum. It is also possible to demonstrate Eq. (13) by means of Eqs. (12.9) and an identity[15] due to G. E. Brown. However, as will be seen later, consideration of the derivatives of the wave functions with respect to energy indicates that $\partial V/\partial|E_s-E_p|$ is large and possibly infinite at $|E_s-E_p|=0$. It has been verified that I_{sp} increases very rapidly with $|E_s-E_p|$.

Using the first terms in the power series expansions of f and g from Eq. (12.6) and fixing on the normalizing factor for the continuum by means of Eqs. (9) and (9.7), there results from Eq. (12.4)

$$V=0.801z_N I_{sp}/[C(E_p)]^{\frac{1}{2}} \tag{13.2}$$

for an $s_{\frac{1}{2}}$ electron perturbed by the $p_{\frac{1}{2}}$ continuum while for a $p_{\frac{1}{2}}$ electron perturbed by the $s_{\frac{1}{2}}$ continuum,

$$V=2.12z_N I_{ps}/[C(E_s)(E_s-\rho)/(E_s+\rho)]^{\frac{1}{2}}. \tag{13.3}$$

The quantity z_N is the charge on the nuclear particle. Assuming interaction with nuclear alpha-particles as will be done here one has a z_N of 2. Since $C(E)$ is readily calculated one needs only evaluate I_{sp} to find V.

The Bessel function expressions for f and g defined by Eq. (12.6) were used for the wave functions describing the bound electron. Using up to 10 terms in the hypergeometric series occurring in Eqs. (12.7) and (12.8), f_p and g_p for the continuum were calculated to beyond the first maximum of rg_p. Employing a suitable reduction[13] of Dirac's equation the wave functions were extended by means of JWKB solutions. These continuum functions were then conveniently normalized to unit linear density by considering the asymptotic forms. The normalization coefficients were checked by noting that f_p and g_p behaved properly for small r by comparison with $C(E)$. From these values of f_p and g_p, f_s and g_s were calculated by the use of Eqs. (12.9). The integrals I_{sp}, I_{ps} were then evaluated by numerical quadrature with a probable error of about five percent. The values of V from Eqs. (13.2) and (13.3) for $z_N=2$ are given in Table I for various energy combinations. The numerical quadratures used for Table I were made from the nuclear radius a on to ∞. The results are very insensitive to the choice of the lower limit.

Comparing with the calculations of Section V it is seen from Table I that the effective V's for the dipole interaction and $z_N=2$ are relatively small. A calculation based on the relation

$$|E^{(2)}/\delta_c E|=(z_N^2/7100)\int_1|E-E_1|^{-1}(E/p)I_{sp}^2 d\dot{E} \tag{13.4}$$

shows that for $E_1=0.9$ (a single nuclear level at 50 kev) the staggering effect due to the dipole term is about three percent of the top slice volume effect. This figure includes an integration up to $E=100$. If only the range $E=1$ to $E=10$ is taken then the corresponding number is 1.5 percent. This result is comparable with values in Table I and the estimate $V=3.8$ obtained soon after Eq. (10.2). Since this V corresponds to 50 percent of the volume effect on the top slice basis one would estimate for 1.5 percent a V of $3.8/[50/1.5]^{\frac{1}{2}}=0.66$, which is approximately the value in Table I.

The figure 1.5 percent was obtained by quadrature based on the calculation of the integrand. The value three percent which was stated for the effect up to $E=100$ is not considered to be nearly so reliable since the integrand was not evaluated from $E=10$ to $E=100$. The relative smallness of the effects under consideration makes this contribution have only a secondary interest.

Calculations on perturbations of $p_{3/2}$ states by the s continuum have been made. It has been found that as the energy of the s electron is increased the effective V decreases rapidly and that these perturbations are much smaller than those of $p_{\frac{1}{2}}$ states. At $E_s=2$ the effect on the $p_{3/2}$ state is $\sim\frac{1}{2}$ of that on the $p_{\frac{1}{2}}$ state.

As a check on the accuracy of the wave functions for the continuum and to get an indication of $\partial V/\partial E$, $(E=1)$, the energy derivatives of the s-wave functions at $E=1$ were computed by two independent methods (derivations included in Appendix). In the first, the quantity $y=f/g$ was used. One obtains[6]

$$\partial y/\partial E=-(rg)^2\int_0^r r^2(f^2+g^2)dr \tag{14}$$

and

$$\partial g/\partial E=g(r)\int_0^r[y+(E+1+\gamma/r)\partial y/\partial E]dr. \tag{14.1}$$

In the second a Bessel function expansion[16] is employed

[15] G. E. Brown, Proc. Nat. Acad. Sci. **36**, 15 (1950).

[16] Yost, Wheeler, and Breit, Phys. Rev. **49**, 174 (1936) employed a similar expansion in the calculation of Coulomb wave functions.

and there results

$$\partial(rf)/\partial E=[(r/3\gamma)-(1/2)]rf +[(2r/3)+(r^2/3\gamma)]d(rf)/dr \quad (14.2)$$

and

$$\partial(rg)/\partial E=[(2r^2/3\gamma)+(5r/3)+(1/2\gamma)-(2\rho^2/3\gamma)]rf -(r/6\gamma)d(rf)/dr. \quad (14.3)$$

The normalization is such that

$$\partial(y, g, f)/\partial E=0, \quad r=0. \quad (14.4)$$

Applying Eqs. (13.2) and (13.3) to the energy derivative of I_{sp} the presence of such factors as $2r^2/3\gamma$ in Eq. (14.3) causes the integrand to diverge at large r. While screening may keep the result finite it appears that the curve of V *vs.* E starts off with a steep slope. This may be of importance in estimating the magnitude of the dipole polarization effect for low lying nuclear energy levels.

An upper bound can be set on the expected dipole effect by means of the f sum rule, if the nuclear excitation energy of the perturbing levels is decided on. According to the f sum rule the sum of the f values is equal to the number of protons. One has for any energy range the inequality

$$\Sigma|r_{nm}|^2<(3/4\pi)(\hbar/mc)|c/\nu_{nm}|(m/M)Z$$

where the sum on the left is taken over the energy range that is under consideration. Account is here taken of the fact that in the f sum there occurs a cancellation of effects owing to omission of transitions between occupied states. The f sum rule consideration may be expected to be of significance mainly for excitations corresponding to an average condition rather than one of exceptionally low excitation. Taking 20 Mev, somewhat arbitrarily, for the excitation energy and $Z=80$ one finds from the previous equation

$$\langle|r_{nm}|\rangle<1.56\times10^{-12}\text{ cm}$$

which may be compared with $a=0.89\times10^{-12}$ cm, the value used in the calculations in this section. The ratio of the two is 1.75.

It should be mentioned that all of the values used here are overestimates because of the omission of the factor

$$(Z_1M_2-Z_2M_1)/[Z_1(M_1+M_2)],$$

which has to be included as a correction for the motion of the residual nuclear mass M_2 having charge Z_2e when one considers the effective dipole moment due to charge Z_1e with mass M_1. With a view toward the application in Section VIII, all the protons will be combined into (Z_1, M_1) and all neutrons into (Z_2, M_2) giving a correction factor of $128/208=0.61$ to the effective matrix element V for Pb^{208}. Since the value of $\langle|r_{nm}|\rangle$ was obtained on the basis of protons rather than alpha-particles there is a further factor $\frac{1}{2}$ for V. Combining these factors one has a net factor $1.75\times0.61\times0.5=0.52$. These estimates indicate that the whole effect will not be more than $(0.52)^2\times3$ percent $=0.8$ percent of the theoretically expected effect on the top slice method. If the mean excitation energy were taken as 2.5 Mev so as to correspond to the calculation in which contributions of the second-order perturbation energy have been summed from $E=1$ to $E=10$ the effect would be increased by a factor 8 on account of the effect of the energy ratio on $\langle r^2\rangle$. It would be decreased because the value 1.5 percent rather than three percent was obtained in the estimate by numerical quadrature from $E=1$ to $E=10$. One would obtain at most $4\times0.8=3.2$ percent of the top slice volume effect expected on the $A^{\frac{1}{3}}$ nuclear radius approximation. The nature of this estimate is such as to exaggerate the expected value of the frequency shift except for the probable overestimate of the volume effect.

VIII. DISCUSSION

Extensive experimental material on the isotope shift of Hg, Pb, and Pt is available through the work of Schüler, Kopfermann and many other investigators. The staggering of the term values of odd isotopes in Hg, Pb, and Pt is in such a direction as though the nuclei of the odd isotopes exerted relatively more attraction on the electron than the even ones. This fact is in agreement with expectation since the odd isotopes are less stable and since they have a larger density of nuclear levels close to the ground state. Quantitative comparison in Hg is difficult because of differences in the indications concerning the magnitude of the staggering effect as obtained from different lines. It is convenient in this connection to express the comparison in terms of a unit of isotope displacement which will be referred to as an isotopic unit. This unit will be defined as one-half the separation between term values of the nearest pair of even isotopes if one is discussing the term value of an odd one. Figure 15 of Schueler and Keyston[17] indicates for λ2536 a polarization effect of about one-third of an isotopic unit for Hg^{201} and about 0.9 for Hg^{199}. For λ6072($7\,^3S_1-8\,^1P_1$) the staggering of Hg^{199} and that of Hg^{201} is about 0.6 isotopic unit. For λ6716($7\,^1S_0-8\,^1P_1$) the staggering is according to the same figure of Schueler and Keyston about 0.75 and 0.55 isotopic unit for these two isotopes.

It appears possible that for λ2537 there has been some interference among the components of the hyperfine structure pattern inasmuch as the separation between isotopes 198 and 200 is appreciably smaller for this line than between 200 and 202 while the interval between the centroid of the pattern of isotope 199 and 198 is anomalously small. The well-known difficulties of hyperfine structure measurements on an isotopic mixture make one doubtful concerning the reality of some of the discrepancies. Additional experiments especially with the now available separated isotopes

[17] H. Schueler and J. E. Keyston, Zeits. f. Physik. **72**, 423 (1931).

TABLE I. Values of equivalent interaction energy matrix element V for various excitation energies E_s, E_p of the electron. Only $p_{\frac{1}{2}}$ electrons covered here.

E_s $[mc^2]$	E_p $[mc^2]$	I_{sp}, I_{ps} $[(\hbar/mc)^{-2}]$	V $[mc^2]$
1	1	0	0
1	2	1.92	0.61
1	6	3.4	0.47
1	10	3.8	0.36
2	1	0.38	0.48
6	1	1.10	0.46
10	1	1.31	0.35

would be helpful in providing a more certain basis for theoretical speculation. There is a possibility that some of the discrepancies are the result of a difference in the staggering effect caused by differences in the behavior of different terms with respect to the participation of perturbations by $s_{\frac{1}{2}}$ and $p_{\frac{1}{2}}$ continua. It is also not clear theoretically that this participation of continua will produce similar effects for different isotopes.

There is some indication in the work of Schueler and Keyston on λ2537 that the separation between Hg^{202} and Hg^{200} is larger than that between Hg^{204} and Hg^{202} or that between Hg^{200} and Hg^{198}. For the other lines in their Fig. 15, however, the phenomenon does not appear as clearly. Differences in the behavior of even isotopes are not excluded by the polarization effect explanation but it appears premature to speculate on this point also.

For Pb the observations of Schueler and Jones,[18] Rose and Granath,[19] Kopfermann[20] again show decided staggering of odd isotopes with respect to the even ones. Here only one odd isotope (207) is present. Taking the mean of results obtained from 11 lines measured by Rose and Granath, one obtains for $[(207)-(206)]/[(208)-(207)] \cong 0.59 \pm 0.06$ where 0.06 is the probable error. Here (206) means the term value of Pb^{206}, (207) the centroid of term values of Pb^{207}. This speaks for a specific staggering effect of 0.26 of an isotopic unit which is somewhat smaller than the value assumed in making estimates of V. There is again considerable variation of the $[(206)-(207)]/[(207)-(208)]$ ratio between different lines. It may be premature to claim too much on the basis of this fact since some variation would result as a consequence of experimental error. Different effectiveness of the $s_{\frac{1}{2}}$, $p_{\frac{1}{2}}$ continua for different terms would not be in contradiction with such a variation, however. There are observations on only three even isotopes of Pb. The spacing between Pb^{204} and Pb^{206} is somewhat smaller than that between Pb^{206} and Pb^{208} according to Schueler and Jones[18] and according to observations of Watson and Anderson,[21] and Manning.[22] This fact may possibly be related to the supposed closing of a stable shell[3] of 126 neutrons in Pb^{208}. The stable shell can be expected to be less polarizable and the addition of the 126th neutron could lead, therefore, to a larger than usual apparent volume effect.

For Pt ($Z=78$) there are measurements of Jaeckel and Kopfermann,[23] Jaeckel,[24] and by Tolansky and Lee.[25] The ratio $[(194)-(195)]/[(195)-(196)]$ is 0.82 for λ5369 and 0.5 for λ5391. There is no apparent reason for considering the staggering to be greater than 0.5 of an isotopic unit and it may be much smaller since a smaller value is indicated by λ5369 for which the whole pattern is more open. The displacements between the even isotopes are approximately equal to each other with possibly a tendency for the ratio $[(194)-(196)]/[(196)-(198)]$ to be slightly less than unity.

The observations of Schueler and Schmidt[26] and of Brix and Kopfermann[2] on Sm ($Z=62$) show a large anomaly for the even isotopes. A related phenomenon is present in Nd according to Klinkenberg.[27] Explanations of this phenomenon have been discussed by Schueler and Schmidt, Klinkenberg, Feather,[28] and by Brix and Kopfermann. Klinkenberg brought out the fact that the specially large separation occurs between isotopes with a number of neutrons $N=88$ and $N=90$ for both $Z=62$ and $Z=60$. Feather points out that the new assignment of α-activity to Sm^{152} is not in striking contradiction to expectation from the occurrence of α-activities for radioactive elements with $Z=84$. He further points out that for Sm the isotopes 144, 148, 150 can be considered as tightly bound while 152, 154 are regarded as loosely bound. The volume of Sm^{152} and of Sm^{154} should be anomalously great, therefore. Similarly according to Feather the volume of Nd^{150} may be expected to be anomalously great because Nd^{150} is loosely bound. On the other hand, Brix and Kopfermann suspect connection between the shape of these nuclei and the quadrupole moment of Eu. As has been mentioned in the Introduction, the explanation of Brix and Kopfermann cannot be maintained in its original form if the nuclei in question have a spin O because the charge distribution is then spherically symmetric. A connection with the occurrence of quadrupole moments for neighboring nuclei may, nevertheless, exist as has been also discussed in the Introduction.

If the anomalies in Sm and Nd are to be explained as polarization effects of the nucleus, then it seems necessary to suppose that neutron shells with $N=90$ are especially tightly bound in the sense of having smaller polarization effects for $N=90$ than $N=88$. Such a view does not fit in especially well with Feather's evidence

[18] H. Schueler and E. G. Jones, Zeits. f. Physik **75**, 563 (1932).
[19] J. L. Rose and L. P. Granath, Phys. Rev. **40**, 760 (1932).
[20] H. Kopfermann, Zeits. f. Physik **75**, 363 (1932).
[21] W. W. Watson and C. E. Anderson (private communication); Manning, Anderson and Watson, Phys. Rev. **78**, 417 (1950).
[22] T. E. Manning, Phys. Rev. **76**, 464A (1949).
[23] B. Jaeckel and H. Kopfermann, Zeits. f. Physik **99**, 492 (1936).
[24] B. Jaeckel, Zeits. f. Physik **100**, 513 (1936).
[25] S. Tolansky and E. Lee, Proc. Roy. Soc. **A158**, 110 (1937).
[26] H. Schueler and Th. Schmidt, Zeits. f. Physik **92**, 148 (1934).
[27] P. F. A. Klinkenberg, Physica **11**, 327 (1945).
[28] N. Feather, Nature **162**, 412 (1948).

which indicates loose binding in Sm for $N=90$, 92 and Nd for $N=90$. The conflict between the views is perhaps not a decided one because looseness of binding in Feather's sense has to do with the energy available for α-emission which is not simply related to relative polarizability of isotopes. The latter depends not only on binding but also on the character of the wave function as in Eq. (11.3). No definite claim can be made for the polarization picture on the basis of the isotope shift in Nd and Sm. The anomalies in these shifts can be explained more easily on the nuclear volume picture, as has been pointed out by Feather.

Returning to the general subject of orders of magnitude of the polarization needed for the explanation of the isotope effect, it is of interest that Goldhaber and Teller[29] consider it likely that the (γ,n) reactions indicate the possibility of exciting nuclear "dipole vibrations" of an exceptionally strong type. In their picture the neutrons move in a direction opposite to that of the protons. Such a vibration corresponds to a larger effective charge z_N than is needed in order to make the dipole terms important for the isotope shift.

The expectation of Goldhaber and Teller that there should be resonance absorption for γ-rays by C^{12} and Cu^{63}, has not been confirmed by the experiments of Gaerttner and Yeater.[30] On the other hand, Lawson and Perlman[31] obtain results for the total cross section which fit Goldhaber and Teller's view. Kubitschek and Dancoff[32] find in a study of a large number of elements that there is evidence in γ-ray capture of frequent emission of γ-rays carrying nearly the whole available energy. These observations appear to speak against a purely statistical treatment of the distribution of nuclear energy levels and the possibility of large matrix elements for the higher energy γ-transitions. This evidence regarding nuclear polarization is not in contradiction with the thesis of Teller-Goldhaber. The experiments of Gaerttner and Yeater do not necessarily exclude the general features of the Teller-Goldhaber view. A strong damping of resonance absorption by (γ,n) processes can reduce the effect and the "reststrahlen" type of vibration is perhaps not taking place in as extreme a manner as originally proposed. Without more definite evidence it appears only fair to draw attention to the relationship which the supposed nuclear dipole vibrations can conceivably have to the odd-even staggering phenomenon.

The discussion at the end of Section VII on the dipole effect made use of the f sum rule consideration. The occurrence of the vibrations of Goldhaber-Teller at high energies makes the larger of the two estimates ($\sim$three percent) improbable because this estimate assumed a concentration of contributions to the second-order perturbation energy from the 2.5-Mev nuclear excitation region, while experiment and the theory of Teller-Goldhaber speak for the concentration of a large part of the f sum at much higher energies. The experimental situation for the heavier elements discussed by Goldhaber and Teller is not quite clear however and the present argument is not certain before the f sum contributions in nuclei are more thoroughly known.

While the manuscript of the present paper was being prepared there appeared a new and very thorough theoretical discussion of the experimental material by Crawford and Schawlow.[33] They employ the point of view that the features of hyperfine structure originating in the coupling of electrons to the nuclear spin may be used to determine the normalization of the electronic wave function close to the nucleus. This is done much more carefully by Crawford and Schawlow than previously and the results are, furthermore, more significant because of the availability of direct measurements of nuclear magnetic moments. Crawford and Schawlow conclude that the ratios of the isotopic shift for different spectroscopic terms are in fair agreement with the volume effect theory. The $A^{\frac{1}{3}}$ law gives, however, an expected isotope shift corresponding to the addition of two neutrons which is too large by a factor of about 2 if the protons are assumed to be uniformly distributed through the nuclear volume. Crawford and Schawlow suggest that the explanation for the smallness of the observed effect might lie in nuclear shell structure along the lines proposed by Mayer,[3] Feenberg and Hammack,[34] and Nordheim.[35] A partial cause of the effect may be nuclear polarization. High electronic excitations do not distinguish markedly between details of the nuclear level systems and would be expected to cause effects varying approximately regularly with the neutron number N.

The nuclear shell structure has to do with comparatively high stability when a certain number of nucleons of the same type exists in the nucleus. The effects are reasonably pronounced on a scale of the binding energy of the last neutron. This fact does not necessarily imply, however, a significant consequence of shell structure regarding the volume effect because the stability of shells is not a marked phenomenon on the scale of the whole nuclear binding energy. For an α-particle compared with a deuteron there would indeed be a strong effect. In the heavier nuclei, however, the conditions can hardly be expected to be as clear cut.

The probable implication of the existence of shell structure is that a certain quota of nucleons has been admitted to available quantum numbers. Such a condition does not have to go with spatial rigidity of the shell. The degree to which shell structure is of im-

[29] M. Goldhaber and E. Teller, Phys. Rev. **74**, 1046 (1948).
[30] E. R. Gaerttner and M. L. Yeater, Phys. Rev. **76**, 363 (1949).
[31] J. J. Lawson and M. L. Perlman, Phys. Rev. **74**, 1190 (1948).
[32] H. E. Kubitschek and S. M. Dancoff, Phys. Rev. **76**, 531 (1949).
[33] M. F. Crawford and A. L. Schawlow, Phys. Rev. **76**, 1310 (1949). The views expressed in this reference are further supported by Schawlow, Hume, and Crawford, Phys. Rev. **76**, 1876 (1949).
[34] E. Feenberg and K. C. Hammack, Phys. Rev. **75**, 1877 (1949).
[35] L. W. Nordheim, Phys. Rev. **75**, 1894 (1949).

portance for the volume effect appears, therefore, to be uncertain.

It should be pointed out that in the present paper the estimates of the ratio of the polarization effect to the volume effect have been made on the basis of a volume effect corresponding to the $A^{\frac{1}{3}}$ law and the top slice (protons on the outside) picture. According to the Crawford-Schawlow reductions and the supposition that the nuclear spin part of the hyperfine structure gives a sufficiently good calibration of the wave function close to the nucleus one has to conclude that the observed isotope effect corresponding to the addition of two neutrons is smaller than the one used in the present paper, as has been previously mentioned. It will also be recalled that the estimates of the staggering effect have been made on the basis of low lying nuclear levels which emphasize contributions from the low energy part of the electronic continuum. So far as an evaluation of the importance of these contributions is concerned, it is immaterial whether the smallness of the effect of *two* neutrons is caused by polarization or by static charge distribution conditions. In either case the relative importance of the theoretically expected effects for odd-even staggering can be considered as having been conservatively presented in the discussion of experimental material since one could claim that it is at least twice as great on account of the too large unit of isotopic displacement which has been used.

The smallness of the observed shift corresponding to the addition of two neutrons increases the probability that nuclear monopole effects contribute to the staggering phenomenon. Instead of $|V|=3.8$ at the end of Section V it would suffice to have $|V|=3.8/\sqrt{2}=2.7$. The equivalent $|V|=1/0.8$ estimated for α-particles in connection with Eq. (11.4) taking into account four levels can be increased to $|V|=2.7$ either by increasing z from 2 to ~ 4 or by using more levels. When it is considered that the discussion of the experimental material does not call for as high a value as $\frac{1}{2}$ for $|\delta E^{(2)}/\delta_c E|$ and that the estimates in the present paper exaggerate the volume effect by employing the top slice cut-off rather than the uniform charge density model it appears possible that the monopole effect can account for the observed staggering.

In order to bring the dipole effect up to the observed values for the staggering one would have to increase the charge z_N by a factor of $\sim(40/3)^{\frac{1}{3}}=3.6$ corresponding to a staggering effect of 40 percent of the regular and to a top slice volume effect of twice the regular isotope shift. The corresponding $z_N\sim 7.2$. Such a value of z_N cannot be used without considering the $Z_1M_2-Z_2M_1$ factor and the sum rule considerations at the end of Section VII. The factor 2 between the volume effect theory and observation changes the 3.2 percent which has been obtained by the f sum rule consideration with the main excitation energy at 2.5 Mev into ~ 6 percent. The discussion of the paper of Goldhaber and Teller which has been attempted indicates, however, that even this number is probably an overestimate of the effect. At this point the writers would like to express their indebtedness to Professor E. Teller for a helpful discussion of the GT paper so often referred to and for pointing out the apparent absence of the "dipole type" vibrations at lower frequencies.

The irregularities in the spacings of the even isotopes of Pb having been briefly mentioned. A tentative explanation of these has been previously attempted.[36] At the time the "magic numbers" for nuclear particles were not known and the conditions of stability of nuclear particles were reasoned about from the viewpoint of Gamow's picture of a potential valley. Since Pb^{208} is decidedly stable it was supposed that it was located near the bottom of the valley and that, therefore, the step from Pb^{206} to Pb^{208} should contribute less to stability than the step from Pb^{204} to Pb^{206}. Accordingly, the nuclear radius was expected to increase somewhat more in the 206 to 208 step than in the one from 204 to 206 in apparent agreement with observation.

From general arguments of stability the polarization picture would lead to the opposite result for such changes in the energy. A decrease in the binding energy of the last neutron in the 206–208 step may be expected to give a larger attraction of the electron by the nucleus as though the nuclear radius increased by an anomalously small step. According to the table at the end of the second volume of the book by Rosenfeld[37] the binding energy per nuclear particle in Mev for these isotopes is 7.825 for 204, 7.827 for 206, and 7.819 for 208. According to these numbers Pb^{208} is relatively more loosely bound, in spite of the closure of the magic number shell consisting of 126 neutrons. In this case the volume effect explanation agrees better with the irregularity of level spacing than the polarization picture. On the other hand, the binding energy per nucleon is 7.820 Mev for Pb^{207} according to the same table. Here the volume picture suggests on anomalously large radius and the corresponding volume anomaly might be expected to have a direction opposite to that observed. While the (208–206)/(206–204) ratios speak against the direct applicability of the polarization view it is hardly justifiable to employ binding energies per nucleon as the deciding criterion since the protons rather than neutrons are instrumental in the process and since a tighter neutron configuration does not necessarily imply a stiffer arrangement of protons. Experiments on the isotope shift of Pb^{210} would be helpful and improved knowledge of binding energies of the isotopes of Pt, Hg and other elements showing the spectroscopic isotope shift would contribute also.

The example of Pb^{207} shows that the binding energy per nuclear particle, which is practically as large for this isotope as for Pb^{208}, cannot be used as the only

[36] G. Breit, Phys. Rev. **46**, 319(L) (1934).

[37] L. Rosenfeld, *Nuclear Forces* (Interscience Publishers, Inc., New York, 1948).

criterion either on the volume effect theory or from the polarization viewpoint. The agreement of the direction of the (208–206)–(206–204) difference with that expected from binding energies and a naive application of the volume effect theory does not exclude the possibility that the difference is in part due to the availability of excited states in Pb^{206} which might contribute to larger polarization of this nucleus than that of Pb^{208} and which might conceivably have its origin in the fact that shell closes for 126 neutrons. A study of the level systems of these isotopes will have to be made in order to reach a decision concerning the relative importance of these effects. At present it appears to be impossible to exclude the combined operation of the two possible causes of the anomaly in this as well as in the cases of isotopes under discussion below. It may be of interest also that the masses of the even Pt isotopes as listed by Mattauch are 198.044, 196.039, 194.039 indicating a greater instability of the 198 isotope than that of the other two. The observed isotope shift is greater for the 198–196 interval than for that between 196 and 194. Here again the volume effect explanation fits the facts more naturally. The errors listed by Mattauch are of the order of the differences under discussion, however. The situation is similar for the 150–148 spacing in Nd as has been discussed in relation to the Sm phenomenon.

Summarizing, it appears that the dipole effect is probably too small to be of real interest, that the monopole effect possibly can be made large enough if the departures from the central field approximation to nuclear wave functions are assumed to be sufficiently drastic; the even-odd isotope shift staggering fits the monopole calculations rather naturally especially if it is supposed that differences in densities of perturbing energy levels in the region of a few Mev are not compensated for as the nuclear excitation is increased to 10 or 20 Mev; irregularities in positions of even isotopes are not necessarily in contradiction with the polarization view but do not fit it especially naturally. There is a possibility that the small value of the observed isotope shift is in part caused by a partial cancellation of the volume effect by that of the polarization.

The authors would like to express their indebtedness to Professor W. W. Watson for informing them of the experimental results on Pb before publication, and to Professor A. C. G. Mitchell for information on nuclear levels of elements of medium mass number.

APPENDIX

Using $y=f/g$ and combining the two Dirac radial equations one obtains[6]

$$(E+1+\gamma/r)y^2+(E-1+\gamma/r)+dy/dr+2y/r=0. \quad \text{(A1)}$$

Differentiating with respect to E and solving for $\partial y/\partial E$ one gets Eq. (14). Equation (14.1) results from the similar treatment of the radial equation containing $\partial g/\partial r$. The normalization convention is that f_s and g_s have been divided by $[C(E)]^{\frac{1}{2}}$ so that the first power of r is energy independent.

While the second method is limited to $E=1$, it gives precise values at all r and is somewhat more convenient than the preceding method for large r. Substituting $rf=F$, $rg=G$, and $r=z^2/8\gamma$, the radial equations may be rewritten

$$\begin{aligned}[(d/dz)+(2/z)]F+[(2\gamma/z)+z(E-1)/4\gamma]G=0,\\ [(d/dz)-(2/z)]G-[(2\gamma/z)+z(E+1)/4\gamma]F=0.\end{aligned} \quad \text{(A2)}$$

It is from this form of the Dirac equations that Eq. (12.6) may be obtained. Expanding F in powers of $(E-1)$,

$$F=F^{(0)}+(E-1)F^{(1)}+\cdots \quad \text{(A3)}$$

and letting[16]

$$\begin{aligned}F^{(0)}=\gamma J_\nu(z), \quad \nu=2\rho,\\ L\equiv d^2/dz^2+1/z+1-\nu^2/z^2\end{aligned} \quad \text{(A4)}$$

one finds

$$LF^{(1)}=(1/2\gamma-\gamma-z^2/8\gamma)J_\nu+(z/4\gamma)dJ_\nu/dz. \quad \text{(A5)}$$

Using

$$L[z^pJ_\nu(z)]=z^p\{2pdJ_\nu/zdz+p^2J_\nu/z^2\} \quad \text{(A6)}$$

and

$$\begin{aligned}L[z^qdJ_\nu(z)/dz]=z^q\{(q-1)^2dJ_\nu/z^2dz\\ +[2\nu^2(q-1)/z^3-2q/z]J_\nu\},\end{aligned} \quad \text{(A7)}$$

it is found that

$$F^{(1)}(z)=[(z^2/24\gamma)-(\gamma/2)]J_{2\rho}+[(z\gamma/3)+(z^3/48\gamma)]dJ_{2\rho}/dz. \quad \text{(A8)}$$

Similarly,

$$\begin{aligned}G^{(1)}(z)=[(z^4/96\gamma^2)+(5z^2/24)+(1/2)-(2\rho^2/3)]J_{2\rho}\\ -(z/12)dJ_{2\rho}/dz.\end{aligned} \quad \text{(A9)}$$

Equations (14.2) and (14.3) follow directly from these.

The Internal Conversion Electrons of Several Short-Lived Neutron Induced Radioactivities*†

RICHARD L. CALDWELL
University of Missouri, Columbia, Missouri and Argonne National Laboratory, Chicago, Illinois
(Received January 30, 1950)

Accurate values of the transition energy were measured for seven neutron-induced radioactivities using a permanent magnet beta-ray spectrograph. A special vacuum gate permitted the introduction of short-lived samples within twelve seconds after the end of bombardment without disturbing the vacuum in the spectrograph. Transition energies, accurate to about one percent, were determined as follows: cesium (3 hr.) 128.0 kev, cobalt (10.7 min.) 58.9 kev, columbium (6.6 min.) 41.5 kev, dysprosium (1.3 min.) 109.0 kev, dysprosium (2.6 hr.) 87.8 kev, iridium (1.5 min.) 57.4 kev, thulium (120 day) 84.8 kev. For the five isomeric transitions, approximate values of the relative intensities of the electron lines were determined, and an assignment was made of the multipole order of the radiation, assuming electric multipole radiation.

1. INTRODUCTION AND METHOD

To study the internal conversion electrons of several short-lived radioactivities, a permanent magnet spectrograph, similar to that described by Hill,[1] was constructed. Because of the integrating action of the photographic film detector, short half-life period radioactivities could be studied by using successive radioactive samples to give an accumulated exposure on a single film. A special vacuum gate was used to introduce into the spectrograph a radioactive sample within twelve seconds after the end of its bombardment without seriously altering the vacuum in the spectrograph. The design of this gate is shown in Fig. 1. It consists of a small forechamber separated from the main spectrograph vacuum chamber by a hand operated gate. A Welch forepump was used to produce the required vacuum of 10^{-3} mm Hg in the main chamber. A second forepump was connected to the forechamber with a hand valve in the pumping line. A circular opening in the forechamber allowed insertion of a sliding cylindrical rod with removable Lucite source holder on its end. An O-ring gasket formed a vacuum seal between the rod and forechamber walls permitting both translational and rotational motion of the rod holding the source.[2] With this arrangement it was possible to insert the rod with the source on it through the O-ring seal into the forechamber and permit rough pumping of the forechamber prior to opening the gate and sliding the rod forward to position the sample in the spectrograph.

The source in powder form was attached to a narrow

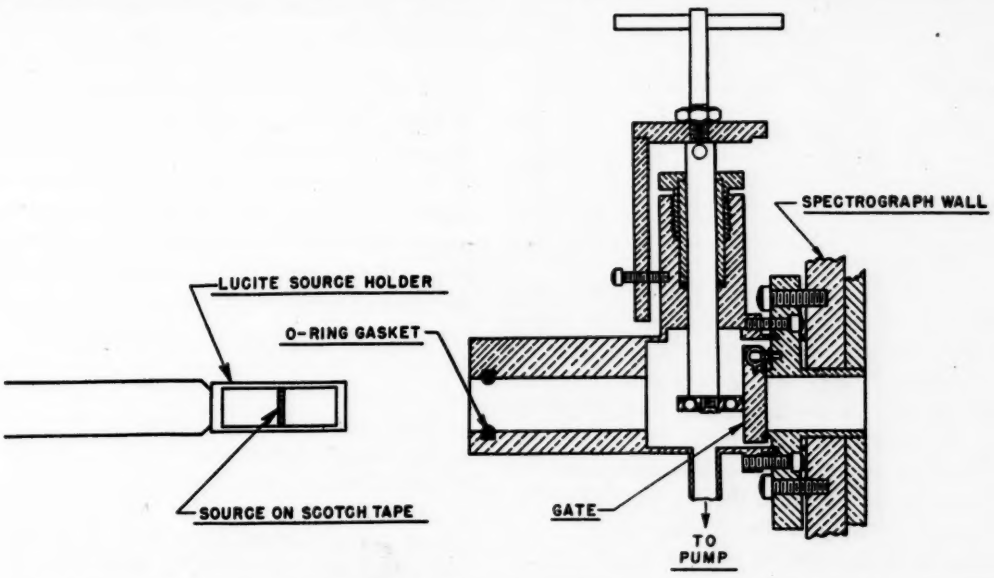

FIG. 1. Vacuum gate for quick source change. This vacuum gate was used to introduce into the spectrograph a radioactive sample within twelve seconds after the end of its bombardment without seriously altering the vacuum in the spectrograph.

* Extract from a thesis submitted in partial fulfillment of the requirements for the degree of Doctor of Philosophy at the University of Missouri. A preliminary report was given by Caldwell, der Mateosian, and Goldhaber, Phys. Rev. 76, 187(A) (1949).
† This work was carried out at the Argonne National Laboratory under auspices of the AEC.
[1] R. D. Hill, Phys. Rev. 74, 78 (1946).
[2] F. N. D. Kurie, Rev. Sci. Inst. 19, 485 (1948).

TABLE I. Electron and transition energies.

Element	Half-life	$H\rho$ (gauss-cm)	Electron energy (kev)	Conversion shell	Transition energy (kev)
Cs	3 hr.	1067.5	92.0	K	128.0
		1251.1	123.0	L	128.0
		1273.5	127.0	M	128.0
					Av.=128.0
Co	10.7 min.	781.9	51.1	K	58.8
		835.8	58.2	L	59.0
		839.9	58.7	M	58.8
					Av.= 58.9
Cb	6.6 min.	510.1	22.5	K	41.5
		678.2	39.0	L	41.5
		695.1	40.8	M	41.2
					Av.= 41.4
Dy	1.3 min.	812.0	55.1	K	109.0
		1117.5	100.2	L_{I}	109.3
		1122.9	101.1	L_{III}	108.9
		1158.6	107.1	M	108.8
		1167.9	108.7	N	109.0
					Av.=109.0
Dy	2.6 hr.	616.2	32.5	K	88.2
		982.1	78.8	L_{I}	88.2
		988.5	80.0	L_{III}	88.1
		1029.8	85.8	M	87.2
		1039.8	87.2	N	87.4
					Av.= 87.8
		1734.3	219.1	K(?)	
Ir	1.5 min.	722.9	44.1	L_{I}	57.5
		739.1	46.0	L_{III}	57.2
		806.6	54.4	M	57.3
		823.0	56.5	N	57.3
					Av. =57.4
Tm	120 days	515.8	22.9	K	84.4
		954.3	74.8	L_{I}	85.3
		961.5	75.9	L_{III}	84.9
		1007.7	82.7	M	84.8
		1018.3	84.3	N	84.8
					Av.= 84.8

piece of Scotch Tape on a source holder which was bombarded with thermal neutrons from the heavy water moderated chain-reacting pile of the Argonne National Laboratory. Since several source holders were used interchangeably, a special jig was constructed for cutting the Scotch Tape to which the source was attached. This jig assured that all sources were the same width and were aligned in the same position with respect to the slit opening of the spectrograph.

The photographic film used was Eastman No-Screen X-Ray film. In order to make approximate measurements of the relative intensities of the various electron lines the film was calibrated by using a thulium source (120-day half-life period). The data of Saxon[3] were used as a "standard" to give the number of electrons at any particular energy.

[3] D. Saxon, and J. Richards, Phys. Rev. **76**, 186 (1949).

Calibration of the magnetic field strength of the spectrograph magnet was made by two independent methods. First, the x-ray critical absorption energies were used to obtain an accurate evaluation of the magnetic field strength in the following way. A provisional assignment of the conversion lines for all the elements studied was made from a reasonably accurate value of the field as measured with a previously standardized coil and fluxmeter. The accurate x-ray energy level values were then used to calculate the value of the field which brought the transition energies derived from the K, L, M, and N conversions into agreement. Second, the accurately known 80-kev gamma-ray of I^{131} was used as a standard for calibrating the magnetic field. Du Mond[4] and his co-workers have measured the gamma-rays from I^{131} using a double crystal spectrometer. They report a value of 80.133±0.005 kev for the low energy gamma-ray. A sample of radioactive separated isotope I^{131} obtained from Oak Ridge was used as a source in the spectrograph. Three conversion electron lines found were assigned to K, L, and M conversions of the 80-kev gamma-ray. Using Du Mond's value for the gamma-ray energy, the measured radii of curvature of the three electron lines, and the x-ray data for the critical absorption energies, a value was assigned to the magnetic field. The values of the magnetic field obtained by the two methods agreed to within 0.1 percent and the weighted mean value of 98.3±0.1 gauss was adopted for the calculation of the electron energies.

The field of the spectrograph magnet was uniform to within 0.2 percent except at points closer than 5 cm from the edge of the pole pieces, which measured 30.5 ×50.8 cm. The maximum useful radius of the spectrograph was 20 cm. The maximum value of the product of field strength and electron radius of curvature obtainable was then 1966 gauss-cm, corresponding to an electron energy of 273 kev. Although electrons of energy as low as 5 kev were focused on the detector, the lower energy limit of the spectrograph was probably about 20 kev because of the low sensitivity of the film to electrons of energy less than 20 kev.

2. TRANSITION ENERGIES

Cesium

Neutron irradiation of cesium, which has but one stable isotope of mass number 133, produces a 3-hour period which is isomeric with a long period of about 2 years. Goldhaber and Muehlhause[5] reported for the 3-hour period strong K_α x-rays of cesium as well as conversion electrons which they assumed to be K electrons of a transition of about 160 kev. Peacock, Jones, and Overman[6] reported a highly converted gam-

[4] Lind, Brown, Klein, Muller, and Du Mond, Phys. Rev. **75**, 1544 (1949).

[5] M. Goldhaber and C. O. Muehlhause, Phys. Rev. **74**, 1904 (1948).

[6] Peacock, Jones, and Overman, Plutonium Project Report, Mon. N-432, 56 (1947).

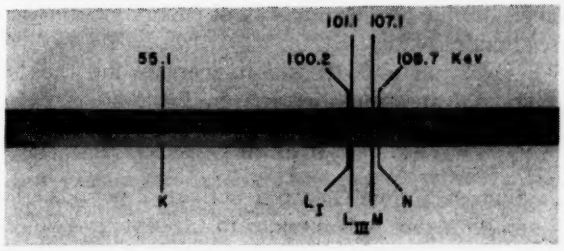

FIG. 2. Internal conversion electrons of Dy^{165} (1.3 min.).

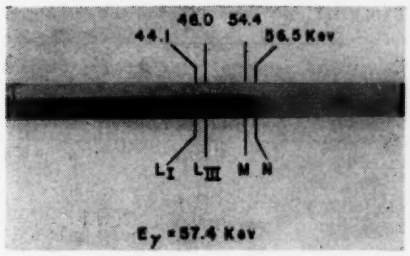

FIG. 3. Internal conversion electrons of Ir^{192} (1.5 min.).

ma-ray of 150 kev±30 kev going to the lower state of Cs^{134} (2 yr.).

A spectrogram of the 3-hour period of cesium showed three electron lines due to a single gamma-ray of energy 128±0.5 kev which converts in the K, L, and M shells. Table I gives the energies of the internal conversion electrons. The previously reported values would be in good agreement with our value if L rather than K electrons had been assumed. An examination of the critical absorption energies[7] for both cesium and barium shows that the $K-L$ electron energy difference and the $L-M$ electron energy difference fit the accurate x-ray absorption difference for these shells for cesium but do not fit the same shell differences for barium. This confirms the critical absorption experiments of Goldhaber and Muehlhause,[8] showing that the transition is an isomeric one in cesium and not a transition following a beta-ray which would require that the transition be in the element barium.

Cobalt

The 10.7-minute period in cobalt produced by neutron irradiation of cobalt metal has been investigated by Deutsch, Elliott, and Roberts.[8] They report that at least ninety percent of the disintegrations are by an isomeric transition of energy 56 kev, presumably to the five-year level. The remaining ten percent of the disintegrations are by a beta-ray of 1.25 Mev, followed by a single gamma-ray of energy 1.50 Mev. They studied the beta-ray spectrum with a spectrometer having a thin window counter and found a peak of conversion electrons at 48.5±2 kev. The K and L peaks were not resolved because a thick source was used. Assigning the conversion electrons to conversion mostly in the K-shell, they obtained a value of 56±3 kev for the energy of the gamma-ray.

In the present work, a spectrogram of the 10.7-minute period of cobalt showed three conversion electron lines which were assigned to K, L, and M conversions of a single gamma-ray of energy 58.9±0.5 kev. The electron energies are shown in Table I.

Columbium

The 6.6-minute period in columbium can be produced by slow neutron irradiation of columbium.[9] Goldhaber, Muehlhause, and Turkel[10] found that very pure Cb exposed to slow neutron irradiation emitted strong K x-rays. By critical absorption they showed these x-rays to be characteristic K radiations of Cb which implies that they arise from an isomeric transition in columbium. The internal conversion electrons were compared with the known internal conversion electrons from Co^{60} (10.7-min. period). A value of 36.5 kev was obtained; adding the Cb K work function of 19.0 kev gave 55.5 kev for the energy of the isomeric transition. Beta-rays of energy 1.3 Mev were also found. No unconverted gamma-rays were found, indicating that practically all of the gamma-rays are internally converted.

A spectrogram of the 6.6-minute internal conversion electrons was obtained using a thin foil (~2 mg/cm²) of columbium metal irradiated with slow neutrons. It was necessary to make 100 bombardments for a sufficient exposure. Three internal conversion electron lines were observed of energies 22.5, 39.0, and 40.8 kev.

TABLE II. Relative intensities of electron lines.

Element and half-life	Electron shell	Electron energy (kev)	Relative intensity (arbitrary units)
Cesium (3 hr.)	K	92.0	21.7
	L	123.0	33.8
	M	127.0	6.3
Cobalt (10.7 min.)	K	51.1	29.5
	L	58.2	6.5
	M	58.7	2.1
Columbium (6.6 min.)	K	22.5	1.4
	L	39.0	4.5
	M	40.8	1.6
Dysprosium (1.3 min.)	K	55.1	1.8
	L_I	100.2	14.3
	L_{III}	101.1	9.4
	M	107.1	6.3
	N	108.7	3.0
Iridium (1.5 min.)	L_I	44.1	26.0
	L_{III}	46.0	16.2
	M	54.4	10.1
	N	56.5	3.2

[7] A. H. Compton and S. K. Allison, *X-Rays in Theory and Experiment* (D. Van Nostrand Company, Inc., New York, 1935).
[8] Deutsch, Elliott, and Roberts, Phys. Rev. 68, 193 (1945).
[9] M. Goldhaber and W. J. Sturm, Phys. Rev. 70, 111A (1946).
[10] Goldhaber, Muehlhause, and Turkel, Plutonium Project Report, CF-3574 (July, 1946).

TABLE III. Multipole order of the radiation.

Element	Half-life	Transition energy (kev)	Multipole order From lifetime —energy relation	Multipole order From K/L ratio
Cs	3 hr.	128.0	2^4 or 2^5	2^4 or 2^5
Co	10.7 min.	58.9	2^4	2^4
Cb	6.6 min.	41.5	2^4	2^4
Dy	1.3 min.	109.0	2^4	2^4
Ir	1.5 min.	57.4	2^4	—

These were assigned to K, L, and M conversions of a single gamma-ray of energy 41.5±0.5 kev. The L conversion line is undoubtedly what Goldhaber *et al.*, interpreted as the K line in their aluminum absorption experiment. The electron energies for columbium are given in Table I.

Dysprosium

When the element dysprosium is subjected to slow neutron bombardment, two periods are observed. The 2.6-hour activity was first reported by Hevesy and Levi[11] and was confirmed by Pool and Quill[12] and by Inghram, Shaw, Hess, and Hayden.[13] The 1.25-minute K-converted gamma-activity was initially reported by Flammersfeld.[14] Inghram *et al.*, showed that both of these activities are produced by neutron irradiation of the stable isotope Dy^{164} and that the 1.25-minute activity is isomeric with the 2.6-hour activity.

For the 1.25-minute activity Flammersfeld has reported conversion electrons of energy 130 kev as measured by absorption in aluminum. He interpreted these as K electrons from which he obtained an energy of about 180 kev for the isomeric transition. Hole,[15] using a beta-ray spectrometer, observed an electron line at 93 kev which he interpreted as an L conversion electron line.

A spectrogram of the 1.25-minute activity, reproduced in Fig. 2, was obtained by making fifteen bombardments to give an accumulated exposure on one film. There were five conversion electron lines, which were assigned to a single gamma-ray of energy 109.0 ±0.5 kev which converts in the K, L_{I}, L_{III}, M, and N shells of dysprosium.

Seaborg and Perlman[16] report for the 2.6-hour activity of dysprosium four gamma-rays of energy 91, 370, 780, and 1100 kev. A spectrogram of the 2.6-hour activity showed six conversion electron lines, five of which were assigned to K, L_{I}, L_{III}, M, and N conversions of a single gamma-ray of energy 87.8±0.7 kev. The sixth line was not assigned, but is probably a K conversion line of a gamma-ray of energy greater than three hundred kev.

The electron and transition energies for the two periods of dysprosium are given in Table I.

Iridium

Iridium has three neutron activated periods. The 1.5-minute period is isomeric with the seventy-two day period and both are assigned to Ir^{194}. Goldhaber Muehlhause, and Turkel[17] report for the 1.5-minute period two gamma-rays of energy approximately 60 kev and 30 kev as well as strong L x-rays of iridium. They were unable, however, by critical absorption to show that there is a unique gamma-ray in the region of about thirty kev.

A spectrogram of the 1.5-minute activity using some of the same sample of iridium as used by Goldhaber *et al.*, was made and is shown in Fig. 3. Four conversion electron lines were seen which were assigned to a single gamma-ray of energy 57.4±0.5 kev which converts in the L_{I}, L_{III}, M, and N shells of iridium. A second spectrogram was made using twice as long an exposure on the film to try to find lower energy electrons supposedly from conversion of the ~30-kev gamma-ray. The results obtained were the same as for the first exposure, indicating no discrete lower energy gamma-rays. The electron energies for iridium are shown in Table I. The following interpretation has been suggested.[18] The transition from the 1.5-minute metastable state to the ground state can take place either by a 2^4-pole isomeric transition or by a competitive "double photon" emission.

A spectrogram of the nineteen-hour activity showed no conversion electron lines in the energy range of the spectrograph.

Thulium

The 120-day period in thulium was produced by neutron irradiation of thulium oxide powder. This period is reported to have a beta-ray spectrum of 1-Mev maximum energy and no gamma-rays.[16] Saxon[3] recently studied this period using a 180° focusing magnetic spectrometer and found superimposed on the beta-ray spectrum three internal conversion electrons of a single gamma-ray of energy[19] 85.5 kev.

Using a sample of irradiated thulium obtained from Mr. Saxon a spectrogram was made in the permanent magnet spectrograph. Five electron lines were clearly seen, which were assigned to K, L_{I}, L_{III}, M, and N conversion electrons of a single gamma-ray of energy 84.8±0.5 kev. The electron energies are given in Table I. The L_{I} and L_{III} conversion electron lines were clearly resolved in the spectrogram as two separate

[11] G. Hevesy and H. Levi, Nature **136**, 103 (1935).
[12] M. L. Pool and L. L. Quill, Phys. Rev. **53**, 437 (1938).
[13] Inghram, Shaw, Hess, and Hayden, Phys. Rev. **72**, 515 (1947).
[14] A. Flammersfeld, Zeits. f. Naturforschung **1**, 190 (1946).
[15] N. Hole, Arkiv. f. Mat. Astr. o. Fys. **36A**, paper 2 (1948).
[16] G. T. Seaborg and I. Perlman, Rev. Mod. Phys. **20**, 585 (1948).
[17] Goldhaber, Muehlhause, and Turkel, Phys. Rev. **71**, 372 (1947).
[18] M. Goldhaber (private communication).
[19] See also R. L. Graham and D. H. Tomlin, Nature **164**, 278 (1949) who find for the gamma-ray an energy of 82.7 kev.

lines although the energy difference between them is only 1.1 kev.

3. RELATIVE INTENSITIES OF ELECTRON LINES AND MULTIPOLE ORDER OF THE RADIATION

Relative intensities of the conversion electron lines were measured for the five isomeric transitions studied. Corrections to the observed densities were made for fog, density-exposure, and for differences in film sensitivity for electrons of different energies. The resulting corrected values of relative intensities of electron lines is given in Table II and are to be considered only as approximate values.

For each of the five isomeric transitions the multipole order of the radiation was obtained by two independent methods. First, the half-life period of each element was checked with the reported value by observing the decay of the radiations from samples bombarded in the pile using an ion-chamber detector. These values of the half-life periods and the spectrograph values of the energies of the transitions were used together with Wiedenbeck's[20] curves to determine the multipole order of the radiation, assuming electric multipole radiation. Second, the ratio of the intensities of the K and L conversion electrons were used together with the theoretical curves of Hebb and Nelson[21] to find the multipole order of the radiation for each of the four isomeric transitions where both K and L conversions were observed.

Table III gives the values obtained for the multipole order assignments as well as a summary of the transition energy data. Axel and Dancoff[22] used some of these data in their recent analysis of isomeric transitions and reached similar conclusions.

The author wishes to express his deep appreciation of the advice and assistance generously given to him by the following: Professor Newell S. Gingrich, University of Missouri, and Professor M. Goldhaber, University of Illinois consultant to the Argonne National Laboratory, for suggesting the problem and for guidance throughout the investigation; Messrs. E. der Mateosian, R. D. Hill, C. O. Muehlhause, and S. B. Burson for many helpful discussions. To the O. M. Stewart Fund of the University of Missouri appreciation is expressed for financial support granted.

[20] M. L. Wiedenbeck, Phys. Rev. **69**, 567 (1946).

[21] M. H. Hebb and E. Nelson, Phys. Rev. **58**, 486 (1940).

[22] P. Axel and S. M. Dancoff, Phys. Rev. **76**, 892 (1949).

PHYSICAL REVIEW VOLUME 78, NUMBER 4 MAY 15, 1950

Cosmic-Ray Intensity Following a Solar Flare*

JAMES W. BROXON AND HOWARD W. BOEHMER
Department of Physics, University of Colorado, Boulder, Colorado

(Received January 30, 1950)

Continuous records of the cosmic-ray intensity measured by a heavily shielded, high pressure ion chamber, were obtained during and following an intense solar flare (of importance 3+) and a subsequent intense magnetic storm. No increase in $C-R$ intensity was observed at or near the time of the flare, such as have been observed by others on similar occasions. At the peak of the magnetic storm there was a decrease of about 1.5 percent in $C-R$ intensity, with full recovery requiring 2 or 3 days. Unshielded $C-R$ telescope readings of low accuracy are included. These indicate that there were no prolonged alterations in the intensity (without shielding) of magnitude much greater than 14 percent associated with either the flare or the storm.

1. INTRODUCTION

IN recent years there have been reported instances of changes in cosmic-ray intensity apparently associated with particular solar flares. For example, Forbush[1] reported that upon examination of 10 years of continuous records with ion chambers shielded by 11 cm Pb, three unusual increases were noted. These occurred on February 28 and March 7, 1942, and July 25, 1946. The first two consisted of sharp increases of about 7 percent which began within 18 minutes after radio fade-outs which were presumed to indicate solar flares. The third represented a sharp increase of about 15 percent beginning one hour after the commencement of a solar flare and fade-out. The peaks were very sharp, being represented on the graphs by only one or two points representing bi-hourly means, with the entire increase above indicated statistical deviations being represented by about 3 to 6 points. After a very few hours, the intensity returned to normal and not long afterward it dropped to some 7 or 8 percent subnormal in the first and third instances. The large subnormal dips followed a few hours after the sudden commencement of magnetic storms, and the upward return toward normal was slow, extending over several days. In the third case, the magnetic storm began 26.8 hours after the solar flare. The reliability of the observations of the

* The experimental work was supported in part by the ONR.

[1] S. E. Forbush, Phys. Rev. **70**, 771 (1946); 1942 increases reported also by I. Lange and S. E. Forbush, Terr. Mag. **47**, 331 (1942).

initial increases is augmented by the fact that they were recorded simultaneously at stations at geomagnetic latitudes 50° N, 78° N, and 48° S, though not on one at 1° S, while the decreases accompanying the magnetic storms were recorded at all four stations.

The 1942 increases were reported also by Duperier[2] in England, though the increase noted by him on February 28 appears to have depended upon a single reading and to have amounted only to about one percent. The increase in cosmic-ray intensity following the solar flare of July 25, 1946, was confirmed both by Dolbear and Elliot[3] and by Neher and Roesch.[4] Using twofold and threefold coincidence counters with hourly rates of 30,000 and 65,000 at Manchester, England, Dolbear and Elliot found an increase of about 17 percent above normal, with the peak between 18.00 and 18.30 GMT, or between 2 and 2.5 hours after commencement of the flare. After the magnetic storm which followed, they observed a decrease of about 8 percent below normal, with a slow recovery during more than a week. Neher and Roesch, by means of an unshielded electroscope at Mount Wilson Observatory, noted an increase of 18 percent following the flare. They found that the increase had largely subsided in about 10 hours, but that the intensity was still 1 or 2 percent above normal when the magnetic storm began, after which they noted the usual decrease. They concluded that while the cosmic-ray increase attained its maximum about two hours later than the visual flare, the two began at about the same time.

Very recently Forbush, Stinchcomb, and Schein[5] have reported very large increases in cosmic-ray intensity accompanying the solar flare of November 19, 1949. Using ion chambers shielded by 12 cm Pb, they observed increases beginning at 10^h 45^m GMT and rising to 43 percent above normal at 11^h GMT at low altitudes at geomagnetic latitudes 50° N and 80° N, with no increase at 11,000 ft. altitude at $\Phi=0°$. At Climax, Colorado, altitude 11,500 ft., they report that the intensity under similar shielding increased to about 180 percent above normal in 15 min. and remained at least 100 percent above normal for about an hour, decreasing "exponential-wise" to near normal in about 7 hours. According to a verbal report by Dr. W. O. Roberts, Dr. Muller of Wendelstein Solar Observatory in Bavaria reported in a letter to Allen Shapley that he observed a solar flare of importance 3 beginning at 10^h 29 on November 19, attaining a maximum at 10:34, and subsiding at 11:19. Thus these extraordinary increases in cosmic-ray intensity appear to have begun only about 16 minutes after the start of the flare and to have attained their maxima about 26 minutes after the flare maximum, while persisting some 6 hours after the flare had subsided.

While the findings are largely negative, it appears that in view of the observations mentioned above it might be of some interest to report on the indications of recording apparatus which was in operation at Boulder, Colorado, altitude 5400 ft., geomagnetic latitude 49° N, during the large solar flare (of importance 3+) of May 10, 1949; it is unfortunate that the apparatus was not in operation on November 19, since Boulder is only about 65 miles from Climax and at nearly half its altitude.

According to a report by Dodson,[6] the flare of May 10, as observed at McMath-Hulbert Observatory, increased very suddenly in brightness, the principal outburst starting at 20^h 02^m, reached a maximum at 20^h 11^m, and was still bright at 22^h 20^m. At the maximum, the brightest regions had 4 times the intensity of the undisturbed $H\alpha$-disk. Shapley and Davis[7] of the National Bureau of Standards reported concurrent bursts of radio noise. They stated that maxima were attained between 20:10.5 and 20:12.5, and that the intensity of the noise burst was about 290 times the normal energy output of the entire disk of the quiet sun on 160 megacycles, while on 480 megacycles it was probably 1000 times the background radiation.

Schein[8] has reported that during a balloon flight on May 11 an increase of 50 percent occurred in the rate of nuclear disintegrations at 95,000 ft. He attributed this unusual increase to the large solar flare observed "a few hours before the balloon flight took place."

2. EXPERIMENTAL PROCEDURE

The ionization-chamber measurements at Boulder were made with the same equipment, slightly modified, that was used in the measurements of a decade earlier. The thick-walled steel chamber was shielded not only by 5 inches of lead immediately surrounding it, but also by the building in whose basement it was maintained at constant temperature. It has been estimated[9] that the shielding afforded by the chamber walls and surrounding lead were roughly equivalent to 18 cm of lead, while that afforded by the building amounted to some 15 cm of lead for any direction and more than 40 cm for certain directions. In place of the air at 160 atmospheres used earlier, the ion chamber was filled with argon at 20 atmospheres for the recent observations. This yielded about the same cosmic-ray ionization current as the air at the higher pressure. The electrometer sensitivity was also increased somewhat so that bursts of 1.2×10^6 ion pairs produced deflections of 1 mm on the photographic record and were regularly read.

[2] A. Duperier, Proc. Phys. Soc. London **57**, 464 (1945).
[3] D. W. N. Dolbear and H. Elliot, Nature **159**, 58 (1947).
[4] H. V. Neher and W. C. Roesch, Rev. Mod. Phys. **20**, 350 (1948).
[5] Forbush, Stinchcomb, and Schein, Bull. Am. Phys. Soc. **25**, 15 (1950).
[6] H. W. Dodson, Astrophys. J. **110**, 382 (1949).
[7] A. H. Shapley and R. M. Davis, Jr., Science **110**, 159 (1949).
[8] M. Schein, Science **111**, 16 (1950).
[9] J. W. Broxon, Phys. Rev. **72**, 1187 (1947).

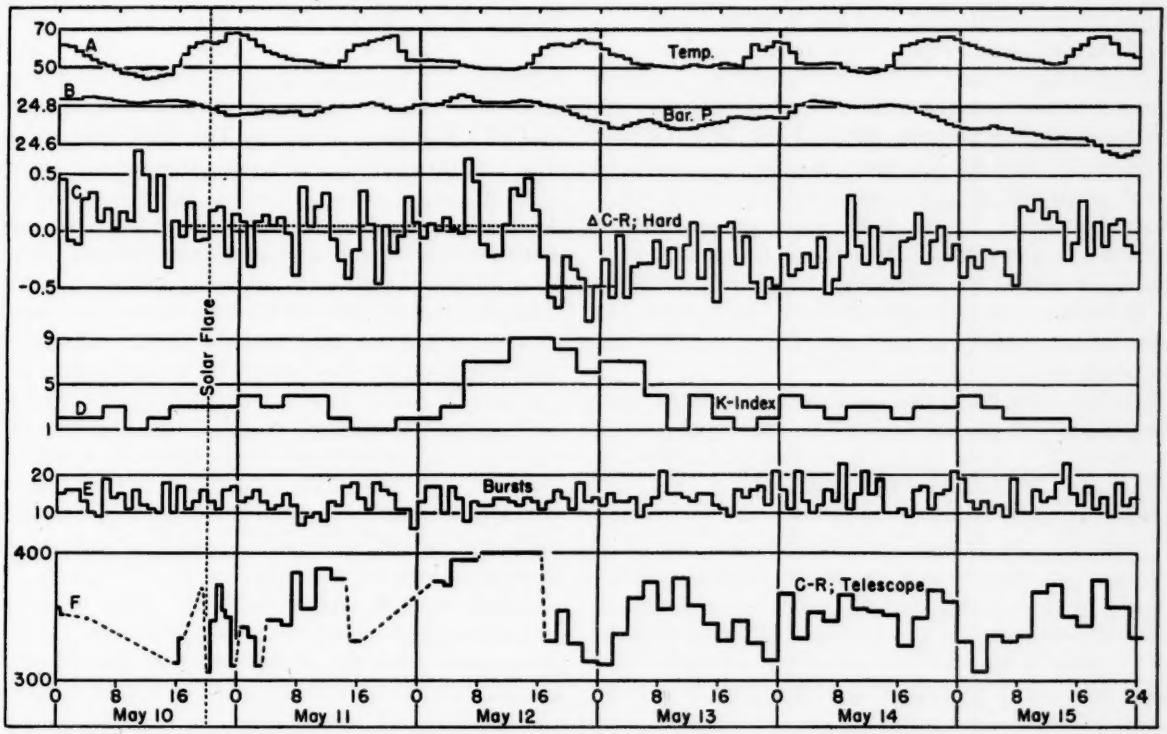

FIG. 1. For all curves the horizontal axis represents GMT. *Curve A* shows hourly average values of the out-door temperature in °F. *Curve B* shows hourly average values of the barometric pressure in inches of mercury. *Curve C* shows (as positive values) hourly average values of the excess of cosmic-ray ionization current over the steady compensating current, expressed in ion pairs per cc of the $C-R$ ion chamber per sec. This curve has been corrected for bursts and for barometric variations. *Curve D* shows magnetic K-indices at Cheltenham for successive 3-hour intervals. *Curve E* shows the number of bursts observed in each hour (59-minute collection interval) including all bursts greater than or equal to 1.2×10^6 ion pairs. *Curve F* shows the number of counts per hour with the telescope axis directed vertically or corrected for azimuth angle, but with no other corrections.

3. DISCUSSION

The data are represented in Fig. 1 for the (GMT) days May 10 to May 15, 1949, inclusive. Curve A, representing hourly means of out-door surface temperature in °F, shows that there were no unusual temperature changes. Curve B, representing hourly means of barometric pressure in inches of Hg, shows that the changes in barometric pressure were rather small and gradual. Hourly means of the excess of the cosmic-ray ionization current over the steady compensating current provided in an auxiliary chamber by gamma-rays from a radium capsule, expressed in ion-pairs per cc of the cosmic-ray ion chamber per sec., are designated in curve C. The values represented here were corrected for bursts (1 mm and greater) and for variations in barometric pressure. The analysis of data being in its initial stages, the barometric coefficient with the present set-up has not been fully investigated; a weighted average coefficient based on daily averages during a period of 10 months was employed.

The ion-chamber readings do not indicate any change (apart from the usual statistical fluctuations) at the time of the intense solar flare nor soon thereafter. Beginning at 17^h on May 12, 45 hours after the solar flare, there appears to be a definite decrease in $C-R$ intensity lasting several hours. For purposes of comparison, averages were determined for the 48-hour period from 16^h May 10 to 16^h May 12, and for the 9-hour period from 17^h May 12 to 2^h May 13. These averages are represented by dotted lines extending over the specified intervals in curve C. The difference between these averages indicates a decrease of 1.5 percent of the estimated average $C-R$ intensity for the 9-hour interval. The difference was found to be 3 times the standard deviation of the hourly values from the average for the 9-hour interval, but only 2.3 times the standard deviation for the 48-hour interval. It seems significant, however, that the $C-R$ intensity appears to have remained somewhat depressed for quite a long time. During the interval of 41 hours from 16^h May 12 to 9^h May 14, the $C-R$ current rose to the average value for the 48-hour interval preceding 16^h May 12 during only 3 hours, and then only barely so. In fact, curve C provides some indication that the pre-depression average may not have been fully attained until about 64 hours after the depression began.

That the decrease in $C-R$ intensity which began 45 hours after the solar flare was much more closely associated with an intense magnetic storm is shown by curve D. In this are shown the K-indices for successive 3-hour intervals determined at the Cheltenham (Maryland) Magnetic Observatory and supplied by the U. S. Coast and Geodetic Survey. A moderate storm is represented by K-index = 5, while moderately severe

storms are represented by 6 or 7, and severe storms by 8 or 9. According to a report from the Tucson (Arizona) Magnetic Observatory, the storm represented by curve *D* had a sudden commencement at $6^h\ 41^m$ on May 12, had its maximum between 15^h and 18^h May 12, and ended at 7^h May 13. (A storm is considered to have ended when the *K*-index remains at 2 or less for a reasonable period, so the storm seems to have ended earlier at Tucson than at Cheltenham.) The range of *H* during the storm was 552γ at Tucson. The decrease in $C-R$ intensity is thus seen to have begun about 11 hours after the storm started and while the storm was at or near its peak.

Because solar flares are commonly associated with sunspots, as was the one of May 10, and because these are often followed by magnetic storms as was the case here, it may be of interest to compare the observations in this particular instance with the results of a statistical investigation by Broxon[10] of the relation of $C-R$ intensity to sunspots and magnetic disturbances by Chree's method of superposed epochs. Employing data obtained during a year and a half in 1938 and 1939, he found statistically that pulses in $C-R$ intensity were associated with inverse pulses in magnetic character and in sunspot area. The peaks of the $C-R$ pulses were found to lag the peaks of the inverse magnetic-character pulses by rather less than a day, while lagging the peaks of the inverse sunspot-area pulses by some 3 or 4 days. The peaks of the $C-R$ pulses represented deviations of about 0.6 or 0.7 percent from the average. $C-R$ disturbances accompanying magnetic disturbances have, of course, been recognized for quite a long while.[11] An interesting fact in this connection is that Duperier[2] observed a decided dip of 8 percent in $C-R$ intensity in England on March 27, 1945, when there was no magnetic storm.

Since many bursts were observed with the ion chamber, it was thought worth noting whether the rate of occurrence of these was affected by the flare or the following magnetic storm. Curve *E* represents the total number of bursts observed in each hour (actually 59 minutes of collection time) during the 6-day interval. The majority of the bursts were small ones, of course, near the lower limit of 1.2×10^6 ion pairs. The burst-frequency curve does not appear to show any particular response either to the flare or to the magnetic storm. Nothing noteworthy was detected with regard either to the frequency or magnitude of large bursts.

Because the ion chamber was heavily shielded, it is worth mentioning some readings taken concurrently with an unshielded $C-R$ telescope, even though this was not designed for the present purpose and the readings are consequently quite inaccurate. The telescope was mounted in a light wooden structure on the roof of a four-story building. The telescope was dual, with its arm shifting at intervals from zenith angles of 0° to 75° in 15° steps, provisions being made for independently recording (simultaneously) triple coincidences with no shielding and with two different amounts of shielding. Factors for reducing counting rates at different zenith angles to 0° were found by operating the equipment for long periods. These differed considerably from the $\cos^{-2}$ law only at the largest angle.

Curve *F* shows the number of counts per hour (reduced to the vertical) obtained with one arm of the telescope and no shielding during the 6 days. Readings given by the other arm were not included because of an apparent instability yielding obviously high and erratic readings; the arm employed appeared to be functioning normally. Because the shifting mechanism was not operating entirely satisfactorily, recordings represented somewhat varying time intervals. These are shown by the length of the line representing the mean counting rate in each interval. Because the camera did not function properly at times, there are gaps in the record indicated by dotted lines. The recorded values have not been corrected for barometric variations or anything but zenith angle. It will be noted that there was very little variation in barometric pressure during the first three days, and only the usual diurnal variations in temperature.

The unshielded telescope does not provide any clear indication of a change in $C-R$ intensity at the time of the solar flare nor soon thereafter. There do appear to be somewhat abnormally high values during the first two-thirds of May 12, followed by a decrease at 17^h on that day. The decrease is not to abnormally low values, however. Also the two longest readings at the highest values were at 75° zenith angle. The triple-coincidence rate is so small and the statistical fluctuations consequently so large that $C-R$ variations of a few percent could not have been detected reliably. Since the extreme variations during the 6-day interval were a little less than 14 percent from the mean of the extremes, it appears that any increase much greater than this and closely following the solar flare would have been detected, since the telescope was functioning at that time.

Aid was also provided by the Graduate School's Council on Research and Creative Work.

[10] J. W. Broxon, Phys. Rev. **62**, 508 (1942).

[11] A. Corlin, Lund Obs. Cir. No. 1 (1931) and No. 4 (1934); Broxon, Merideth, and Strait, Phys. Rev. **44**, 253 (1933); W. Messerschmidt, Zeits. f. Physik **85**, 332 (1933); J. W. Broxon, Terr. Mag. **39**, 121 (1934); V. F. Hess and A. Demmelmair, Nature **140**, 316 (1937); S. E. Forbush, Phys. Rev. **51**, 1108 (1937); J. Clay and E. M. Bruins, Physica **5**, 111 (1938) and K. Amsterdam Proc. **41**, 215 (1938); T. H. Johnson, Terr. Mag. **43**, 1 (1938); V. F. Hess, A. Demmelmair and R. Steinmaurer, Terr. Mag. **43**, 7 (1938); W. Kolhorster, Naturwiss. **26**, 159 (1938); S. E. Forbush, Phys. Rev. **54**, 975 (1938).

Note added March 18, 1950: We have just received copies of papers by J. Clay, H. F. Jongen and A. J. Dijker [Koninklijke Nederlandsche Akad. V. Wetenschappen, Proc. **LII**, 897–914 and 923–926 (1949)] in which they report numerous correlations of $C-R$ fluctuations associated with solar flares, e.g., 30 cases of considerable increase (some extending to 3 or 5 percent) and 30 smaller ones during the year 1947, alone. For the intense solar flare of May 10, 1949, however, they observed no $C-R$ effect in a chamber shielded with 110 cm Fe, and an increase of only 1 percent in an unshielded chamber.

A Note on the Centrifugal Stretching in Axially Symmetric Molecules

HARALD H. NIELSEN
Mendenhall Laboratory of Physics, Ohio State University, Columbus, Ohio
(Received February 1, 1950)

It is demonstrated that the degenerate Coriolis splitting of a rotational level, $K\neq 0$, of a molecule which is in an excited perpendicular vibration state is influenced by centrifugal distortion. The effect is of the form $a\,K^3+bJ(J+1)K$. The effect of this distortion on the infra-red spectrum is of the same order of magnitude as the ordinary centrifugal distortion. It is further shown that by redefining the Coriolis coupling coefficient ζ_t the rotational energy of a symmetric molecule may be written in the form $(E/hc)=[J(J+1)-K^2]B_v+L^2C_v-[J(J+1)-K^2]^2D_J-[J(J+1)-K^2]L^2D_{JL}-L^4D_L$ where $L=K-\Sigma_t l_t\zeta_t^{(z)}$.

THE problem of centrifugal stretching of axially symmetric molecules in their normal vibration states has been dealt with by Slawsky and Dennison.[1] They have also made estimates of the magnitudes of the centrifugal distortion coefficients D_J, D_{JK}, and D_K for molecules of the variety CH_3X. It is known that the coefficients D must vary with the vibration quantum numbers. This variation is, however, small in general and it has been the practice to set the D_v equal to the equilibrium value D_e. The centrifugal distortion of a molecule for a given set of rotational quantum numbers would then be the same in the excited vibration states as in the normal vibration state when this simplification is made. It is the purpose of this note to point out that this is not actually so in an axially symmetric molecule when its perpendicular vibrations are excited.

The terms in the energy which represent the centrifugal distortion originate with a second-order perturbation calculation of the first-order corrections to the moments of inertia and the products of inertia of a molecule and may be written:

$$H^{(1)}=\cdots-\tfrac{1}{2}\sum_{s\sigma}(\hbar^2/\lambda_s)^{\frac{1}{2}}\times\{\sum_{\alpha\beta}a_{s\sigma}{}^{(\alpha\beta)}(P_\alpha P_\beta/I_{\alpha\alpha}{}^{(e)}I_{\beta\beta}{}^{(e)})\}q_{s\sigma},\quad(\alpha,\beta=x,y,z),\quad(1)$$

where the $a_{s\sigma}{}^{(\alpha\alpha)}$ are the quantities $a_{s\sigma}$, $b_{s\sigma}$, etc., and the $a_{s\sigma}{}^{(\alpha\beta)}$ the $-d_{s\sigma}$, $-e_{s\sigma}$, etc., defined in an earlier work[2] and where $\lambda_s=4\pi^2c^2\omega_s^2$. These give rise to second-order terms proportional to $P_\alpha P_\beta P_\gamma P_\delta$ which yield energy contributions which, in general, depend upon the fourth power of the rotational quantum numbers.

There occur terms in the second-order Hamiltonian for a molecule of the form

$$H^{(2)}=\cdots\sum_{s\sigma}(\hbar^2/\lambda_s)^{\frac{1}{2}}\{\sum_{\alpha\beta}a_{s\sigma}{}^{(\alpha\beta)}(p_\alpha P_\beta/I_{\alpha\alpha}{}^{(e)}I_{\beta\beta}{}^{(e)})\}q_{s\sigma},\quad(2)$$

where p_α will be

$$\sum_{s'\sigma'}\sum_{s''\sigma''}\zeta^{(\alpha)}_{s'\sigma's''\sigma''}[(\lambda_{s''}/\lambda_{s'})^{\frac{1}{2}}q_{s'\sigma'}p_{s''\sigma''}-(\lambda_{s'}/\lambda_{s''})^{\frac{1}{2}}q_{s''\sigma''}p_{s'\sigma'}]$$

in which the $\zeta^{(\alpha)}_{s'\sigma's''\sigma''}$ are the Coriolis coupling coefficients. These are the first-order corrections to the Coriolis contribution or the second-order Coriolis terms which, in general, do not contribute to the energy in second order of approximation. An exception to this rule occurs, however, in the case of a perpendicular vibration which in an axially symmetric molecule is twofold degenerate. In this event $s'=s''$ and $\lambda_{s'}=\lambda_{s''}$. It is then convenient to replace $q_{s'1}$ and $q_{s'2}$ by $r_{s'}\cos\chi_{s'}$ and $r_{s'}\sin\chi_{s'}$, respectively.

The solution to the two dimensionally isotropic oscillator in quantum mechanics has been studied by Dennison[3] and by Shaffer[4] and the solution is known to be of the form $\psi=e^{\pm il\chi}R_v(r)$, where $R_v(r)$ is a function of r only which may be expressed in terms of the associated Laguerre polynomial. The quantum number v is the total vibration quantum number and l is a quantum number signifying the angular momentum associated with the vibration state which takes the values v, $v-2$, $v-4$, $\cdots 1$ or 0. The operator p_z, when $q_{s'\sigma'}$ and $p_{s'\sigma'}$ have been replaced by their equivalents in $r_{s'}$ and $\chi_{s'}$, will contain a term

$$-i\hbar\sum_{s'}\zeta_{s'}{}^{(z)}\partial/\partial\chi_{s'}$$

and then (2) becomes of the same order of magnitude as (1) in the states where $l_{s'}$ is different from zero. It is, therefore, an advantage to include the portions of (2), each of which depends upon a single twofold degenerate frequency with $H^{(1)}$ before carrying out the perturbation calculation which yields the centrifugal distortion. When this is done, we have:

$$H^{(1)}=\cdots-\tfrac{1}{2}\sum_{s\sigma}(\hbar^2/\lambda_s)^{\frac{1}{2}}\{\sum_{\alpha\beta}a_{s\sigma}{}^{(\alpha\beta)}(P_\alpha-2p_\alpha{}^*)P_\beta/I_{\alpha\alpha}{}^{(e)}I_{\beta\beta}{}^{(e)}\}q_{s\sigma}.\quad(3)$$

The perturbation calculation is straightforward and leads to the following terms which are diagonal in K and $l_{s'}$ in addition to the usual ones which depend upon the fourth power of the rotational quantum numbers.

$$hc\sum_{s'}l_{s'}\zeta_{s'}{}^{(z)}\{(4D_K+2D_{JK})K^3+2(2D_J+D_{JK})J(J+1)K\}.\quad(4)$$

[1] Z. I. Slawsky and D. M. Dennison, J. Chem. Phys. **7**, 509 (1939).
[2] H. H. Nielsen, Phys. Rev. **60**, 794 (1941).
[3] D. M. Dennison, Phys. Rev. **41**, 304 (1932).
[4] W. H. Shaffer, Rev. Mod. Phys. **16**, 245 (1944).

The relation (4) shows that the centrifugal stretching now depends also upon the third power of the rotational quantum numbers. This is tantamount to stating that not only the positions of the centers of gravity of the two components into which a rotation level of a molecule in an excited perpendicular vibration state where $K\neq 0$ is split by the degenerate Coriolis forces, but the actual splitting itself is influenced by the centrifugal forces. This is, what might be expected, of course, if the centrifugal distortion is regarded as the effect of the change of the moment of inertia by the rotational motion itself. It may be seen further that the effect upon the infra-red spectrum will be of the same order of magnitude as will the usual centrifugal distortion effects. The terms here described are proportional to l_s'. In the normal vibration state $l_{s'}=0$. The terms will therefore be zero in the normal state, but will occur in a state where $l_{s'}\neq 0$. The position of a line in a perpendicular band in the spectrum is the difference of a spectral term in the excited state where $l_{s'}\neq 0$ and a term level in the normal state where $l_{s'}=0$. The effect upon the spectrum is, therefore, proportional to the third power of the rotational quantum numbers just as is the effect due to the usual centrifugal distortion. It has already been pointed out by Nielsen[5] that this effect is measurable and necessary to explain the positions of lines in the microwave spectrum of symmetric molecules.

It may be regarded as convenient to combine the contribution (4) with the usual energy of a symmetric molecule. This may be done in the following manner. The energy is normally written

$$(E/hc)=(E_{\text{vib}}/hc)+[J(J+1)B_v+K^2(C_v-B_v)]\pm 2K\sum l_{s'}\zeta_{s'}^{(z)}\bar{C}_v-D_JJ^2(J+1)^2-D_{JK}J(J+1)K^2-D_KK^4, \quad (5)$$

where[6]

$$B_v=B_e-\sum_s \alpha_s(v_s+g_s/2), \quad C_v=C_e-\sum_s \gamma_s(v_s+g_s/2),$$

$$\bar{C}_v=C_e-\sum_s \bar{\gamma}_s(v_s+g_s/2), \quad B_e=(h/8\pi^2 I_{xx}^{(e)}c)$$

and $C_e=h/8\pi^2 I_{zz}^{(e)}c$. The constant $\bar{\gamma}_s$ is equal to

$$\gamma_s+\sum_{s''}(C_e^2/\omega_s)[(3\lambda_s+\lambda_{s''})/(\lambda_s-\lambda_{s''})](\zeta_{ss''}^{(z)}{}_{s''})^2.$$

[5] H. H. Nielsen, Phys. Rev. **77**, 130 (1950).
[6] H. H. Nielsen, Phys. Rev. **70**, 184 (1946).

The coefficient $\bar{C}_v$ may be replaced by C_v in (5) if we set

$$\sum_{s'} l_{s'}(\zeta_{s'}^{(z)})_v C_v=\sum_{s'} l_{s'}\zeta_{s'}^{(z)}\bar{C}_v.$$

One obtains then for $(\zeta_{s'}^{(z)})_v$

$$(\zeta_{s'}^{(z)})_v=\zeta_{s'}^{(z)}\{1-2\sum_{s\sigma}\sum_{s''\sigma''}(C_e/\omega_s g_s)\times[(3\lambda_s+\lambda_{s''})/(\lambda_s-\lambda_{s''})]\times(\zeta_{ss''}^{(z)}{}_{\sigma''})^2](v_s+g_s/2)\}. \quad (6)$$

The vibration energy contains the constants $xl_{s'}l_{s'}$ and $xl_{s'}l_{s'''}$. These in turn are proportional to $(l_{s'}\zeta_{s'}^{(z)})^2C_e$ and $(l_{s'}l_{s'''}\zeta_{s'}^{(z)}\zeta_{s'''}^{(z)})C_e$. We may to this approximation replace these by $[l_{s'}(\zeta_{s'}^{(z)})_v]^2C_v$ and $[l_{s'}l_{s'''}(\zeta_{s'}^{(z)})_v\times(\zeta_{s'''}^{(z)})_v]C_v$. The rotational energy may now be written in the form

$$(E_{\text{rot}}/hc)=[J(J+1)-K^2]B_v+L^2C_v-[J(J+1)-K^2]^2D_J-[J(J+1)-K^2]L^2D_{JL}-L^4D_L \quad (7)$$

if the portion of $xl_{s'}l_{s'}$ and $xl_{s'}l_{s'''}$ which depends upon $(\zeta_{s'}^{(z)})^2$ and $\zeta_{s'}^{(z)}\zeta_{s'''}^{(z)}$ is included with the rotational energy. The number L will in general not be quantized and will be equal to

$$L=K-\sum_{s'} l_{s'}(\zeta_{s'}^{(z)})_v.$$

The new centrifugal distortion coefficients D_{JL} and D_L may be shown to be expressible in terms of the usual D_{JK} and D_K as

$$D_{JL}=2D_J+D_{JK}, \quad D_L=D_J+D_K+D_{JK}. \quad (8)$$

It is of interest to note that for a linear molecule where the Sayvetz[7] condition demands that

$$K=\sum_{s'} l_{s'}\zeta_{s'}^{(z)},$$

i.e., $L=0$, the relation (8) becomes exactly that for a linear molecule.

The author wishes to express his gratitude to the Guggenheim Memorial Foundation for a fellowship which has permitted him to work at Cambridge University, England. He is grateful to his many friends here also who have made facilities available to him, in particular the excellent Faculty of Mathematics and Philosophical Library.

[7] A. Sayvetz, J. Chem. Phys. **7**, 282 (1939).

Isotope Shift in the Spectrum of Neutral Lead*

THURSTON E. MANNING,† C. E. ANDERSON, AND W. W. WATSON
Sloane Physics Laboratory, Yale University,‡ New Haven, Connecticut

(Received February 6, 1950)

The isotope shift and the Pb^{207} h.f.s. in nine of the strongest PbI lines in the violet and ultraviolet regions have been measured, using material enriched in the 204 isotope. For all lines with measurable structure the 204–206 interval is less than the 206–208 interval. In the resonance line λ2833 and in λ3639, for both of which the measurements are almost completely unaffected by superposed h.f.s., the ratio of the 204–206 to the 206–208 interval is 0.89 and 0.82 respectively. The average of our observations and others for the staggering of the center of gravity of the 207 components for all lines is about 0.63 for the ratio of the 206–207 and 207–208 intervals. Isotope splitting of about 0.050 cm^{-1} in the $6p6d$ levels contributes further evidence of perturbations by $6p7s$ and $6p8s$ levels. The staggering is discussed in terms of Breit's theory of polarizability of nuclei by electrons. These Pb isotope shifts indicate decreasing nuclear stability in the progression 204 to 208.

1. INTRODUCTION

THE arc spectrum of ordinary lead, as well as radiogenic lead, has been well examined to determine the wave-lengths of the line components from the three most abundant stable isotopes of masses 206, 207, and 208.[1–3] The fourth stable isotope of mass 204 comprises only 1.5 percent of natural lead, and is not the end product of a natural radioactive series; hence the examination of its spectrum is extremely difficult if natural lead is used. Despite this, Schüler and Jones[3] succeeded with long exposures in photographing the 204 component in a few PbI lines in the visible region. Since other workers have not been able to confirm their results, using ordinary lead, and since there is considerable interest in the staggering phenomenon in the isotope splittings in the spectral lines of the heavy elements, we decided to examine the structure of some of the Pb lines, using Pb^{204} enriched material in the source.

This lead, in the form of lead sulfate, enriched in the light isotopes by the electromagnetic process,[4] has the following isotopic composition as compared to ordinary lead:

Mass:	204	206	207	208
Ordinary Pb:	1.5%	23.6%	22.6%	52.3%
Enriched Pb:	27.0%	33.7%	16.2%	23.1%

These changes in the relative abundances of the four Pb isotopes have proved to be just about ideal for the examination of the structure of the Pb lines. Because of the necessity of using this lead sulfate sparingly, however, good measurements could be made only on the stronger Pb arc lines.

2. EXPERIMENTAL PROCEDURE

Two forms of Schüler lamp have been employed. Of necessity these are constructed with small hollow cathodes and other features to minimize consumption of the lead sulfate and to facilitate later recovery of this material. One of our sources was modified from a design given by Schüler and Gollnow.[5] It is a horizontal, water-cooled lamp, having a cavity $\frac{1}{2}$ in. deep and $\frac{3}{16}$ in. in diameter in the Al cathode. The circulating helium gas is led through radial canals near the opening to this cavity so as to tend to form a "gas window" over the hollow, thus retaining the lead material in the cavity. The other source is of the vertical type, also having the essential small cavity in the cathode and the "gas window," and is operated immersed in liquid nitrogen or in a dry ice-aceton mixture. For a heavy atom such as lead, this low temperature source to decrease the Doppler broadening of the lines is needed only when working in the ultraviolet.

The helium sustaining the discharge was circulated continuously through the lamp and a liquid-nitrogen-cooled charcoal trap, at a pressure of about 1 to 2 mm of Hg. Powered by a 1000-volt d.c. generator, the current through the lamp was held to the range 200–400 ma, or always under "condition A" of Rose and Granath.[1]

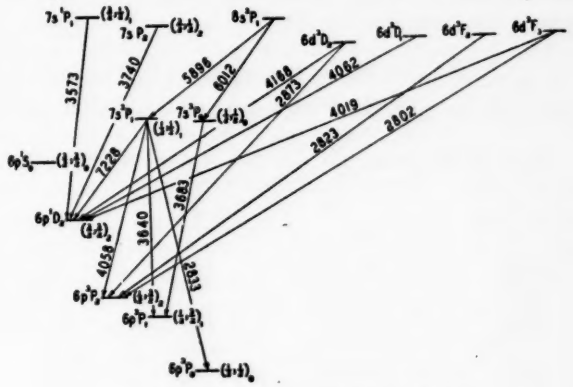

FIG. 1. Low lying energy levels of PbI.

* A portion of this research constituted a part of a dissertation submitted by T.E.M. to the Faculty of the Graduate School of Yale University in partial fulfillment of the requirements for the degree of Doctor of Philosophy.

† Now at Oberlin College, Oberlin, Ohio.

‡ Assisted by the AEC.

[1] J. L. Rose and L. P. Granath, Phys. Rev. **40**, 760 (1932).

[2] H. Kopfermann, Zeits. f. Physik **75**, 363 (1932).

[3] H. Schüler and E. J. Jones, Zeits. f. Physik **75**, 563 (1932).

[4] Sample allocated by the Isotopes Division, U.S. AEC.

[5] H. Schüller and H. Gollnow, Zeits. f. Physik **93**, 611 (1935).

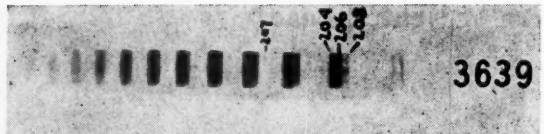

FIG. 2. Typical Pb line-patterns. The 208 components are on the high frequency side.

Our exposure times varied from 10 to 30 minutes. The success of the methods used to conserve the material placed in the cathode is indicated by the fact that over 30 hours of operation were possible with a charge of 25 mg of lead sulfate in the cavity, after which time the material could be recovered from the anode and other parts of the lamp where it had been carried by the action of the discharge.

To resolve the close isotope components, spaced from each other in these Pb lines by 0.06 to 0.08 cm^{-1}, we have used a Hilger quartz Lummer-Gehrcke interferometer having dimensions 200 mm×30 mm×7.34 mm. The interferometer was mounted in parallel light. The fringes formed by the extraordinary ray in the quartz were isolated for wave-lengths longer than 4000A by the use of a Nicol prism placed in the optical train before the Lummer plate, while for shorter wave-lengths by just the double refraction of the quartz together with the correct angle of inclination of the interferometer. For auxiliary dispersion a Hilger E-1 quartz spectrograph was used.

The photographed fringes were measured with a comparator, and some of the values of the intervals so obtained were checked with microdensitometer traces of the fringe systems. Behrens' method[6] for the reduction of Lummer-plate fringes was used. It is believed that our results have a probable error of about 0.005 cm^{-1}.

TABLE I. Isotope splittings for PbI lines in the ultraviolet.

Wave-length A.	Levels	$\Delta\nu_{208-206}$ cm^{-1}	$\Delta\nu_{206-204}$ cm^{-1}
4058	$6p^3P_2-7s^3P_1$	0.080	0.068
3740	$6p^1D_2-7s^3P_2$	0.080	0.068
3683	$6p^3P_1-7s^3P_2$	0.074	0.070
3640	$6p^3P_1-7s^3P_1$	0.084	0.069
3573	$6p^1D_2-7s^1P_1$	~0.08	~0.07
2873	$6p^3P_2-6d^3D_2$	~0.05	~0.05
2833	$6p^3P_0-7s^3P_1$	0.081	0.072
2823	$6p^3P_2-6d^3F_2$	~0.05	~0.05
2802	$6p^3P_2-6d^3F_3$	~0.05	~0.05

3. RESULTS

In Fig. 1 are sketched the low lying levels of PbI and we indicate all the transitions mentioned in our discussion. Although it is customary to designate these levels with *LS* notation, it should be remembered that the coupling of the two outer electrons is almost pure *jj*. We display in Table I the average values of all our measurements on the intervals between the three even-isotope components for nine of these lines. Except for the three lines λλ2873, 2823, and 2802 originating in levels of the $6p6d$ configuration, and for which the resolution is insufficient to make accurate measurement, it is seen that the 206–204 interval is smaller than the 208–206 interval. The average ratio of the 206–204 interval to the 208–206 interval for the six lines representing transitions between levels of the $6p7s$ configuration to levels of the ground state $6p^2$ is 0.87. A few of our typical fringe systems are shown in Fig. 2. In all cases the 208 component is on the high frequency side.

Because of either the low intensity or partial fusion with even-isotope components, it is possible to measure the complete Pb^{207} h.f.s. pattern for only three of these lines. Our measurements of the intervals from the 207 components to the 208 component in each case are listed in Table II. We also list in Table III the center of gravity of the 207 components not only for these three lines but also the obviously good measurements for λ7228 (Schüler) and for λ3640 (Rose and Granath). The marked staggering of the 207 position in the succession of isotope components is indicated by the ratios of the 206–207 to the 208–207 intervals which average to about 0.63 for all the lines excluding λ3683.

In general our values of the 208–206 intervals agree with the earlier measurements of others except for

TABLE II. Pb^{207} hyperfine structure intervals from Pb^{208} component (cm^{-1}).

λ	Intensity ratios	$\Delta\nu_{208-207a}$	$\Delta\nu_{208-207b}$	$\Delta\nu_{208-207c}$
4058	5, 1, 9	+0.224	+0.098	−0.216
3683	1, 2	+0.156	−0.130	
2833	1, 2	−0.345	+0.098	

TABLE III. Interval of center of gravity of Pb^{207} h.f.s. components from Pb^{208} component (cm^{-1}).

λ	$\Delta\nu_{208-207}$	$\Delta\nu_{206-207}/\Delta\nu_{208-207}$	Obs. by
7228	−0.055	0.63	Schüler
4058	−0.048	0.66	present authors
3683	~−0.035	1.11	present authors
3640	−0.052	0.62	Rose and Granath
2833	−0.050	0.62	present authors

[6] D. J. Behrens, J. Sci. Inst. 18, 239 (1941).

λλ4058, 3683 and 3740. For the last two of these lines there is obvious over-lapping of 207 components with those from 208 and 206. Since the isotopes have been changed in relative abundance in our lead, the apparent intervals would be expected to differ some. With ordinary lead we do obtain the same 208–206 interval as the others for λ3683. We agree with Murakawa[7] but not with Kopfermann[2] in our measurements of the Pb^{207} h.f.s. pattern for λ4058, and judging from our spectrograms in which λ4062 is visible we do not believe that there is any interference from this much weaker line. The two 207 components of λ3683 are completely resolved, but owing to their very low intensity (lower than one would expect from the relative abundance of Pb^{207}), the accuracy of measurement is decreased to such an extent that we must take the 208–207 interval of -0.035 cm^{-1} as only an approximate value. Although for λλ2873, 2823, and 2802 the components are not quite resolved, our observation that the 208–206 and 206–204 intervals are about 0.050 cm^{-1} is of some interest in connection with our discussion below.

4. DISCUSSION

In order to establish term splittings from these observed isotope shifts of the spectral lines it is necessary to choose arbitrarily a level of zero splitting. One can with good reason assume that the $6p^2\ {}^1D_2$ level shows no splitting,[8] for both of the $6p$ electrons are $p_{3/2}$. Then the large splittings occur in the levels of the $6p7s$ configuration with the Pb^{208} component levels lying highest. The splittings in the $6p^2\ {}^3P_{0,1,2}$ levels are all about 0.01 cm^{-1} in the same sense, and our observation that the splittings in λλ2873, 2823 and 2802 are about 0.050 cm^{-1} indicates then that the $6p6d$ levels have also a sizeable splitting of about 0.060 cm^{-1}. This is in good agreement with the measurements of Kopfermann,[2] who found 208–206 splittings of 0.063, 0.062, and 0.061 cm^{-1} in λλ4019, 4062, and 4168 respectively. The observation by Schüler and Jones[3] that λλ5896 and 6012 exhibit a 208–206 splitting of about 0.015 in the opposite sense indicates that the $6p8s\ {}^3P_1$ level has the same isotope splitting as the $6p7s$ levels, but smaller in magnitude by 0.015 cm^{-1}.

It has been remarked by Breit[8] that the size of this isotope splitting in terms of the $6p6d$ configuration is surprising and that it may perhaps be an indication of perturbations of these terms by the $6p7s$ and $6p8s$ configurations. Other evidence for the existence of perturbations between these terms is (a) irregularities in the quantum defect *vs.* n plot for these lowest d terms,[9] (b) in the series of terms beginning with $7s$ the terms $ns\ {}^3P_0$ lie above the terms $ns\ {}^3P_1$ with the exception of the $8s$ terms where the reverse is true,[9] and (c) intensity anomalies in the lines involving transitions from these $6p6d$ terms down to the $6p^2$ terms.

The relative isotope shifts for one of the heavy elements such as lead are known to be approximately explained by the nuclear volume effect theory[8,10–13] According to Breit, Arfken, and Clendenin,[14] the staggered position of the center of gravity of the Pb^{207} components can be explained, at least qualitatively, as due to the greater polarizability of this odd nucleus than the even 204, 206 nuclei by the penetrating $s_{\frac{1}{2}}$ and $p_{\frac{1}{2}}$ electrons not in closed shells. Breit *et al.* further suggest that the smallness of the observed isotope shifts such as these in neutral Pb and departure from regular spacings for even isotopes may perhaps be in part attributable to this polarization of the nucleus.

Since Pb^{208} has the high stability associated with two of the "magic numbers" 82 and 126, at first thought one would say that the order of nuclear stability is $Pb^{208} > Pb^{206} > Pb^{204}$. But then from nuclear volume effect alone the 204–206 isotope shift should be greater than the 206–208 shift. Calculation of the relative binding energy of successive nucleons in nuclei in this region of the periodic table indicates,[15] however, that the order of nuclear stability from the point of view of changes in binding energy per nucleon may indeed be $Pb^{204} > Pb^{206} > Pb^{208}$. This suggests that the volume effect might be an important factor in producing the observed shifts of the line components from the even Pb isotopes.

We wish to thank Professor Breit for his most helpful suggestions and comments.

[7] K. Murakawa, Zeits. f. Physik **72**, 793 (1931).
[8] G. Breit, Phys. Rev. **42**, 348 (1932).
[9] H. Gieseler and W. Grotrian, Zeits. f. Physik **39**, 377 (1926).
[10] J. H. Bartlett, Jr., Nature **128**, 408 (1931).
[11] J. Racah, Nature **129**, 723 (1932).
[12] J. Rosenthal and G. Breit, Phys. Rev. **41**, 459 (1932).
[13] M. F. Crawford and A. L. Schawlow, Phys. Rev. **76**, 1310 (1949).
[14] G. Breit, G. B. Arfken, and W. W. Clendenin, Phys. Rev. **77**, 569 (1950).
[15] G. Breit (private communication). This matter is discussed in a preceding paper by Breit, Arfken, and Clendenin, Phys. Rev. **78**, 390 (1950).

Anomalous Internal Friction Associated with the Precipitation of Copper in Cold-Worked Al—Cu Alloys*

T'ING-SUI KÊ†
Institute for the Study of Metals, University of Chicago, Chicago, Illinois
(Received January 10, 1950)

Anomalous internal friction at very small stress levels has been observed in cold-worked aluminum containing one-half percent of copper. This internal friction, which was not observed in high purity aluminum after similar treatment, can be eliminated by annealing at high temperatures so that the specimen completely recrystallizes. This anomalous behavior is shown to be associated with an early stage "precipitation" of copper from the solid solution with aluminum. The temperature range within which such anomalous internal friction was observed is −5°C to 125°C when the cold-worked specimen was annealed at 300°C for one hour. At each temperature within this range the anomalous behavior first increases and then decreases with the aging time at that temperature.

The internal friction associated with this behavior is anomalous in the following aspects: (1) At a given temperature the internal friction first increases and then decreases with an increase of stress amplitude even when the stress amplitude is extremely small. There is an optimum stress amplitude at which the internal friction is a maximum. (2) At each stress amplitude there is an optimum temperature of measurement at which this anomalous internal friction is a maximum.

These observed phenomena are consistent with the concept that atmospheres of foreign atoms are formed around the dislocations created in the specimen by cold-working. Such an "atmosphere" concept was originally suggested by Cottrell for the explanation of the yield points in iron containing carbon or nitrogen.

1. INTRODUCTION

SNOEK[1] has observed in cold-worked iron a type of internal friction which can be eliminated by annealing at high temperatures or by removing the carbon or nitrogen from the specimen. Later work by this writer[2] has confirmed Snoek's observation that this internal friction requires for its occurrence both cold-working and the presence of either carbon or nitrogen. This internal friction is presumably caused by the stress-induced diffusion of foreign atoms within some peculiar type of stress regions created in the specimen by cold-work.

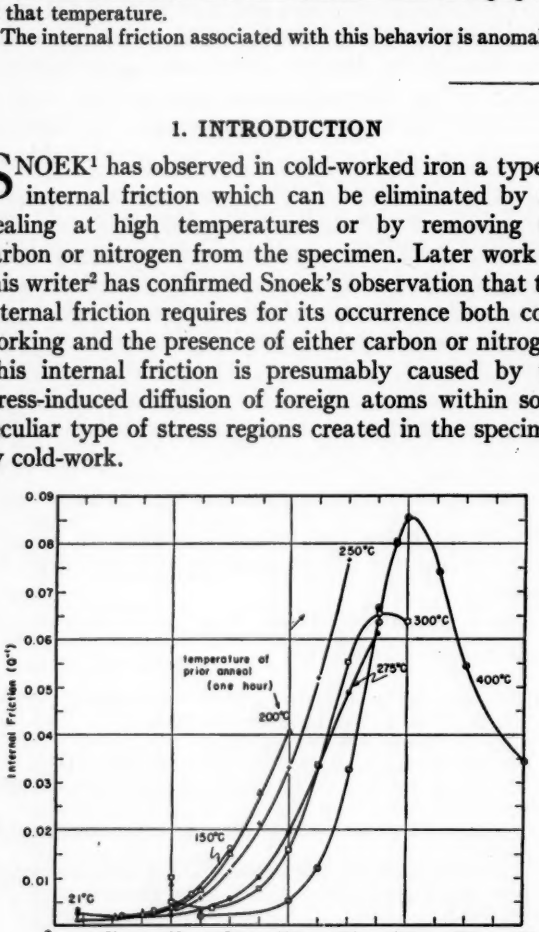

FIG. 1. Variation of internal friction with temperature of cold-worked aluminum containing one-half percent of copper after successive annealing at various temperatures.

A similar type of internal friction has recently been observed in commercially pure aluminum, both in polycrystalline[3] and in single crystal[4] specimens. The foreign atom responsible for this anomalous internal friction is believed to be copper. These observations suggest that the internal friction concerned may be a general feature of cold-worked metals containing appropriate foreign atoms. The purpose of this paper is to report the results of an investigation on this type of internal friction in 99.991 aluminum alloyed with 0.5 percent of copper.[5] The physical origin of this internal friction is discussed in the light of current dislocation theory.

The internal friction was measured with a torsion pendulum with a frequency of vibration of about one cycle per second. The maximum shearing strain on the surface of the specimen was about 10^{-5}. The apparatus and procedure for measurement has been previously described.[6]

2. EXPERIMENTS

The specimens used in this investigation were prepared by melting in vacuum 99.991 percent aluminum ingots with additions of electrolytic copper shots similar to those used by McReynolds[7] in his study of the stress-strain curve of Al—Cu alloys. Chemical analysis showed that the copper content in the alloy is 0.5 percent and the Si and Fe content is less than 0.01 percent. After homogenization the cast of the alloy was machined and swaged down with several intermediate annealings at 500°C. The final cold-working was done by drawing

* This research was supported in part by the ONR, Contract No. N-6ori-20-IV, NR 019 302.
† Now in the Department of Physics, National Tsing Hua University, Peking, China.
[1] J. L. Snoek, Physica 8, 711 (1941).
[2] T. S. Kê, Trans. A.I.M.E. 176, 448 (1948); (Tech. Pub. No. 2370).
[3] T. S. Kê, "Internal friction of cold-worked metals at various temperatures," J. Metals 188, 575 (1950).
[4] T. S. Kê, unpublished results.
[5] A brief account of this work has been reported before the Cambridge, Massachusetts Meeting of the Am. Phys. Soc. (June 16–18, 1949). See T. S. Kê, Phys. Rev. 76, 47(A) (1949).
[6] T. S. Kê, Phys. Rev. 71, 533 (1947).
[7] A. W. McReynolds, J. Metals Trans. 1, 32 (1949).

through dies to give a 95 percent reduction in area (95 percent *RA*).

The internal friction of this cold-worked specimen, having a diameter of 0.033 inch and a length of one foot, was measured at room temperature (21°C). It was then annealed at 150°C for one hour and the internal friction measured at 150°C and at lower temperatures. The same wire was successively annealed at higher temperatures for one hour and measurements were taken at the annealing temperatures and at lower temperatures as before. The variation of internal friction with temperature after successive annealings is shown in Fig. 1. It is seen that up to the annealing temperature of 250°C, the internal friction curve for a higher prior anneal is always lower than that for a lower prior anneal. This behavior is similar to that observed in the case of high purity aluminum.[3] However, as is shown in Fig. 1, when the specimen was annealed at 275°C for one hour, and the internal friction measured at this and at lower temperatures, the internal friction curve began to cross the 250°C and 200°C curve at a temperature of about 50°C. Such an anomalous behavior has not been observed in high purity aluminum. This behavior was more pronounced after the specimen had been annealed at 300°C for one hour. In this case the internal friction at 100°C is higher than the corresponding values for the 150°C, 200°C, and 250°C annealings. This high internal friction at 100°C has also been found to increase with time when the temperature of the specimen was kept at 100°C. The increase with aging time is indicated by an arrow in Fig. 1. The increase was threefold for an aging time of about an hour. Such an anomalous internal friction has also been observed at temperatures below 100°C.

Metallographic examinations showed that recrystallization was well under way after the 275° and the 300°C annealings. However, the majority of the grains are still imperfect with distorted regions and irregular grain boundaries.

A 400°C anneal for two hours resulted in the formation of perfect grains with smooth and straight grain boundaries shown by metallographic examinations. After this anneal it is seen from Fig. 1 that the internal friction peak associated with the viscous behavior of the grain boundaries was well developed, indicating that the specimen has been completely recrystallized.[8] The internal friction at various temperatures after this annealing behaves in a similar manner as in the case of high purity aluminum before the addition of copper. No anomalous internal friction was observed at 100°C or at lower temperatures.

These observations show, thus, that the anomalous internal friction described is caused by the presence of copper in cold-worked aluminum. It was not observed in high purity aluminum under similar conditions. It was eliminated after the copper bearing aluminum, originally cold-worked, was completely recrystallized.

[8] T. S. Kê, "A study of recrystallization and grain growth by measurement of internal friction," J. Metals 188, 581 (1950).

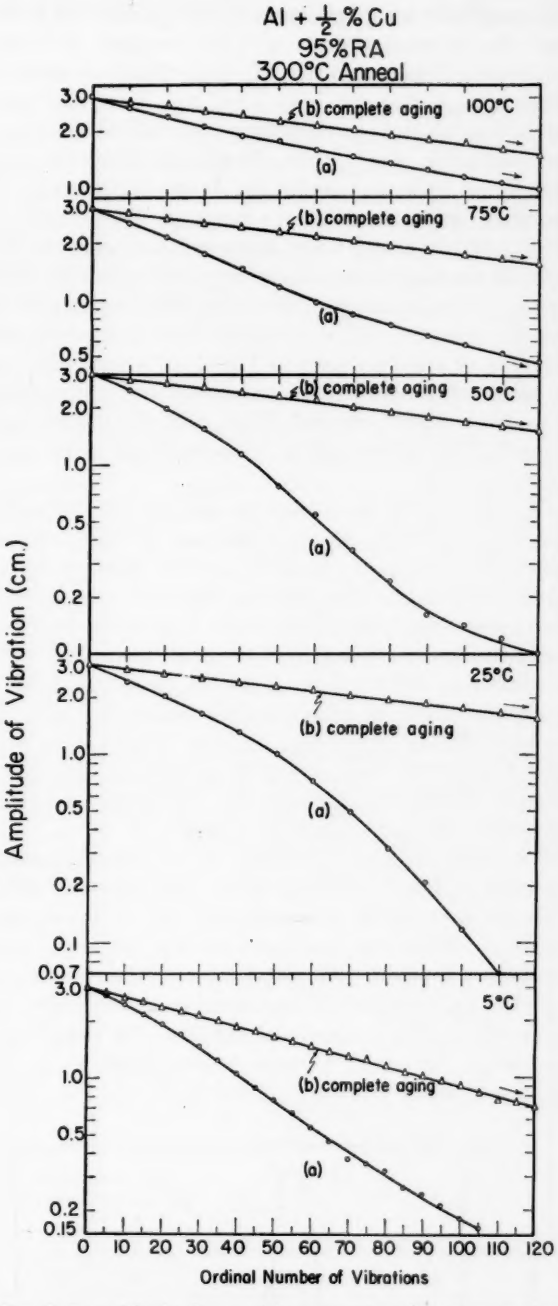

FIG. 2. Logarithmic decrement curves at various temperatures for cold-worked Al containing one-half percent Cu after one hour annealing at 300°C.

The following is a detailed description of the anomalous internal friction observed after the 300°C annealing. Typical measurements are reproduced in Fig. 2. The logarithm of the amplitude of vibration observed on a scale three meters away from the torsion apparatus was plotted against the ordinal number of vibrations. The slope of the curve is a measure of the logarithmic decrement, and the internal friction was taken as this logarithmic decrement divided by π. In all the relaxation experiments we have previously been concerned with,

the amplitude of vibration was always kept so small that the internal friction was independent of stress amplitude. This means that the logarithmic decrement curve was a straight line. This condition has been fulfilled in all the corresponding internal friction measurements for high purity aluminum. This has also been found to be the case for the Al one-half percent Cu specimen in the temperature range of 300°C down to 150°C. At 120°C and lower temperatures, however, the slope of the logarithmic decrement curve changes with stress amplitude although the range of stress amplitude was the same in all the measurements. Following the sequence of graphs shown in Fig. 2, it is seen that the anomalous behavior is more marked as the temperature of measurement is lowered. Maximum effect is reached around 25°C, below which it becomes again less pronounced.

Considerable caution must be used in the interpretation of curves such as are presented in Fig. 2. As an example, one cannot conclude *a priori* from curve (*a*) taken at 25°C that the internal friction increases with decreasing amplitude of vibration. The internal friction may possibly be a function of the prior history of stress amplitude as well as of the instantaneous level of stress amplitude. Such is indeed found to be the case. If, however, the specimen was first set in oscillation at a higher stress level than was to be used subsequently, the internal friction was found to be essentially a function only of the instantaneous stress level.

We have mentioned above that the anomalous behavior at 100°C increases with aging time at 100°C. This has been found also to be the case at lower temperatures. When the specimen was aged at room temperature the effect first increased and then decreased with the aging time. It disappeared completely after an aging of two days at room temperature. The logarithmic decrement curves at various temperatures after this aging treatment are shown respectively by the curves marked *b*. It is seen that all of them are straight lines and the anomalous behavior has all disappeared. It is thus believed that the anomalous effect observed is associated with some stage of the precipitation of copper from the solid solution of the specimen. The effect disappears after the completion of the precipitation or after the completion of certain early stages of the precipitation. This viewpoint was strengthened by the following observations. When an aged specimen in which the anomalous behavior had disappeared was again annealed at 300°C for one hour and the measurements of internal friction repeated as before, the anomalous behavior reappears in a similar manner as in the first trial. This one hour annealing at 300°C apparently has redissolved the precipitated copper. Accordingly, the precipitation of copper from solid solution starts over again when the temperature is lowered.

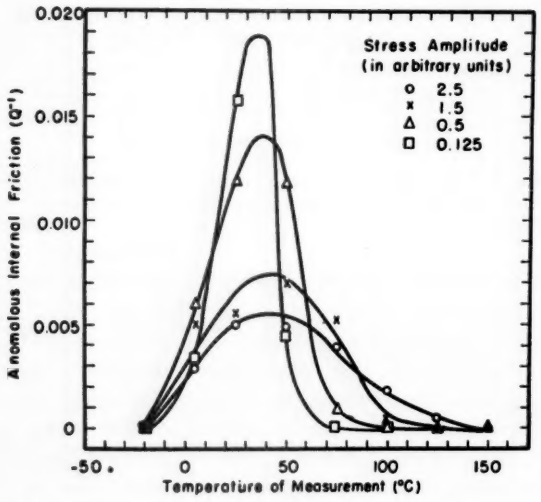

FIG. 3. Temperature dependence of the anomalous internal friction at various stress amplitudes.

From Fig. 2 we can determine the variation of the anomalous internal friction with the temperature of measurement at various stress amplitudes. The anomalous internal friction is here defined as that associated with an *a* curve in Fig. 2 minus that associated with the corresponding *b* curve. A few representative cases are shown in Fig. 3. It is seen that in every case there is an optimum temperature at which the anomalous internal friction is a maximum. This internal friction peak is broad at high stress amplitudes and is very sharp at the lowest stress amplitude studied, which is 0.125 in arbitrary units. This corresponds to a maximum shearing strain on the surface of the wire specimen of about 5×10^{-7}. The height of the peak is also seen to rise with decreasing stress amplitude.

3. DISCUSSION

The effects described above could be interpreted by a variety of models. A unique choice between the possible models must await further experiments. All models, however, utilize the concept of the interaction between solute atoms and dislocations whereby solute atoms are trapped by dislocations, and conversely dislocations are immobilized by solute atoms. The theory of this mutual trapping of solute atoms by dislocations has been discussed at great length by Cottrell.[9] The total strain-free energy of a solute atom and of a dislocation is lower when the solute atom is at the center of, or in the vicinity of, the dislocation than when the two are separated. A solute atom will thereby be trapped by a dislocation. Conversely, a dislocation which, if free of all solute atoms, would move along its entire length under the action of a small applied stress, will be anchored at those regions in which solute atoms are located. The trapping of solute atoms by dislocations has been demonstrated experimentally by Dijkstra[10] in

[9] A. H. Cottrell, *Report on the Strength of Solids* (Physical Society, London, 1948), p. 30; Proc. Phys. Soc. (London) **62**, 49 (1949); in *Progress in Metal Physics* (Interscience Publishers, Inc., New York, 1949), Chapter 2; "Theory of the yield point of iron" (British Iron and Steel Res. Assoc., 1948).

[10] L. Dijksta, J. Metals **185**, 252 (1949).

his study of the solubility of nitrogen in alpha-iron. Dijkstra found that the nitrogen atoms are bound more tightly to dislocations than to the precipitate phases of iron-carbide or iron-nitride, respectively.

We shall now describe one possible model which is capable of interpreting the experiments reported in this paper. Towards this end we shall consider that after an annealing at 275°C, and before appreciable trapping of solute atoms has occurred, all remaining dislocations are in an equilibrium configuration determined by their line tensions and by their mutual interaction. This equilibrium configuration will be altered, however, by an applied stress, the magnitude of the change in the dislocation being proportional to the applied stress, at least for sufficiently low stress levels. We shall further suppose that the adjustment of the dislocations to changes in applied stress occurs in a time very short compared to the period of oscillation in our experiments, which was about one second. The stress induced movement of the dislocations will not then result in any damping, since their configuration will at all times be a unique function of the instantaneous stress. In other words, the time of relaxation τ for the establishment of an equilibrium configuration is very low compared to the period of vibration, and hence vibrations at one cycle per second lie on the extreme low frequency side of a relaxation peak of the internal friction spectrum. When now a dislocation traps solute atoms, its mobility under an applied stress is considerably impeded since the dislocation must now pull along the trapped solute atoms. The trapping of solute atoms thus lengthens the time of relaxation τ for the establishment of the equilibrium configuration of the dislocations. Since the mobility of the solute atoms increases rapidly as the temperature rises, we anticipate that τ will decrease as the temperature is raised. At a sufficiently low temperature, where τ is very long compared to the period of vibration, no appreciable movement of the dislocations will occur, and hence the internal friction will be very low. As the temperature is now raised from such a low value the internal friction will pass through a maximum in that temperature range where τ is comparable to the period of vibration, in which range the dislocations experience both appreciable movement and appreciable resistance to movement. Thus, in terms of this model, the internal friction peaks in Fig. 3 are interpreted in the same formal manner as have so many other internal friction peaks[11] in other systems.

The effect of overaging in removing the anomalous internal friction finds a ready interpretation in our model. It appears as if the copper atoms are bound less strongly to the dislocations than to the stable precipitate phase (Al_2Cu). The stable precipitate phase will, therefore, grow not only at the expense of the solute atoms in solid solution, but also of those attached to the dislocations. This stable precipitate phase is redissolved by heating to 300°C.

---

[11] C. Zener, *Elasticity and Anelasticity of Metals* (The University of Chicago Press, Chicago, 1948), Chapter VII.

On the Diffusion of Imprisoned Resonance Radiation

FRANK N. EDMONDS, JR.
Yerkes Observatory, University of Chicago, Williams Bay, Wisconsin
(Received February 2, 1950)

The solution of the problem of diffusion of imprisoned resonance radiation obtained by Chandrasekhar is worked out in detail in the second approximation. Decay constants, characteristic roots and eigenfunction coefficients necessary for an explicit solution are tabulated for both large and small optical thicknesses. A comparison is made between computed and measured decay constants for the Hg 2537A resonance line.

1. INTRODUCTION

DIFFUSION of imprisoned resonance radiation has been the subject of both experimental and theoretical investigation and can be explained simply in terms of excitation of atoms. In escaping from a gas of atoms in their normal state, radiation at the frequency of a resonance line of the atoms will be absorbed and emitted many times. This transfer of excitation from atom to atom delays the escape of the resonance quanta from the gas because they are "imprisoned" within each atom for an average time equal to the mean life of the excited state. The escape of resonance quanta, therefore, can be considered statistically as a decay of atoms in the excited state, and it can be analyzed as a diffusion process, if the frequency dependence of the atomic absorption coefficient for the resonance line $\sigma(\nu)$ is approximated by assigning a constant value σ over a given frequency interval $\Delta\nu$ such that

$$\int \sigma(\nu)d\nu=\sigma\Delta\nu. \tag{1}$$

The equations of radiative transfer and radiative equilibrium for this diffusion process were first formulated and solved approximately by Milne.[1] Chandrasekhar[2] has analyzed this problem in a similar manner obtaining solutions in finite approximations. The solution in the first approximation, which is essentially equivalent to Milne's solution, is worked out and presented in detail.

In this paper Chandrasekhar's solution in the second approximation will be presented in a similar manner, including tabulation of decay constants of the exponential decay of excited atoms, characteristic roots and dominant eigenfunction coefficients necessary for an explicit solution. Also the decay constants for the Hg 2537A resonance line, as calculated in the first and second approximations and in other investigations, will be compared with laboratory measurements.

2. CHARACTERISTIC ROOTS AND DECAY CONSTANTS FOR THE SECOND APPROXIMATION

The characteristic equation (reference 2, p. 360) in the second approximation is

$$\frac{1}{\omega}=\frac{a_1}{1+(\mu_1 k)^2}+\frac{a_2}{1+(\mu_2 k)^2} \tag{2}$$

where the Gaussian weights a_1, a_2 and divisions μ_1, μ_2 have the values

$$a_1=0.652145, \quad \mu_1=0.339981,$$
$$a_2=0.347855, \quad \mu_2=0.861136,$$

and where ω takes one of its eigenvalues $\omega^{(l,m)}$ or $\omega^{(0,m)}$ with $m=1, 2, \cdots, \infty$. The characteristic roots of (2) corresponding to these eigenvalues consists of the real roots $k_1^{(l,m)}$ or $k_1^{(0,m)}$ and the imaginary roots $ik_2^{(l,m)}$ or $ik_2^{(0,m)}$. Using the definition of θ_{ij} (reference 2, p. 361), we have

$$\begin{aligned}
&\theta_{11}^{(l,m)}=\tan^{-1}\mu_1 k_1^{(l,m)}, \quad &&\theta_{11}^{(0,m)}=\tan^{-1}\mu_1 k_1^{(0,m)},\\
&\theta_{12}^{(l,m)}=\tan^{-1}\mu_2 k_1^{(l,m)}, \quad &&\theta_{12}^{(0,m)}=\tan^{-1}\mu_2 k_1^{(0,m)},\\
&\theta_{21}^{(l,m)}=\tanh^{-1}\mu_1 k_2^{(l,m)}, \quad &&\theta_{21}^{(0,m)}=\tanh^{-1}\mu_1 k_2^{(0,m)}.
\end{aligned} \tag{3}$$

Similar definitions for $\theta_{22}^{(l,m)}$ and $\theta_{22}^{(0,m)}$ are not valid since

$$\mu_2 k_2^{(l,m)}>1; \quad \mu_2 k_2^{(0,m)}>1 \tag{4}$$

for all values of m. Therefore the equations which determine the eigenvalues of ω (reference 2, p. 361) take the modified forms,

$$\begin{vmatrix}
\cos\theta_{11}^{(l,m)}\cos(\theta_{11}^{(l,m)}+k_1^{(l,m)}\tau_1) & \cos\theta_{12}^{(l,m)}\cos(\theta_{12}^{(l,m)}+k_1^{(l,m)}\tau_1)\\
\cosh\theta_{21}^{(l,m)}\cosh(\theta_{21}^{(l,m)}+k_2^{(l,m)}\tau_1) & \dfrac{\cosh k_2^{(l,m)}\tau_1+\mu_2 k_2^{(l,m)}\sinh k_2^{(l,m)}\tau_1}{1-(\mu_2 k_2^{(l,m)})^2}
\end{vmatrix}=0, \tag{5}$$

which is satisfied by $\omega^{(l,m)}$, and

$$\begin{vmatrix}
\cos\theta_{11}^{(0,m)}\sin(\theta_{11}^{(0,m)}+k_1^{(0,m)}\tau_1) & \cos\theta_{12}^{(0,m)}\sin(\theta_{12}^{(0,m)}+k_1^{(0,m)}\tau_1)\\
\cosh\theta_{21}^{(0,m)}\sinh(\theta_{21}^{(0,m)}+k_2^{(0,m)}\tau_1) & \dfrac{\mu_2 k_2^{(0,m)}\cosh k_2^{(0,m)}\tau_1+\sinh k_2^{(0,m)}\tau_1}{1-(\mu_2 k_2^{(0,m)})^2}
\end{vmatrix}=0, \tag{6}$$

[1] E. A. Milne, J. Math. Soc. London **1**, 40 (1926).
[2] S. Chandrasekhar, *Radiative Transfer* (Clarendon Press, Oxford, 1950), p. 354.

TABLE I. Decay constant, characteristic roots and dominant eigengunction coefficients appearing in the second approximation solution for large optical thicknesses.

Decay constant*		Characteristic roots		Dominant eigenfunction coefficients		Optical thickness τ_1 for	
$(\omega^{(l,m)}-1)/\omega^{(l,m)}$ or $(\omega^{(0,m)}-1)/\omega^{(0,m)}$	$-\log\left(\frac{\omega^{(l,m)}-1}{\omega^{(l,m)}}\right)$ or $-\log\left(\frac{\omega^{(0,m)}-1}{\omega^{(0,m)}}\right)$	$k_1^{(l,m)}$ or $k_1^{(0,m)}$	$k_2^{(l,m)}$ or $k_2^{(0,m)}$	$\frac{a^{(l,1)}A_1^{(1)}}{I^{(0)}}$	$-\log_e\left(\frac{-a^{(l,1)}A_2^{(1)}}{I^{(0)}}\right)$	$(l, 1)$	$(0, 2)$
1.0000×10^{-6}	6.00000	0.00173205	1.9720	0.6367	1795.20441	906.182	...
3.1623×10^{-6}	5.50000	0.00308008	1.9720	0.6366	1012.00442	509.289	1019.28
1.0000×10^{-5}	5.00000	0.00547723	1.9720	0.6366	571.35874	286.107	572.904
3.1623×10^{-5}	4.50000	0.00974064	1.9720	0.6366	313.18413	160.569	321.832
1.0000×10^{-4}	4.00000	0.0173222	1.9720	0.6366	183.41917	89.9873	180.669
3.1623×10^{-4}	3.50000	0.0308096	1.9718	0.6365	104.55968	50.2903	101.274
1.0000×10^{-3}	3.00000	0.0548215	1.9712	0.6361	59.92813	27.9597	56.6157
3.1623×10^{-3}	2.50000	0.0976786	1.9695	0.6349	34.65068	15.3897	31.4710
1.0000×10^{-2}	2.00000	0.174780	1.9641	0.6315	19.97762	8.3009	17.2882
3.1623×10^{-2}	1.50000	0.317058	1.9468	0.6218	11.46733	4.2842	9.2386
1.0000×10^{-1}	1.00000	0.60235	1.8902	0.5981	6.43080	1.9942	4.5979
3.1623×10^{-1}	0.50000	1.3605	1.7071	0.5480	3.71399	0.6919	1.850

* $(\omega^{(0,1)}-1)/\omega^{(0,1)}\equiv0$.

which is satisfied by $\omega^{(0,m)}$. These equations are for a slab of gas of infinite extent and a total optical thickness of $2\tau_1$.

It is simpler to solve (5) or (6) together with (2) and (3) for τ_1 for assigned values of the decay constants $(\omega^{(l,m)}-1)/\omega^{(l,m)}$ or $(\omega^{(0,m)}-1)/\omega^{(0,m)}$, rather than solving for decay constants for assigned values of the optical thickness. The results, together with characteristic roots, are tabulated in Table I for large values of τ_1 and in Table II for small values of τ_1, using a sufficient number of values of m to give the final solution of the problem the same order of accuracy as the tables. This accuracy is better than ±5 in the last digit. The decay constants are given in units in which the mean life of the excited state is unity.

3. NORMALIZED EIGENFUNCTIONS AND THE SECOND APPROXIMATION SOLUTION

The orthogonal, normalized eigenfunctions used in the final solution of the problem are in the second approximation (reference 2, p. 362)

$$\psi^{(l,m)}(\tau)=A_1{}^{(m)}[\cos k_1{}^{(l,m)}\tau+(A_2{}^{(m)}/A_1{}^{(m)})\cosh k_2{}^{(l,m)}\tau] \tag{7}$$

TABLE II. Decay constant, characteristic roots and dominant eigenfunction coefficients appearing in the second approximation solution for small optical thicknesses.

Decay constant*		Characteristic roots		Dominant eigenfunction coefficients		Optical thickness τ_1 for						
$(\omega^{(l,m)}-1)/\omega^{(l,m)}$ or $(\omega^{(0,m)}-1)/\omega^{(0,m)}$	$\log\omega^{(l,m)}$ or $\log\omega^{(0,m)}$	$k_1^{(l,m)}$ or $k_1^{(0,m)}$	$k_2^{(l,m)}$ or $k_2^{(0,m)}$	$\frac{a^{(l,1)}A_1^{(1)}}{I^{(0)}}$	$-\frac{a^{(l,1)}A_2^{(1)}}{I^{(0)}}$	$(l, 1)$	$(0, 2)$	$(l, 2)$	$(0, 3)$	$(l, 3)$	$(0, 4)$	$(l, 4)$
0.100	...	0.6024	1.8902	0.5981	0.001611	1.9942	...	...	...	...	...	...
0.150	...	0.7766	1.8476	0.5815	0.005919	1.4435	...	...	...	...	...	...
0.200	0.09691	0.9464	1.8046	0.5695	0.01113	1.1177	...	...	...	...	...	...
0.250	...	1.1192	1.7620	0.5601	0.01720	0.8975	...	...	...	...	...	...
0.300	...	1.2998	1.7203	0.5507	0.02283	0.7354	1.9473	...	...	...	...	...
0.350	...	1.4912	1.6803	0.5432	0.02704	0.6117	1.6694	...	...	...	...	...
0.400	...	1.6979	1.6425	0.5369	0.02976	0.5121	1.4426	...	...	...	...	...
0.450	...	1.9222	1.6074	0.5317	0.03084	0.4305	1.2537	2.0699	...	...	...	...
0.500	...	2.1686	1.5750	0.5277	0.03082	0.3613	1.0930	1.8162	...	...	...	...
0.550	...	2.4432	1.5456	0.5248	0.02901	0.3035	0.9535	1.5957	...	...	...	...
0.600	0.39794	2.7541	1.5189	0.5221	0.02662	0.2528	0.8303	1.3995	1.9701	...	...	...
0.650	...	3.1137	1.4949	0.5199	0.02368	0.2083	0.7194	1.2227	1.7275	...	...	...
0.700	...	3.5413	1.4733	0.5173	0.0202	0.1690	0.6185	1.0597	1.5046	1.9481	...	...
0.7500	...	4.0692	1.4539	0.5147	0.0168	0.1336	0.5254	0.9094	1.2973	1.6822	2.0681	...
0.7750	...	4.3881	1.4449	...	...	...	...	...	...	...	1.9120	...
0.8000	0.69897	4.7559	1.4364	0.512	0.013	0.1019	0.4375	0.7653	1.0967	1.4262	1.7567	2.0870
0.8250	...	5.198	1.4283	...	...	...	...	...	...	...	1.6023	1.9038
0.8500	...	5.7235	1.4206	0.509	0.010	0.0730	0.3502	0.6238	0.8987	1.1729	1.4475	1.7220
0.8750	...	6.3942	1.4133	...	...	...	...	...	...	...	1.2899	1.5371
0.9000	1.00000	7.2862	1.4064	...	...	...	0.2646	0.4789	0.6952	0.9104	1.1262	1.3417
0.9250	...	8.5698	1.3997	...	...	...	...	...	...	...	0.9526	1.1351
0.9500	1.30103	10.6848	1.3934	...	...	...	0.1707	0.3168	0.4644	0.6110	0.7583	0.9051
0.97500	1.60206	15.3743	1.3874	...	...	...	0.1137	0.2155	0.3180	0.4199	0.5223	0.6244
0.98750	1.90309	21.9273	1.3845	...	...	...	0.0774	0.1488	0.2206	0.2920	0.3639	0.4355
0.993750	2.20412	31.1398	1.3831	...	...	...	...	0.1037	0.1543	0.2047	0.2552	0.3056
0.9968750	2.50515	44.1302	1.3824	...	...	...	...	0.0725	0.1082	0.1438	0.1794	0.2150
0.99843750	2.80618	62.4742	1.3821	...	...	...	...	...	0.0761	0.1013	0.1265	0.1516
0.999218750	3.10721	88.3976	1.3819	...	...	...	...	...	...	0.0714	0.0892	0.1070

* $(\omega^{(0,1)}-1)/\omega^{(0,1)}\equiv0$.

and

$$\psi^{(0,m)}(\tau)=B_1^{(m)}[\sin k_1^{(0,m)}\tau+(iB_2^{(m)}/B_1^{(m)})\sinh k_2^{(0,m)}\tau], \tag{8}$$

where by the boundary conditions (reference 2, p. 362)

$$A_2^{(m)}/A_1^{(m)}=-\cos\theta_{11}^{(l,m)}\cos(\theta_{11}^{(l,m)}+k_1^{(l,m)}\tau_1)/\cosh\theta_{21}^{(l,m)}\cosh(\theta_{21}^{(l,m)}+k_2^{(l,m)}\tau_1) \tag{9}$$

and

$$iB_2^{(m)}/B_1^{(m)}=-\cos\theta_{11}^{(0,m)}\sin(\theta_{11}^{(0,m)}+k_1^{(0,m)}\tau_1)/\cosh\theta_{21}^{(0,m)}\sinh(\theta_{21}^{(0,m)}+k_2^{(0,m)}\tau_1), \tag{10}$$

and by the normalizing conditions

$$\frac{1}{(A_1^{(m)})^2}=\tau_1+\frac{\sin 2k_1^{(l,m)}\tau_1}{2k_1^{(l,m)}}+\left[\frac{A_2^{(m)}}{A_1^{(m)}}\right]^2\left[\tau_1+\frac{\sinh 2k_2^{(l,m)}\tau_1}{2k_2^{(l,m)}}\right]$$
$$+4\left[\frac{A_2^{(m)}}{A_1^{(m)}}\right]\left[\frac{k_1^{(l,m)}\sin k_1^{(l,m)}\tau_1\cosh k_2^{(l,m)}\tau_1+k_2^{(l,m)}\cos k_1^{(l,m)}\tau_1\sinh k_2^{(l,m)}\tau_1}{(k_1^{(l,m)})^2+(k_2^{(l,m)})^2}\right] \tag{11}$$

and

$$\frac{1}{(B_1^{(m)})^2}=\tau_1-\frac{\sin 2k_1^{(0,m)}\tau_1}{2k_1^{(0,m)}}-\left[\frac{iB_2^{(m)}}{B_1^{(m)}}\right]^2\left[\tau_1-\frac{\sinh 2k_2^{(0,m)}\tau_1}{2k_2^{(0,m)}}\right]$$
$$+4\left[\frac{iB_2^{(m)}}{B_1^{(m)}}\right]\left[\frac{k_2^{(0,m)}\sin k_1^{(0,m)}\tau_1\cosh k_2^{(0,m)}\tau_1-k_1^{(0,m)}\cos k_1^{(0,m)}\tau_1\sinh k_2^{(0,m)}\tau_1}{(k_1^{(0,m)})^2+(k_2^{(0,m)})^2}\right]. \tag{12}$$

The expansions in terms of these eigenfunctions of the mean intensity $J(t,\tau)$ and the number of excited atoms per cm^3 $N(t,\tau)$ constitute the final solution of the problem. These expansions (reference 2, p. 362) in the second approximation are

$$J(t,\tau)=\sum_{m=1}^{\infty}a^{(l,m)}\psi^{(l,m)}(\tau)\times\exp\{-(\omega^{(l,m)}-1)t/\omega^{(l,m)}\}$$
$$+\sum_{m=2}^{\infty}a^{(0,m)}\psi^{(0,m)}(\tau)\times\exp\{-(\omega^{(0,m)}-1)t/\omega^{(0,m)}\} \tag{13}$$

and

$$N(t,\tau)=\sum_{m=1}^{\infty}a^{(l,m)}\omega^{(l,m)}\psi^{(l,m)}(\tau)\times\exp\{-(\omega^{(l,m)}-1)t/\omega^{(l,m)}\}$$
$$+\sum_{m=2}^{\infty}a^{(0,m)}\omega^{(0,m)}\psi^{(0,m)}(\tau)\times\exp\{-(\omega^{(0,m)}-1)t/\omega^{(0,m)}\}, \tag{14}$$

where the summation of $\psi^{(0,m)}(\tau)$ starts with $m=2$, since $\psi^{(0,1)}(\tau)$ is identically zero. These solutions are for the time interval $t>0$ where $t=0$ marks the cutting off of all radiation incident on the gas and hence the starting of the diffusion process. Examination of Tables I and II shows that for a given τ_1, the decay constant $(\omega^{(l,1)}-1)/\omega^{(l,1)}$ is the smallest, and so the term containing $\psi^{(l,1)}(\tau)$ in (13) and (14) will dominate for sufficiently large values of t, this domination being more pronounced for large values of τ_1. Hence $\psi^{(l,1)}(\tau)$ will be designated the dominant eigenfunction, and its associated decay constant, the dominant decay constant.

The coefficients of expansion $a^{(l,m)}$ and $a^{(0,m)}$ are determined by equating $J(t=0,\tau)$ to the mean intensity $J(\tau)$ obtained from the solution of the stationary Schuster problem for the time interval $t<0$. In the second approximation this solution for the steady state conditions when radiation is incident on the gas, gives (reference 2, p. 363)

$$J(\tau)=L_0\tau-2L_1\sinh k^{(0)}\tau+L_2, \tag{15}$$

where

$$k^{(0)}=1.972027$$

is a root of the characteristic equation (reference 2, p. 363). The coefficients in (15) as determined by the boundary conditions (reference 2, p. 363) are

$$L_0=\tfrac{1}{2}I^{(0)}[0.228020\exp\{-k^{(0)}\tau_1\}-4.466748\exp\{k^{(0)}\tau_1\}]/L^*, \tag{16}$$

$$L_1=\tfrac{1}{2}I^{(0)}[0.521155]/L^* \tag{17}$$

and

$$L_2=\tfrac{1}{2}I^{(0)}, \tag{18}$$

where

$$L^*=(0.228020\tau_1+0.389506)\exp\{-k^{(0)}\tau_1\}-(4.466748\tau_1+3.100033)\exp\{k^{(0)}\tau_1\}, \tag{19}$$

and $I^{(0)}$ is the intensity of the isotropic radiation incident at $\tau=-\tau_1$ Expressions for the coefficients of expansion can be obtained in the usual manner, employing the orthogonality of the eigenfunctions and substituting $J(\tau)$ for $J(l=0, \tau)$. These coefficients of expansion are

$$a^{(l,m)}=\int_{-\tau_1}^{\tau_1} J(\tau)\psi^{(l,m)}(\tau)d\tau=2L_2A_1{}^{(m)}\left[\frac{\sin k_1{}^{(l,m)}\tau_1}{k_1{}^{(l,m)}}+\left(\frac{A_2{}^{(m)}}{A_1{}^{(m)}}\right)\frac{\sinh k_2{}^{(l,m)}\tau_1}{k_2{}^{(l,m)}}\right] \tag{20}$$

and

$$\begin{aligned}a^{(0,m)}=\int_{-\tau_1}^{\tau_1} J(\tau)\psi^{(0,m)}(\tau)d\tau=2L_0B_1{}^{(m)}&\left\{\frac{\sin k_1{}^{(0,m)}\tau_1}{(k_1{}^{(0,m)})^2}-\frac{\tau_1\cos k_1{}^{(0,m)}\tau_1}{k_1{}^{(0,m)}}\right.\\&\left.-\left[\frac{iB_2{}^{(m)}}{B_1{}^{(m)}}\right]\left[\frac{\sinh k_2{}^{(0,m)}\tau_1}{(k_2{}^{(0,m)})^2}-\frac{\tau_1\cosh k_2{}^{(0,m)}\tau_1}{k_2{}^{(0,m)}}\right]\right\}\\&+4L_1B_1{}^{(m)}\left\{\frac{k_1{}^{(0,m)}\cos k_1{}^{(0,m)}\tau_1\sinh k^{(0)}\tau_1-k^{(0)}\sin k_1{}^{(0,m)}\tau_1\cosh k^{(0)}\tau_1}{(k^{(0)})^2+(k_1{}^{(0,m)})^2}\right.\\&\left.+\left[\frac{iB_2{}^{(m)}}{B_1{}^{(m)}}\right]\left[\frac{k_2{}^{(0,m)}\cosh k_2{}^{(0,m)}\tau_1\sinh k^{(0)}\tau_1-k^{(0)}\sinh k_2{}^{(0,m)}\tau_1\cosh k^{(0)}\tau_1}{(k^{(0)})^2-(k_2{}^{(0,m)})^2}\right]\right\}.\end{aligned} \tag{21}$$

The coefficients of the dominant eigenfunction in the expression for $J(l, \tau)$ have been obtained in terms of $I^{(0)}$, using (9), (11), (18) and (20), and the results are included in Tables I and II.

4. DECAY CONSTANT FOR THE MERCURY 2537A RESONANCE LINE

Zemansky[3] and Alpert *et al.*[4] have measured the dominant decay constant for the Hg 2537A resonance line in the normal time scale

$$\beta=A_{21}(\omega^{(l,1)}-1)/\omega^{(l,1)} \tag{22}$$

where A_{21} is the Einstein coefficient for spontaneous emission. These measurements were made for several values of N, the number of absorbing atoms per cm³, which is related to the optical thickness by the expression

$$\tau_1=\tfrac{1}{2}N\sigma l, \tag{23}$$

where l is the geometric thickness of a mercury vapor cell, and σ is the mean absorption coefficient as defied by (1).

Determining the correct value of σ for diffusion of resonance radiation, however, is not a simple matter of determining a line breadth $\Delta\nu$ from the Doppler breadth and fine structure splitting, as such calculations give a value for σ several times too large. As Zanstra[5] among others has pointed out, Doppler shifts arising from thermal motions of the Hg atoms will produce noncoherent scattering of the resonance radiation, and this will speed up the diffusion process since the probability of escape for a resonance quantum at the center of the line is much less than the product of the probability of its being scattered to the wings and the probability of escape at the scattered frequency. This phenomenon will qualitatively explain the necessary reduction in σ, but a satisfactory quantitative theory is still needed. An approximate method for determining σ is provided by Zemansky[6] who has equated a diffusion coefficient derived by Kenty[7] to $A_{21}/4N^2\sigma^2$ which appears as a diffusion coefficient in Milne's[1] theory. In obtaining his diffusion coefficient as a function of N, l and atomic constants, Kenty has taken account of incoherent

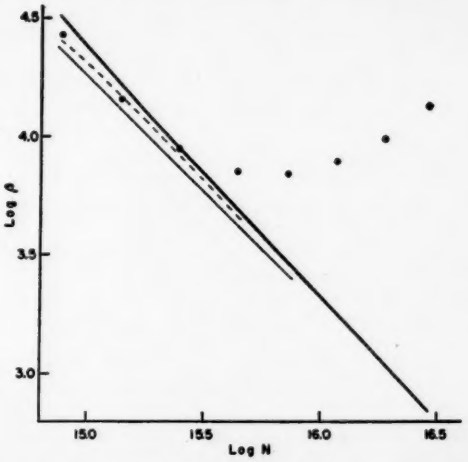

FIG. 1. Logarithm of β, the dominant decay constant for the Hg 2537A resonance line in reciprocal seconds, as a function of the logarithm of N, the number of absorbing atoms per cm³ in a cell 1.95 cm thick. The thick solid curve represents computations using the second approximation; the thin solid curve, computations of Holstein; the broken curve, computations of Zemansky using Milne's theory. The black circles represent laboratory measurements by Zemansky.

[3] M. W. Zemansky, Phys. Rev. **29**, 513 (1927).
[4] Alpert, McCoubray, and Holstein, Phys. Rev. **76**, 1257 (1949).
[5] H. Zanstra, Bull. Astronom. Insts. Netherlands **X1**, No. 401 (1949).
[6] M. W. Zemansky, Phys. Rev. **42**, 843 (1932).
[7] C. Kenty, Phys. Rev. **42**, 823 (1932).

scattering due to thermal motions. However, as Holstein[8] has pointed out, the use of such kinetic theory concepts as a mean free path and a diffusion coefficient in this calculation of σ is not completely satisfactory in describing accurately the diffusion of imprisoned resonance radiation, where the atomic absorption coefficient varies considerably with frequency. Holstein has circumvented these difficulties by analyzing the diffusion process in terms of the probability of a resonance quantum going a given distance between successive absorptions. The averaging of this probability over the resonance line takes account of incoherent scattering due to thermal motions, and this averaged probability is used in an equation of radiative equilibrium which is solved approximately by variational methods for the decay constant. However, Zemansky's method for calculating σ, which gives the right order of magnitude, is used in this paper.

The optical thicknesses obtained from (23) for the values of N and l involved in the laboratory measurements of the decay constant are large, ranging from ten to one hundred. In this range $\log\beta$ as calculated by the first approximation is less than one percent larger than $\log\beta$ as calculated by the second approximation. In Fig. 1, values of $\log\beta$ are plotted for various values of $\log N$ and for $l=1.95$ cm, as calculated for the second approximation, as calculated by Zemansky[6] using Milne's theory and as calculated by Holstein.[8] The measurements of Zemansky[3] for the same value of l are also plotted. Better agreement between measured and calculated decay constants have been obtained with the improved measuring techniques of Alpert *et al.*[4] The discrepancy between measured and calculated values of $\log\beta$ for large values of $\log N$ can be explained in part by the effects of collisional broadening which have been neglected in the computations.

It is a pleasure to express my appreciation to Dr. S. Chandrasekhar for suggesting this problem and for helpful discussions concerning it.

[8] T. Holstein, Phys. Rev. **72**, 1212 (1947).

PHYSICAL REVIEW VOLUME 78, NUMBER 4 MAY 15, 1950

The Growth of Circularly Polarized Waves in the Sun's Atmosphere and Their Escape into Space

V. A. BAILEY
School of Physics, University of Sydney, Sydney, Australia
(Received May 24, 1949)

The theory, previously published, of plane waves in an ionized medium pervaded by static electric and magnetic fields is shown to predict wave amplification, and consequent electromagnetic noise, in certain frequency bands. It is then developed in detail for the case in which the static fields are both parallel to the direction of wave propagation and the perturbations are transverse to this direction.

It is shown that for any given frequency and electron drift velocity there are two trios of such waves, E_1 and E_2 waves, all circularly polarized; the E_1 and E_2 waves are oppositely polarized. It is found that any transverse perturbation temporally prescribed at a given plane can be split up into two such trios which can then be considered independently.

Necessary and sufficient conditions are then found under which a growing flux of energy carried by E_1 or E_2 waves can pass normally through the boundary between two different ionized media.

The theory is applied to show that under simple hypotheses about the drift of electrons in the atmosphere above a large sunspot strong circular waves can arise by growth of random transverse perturbations and can then escape from the sun. The consequences of two such hypotheses are compared with known observations of solar noise and used to interpret them.

It is concluded that the general hypothesis that electrons in a sunspot have a drift motion leads to results which are in good agreement with many facts about strong solar noise and which do not disagree with any others.

The ultimate intensity which a growing perturbation can attain is also discussed.

1. INTRODUCTION

IN two previous publications[1,2] the general equations which specify the dispersion and polarization of plane waves in an ionized medium, pervaded by static electric and magnetic fields, have been derived. This theory may be conveniently referred to as the electromagneto-ionic theory of wave propagation and more briefly as the E.M.I. theory. As a limiting case it includes the well-known magneto-ionic theory (M.I. theory) and its application is in general subject to the same conditions of validity as the latter.

We shall here apply the E.M.I. theory to the important solar phenomenon of emission of strong circularly polarized radio noise by a large sunspot.

As it appears that the Australian publications referred to above are not yet readily available in the United States and elsewhere, a summary of the E.M.I. theory is given here in the approximation which neglects the motions of the positive ions.

In Appendix 1 we also give the relativistic form of the

[1] V. A. Bailey, J. Roy. Soc. N.S.W. **82**, 107 (1948).
[2] V. A. Bailey, Australian J. Sci. Res. **A, 1**, 351 (1948).

equation of dispersion which is needed for certain purposes.

The physical problem is to determine the wave properties of an ionized medium which, in the steady state, consists of N_0 electrons per cc, N_{i0} positive ions per cc and gas molecules, and is pervaded by a static electric field $\mathbf{E}_0$ and a static magnetic field $\mathbf{H}_0$. Consequently in the steady state the electrons and ions have the mean drift velocities $\mathbf{U}_0$ and $\mathbf{U}_{i0}$, respectively, relative to a frame of reference in which the gas is at rest. In general also the electrons and ions will have random motions specified by the temperatures θ and θ_i, respectively, and frequencies of collision (with gas molecules) ν and ν_i, respectively. It has been found more convenient to specify the random motions by the quantities τ and τ_i which are equal to one-third of the mean square velocities of agitation of the electrons and ions, respectively. According to circumstances we may have $\tau \lesseqgtr U_0^2$ and $\tau_i \lesseqgtr U_{i0}^2$ (as for example in traveling-wave tubes and the ionosphere, respectively).

In the theory it is assumed as a first approximation that ν, ν_i, τ, τ_i are constants and that the distribution of random velocities is constant. Of course ν and ν_i are related to τ and τ_i and to U_0 and U_{i0} through the mean free paths, but the actual relations are best considered when the general theory is applied to a particular problem, for then known experimental data may be available or can be obtained. When the gas pressure is very low, as in electron-beam tubes or in the sun's atmosphere above 2000 km from its surface, the quantities ν, ν_i may in general be neglected when waves of several Mc/sec. frequency are being considered. The motions of the positive ions may also be neglected when the ionic density-frequency and gyro-frequency are both much less than the wave frequency.

The E.M.I. theory is developed from the following laws of physics:

I. Maxwell's laws of the electromagnetic field.
II. The conservation of electrons and positive ions.
III. Maxwell's laws of the transfer of momentum in mixtures of different kinds of particles which are also subject to fields of force.

As is well known, III represents only a first approximation to the exact laws. But the exact laws are in general much more complicated than Maxwell's and cannot be used without an exact knowledge of the laws of force which operate at collisions and which will differ according to the nature of the molecules and positive ions present. In any event it is known that in the few cases which have been studied rigorously the results show that Maxwell's laws of transfer are very good approximations. Also these laws become exact when the effects of collisions are negligible.

The laws of transfer of energy of agitation are here neglected in the interests of simplicity. The effect is unimportant when ν, ν_i, τ, and τ_i are negligible, but even when they are not, the effect may be important only in special circumstances. The analogous problem of the propagation of sound waves in air shows that the corresponding neglect of energy transfer leads only to the correction which Laplace made in Newton's estimate of the velocity of sound, namely about ten percent. In the E.M.I. theory we therefore neglect possible perturbations of ν, ν_i, τ, and τ_i and treat them as constants.

It has also been found convenient to introduce the vector and scalar potentials $\mathbf{A}$ and V.

The physical problem now consists of the study of perturbations of the quantities N_0, N_{i0}, $\mathbf{E}_0$, $\mathbf{H}_0$, $\mathbf{U}_0$, $\mathbf{U}_{i0}$, $\mathbf{A}_0$ and V_0. These perturbations are denoted by the corresponding lower case symbols n, n_i, $\mathbf{e}$, $\mathbf{h}$, $\mathbf{u}$, $\mathbf{u}_i$, $\mathbf{a}$ and v.

The resulting equations for the perturbations are non-linear. In a first approximation to their solutions we retain only the linear terms and so can obtain plane wave (or cylindrical wave) solutions of the form

$$Ae^{i(\omega t - Lx)}.$$

This first approximation therefore holds true only when the perturbations are small. But when the angular frequency ω lies within certain frequency bands,* the perturbations may grow sufficiently to make it necessary to retain the non-linear terms, and then the solutions become much more complicated and difficult to apply except in special cases. With such growing perturbations their reaction on the medium may become large enough to consider. It is clear that one important result is that the wave energy grows at the expense of the kinetic energies $\frac{1}{2}mU^2$, $\frac{1}{2}m_iU_i^2$, of the electrons and ions, which in turn draw upon the energy associated with the static electric and magnetic fields.

In this paper we cannot make an exhaustive study of all these questions as this would require too much space. We will therefore limit ourselves to a fairly exact study of the origin and escape of circularly polarized waves from a large, isolated sun spot and to a discussion of the reaction of such waves on the medium. For the same reason we shall postpone to a future occasion the full discussion of any longitudinal (plasma) growing waves and their interaction with the circular waves through non-linear terms in the equations or otherwise.

It may also be stated here that when the relativistic E.M.I. theory (in Appendix 1) is used it is found that as the drift velocity U_0 approaches c, the velocity of light, the possibility of growth tends to disappear. We will therefore restrict our discussion to situations in which $U_0^2 \ll c^2$.

The principal symbols used here are set out as follows, mostly in alphabetical order. Considerable use has been made of auxiliary symbols in order to keep the formulas and some of the discussion from becoming unwieldy.

* In which, for example, two possible values of L are conjugate complex numbers.

$\mathbf{A}_0, \mathbf{a}$ the static and varying vector potentials respectively.
βi the imaginary part of M.
c the velocity of light.
$\nabla = \mathbf{i}(\partial/\partial x) + \mathbf{j}(\partial/\partial y) + \mathbf{k}(\partial/\partial z)$.
$D_t = \partial/\partial t$.
$\Box^2 = \nabla^2 - c^{-2}D_t^2$.
$D = D_t + (\mathbf{U}\cdot\nabla)$.
e the electronic charge, in e.s.u.
$\mathbf{E}_0, \mathbf{e}$ the static and varying electric field vectors respectively.
E_1, E_2 denote circularly polarized waves defined under (20) or (20.1) and in Appendix 2.
$f = \omega/2\pi$, the wave frequency in Mc/sec.
$f_0 = p_0/2\pi$, the electron density frequency (or plasma frequency) in Mc/sec.
$f_H = \Omega_0/2\pi$, the electron gyro-frequency in Mc/sec.
$f_x, f_x' = \frac{1}{2}[(f_H^2 + 4f_0^2)^{\frac{1}{2}} \pm |f_H|]$ at x km above the sun's surface.
$\mathbf{H}_0, \mathbf{h}$ the static and varying magnetic field vectors respectively.
$\mathbf{i}, \mathbf{j}, \mathbf{k}$ unit vectors parallel to the x, y, and z axes respectively.
$k_n = (-)^{n-1}$ with $n = 1$ or 2.
L the angular wave number (complex).
M the complex refractive index.
μ the real part of M.
m the electronic mass.
N_0, n the static and varying number-density of electrons.
ν the frequency of collisions of an electron with other kinds of particles.
$p_0 = (4\pi N_0 e^2/m)^{\frac{1}{2}}$ the angular electron density frequency (or plasma frequency).
P the Poynting flux of energy.
$R = \omega - U_x L$.
$\rho = \nu/\omega$.
$\sigma_n = 1 - k_n\eta$.
τ one-third of the mean square velocity of electron agitation.
$\mathbf{U}_0, \mathbf{u}$ the mean steady drift velocity and varying velocity, respectively, of the electrons.
U_x, U_y, U_z the components of $\mathbf{U}_0$.
U an abbreviation for U_0.
V_0, v the static and varying scalar potentials.
$\mathbf{V}_0 = \mathbf{U}_0/c$.
$\mathbf{\Omega}_0 = (-e/mc)\mathbf{H}_0$ the angular electron gyro-frequency vector.
$\Omega_x, \Omega_y, \Omega_z$ the components of $\mathbf{\Omega}_0$.
Ω an abbreviation for Ω_0.
ω the angular wave frequency, always taken as positive.
$\omega_1, \omega_2 = \frac{1}{2}[(\Omega^2 + 4p_0^2)^{\frac{1}{2}} \pm |\Omega|]$.
ω_a, ω_a' values of ω_1, ω_2 respectively in a medium A.
$X = R^2 - \tau L^2 - p_0^2 - i\nu R$.
$\xi = p_0^2/\omega^2$.
$Y = R(Z + p_0^2) - i\nu Z$.
$\eta = \Omega/\omega$.
$Z = c^2L^2 - \omega^2$.
x, y, z space coordinates.
t time.

With the notation

$$\left.\begin{array}{lll} N = N_0 + n, & \mathbf{E} = \mathbf{E}_0 + \mathbf{e}, & \mathbf{H} = \mathbf{H}_0 + \mathbf{h}, \\ \mathbf{U} = \mathbf{U}_0 + \mathbf{u}, & \mathbf{A} = \mathbf{A}_0 + \mathbf{a}, & V = V_0 + v, \end{array}\right\} \quad \text{(A)}$$

and the motions of the positive ions neglected, the complete set (S) of fundamental equations which express the laws I, II and III are

$$\mathbf{E} = c^{-1}D_t\mathbf{A} - \nabla V, \tag{1}$$

$$\mathbf{H} = \nabla\times\mathbf{A}, \tag{2}$$

$$4\pi e(N - N_{i0}) = -\Box^2 V, \tag{3}$$

$$4\pi e N\mathbf{U} = -\Box^2\mathbf{A}, \tag{4}$$

$$D_t N = -\nabla(N\mathbf{U}), \tag{5}$$

$$D\mathbf{U} + \nu\mathbf{U} + N^{-1}\nabla\tau N = (e/m)(\mathbf{E} + c^{-1}\mathbf{U}\times\mathbf{H}). \tag{6}$$

The set (S_0) of equations for the steady state of the medium are obtained from this set (S) by adding the suffix 0 to all the variables and omitting all the terms in which D_t occurs.

As a check it will be found that the Eq. (6_0) obtained from (6) is consistent with the classical formulas of J. S. Townsend[3] for the steady motions of electrons under the action of uniform electric and magnetic fields. When N_0 is uniform in the steady state (6_0) becomes

$$(\mathbf{U}_0\cdot\nabla)\mathbf{U}_0 + \nu\mathbf{U}_0 - (e/mc)\mathbf{U}_0\times\mathbf{H}_0 = (e/m)\mathbf{E}_0; \tag{7}$$

this equation determines the drift velocity $\mathbf{U}_0$ in terms of the static electric and magnetic fields and the collision frequency or, alternatively, determines the electric field required to set up a given drift velocity.

To obtain the set of equations (S_p) for the perturbations we substitute in the set (S) given above the expressions for N, $\mathbf{E}$, $\mathbf{H}$, etc., given under (A), and subtract the corresponding equations in the set (S_0). As some of (S_p) are non-linear, we may in a first approximation, which is valid for sufficiently small pertubations, retain only the linear terms.

When the medium and the static fields are uniform in the steady state the quantities with suffix 0 are all constants and $N_{i0} = N_0$. To study any (small) plane perturbation of this state it is sufficient, by Fourier's integral theorem, to take all the lower case variables in the linear equations (S_p) to be proportional to

$$e^{i(\omega t - Lx)}. \tag{8}$$

Then (S_p) reduces to the following set:

$$\mathbf{e} = -ic^{-1}\omega\mathbf{a} + iL v\mathbf{i}, \tag{1.1}$$

$$\mathbf{h} = -iL\mathbf{i}\times\mathbf{a}, \tag{2.1}$$

$$n = (Z/4\pi ec^2)v, \tag{3.1}$$

$$N_0\mathbf{u} + \mathbf{U}_0 n = (Z/4\pi ec)\mathbf{a}, \tag{4.1}$$

$$Rn = N_0 L u_x, \tag{5.1}$$

$$\delta\mathbf{u} - \mathbf{\Omega}_0\times\mathbf{u} - i\tau N_0^{-1}Ln\mathbf{i} = (e/m)(\mathbf{e} + c^{-1}\mathbf{U}_0\times\mathbf{h}), \tag{6.1}$$

where Z, R, δ and $\mathbf{\Omega}_0$ are defined below under (11).

Without loss of generality we shall take the xy plane so that it contains the direction of the drift velocity, i.e., we take $U_z = 0$.

On eliminating $\mathbf{e}$, $\mathbf{h}$, n and $\mathbf{u}$ from (6.1) by means of the Eqs. (1.1) to (5.1) we obtain the following equations

[3] J. S. Townsend, *Electricity in Gases* (Clarendon Press, Oxford, 1915), Sections 91 and 92.

in the components a_x, a_y, a_z of $\mathbf{a}$:

$$\left.\begin{aligned}\alpha_x a_x+\alpha_y a_y+\alpha_z a_z&=0,\\ \beta_x a_x+\beta_y a_y+\beta_z a_z&=0,\\ \gamma_x a_x+\gamma_y a_y+\gamma_z a_z&=0,\end{aligned}\right\} \quad (9)$$

where

$$\left.\begin{aligned}&\alpha_x=X+iL\Omega_z U_y, \quad \alpha_y=-i\omega\Omega_z+p_0^2\omega L U_y Z^{-1}, \quad \alpha_z=i\omega\Omega_y,\\ &\beta_x=-(\Omega_z R+L\delta U_y)Z, \quad \beta_y=i\omega Y, \quad \beta_z=\omega\Omega_z Z,\\ &\gamma_x=(\Omega_y R+L\Omega_z U_y)Z, \quad \gamma_y=-\omega\Omega_z Z, \quad \gamma_z=i\omega Y,\end{aligned}\right\} \quad (10)$$

with

$$\left.\begin{aligned}X&=R^2-\tau L^2-p_0^2-i\nu R,\\ Y&=R(Z+p_0^2)-i\nu Z,\\ Z&=c^2L^2-\omega^2,\\ R&=\omega-U_x L,\\ \delta&=iR+\nu,\\ p_0^2&=4\pi N_0 e^2/m,\\ \boldsymbol{\Omega}_0&=(-e/mc)\mathbf{H}_0=(\Omega_x,\ \Omega_y,\ \Omega_z).\end{aligned}\right\} \quad (11)$$

The necessary and sufficient condition for a non-zero solution of (9) is that the determinant Δ formed by the coefficients is zero; this yields the equation of dispersion.

When we take into account the fact that $U_y^2 \ll c^2$ it is found that the terms in U_y^2 are always small compared with certain others. On neglecting the terms in U_y^2 the equation of dispersion reduces to the form

$$X(Y^2-\Omega_x^2 Z^2)-(\Omega_y^2+\Omega_z^2)RYZ -2p_0^2 LRZ\Omega_x U_y\Omega_y=0, \quad (12)$$

which is of the eighth degree in L and ω.

This form differs from the Eq. (3A) in Appendix 1, which is derived by means of a relativistic theory, only by quantities which are of the second or higher orders of smallness in U_x, U_y and τ.

When (12) is satisfied then, by (9), a_x, a_y, a_z are proportional to the co-factors of any row of the determinant.

Then $\mathbf{e}$ and $\mathbf{h}$ are given by

$$\left.\begin{aligned}e_x&=-\phi\omega^{-2}Z a_x, \quad e_y=\phi a_y, \quad e_z=\phi a_z,\\ h_x&=0, \quad h_y=-\phi M a_z, \quad h_z=\phi M a_y,\end{aligned}\right\} \quad (13)$$

where $\phi=-i\omega/c$, $M=cL/\omega$.

When the drift velocity $\mathbf{U}_0$ and the electron temperature (proportional to τ) are negligible (12) reduces to the (bi-quadratic) equation of dispersion in the M.I. theory. For small enough collision frequencies (e.g., $\nu \ll \omega$) the latter equation reduces to

$$(\omega^2-p_0^2)[\omega^2(Z+p_0^2)^2-\Omega_x^2 Z^2] -\Omega_T^2\omega^2 Z(Z+p_0^2)=0, \quad (12.0)$$

where

$$Z=c^2L^2-\omega^2=\omega^2(M^2-1), \quad \Omega_T^2=\Omega_y^2+\Omega_z^2.$$

The (ω, L) curve corresponding to (12.0) is symmetrical about both axes. It cuts the ω-axis at the points ± 0, $\pm p_0$, $\pm\omega_1$, $\pm\omega_2$, where

$$\omega_1, \omega_2=\tfrac{1}{2}[(\Omega_0^2+4p_0^2)^{\frac{1}{2}}\pm|\Omega_0|]. \quad (14)$$

It has the oblique asymptotes $cL=\pm\omega$ and the asymptotes $\omega=\pm\omega_3$, $\omega=\pm\omega_4$ parallel to the L axis where

$$\omega_3, \omega_4=+[\tfrac{1}{2}(\Omega_0^2+p_0^2)\pm(\tfrac{1}{4}(\Omega_0^2+p_0^2)^2-\Omega_x^2 p_0^2)^{\frac{1}{2}}]^{\frac{1}{2}}. \quad (15)$$

For example when the plasma frequency is 100 Mc/sec., the gyro-frequency is 600 Mc/sec. and the angle θ between the directions of the magnetic field and of propagation is more than 45°, then

$$\omega_1/2\pi \doteqdot 616, \quad \omega_2/2\pi \doteqdot 16.5,$$
$$\omega_3/2\pi \doteqdot 605, \quad \omega_4/2\pi \doteqdot 100\cos\theta \text{ Mc/sec.}$$

The frequencies 0, p_0, ω_1, ω_2, ω_3 and ω_4 are the edges of frequency bands within which the wave number L (and the refractive index M) is purely imaginary. In these bands waves cannot propagate through the given medium.

It can be shown that in general

$$\omega_1>(\Omega_0^2+p_0^2)^{\frac{1}{2}}>\omega_3>(\tfrac{1}{2}(\Omega_0^2+p_0^2))^{\frac{1}{2}}>\omega_4$$

and

$$\omega_2<p_0^2/(\Omega_0^2+p_0^2)^{\frac{1}{2}}<\omega_1,$$

and that when $\Omega_0^2>p_0^2$ than $\omega_1>\omega_3>\omega_2$ and ω_4.

One of the bands then lies between ω_1 and ω_3 and one of the other bands lies between ω_2 and 0.

When an electron drift velocity $\mathbf{U}_0$ exists the corresponding (ω, L) curve has some branches which are similar to the ones just considered but distorted in a skew manner so that they become *unsymmetrical* about the ω-axis. The principal consequence is that in general we now obtain bands in which L (and M) is a *complex* number $a\pm ib$.

These bands approximate to the bands considered above in the M.I. theory. We thus see that the effect of electron drift is to create wave amplification and consequent electromagnetic noise in frequency bands in which otherwise waves cannot propagate.† If $L=a\pm ib$ the phase velocity is ω/a and one of the two corresponding waves or wave groups grows by the factor $\exp|bx|$ in the distance x.

No wave amplification is possible when the wave is propagated transversely to the drift velocity and at the same time the magnetic field is perpendicular to either the direction of propagation or the drift velocity. This follows from the fact that when $U_x=0$ and $\Omega_x U_y\Omega_y=0$ then (12) reduces to the Eq. (12.0) corresponding to the M.I. theory.

In particular when the drift and magnetic field have a common direction (as in the case (C 11) considered below) wave growth is in general increasingly favored by orientation of the direction of propagation towards this common direction.

In general a root of (12) can be determined only by some method of successive approximation, like Newton's, from some first approximation. In one method of

† This prediction of noise occurring in separate bands has now been confirmed by means of experiments carried out in collaboration with Dr. K. Landecker. These experiments will be described elsewhere.

TABLE I.

Height x in km.	ϵ_1 <	ϵ_2 <	ϵ_3 <	ϵ_4 <	ϵ_5 <
$>2\times10^3$	2×10^{-4}	10^{-4}	2×10^{-3}	50	10^{-2}
$>10^4$	10^{-8}	10^{-9}	2×10^{-8}	50	5×10^{-7}

getting the first approximation we take $\nu=0$ and in another $U_0=0$. Both have their special uses. The second method has the special virtue that it develops four of the roots from those of the M.I. theory; moreover the latter are expressible in a closed form.

We shall now consider in detail the important case in which the drift and magnetic field are both in the direction of propagation, i.e., when

$$U_x=U_0,\ U_y=U_z=0 \text{ and } \Omega_x=\Omega_0,\ \Omega_y=\Omega_z=0. \quad \text{(C 11)}$$

From now on we may conveniently drop the subscript 0 from the symbols U_0 and Ω_0.

Then (10) and (9) combined with (13), yield

$$\left.\begin{aligned} Xe_x&=0,\\ iYe_y+\Omega_x Ze_z&=0,\\ -\Omega_x Ze_y+iYe_z&=0,\end{aligned}\right\} \quad (16)$$

The first equation yields two waves with the dispersion equation $X=0$, i.e.,

$$(\omega-UL)^2-\tau L^2-p_0^2-i\nu(\omega-UL)=0, \quad (17)$$

which have their electric vectors in the direction of propagation and no magnetic vectors. These waves will grow when

$$\tau>U^2>0 \quad \text{and} \quad \nu^2\ll\omega^2<p_0^2(1-U^2/\tau).$$

Since they have no corresponding Poynting flux they are not of primary importance in considering observed circular solar noise. In a more exhaustive study they may require to be considered when (and only when) account is taken of the neglected non-linear terms. Otherwise, as will be seen, the origin and escape of circular solar noise can be adequately accounted for quite independently of these waves. For these reasons their detailed discussion here is omitted.‡

The second and third equation under (16), combined with (13) yield the following results:

There are two types of waves with dispersion equations given by

$$Y-k_n\Omega Z=0, \quad (n=1, 2), \quad (18)$$

where

$$k_1=1, \quad k_2=-1,$$

and polarizations given by

$$h_z/h_y=-k_n i. \quad (19)$$

These two types may be conveniently labeled

$$\left.\begin{aligned} &E_1 \text{ waves when } k_n\Omega>0;\\ &E_2 \text{ waves when } k_n\Omega<0.\end{aligned}\right\} \quad (20)$$

In conformity with the M.I. theory (as shown in Appendix 2) the E_1 and E_2 waves may be termed extraordinary and ordinary waves, respectively.

By (19) they are both circularly polarized, but in opposite senses. Also by (18) and (19),

$$\left.\begin{aligned} &E_1 \text{ waves are } RH \text{ or } LH \text{ and } E_2 \text{ waves are}\\ &LH \text{ or } RH \text{ according as } \Omega\gtrless0, \text{ i.e., } H\gtrless0,\end{aligned}\right\} \quad (20.1)$$

where *RH* and *LH* mean, respectively, right-handed and left-handed direction of rotation of the magnetic vector when viewed in the direction of $0x$.

From (16), (1.1), (3.1), and (5.1) we see that for these waves e_x, v, n and u_x are zero, i.e., the electric and magnetic vectors and the electron vibrations are purely

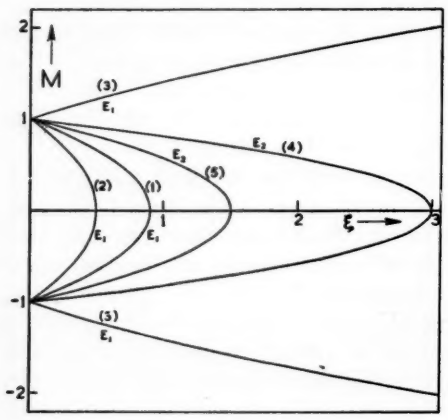

FIG. 1. Curves of (ξ, M) for E_1 and E_2 waves with $V=0$ and the following values of $k_n\eta$: (1) 0.1; (2) 0.5; (3) 2; (4) −2; (5) −0.5.

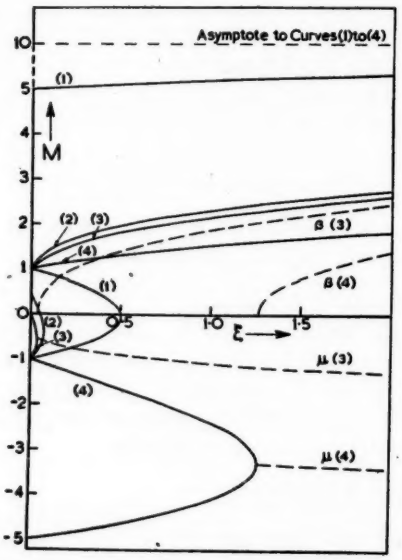

FIG. 2. Curves of (ξ, M) for E_1 waves with $V=0.1$ and the following values of $k_n\eta$: (1) 0.5; (2) 0.95; (3) 1; (4) 1.5.

‡ Some numerical examples of such longitudinal waves are given in reference 2 and in a joint paper with J. A. Roberts in the Australian J. Sci. Res. A, 2, 307 (1949). Also it now appears that such waves have been previously discussed by W. O. Schumann in Zeits. f. Physik 121, 7 (1943).

transverse, and there are no perturbations of the electron density.

Also from (4.1) and (13) we have

$$\mathbf{u}=(1/4\pi N_0 e)i\omega(M^2-1)\mathbf{e}. \tag{21}$$

These circular waves and the longitudinal waves (corresponding to (17)) thus form a complete contrast. Also they are entirely without mutual interactions (i.e., coupling) unless and until one of them can grow so large that the non-linear terms of the theory become important. Therefore in considering the growth of the circular waves it is initially unnecessary to consider the possibility of having growing longitudinal waves.

2. THE CIRCULARLY POLARIZED WAVES

The dispersion Eqs. (18) of circular waves, when expanded by means of (11), are the two cubics

$$(VM-1)\{\omega^2(M^2-1)+p_0^2\}+(k_n\Omega+i\nu)\omega(M^2-1)=0, \tag{22}$$

where M is the complex refractive index; $V=U/c$ and $V^2\ll 1$.

These show that the circular waves depend on the random motions of the electrons only through the terms in ν.

In order to discuss the propagation of waves in a medium which is gradually varying in space we shall adopt the following convenient notation¶

$$\xi=p_0^2/\omega^2, \quad \eta=\Omega/\omega, \quad \sigma_n=1-k_n\eta, \quad \rho=\nu/\omega. \tag{23}$$

Then the cubics (22) assume the form

$$f(M)\equiv VM^3-(\sigma_n-i\rho)M^2+V(\xi-1)M+\sigma_n-\xi-i\rho=0. \tag{24}$$

In general the roots of each cubic are unequal.

In our applications of the theory of the sun's atmosphere (in Section 5) the adopted numerical values of p_0, Ω and ν are those given by Smerd,[4] the magnetic field H being that above the center of a large sunspot. His values of $f_0=p_0/2\pi$ and $f_H=|\Omega|/2\pi$ are also indicated in our Fig. 4 by means of curves.

From such data we find that in regions at different heights x above the sun's surface and for waves of frequencies ω such that they can grow in these regions, the following relations exist:

$$\nu=\epsilon_1 p_0, \quad \nu=\epsilon_2|\Omega|, \quad \nu=\epsilon_3\omega, \quad \omega=\epsilon_4 p_0, \quad \rho=\epsilon_5\xi,$$

where ϵ_1, ϵ_2, ϵ_3, ϵ_4 and ϵ_5 $(=\epsilon_1\epsilon_4)$ have values less than the numbers given in the corresponding columns of Table I.

Thus in our application we have:

Above the heights 2×10^3 and 10^4 km, respectively,
$\rho<2\times10^{-3}$ and 2×10^{-8},
$\rho<10^{-4}|k_n\eta|$ and $10^{-9}|k_n\eta|$,
$\rho<10^{-2}\xi$ and $5\times10^{-7}\xi$. (25)

¶ This is in part similar to one often used in discussing propagation in the ionosphere.

[4] S. F. Smerd, Australian Council for Scientific and Industrial Research, R. P. L. 14 (January, 1948).

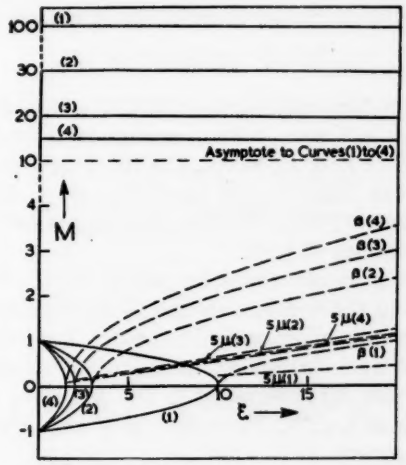

FIG. 3. Curves of (ξ, M) for E_2 waves with $V=0.1$ and the following values of $k_n\eta$: (1) -9; (2) -2; (3) -1; (4) -0.5.

Therefore in (24) the terms in ρ may be neglected except perhaps when $|\xi-\sigma_n|$ or $|\sigma_n|$ is comparable with, or less than, ρ.

We shall first consider the general circumstances in which ρ is negligible, i.e., when (24) approximates to

$$f(M)\equiv VM^3-\sigma_nM^2+V(\xi-1)M+\sigma_n-\xi=0. \tag{24.0}$$

In general neither of these cubics has more than two roots equal.

The six roots of these equations will be denoted by M_1, M_2, M_3 for the E_1 waves (when $\sigma_n<1$), and by M_{-1}, M_{-2}, M_{-3} for the E_2 waves (when $\sigma_n>1$).

The dependence of real values of M on the electron density N_0 is conveniently shown by drawing curves with ξ and M as coordinates for given values of η and V and for $\xi>0$. Such curves are illustrated by Figs. 1 to 3.

Points on the curve defined by (24.0) are most easily determined by calculating ξ for real values of M.

The intercept on the ξ-axis is σ_n and the intercepts on the M axis are 1, -1, $V^{-1}\sigma_n$. The only asymptote to the curve is

$$M=V^{-1}$$

and is approached from above or below according as $\sigma_n\gtrless 1$.

The important ranges of values of ξ in which growing waves can occur are indicated by means of the vertical tangents. These tangents occur at points P_1, P_2, P_3 determined by (24.0) and the equation

$$M=V^{-1}\theta,$$

where θ is a root of

$$\theta^3-\tfrac{1}{2}(\sigma_n+3)\theta^2+\sigma_n\theta-\tfrac{1}{2}V^2(\sigma_n-1)=0.$$

Since $V^2\ll 1$ and in general $\sigma_n\neq 0$ the two larger roots θ_1, θ_2 and the third root are given approximately by

$$\theta_1, \theta_2\doteqdot\tfrac{1}{4}\{(\sigma_n+3)\pm(\sigma_n^2-10\sigma_n+9)^{\frac{1}{2}}\}, \quad \theta_3\doteqdot\tfrac{1}{2}V^2(1-\sigma_n^{-1}).$$

The values of ξ at the vertical tangents are given by

$$\xi=(1-V^{-2}\theta^2)(\sigma_n-\theta)/(1-\theta).$$

The two tangents corresponding to θ_1 and θ_2 exist only when $\sigma_n\leqslant 1$ or $\geqslant 9$ i.e., always for E_1 waves and when $k_n\eta<-8$ for E_2 waves. The third vertical tangent, occurs near (but not at) the point $\xi=\sigma_n$ where the curve cuts the ξ-axis. When $\sigma_n<0$ this tangent does not exist for values of $\xi>0$.

Figure 1 shows examples when $V=0$. This corresponds to the well-known case of longitudinal propagation in the magneto-ionic theory. The curves are parabolas and correspond to the usual straight lines which depict M^2 in terms of ξ. The waves are E_1 or E_2 according as $k_n\eta\gtrless 0$. The values of M are either real or pure imaginary.

Figures 2 and 3, respectively, give examples of E_1 and E_2 waves when $V>0$ i.e., when the electrons have a motion of drift in the direction of $0x$. These show that the values of M are in general either real or complex with non-zero real parts. Thus for a given frequency and type E_n there are values of the electron density for which all the waves remain constant in amplitude, apart from attenuation due to electron collisions. These may be called waves of the First Species. With other values of the electron density one of the waves grows and another attenuates (apart from the results of collisions) as they travel. These may be called waves of the Second Species.

For *all* values of the electron density at least two progressive waves of each type can exist. The only values of electron density at which just two such waves can exist are those corresponding to the points $\xi=\sigma_n$, where $M=0$.

In those parts of Figs. 2 and 3 where only one real root M_3 occurs the complex roots M_1, M_2 can be calculated as follows by means of the values of M_3:

$$M_1=\mu+i\beta, \quad M_2=\mu-i\beta, \tag{26}$$

where

$$\left.\begin{aligned}\mu&=\tfrac{1}{2}(V^{-1}\sigma_n-M_3),\\ \beta&=[V^{-1}M_3^{-1}(\xi-\sigma_n)-\tfrac{1}{4}(V^{-1}\sigma_n-M_3)^2]^{\frac{1}{2}}.\end{aligned}\right\} \tag{27}$$

From (27) and (24.0) we have

$$\frac{\xi}{2\mu}=\frac{M_3^2-1}{M_3-V^{-1}},$$

and since $\xi>0$ it follows that $\mu>0$ when $M_3<V^{-1}\sigma_n$ and either (a) $V>0$ with $|M_3|<1$ or $M_3>V^{-1}$, or (b) $V<0$ with $|M_3|>1$ and $M_3>V^{-1}$.

From this we deduce that

$$\left.\begin{aligned}&\mu>0 \text{ only when}\\ &V>0 \text{ and } k_n\eta<1+V,\\ \text{or}\quad &V<0 \text{ and } k_n\eta>0.\end{aligned}\right\} \tag{28}$$

Similar remarks may be made about M_{-3}, M_{-1}, M_{-2}.

The dashed curves in Figs. 2 and 3 show μ and β in terms of ξ. They relate to E_1 or E_2 waves according as $k_n\Omega\gtrless 0$.

Physically μ is the real refractive index and β is the index of growth or attenuation.

When $|V|\ll 1$, direct approximations to the roots M_1, M_2 can be made as follows.

As first approximations to them we take the roots M_{10}, M_{20} of the equation derived from (24.0) when V is made zero, namely

$$M_{10}, M_{20}=\pm ia=\pm i(\xi\sigma_n^{-1}-1)^{\frac{1}{2}}.$$

Then by Newton's method of iteration applied to (24.0) we obtain the second approximations

$$M_1, M_2=\pm ia\pm\frac{Va\xi(1-\sigma_n^{-1})}{\pm 2\sigma_n a+iV(2+\xi-3\xi\sigma_n^{-1})}.$$

Hence, if

$$\left.\begin{aligned}a&=(\xi\sigma_n^{-1}-1)^{\frac{1}{2}},\\ b&=\{1+\tfrac{1}{2}\xi(1-3\sigma_n^{-1})\}a^{-1},\\ \psi&=k_n\eta\xi/2(\sigma_n^2+V^2b^2),\end{aligned}\right\} \tag{29}$$

then,

$$M_1, M_2=\mu\pm i\beta, \tag{30}$$

where

$$\mu\doteqdot -V\psi, \quad \beta\doteqdot a+V^2\psi\sigma_n^{-1}b. \tag{31}$$

Clearly in this approximation M_1, M_2 are complex when $\xi>\sigma_n>0$, i.e., when $0<\omega<\delta\omega_2$ and $|\Omega|<\omega<\omega_1$, where ω_1, ω_2 are defined under (14).

For E_1 waves in the critical case $\sigma_n=0$ we have to proceed otherwise. Thus, when in (24.0)

$$\sigma_n=0 \quad \text{and} \quad |V|\ll|\xi(\xi-1)^{-\frac{1}{2}}|$$

we may take $M_3\doteqdot(V^{-1}\xi)^{\frac{1}{3}}$ and then (27) yields the following result:

$$\left.\begin{aligned}&\text{When } \omega=k_n\Omega \text{ and } |V|\ll|\xi(\xi-1)^{-\frac{1}{2}}|,\\ &\text{then}\\ &\mu\doteqdot -\tfrac{1}{2}(V^{-1}\xi)^{\frac{1}{3}}, \quad \beta\doteqdot \tfrac{1}{2}\sqrt{3}(V^{-1}\xi)^{\frac{1}{3}}.\end{aligned}\right\} \tag{31.1}$$

The corresponding waves may be termed E_1 gyro waves of the Second Species.

Values of M, μ, and β calculated by means of (31) and (31.1) are found to agree well with those given by the curves in Figs. 2 and 3.

The formulas (31), (20), and (31.1) yield the following conditions for μ to be positive:

$$\left.\begin{aligned}&\text{When } |V|\ll 1 \text{ and } \sigma_n\gtrless 0 \text{ then } \mu>0 \text{ only}\\ &\quad\text{with } E_1 \text{ waves and } V<0, \text{ or}\\ &\quad\quad E_2 \text{ waves and } V>0.\end{aligned}\right\} \tag{28.1}$$

These conclusions are substantially independent of collisions when the terms in ρ of (24) are negligible. As mentioned earlier this is so when $|\xi-\sigma_n|$ and $|\sigma_n|$ are large compared with ρ, i.e., when the wave frequency does not lie near one of the frequencies ω_1, ω_2 or $|\Omega|$.

When $|\xi-\sigma_n|$ or $|\sigma_n|$ is either (a) comparable with ρ, or (b) less than ρ, a special investigation is necessary.

Under (a) the calculations are very lengthy whereas under (b) they are both relatively simple and more sensitive to the effects of collisions. Accordingly we shall here consider only the following special cases:

I. $|\xi-\sigma_n|\ll\rho\ll\sigma_n$ and ξ;
II. $|\sigma_n|\ll\rho\ll\xi$.

The condition $\rho\ll\xi$ is added on account of (25). In the case I we obtain from (24)

$$M_1\doteq(-k_nV\eta/\sigma_n)(1+i\rho/\sigma_n),\quad M_2\doteq-i\rho/k_nV\eta.$$

This shows that for $\mu=\mu_1$ (28.1) also holds true in I.

In the case II we obtain the same approximate results as under (31.1) and (28.1) when $|V|\gg\rho$.

We may therefore conclude, with the help of (25), that in our application to the sun's atmosphere, as exemplified by Fig. 4, the effect of collisions on growth may be neglected in regions above 2000 km when the drift velocity $|U|\gg6\times10^7$ cm/sec. and in regions above 10^4 km when $|U|\gg600$ cm/sec.

3. THE WAVES WHICH CORRESPOND TO ANY TRANSVERSE PERTURBATION TEMPORALLY PRESCRIBED AT THE PLANE $x=0$

In this section it will be shown that (a) any transverse perturbation at a given plane gives rise to two trios of circular waves which are oppositely polarized and can be treated independently of each other; (b) within certain frequency bands each trio will in general grow; (c) the mean Poynting flux of a wave with refractive index $M_m=\mu_m+i\beta_m$ is in the direction of propagation $0x$ and grows in that direction when μ_m and β_m are both positive.

Also the type of growing waves (E_1 or E_2) is found which carries field energy in the direction of $0x$ under different conditions ((48) and (48.1)).

The arguments are set out in some detail partly for the sake of clarity and partly because some of the relevant formulas ((32), (33), (42.1), and (42.2)) are required in the next section.

The vital question of escape of field energy from the sun's atmosphere makes the discussion of the Poynting flux of primary importance. It has not been found necessary here to consider the behavior of wave groups, i.e., of integral expressions like those in (32) but with the limits of integration replaced by $\omega_0+\delta\omega$ and $\omega_0-\delta\omega$, respectively. This is fortunate since the mathematical definition of a wave group is apt to become physically vague (and perhaps misleading) when the rate of growth is very large.‖

We shall represent the given transverse perturbation by the electric vector **e**, the magnetic vector **h** and the electron velocity **u**. Their dependence on time will be indicated, when necessary, by the notation $\mathbf{e}(t)$, $\mathbf{h}(t)$, $\mathbf{u}(t)$.

We shall now determine the values of the corresponding vectors at the plane x, namely

$$\mathbf{e}(t,x),\quad \mathbf{h}(t,x),\quad \mathbf{u}(t,x).$$

These can be expressed in the following general forms which all satisfy the fundamental Eqs. (1.1) to (6.1).

$$\left.\begin{aligned}\mathbf{e}(t,x)&=\int_0^\infty\sum_m\mathbf{A}_me^{i\omega(t-M_mx)}d\omega,\\ \mathbf{h}(t,x)&=\int_0^\infty\sum_m\mathbf{B}_me^{i\omega(t-M_mx)}d\omega,\\ \mathbf{u}(t,x)&=\int_0^\infty\sum_m\mathbf{C}_me^{i\omega(t-M_mx)}d\omega,\end{aligned}\right\}\quad(32)$$

where $m=1,2,3,-1,-2,-3$, and for convenience the velocity of light c is taken as the unit of velocity.

M_m is a known function of ω derivable from (24.0), and $\mathbf{A}_m$, $\mathbf{B}_m$, $\mathbf{C}_m$ are functions of ω which remain to be determined.

On setting $x=0$ and inverting the resulting Fourier integrals we obtain

$$\left.\begin{aligned}\sum_m\mathbf{A}_m=\mathbf{I}_e&\equiv1/\pi\int_0^\infty\mathbf{e}(\alpha)e^{-i\omega\alpha}d\alpha,\\ \sum_m\mathbf{B}_m=\mathbf{I}_h&\equiv1/\pi\int_0^\infty\mathbf{h}(\alpha)e^{-i\omega\alpha}d\alpha,\\ \sum_m\mathbf{C}_m=\mathbf{I}_u&\equiv1/\pi\int_0^\infty\mathbf{u}(\alpha)e^{-i\omega\alpha}d\alpha.\end{aligned}\right\}\quad(33)$$

The quantities $\mathbf{I}_e$, $\mathbf{I}_h$, $\mathbf{I}_u$ are thus known in terms of the given perturbation.

Since the component waves are circularly polarized we may by (13) and (19) write

$$\mathbf{A}_m=(\mathbf{j}-ik_n\mathbf{k})A_m,\quad(34)$$

where, according as $\Omega\gtrless0$,

$k_n=\pm1$ for E_1 waves and $k_n=\mp1$ for E_2 waves.

Hence from (33) we obtain

$$A_1+A_2+A_3=J_e^1,\quad(35.1)$$

$$A_{-1}+A_{-2}+A_{-3}=J_e^2,\quad(35.2)$$

where

$$J_e^1=\tfrac12(I_{ex}\pm iI_{ez}),\quad J_e^2=\tfrac12(I_{ex}\mp iI_{ez}),\quad(36)$$

and we take the upper or lower signs according as $\Omega\gtrless0$. Similarly we have

$$B_1+B_2+B_3=J_h^1,\quad(37.1)$$

$$C_1+C_2+C_3=J_u^1,\quad(38.1)$$

and analogous relations (37.2), (38.2).

But from (13) and (19) we obtain

$$B_m=ik_nM_mA_m,\quad(39)$$

‖ This difficulty is absent in the M.I. theory and so the notion of group-velocity may there be profitably used.

and from (21) combining with (13),

$$\mathbf{C}_m = iK^{-1}\omega(M_m^2-1)\mathbf{A}_m, \tag{40}$$

where

$$K = 4\pi N_0 e. \tag{41}$$

Thus (35.1), (37.1), and (38.1) yield the following system of three simultaneous equations:

$$\left.\begin{aligned} A_1+A_2+A_3 &= J_e^1, \\ M_1A_1+M_2A_2+M_3A_3 &= -k_nJ_h^1, \\ M_1^2A_1+M_2^2A_2+M_3^2A_3 &= -K\omega^{-1}J_u^1+J_e^1. \end{aligned}\right\} \tag{42.1}$$

A similar set (42.2) relates A_{-1}, A_{-2}, A_{-3}.

These results show that the original perturbation can be split up into two kinds of circular waves which are oppositely polarized.

Thus (32) may be replaced by two similar sets of Eqs. (32.1) and (32.2). In (32.1), $\mathbf{e}(t, x)$, etc., are replaced by $\mathbf{e}_1(t, x)$ etc., and m takes the values 1, 2, 3, while in (32.2) $\mathbf{e}(t, x)$ etc., are replaced by $\mathbf{e}_2(t, x)$ etc., and m takes the values -1, -2, -3.

Accordingly each trio of waves may be treated in every respect independently of the other.

When M_1, M_2, M_3 are all different (42.1) always yields finite values of A_1, A_2, A_3.

When $M_1=M_2\neq M_3$ the terms A_2, M_2A_2 and $M_2^2A_2$ in (42.1) are replaced respectively by 0, $i\omega^{-1}A_2'$ and $2i\omega^{-1}M_1A_2'$, but finite values of A_1, A_2' and A_3 are always obtained.

As (24.0) cannot in general have three equal roots this case need not be considered.

Similarly we always obtain finite values of A_{-1}, A_{-2}, A_{-3}.

When

$$M_m = \mu_m + i\beta_m,$$

with μ_m, β_m both real functions of ω, the corresponding term in (32.1) is

$$\int_0^\infty \mathbf{A}_m e^{\omega\beta_m x}\cdot e^{i\omega(t-\mu_m x)}d\omega. \tag{43}$$

From (24.0) we see that when ω exceeds a certain finite value ω_0 all the values of M_m are real, i.e., $\beta_m=0$. It then follows that all the integrals (43) are finite.

Also when $\omega<\omega_0$, β_m has two equal non-zero values of opposite signs and therefore the E_1 perturbations represented by (32.1) will in general ultimately grow with increasing $|x|$.

Similar results hold for (32.2).

The mean Poynting flux for the wave with index M_m is given by

$$\bar{P}_m = c/4\pi|A_m|^2\mu_m e^{2\omega\beta_m x}, \tag{44}$$

where

$$M_m = \mu_m + i\beta_m. \tag{45}$$

Thus

$$\bar{P}_m>0 \text{ when } \mu_m>0 \tag{46}$$

and

$$\bar{P}_m \text{ increases with } x \text{ when } \beta_m>0. \tag{47}$$

From (46), (28), and (28.1) we derive these results:

The only growing waves which carry field energy in the direction of $0x$ are as follows:
With $V>0$ they are growing E_1 or E_2 waves according as $0<k_n\eta<1+V$ or $k_n\eta<0$.
With $V<0$ they are always E_1 waves. (48)

When $|V|\ll 1$, the only growing waves which carry field energy in the direction of $0x$ are E_2 or E_1 waves according as $V\gtrless 0$. (48.1)

When $V>0$ these waves may in general be either RH or LH but when $1\gg V>0$ they are LH or RH according as $\mathbf{H}$ and $0x$ have the same or opposite directions. Also when $V<0$ they are RH or LH according as $\mathbf{H}$ and $0x$ have the same or opposite directions.

By (31), (31.1) and (44) when $|V|\ll 1$ then for a growing wave $\bar{P}_m$ is nearly proportional to V, except when the wave is an E_1 gyro wave.

For the waves of constant amplitude $\bar{P}_m$ is positive when $M_m>0$.

4. PASSAGE OF A GROWING CIRCULARLY POLARIZED PERTURBATION NORMALLY THROUGH THE BOUNDARY BETWEEN TWO DIFFERENT MEDIA

In this section it is proposed first to determine the transverse perturbations in a medium A which lead to a given transverse perturbation, in a second medium B, for which the mean energy flux $\bar{P}$ travels away from A, with $V\neq 0$ in one or both media.

This is done in the following way. First the wave components on one side of the common boundary of A and B are related to those on the other side and then expressed separately in terms of the latter. Next it is shown that these expressions always yield finite values for the components sought. Then it is shown that even with $V=0$ in either A or B, waves of sufficiently high frequency which exist in one medium must lead to waves in the other. Lastly, necessary and sufficient conditions are found under which growing energy fluxes in A can pass into B.

It is also proposed to determine G_{11} the factor by which the mean flux of a growing wave increases when passing from a plane in the medium A to a distant plane in B.

The boundary is here taken normal to the direction of propagation, i.e., to the x axis.

At the boundary the necessary and sufficient conditions which must be satisfied are that the three vectors $\mathbf{e}$, $\mathbf{h}$, and $\mathbf{u}$ vary continuously across it. The first two need not be justified here, while the third is imposed by the fact that the electrons are drifting across the boundary and that under finite forces they cannot suddenly change their transverse velocity $\mathbf{u}$.

From these boundary conditions we deduce that the Poynting flux $\mathbf{P}$ also varies continuously across the boundary.

If a new origin of coordinates be taken in the boundary plane, we may use the formulas of Section 3 for the present discussion. Thus we will take the vectors $\mathbf{e}(t)$, $\mathbf{h}(t)$, $\mathbf{u}(t)$ to represent the perturbations at the boundary $x=0$ and regard the expressions (32) as representing the perturbations in the medium A, when $x<0$ and M_m, $\mathbf{A}_m$, etc., are replaced by M_{am}, $\mathbf{A}_{am}$, etc., and those in the medium B when $x>0$ and M_m, $\mathbf{A}_m$, etc., are replaced by M_{bm}, $\mathbf{A}_{bm}$, etc.

The quantities $\mathbf{I}_e$, $\mathbf{I}_h$, $\mathbf{I}_u$ defined in (33) now represent the perturbations of frequency ω at, and near, the boundary. The same is therefore true of the quantities on the right of (42.1) and (42.2) which determine the two constituent trios of waves.

From (42.1) we obtain the following relations between the amplitudes A_m of the trio of E_1 waves in the two media.

$$\left.\begin{aligned} \sum_m A_{am} &= \sum_m A_{bm} \\ \sum_m M_{am}A_{am} &= \sum_m M_{bm}A_{bm} \\ \sum_m M_{am}^2 A_{am} &= \sum_m M_{bm}^2 A_{bm} \end{aligned}\right\} (m=1,2,3). \quad (49.1)$$

As was proved in Section 3, for (42.1), when M_{a1}, M_{a2}, M_{a3} are all different the system of Eqs. (49.1) always yields finite values of A_{a1}, A_{a2}, A_{a3}, namely

$$A_{a1}=(M_{a1}-M_{a2})^{-1}(M_{a1}-M_{a3})^{-1} \times\sum_m (M_{bm}-M_{a2})(M_{bm}-M_{a3})A_{bm}, \quad (50.1)$$

and formulas for A_{a2}, A_{a3} obtained from this by cyclic permutation of subscripts.

Similar expressions are obtained when, exceptionally, two of these indices are equal.

On calculating $\bar{P}$, the mean value in time of the Poynting flux $\mathbf{P}$ of the E_1 perturbation, we find that it consists of terms which are periodic in x and three terms $\bar{P}_1$, $\bar{P}_2$, $\bar{P}_3$ which are not. The average value of $\bar{P}$ in a given region of space is therefore given approximately by the formula

$$\bar{P}=\bar{P}_1+\bar{P}_2+\bar{P}_3. \quad (51.1)$$

For the trio of E_2 waves we have similar relations (49.2), (50.2), and (51.2) and can draw similar conclusions.

From (50.1) and (50.2) it follows that when progressive waves can exist in both media then such waves can in general pass from A to B or B to A.

Waves cannot exist in a medium when $V=0$ and $\xi>\sigma_n$, i.e., $\omega^2-k_n\Omega\omega-p^2<0$.

Hence, if

$$\left.\begin{aligned} \omega_a,\ \omega_a' &= \tfrac{1}{2}[(\Omega_a^2+4p_a^2)^{\frac{1}{2}} \pm |\Omega_a|], \\ \omega_b,\ \omega_b' &= \tfrac{1}{2}[(\Omega_b^2+4p_b^2)^{\frac{1}{2}} \pm |\Omega_b|], \end{aligned}\right\} \quad (52)$$

it follows that

When $V_a=0$ there can be an energy flux in medium A with E_1 waves only when $\omega>\omega_a$ and with E_2 waves only when $\omega>\omega_a'$. (52A)

A similar conclusion** (52B) holds true for medium B when $V_b=0$.

We shall now establish the following result when $V=0$ in one of the media alone.

When $V=0$ in either A or B alone and transverse waves, of frequencies $\omega>\omega_a'$ or ω_b', respectively, exist in one of these media, then such waves always exist in the other. (53)

For to suppose the contrary is equivalent to having a non-zero solution of equations like (49.1) when their right-hand sides or left-hand sides are all zero; this is impossible because in general the three numbers M_1, M_2, M_3 for either case are all different. Even when $M_1=M_2\neq M_3$ the result (53) is still derived, for the terms in A_2 of (49.1) are then modified as indicated in Section 3.

We shall now determine the conditions under which a mean outward flux in medium B can exist, i.e.,

$$\bar{P}_b>0. \quad (54)$$

Three possible cases, covering growing waves, which can arise will now be considered in detail sufficient for use in later sections.

Case I: $V_a\neq 0$, $V_b\neq 0$

From (50.1) and (50.2) we see that both E_1 and E_2 waves can pass from A to B.

An E_1 wave which grows in A will or will not lead to a growing wave in B with a positive flux, according as

(a) $A_{b1}\neq 0$ and $\mu_b>0$ or (b) $A_{b1}=0$.

With (a) $\bar{P}_{b1}>0$ and at a sufficiently large distance $x_b>0$ the flux $\bar{P}_{b1}$ is much larger than $\bar{P}_{b2}$ and $\bar{P}_{b3}$. We

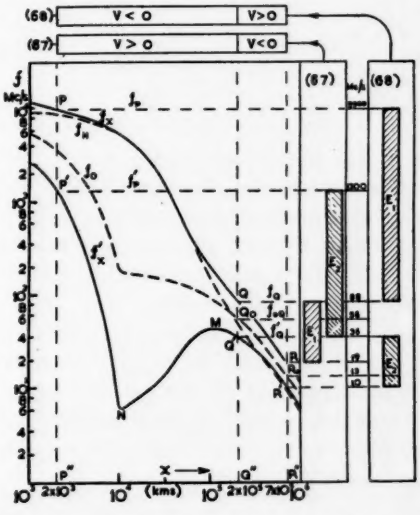

FIG. 4. Illustrating the determination of the frequency bands of growing E_1 and E_2 waves which can escape from the sun's atmosphere over a large sunspot, under hypotheses (67) and (68) about the drift velocity.

** These results are well-known in the magneto-ionic theory of propagation.

TABLE II. Summary of results from hypotheses (67) and (68). $x_P=2\times10^3$, $x_Q=2\times10^5$, $x_R=7\times10^5$ km.

Hypothesis	Drift V_{PQ}	Drift V_{QR}	Frequency bands of escaping waves (Mc/sec.) E_2	Frequency bands of escaping waves (Mc/sec.) E_1
67	>0	<0	1300 to 56 or 36* growing in PQ below 8×10^3 km. 44* to 36* growing partly above 10^5 km.	88 to 19 growing in QR, within broad regions.
68	<0	>0	36 to 13 or 10* growing in QR.	9900 to 88 growing in PQ. 6000 to 600 growing in narrow regions below 5×10^4 km.

* If the region near Q is penetrated.

can therefore simplify the discussion by taking A_{b2} and A_{b3} to be zero since other values will give approximately the same value for $\bar{P}_b$.

On doing so we obtain from (50.1)

$$A_{a1}=\rho_{11}^{-1}A_{b1}, \tag{55}$$

where

$$\rho_{11}=\frac{(M_{a1}-M_{a2})(M_{a1}-M_{a3})}{(M_{b1}-M_{a2})(M_{b1}-M_{a3})}. \tag{56}$$

Also the growing wave amplitude $A_{a1}(x_a)$, at the plane $x=x_a<0$ inside the medium A is given by

$$A_{a1}(x_a)=A_{a1}e^{\omega\beta_a x_a}. \tag{57}$$

From (56), (57), (51.1), and (44) (and on reversion to the unit of velocity 1 cm/sec.) we obtain

$$G_{11}\equiv\frac{P_b(x_b)}{P_{a1}(x_a)}\doteqdot|\rho_{11}|^2\frac{\mu_b}{\mu_a}\exp[2\omega(\beta_b x_b-\beta_a x_a)/c], \tag{58}$$

with $\mu_b>0$.

When $\mu_a>0$ the formula (58) gives the factor of increase G_{11} of a growing flux in passing from the plane $x_a<0$ in A to a distant plane $x_b>0$ in B.

G_{11} can never be zero since μ_a is always finite and since, in (56), M_{a1} cannot be equal to either M_{a2} (for $\beta_a\neq0$) or to M_{a3} (which is real).

With (b) we can similarly for a sufficiently large distance set $A_{b2}=0$ and so obtain a similar, simple approximate expression for the ratio G_{11}. Also a necessary and sufficient condition for a perturbation in A to give rise to a positive flux $\bar{P}_b$ in B is, by (44) and the boundary conditions, that

$$\{|A_{a1}|^2+|A_{a2}|^2\}\mu_a+|A_{a3}|^2M_{a3}=4\pi c^{-1}\bar{P}_b. \tag{59}$$

Similar results hold true for an E_2 wave which grows in A.

Among the random perturbations which can occur at the plane $x=x_a$ in the medium A there can arise some which lead to the situation (a) and others which lead to (b). We may therefore conclude as follows:

When $V_a\neq0$ and $V_b\neq0$, certain transverse perturbations in medium A can lead to a positive mean flux of energy in medium B which grows in the direction A to B; also certain other transverse perturbations in A can lead ultimately to a positive, constant mean flux in B. (60)

By (48) the first kind of perturbations are E_1 or E_2 waves when $V_b>0$ but only E_1 waves when $V_b<0$. Also when $1\gg V_b>0$ they are only E_2 waves.

Case II: $V_a\neq0$, $V_b=0$

We have here the following necessary condition (which is similar to (52A)):

When $V_b=0$ there can be an energy flux in B, with E_1 waves only when $\omega>\omega_b$, and with E_2 waves only when $\omega>\omega_b'$. (61)

Also by (53) it follows that in general when transverse waves of different frequencies $\omega>\omega_b'$ exist in A there is an energy flux in B. Hence,

An energy flux in B can arise from a growing wave in A when, and only when, Eq. (24.0) has complex roots with

$\omega>\omega_b$, $\xi=p_a^2/\omega^2$, $\sigma_n=1-|\Omega_a|/\omega$ for E_1 waves

and with

$\omega>\omega_b'$, $\xi=p_a^2/\omega^2$, $\sigma_n=1+|\Omega_a|/\omega$ for E_2 waves. (62)

The occurrence of such complex roots can be examined by means of curves like those in Figs. 2 and 3, by means of the discriminant of a cubic or, approximately, by means of the formulas (29), (31), and (31.1). Thus, for example,

Complex roots of (24.0) occur when $|V|\ll1$, $\sigma_n>0$ and approximately $\xi>\sigma_n$, i.e., for E_1 waves when $|\Omega_a|<\omega<\omega_a$ and for E_2 waves when $\omega<\omega_a'$, (63)

where ω_a, ω_a' are defined in (52).

When $|V_a|\ll1$ we deduce from (62) and (63) the following approximate necessary and sufficient conditions under which growing energy fluxes in A can pass into B:

With $|V_a|\ll1$ and $V_b=0$, E_1 growing waves can pass when $\omega_a>\omega>\omega_b$ and $|\Omega_a|$ and E_2 growing waves can pass when $\omega_a'>\omega>\omega_b'$. (64)

Case III: $V_a=0$, $V_b\neq0$

Here we deduce, from (53), that:

With $V_a=0$ and $V_b\neq0$ a part of the waves in A (with frequencies $\omega>\omega_a'$) can pass into B. (65)

5. ESCAPE FROM THE SUN OF CIRCULAR WAVES GROWING IN THE ATMOSPHERE ABOVE A LARGE ISOLATED SUNSPOT

We will now apply some of our theoretical conclusions to the waves which can arise by growth of random transverse perturbations in the sun's atmosphere above the center of a large sunpot on the equator.

For this purpose four curves are drawn, as in Fig. 4, with x the distance above the sun's surface as abscissa and f_0, f_H, f_x, f_x' as ordinates, where f_0, f_H are respectively the corresponding electron density frequency and the electron gyro frequency (in cycles/sec.) and

$$f_x, f_x' = \tfrac{1}{2}[(f_H^2+4f_0^2)^{\frac{1}{2}} \pm |f_H|]. \qquad (66)$$

The values of f_0 and f_H are those given by Smerd,[4] H being the magnetic field above the center of a sunspot with a maximum field at the spot of 3600 gauss.

With this spot the curve for f_x' has a valley N in the region between 10^4 and 10^5 km and a peak M at $x=1.1\times10^5$ km with the corresponding frequency $f_M'=44$ Mc/sec.

In the language of the magneto-ionic theory of propagation f_x is the frequency of the extraordinary wave and f_x' that of the ordinary wave for which $\mu=0$ in a medium with no electron drift.†† As the literature on solar noise often uses these terms it is necessary here to relate them to the E_1 and E_2 waves considered in the present theory with the electrons drifting. In Appendix 2 it is shown that we may term the E_1 waves extraordinary and the E_2 waves ordinary.

Following a well-known method of approximation we may consider the sun's atmosphere as composed of a succession of uniform strata each differing slightly from the preceding one.

We shall now suppose that throughout the sun's atmosphere above the spot the electrons drift relatively to the ions with a vertical velocity V which is a continuous function of the distance x.

Since very little is known concerning V, we are at liberty to adopt various hypotheses about it and then compare the theoretical consequences with known observations.

As an example we shall adopt the following hypothesis concerning V in the regions bounded by the lines PP', QQ' and RR', in Fig. 4, which are at the respective distances

$$x_P=2\times10^3, \quad x_Q=2\times10^5, \quad x_R=7\times10^5 \text{ km}.$$

These lines will be named the lines P, Q, and R, respectively.

$$\left.\begin{aligned} &|V|\ll1 \text{ everywhere};\\ &V>0 \text{ in the region } P \text{ to } Q;\\ &V<0 \text{ in the region } Q \text{ to } R;\\ &V \text{ negligible near } Q \text{ and beyond } R. \end{aligned}\right\} \qquad (67)$$

†† The term ordinary is sometimes used exclusively for that wave for which, when propagated transversely to the magnetic field, $f=f_0$ when $\mu=0$. The current terminology is unfortunately somewhat confused.

Let f_P, f_P'; f_Q, f_Q'; f_R, f_R' denote the pairs of frequencies given by (66) which correspond to P, Q, R, respectively.

On applying (60) and (48.1) we see that in the region P to Q there can be growing waves which proceed outward and that these are E_2 waves. By (63) each such wave grows only in the regions for which its frequency lies below the curve for f_x'.

All these E_2 waves with frequencies $f>f_0$ will, by the usual considerations of ray propagation in the magneto-ionic theory, be able to pass into the region near Q where V is negligible. They lie in the band of frequencies f_P' to f_{0Q} where f_{0Q} is the value of f_0 corresponding to the distance x_Q.

By (53) or (65) a part of the waves in this band can pass into the region between Q and R and then into the region beyond R, thus escaping from the sun. All these escaping E_2 waves have grown solely in regions below $x=10^4$ km. Their frequencies lie in the band 1300 to 56 Mc/sec.

Similarly by (60) and (48) there can be growing waves in the region Q to R and these are necessarily E_1 waves. By (63) they grow in the regions bounded by the curves for f_H and f_x. Then, by (64), these waves can pass into the region beyond R and so escape from the sun. Each of these escaping E_1 waves has grown in some part of the region above $x=2\times10^5$ km. Their frequencies lie in the band f_Q to f_R, i.e., 88 to 19 Mc/sec.

The lower frequency limit f_{0Q} for E_2 waves which was adopted above is based on a ray treatment of propagation (with no electron drift) which assumes that when $f_0=f$ then $\mu=0$ and as a result E_2 waves cannot penetrate the region concerned. The universal correctness of this treatment and its consequence has been called into question by Saha and his co-workers[5] and it appears also to be at variance with certain observations of Toshniwal,[6] Harang,[7] and Newstead.[8] It is therefore possible that the lower limit of the E_2 band is set by (64), i.e., by f_Q'. This entails replacing the frequency 56 Mc/sec. given above by 36 Mc/sec.

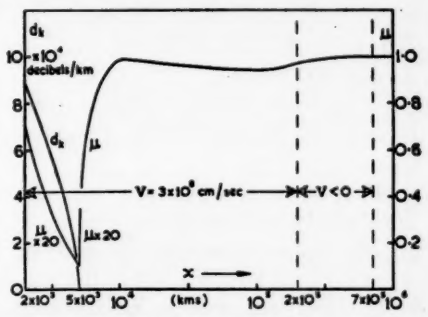

FIG. 5. Curves giving the refractive index μ and rate of growth of intensity d_k for an escaping E_2 wave of frequency 200 Mc/sec. under hypothesis (67) with $V=3\times10^8$ cm/sec.

[5] M. N. Saha *et al.*, Nature **158**, 549 (1946); Ind. J. Phys. **21**, 181, 199 (1947).
[6] G. R. Toshniwal, Nature **135**, 471 (1935).
[7] L. Harang, Terr. Mag. **41**, 143 (1936).
[8] G. Newstead, Nature **161**, 312 (1948).

As another example we shall take the hypothesis complementary to (67), namely:

$$\left.\begin{array}{l} |V| \ll 1 \text{ everywhere;} \\ V<0 \text{ in the region } P \text{ to } Q; \\ V>0 \text{ in the region } Q \text{ to } R; \\ V \text{ negligible near } Q \text{ and beyond } R. \end{array}\right\} \quad (68)$$

By reasoning as before we obtain the following results: E_2 waves in the band 36 to 13 (or 10) Mc/sec. grow in the region Q to R and escape from the sun. E_1 waves in the band 9900 to 88 Mc/sec. grow in those parts of the region P to Q which lie between the curves for f_H and f_x and also escape. Of these the E_1 waves with frequencies between 6000 and 600 Mc/sec. grow in the relatively small regions (below 5×10^4 km) where the f_H curve lies very close to the f_x curve. A simple calculation shows that the lengths Δx of these regions are approximately

$$f_x'/\tan\theta,$$

where $\tan\theta$ is the slope of the f_H curve; therefore Δx is of the order of 20 km for f about 4000 Mc/sec.

This distance is about 0.004 times the distance over which the E_2 waves of frequency 200 Mc/sec. (for example) in the complementary situation (67) can grow. It may therefore result that the latter waves escape with much larger intensities than the E_1 waves of frequencies between 6000 and 600 Mc/sec. in the situation (68). To decide this question definitely it would be necessary to use the exact statement (62) in the place of the approximate ones (63) and (64) and make an estimate of the fraction of the energy flux which escapes. This will not be attempted here.

These results are summarized in Table II.

An example of an E_2 wave which can grow and escape in the situation (67) is illustrated in Fig. 5 by the curves representing the refractive index μ and the rate of growth of intensity d_k, in decibels/km, for a frequency of 200 Mc/sec. and a drift velocity of 3×10^8 cm/sec. These show that the wave grows in the region between $x=2\times10^3$ and $x=5\times10^3$ km at different rates between 9×10^4 decibels/km‡‡ and zero and has wave-lengths between 43 and 300 meters.

It will be seen from Table II that in each region of growth the escaping E_1 waves lie in a higher frequency band.

Also by (48.1) when E_2 waves are observed to escape we may conclude that $V>0$ in the regions where they grew. Similarly when E_1 waves are observed we may conclude that if $|V|\ll1$ then $V<0$ in the regions where they grew. In the language of the magneto-ionic theory these conclusions may be expressed as follows:

When ordinary circular waves escape then the electrons in the regions of growth must drift outward. (69)

When extraordinary circular waves escape the corresponding electrons, if not too fast, must drift inward. (70)

Also from (20.1) we deduce the following:

According as the sunspot is a positive or negative pole, the escaping ordinary waves are respectively LH or RH and the extraordinary waves are RH or LH. (71)

These theoretical conclusions for a large sunspot may now be compared with observation.

During a period of sunspot activity in February, 1946, Appleton and Hey[9] found that the observed strong solar noise was most intense when the sunspot concerned was near the central meridian. During the period of activity in the following July they[10] observed that the solar noise was circularly polarized.

The work of Pawsey, Payne-Scott, and McCready[11] and of Allen[12] shows that peaks of power received on 200 Mc/sec. coincide with the passage of large sunspot groups across the meridian.

Similar observations have been reported by Ryle and Vonberg[13] who, on 175 Mc/sec., also found the responsible solar waves to be largely circular. These observations show that in general the strongest solar noise is emitted normally to the sunspot group from which it originates.

The observation by Martyn,[14] that on 200 Mc/sec. the dominant polarization of the waves from a large northern group of sunspots changed from RH to LH as it crossed the meridian, does not contradict this view.

Dr. Pawsey has very kindly supplied the following as yet unpublished information. During the eclipse of November 1, 1948, Christiansen, Yabsley, and Mills¶¶ observed the following facts on a wave-length of 50 cm:

(1) Strong noise came from small areas located near visible sunspots or near places at which a visible sunspot existed one solar rotation earlier.

(2) The noise radiation from these areas was notably circularly polarized.

(3) As the edge of the Moon's disk crossed these areas the RH waves and the LH waves alternated in becoming the stronger.

These observations are consistent with the view that strong circular waves were traveling outward from *each* spot (visible or invisible). They are also consistent with the theoretical conclusion, given in Section 1, that wave growth is increasingly favored by orientation of the direction of propagation toward the common direction of the drift and the magnetic field.

‡‡ I.e., 10^{90} in about one-quarter of a wave-length.

[9] E. V. Appleton and J. S. Hey, Phil. Mag. **37**, 73 (1946).
[10] E. V. Appleton and J. S. Hey, Nature **158**, 339 (1946).
[11] Pawsey, Payne-Scott, and McCready, Nature **157**, 158 (1946).
[12] C. W. Allen, M. N. R. A. S. **107**, 396 (1947).
[13] M. Ryle and D. D. Vonberg, Nature **158**, 339 (1946).
[14] D. F. Martyn, Nature **158**, 308 (1946).

¶¶ All of the Radiophysics Division of the Australian Council for Scientific and Industrial Research.

Ryle and Vonberg[15] also found that out of sixteen observations of polarization at 175 Mc/sec. nine corresponded to ordinary waves, three corresponded to extraordinary waves, and four were inconclusive. According to (69) and (70) the corresponding electron drift would be outward for nine of these observations and inward for three. Also under our hypotheses (67) and (68) the nine observations would relate to ordinary waves growing in the chromosphere or lower and the three observations would relate to extraordinary waves growing in the corona near or below 10^5 km.

In Martyn's observations mentioned above the (northern) negative sunspots would have preceded the positive spots in their passage across the meridian. It therefore follows from his observations and (71) that the dominant waves concerned were ordinary. Also under our hypothesis (67) they would have grown in the chromosphere or lower. His own theoretical view was contrary to this conclusion.

Bolton[16] found on 100 Mc/sec. that the dominant waves from a southern group of sunspots changed from LH to RH as they crossed the central meridian. By (71) and (67) these also would relate to ordinary waves growing in the chromosphere or lower.

We may therefore conclude that under the hypothesis (67) most of the strong circular waves, the polarization of which has been determined, were ordinary waves and originated in the chromosphere, or lower, with the electrons drifting out of the sunspots concerned.

The consequences of our two hypotheses may also be compared with the observations of Appleton and Hey[9] made in February, 1946. They found that the noise intensity increased rapidly with the wave-length between 2 and 5 meters and then decreased between 5 and 12 meters. Table II shows that under hypothesis (68) no waves between 88 and 36 Mc/sec., i.e., 3.4 and 8.3 meters, escape; so this hypothesis is here excluded. But under hypothesis (67) the observed waves between 2 and 3.4 meters would have been ordinary ones which have grown in the chromosphere, those between 3.4 and 5.3 (or 8.3) meters would have been a mixture of ordinary and extraordinary waves and those between 5.3 (or 8.3) and 12 meters would have been extraordinary waves which have grown in the corona.

The scarcity of observed strong, circular solar waves of frequencies below about 20 Mc/sec. is explained under hypothesis (67) by the fact that according to Table II the lowest possible frequency for an escaping wave is then 19 Mc/sec.

When the region Q, where V changes sign, occurs near the top of the chromosphere then under hypothesis (67) the frequency band of the ordinary waves would lie entirely within the band of the extraordinary waves, but under the hypothesis (68) they would separate widely, with the ordinary band below the extraordinary band.

These results and the corresponding ones which can be similarly derived for smaller sunspots may be used to guide future observations of solar noise.

For a more exact study of the rate of growth and attenuation of waves in the solar atmosphere it is necessary to consider in greater detail the effects due to the collisions of electrons with other particles. This should be done in general for $x<2\times10^3$ km and in particular for E_1 waves of frequencies near the local gyro-frequency f_H in higher regions. One such effect is that in regions where V is negligible the E_1 waves of the lower frequencies would tend to be strongly absorbed.

From all the foregoing theoretical and observational results we may conclude that observed strong circular solar noise of wave-lengths less than 15 meters can originate from random disturbances in different regions of the solar atmosphere over sunspots whenever the electrons in those regions have a drift motion relative to the positive ions, e.g., when a constant (or slowly varying) electric field exists with a component parallel to the spot's magnetic field. That such an electric field can occur has been shown by Giovanelli.[17]

This conclusion is a particular example of the theory previously published[18] that in general abnormal solar noise may be attributed to growing waves which can arise when static electric and magnetic fields are present in the sun's atmosphere.

It also appears possible that the observed waves with frequencies above 60 Mc/sec. have been mainly ordinary waves which grew in the chromosphere by interaction with electrons drifting outward, and that those with frequencies below 60 Mc/sec. have been mainly extraordinary waves which grew in the corona by interaction with electrons drifting inwards.

This suggests that other possible causes of the drift are: (a) Electron emission from low regions over the sunspot, and (b) greater absorption of outgoing radiation by electrons than by ions. either when free or when being freed from one another.

These suggestions of course need closer examination.

It is interesting to note that our conclusion that ordinary waves can escape from the lower regions of the solar atmosphere is in agreement with Saha's[5] view; but, unlike the latter, it is substantially independent of the question whether an ordinary wave in the magneto-ionic theory can penetrate the region in which $f_0=f$.

Summing up, we can see how the single hypothesis that the electrons in a sunspot have a drift motion leads us, through Maxwell's equations and generally accepted data about the sun's atmosphere, to conclusions which are in good agreement with many of the well-established facts about strong solar noise and which do not appear to disagree with the remainder.

An important feature of this theory is that it does not require us to invoke large temperatures of an order exceeding 10^4 °K.

[15] M. Ryle and D. D. Vonberg, Proc. Roy. Soc. **193**, 98 (1948).
[16] See J. L. Pawsey, J. Inst. Elec. Eng. (to be published).
[17] R. G. Giovanelli, M. N. R. A. S. **107**, 338 (1947).
[18] V. A. Bailey, Nature **161**, 559 (1948).

This is in contrast to the theory published recently by Ryle[19] in which, among others, the following two hypotheses are adopted: (1) An electric field exists; (2) this electric field causes the electrons near sunspots to have mean temperatures of from 10^6 to 10^8 °K and sometimes to 10^{10} °K.

The first hypothesis alone is sufficient, on our present theory, to account for strong, circular solar noise.

The second hypothesis may or may not be true, but it does not appear to be necessary.

Also recently a theory has been proposed by Haeff[20] which resembles the present one in that it too makes use of growing plane waves. In that theory the electrons are supposed to be divided into two or more streams with different but parallel drift velocities, and magnetic fields are not considered. The resulting growing waves are longitudinal with no Poynting flux or polarization[21] and the theory gives no information on the process by which these waves give rise to the observed radiation which is necessarily accompanied by a Poynting flux. Also in order "to interpret the observed data on the intensity of solar radiation and its spectral distribution" in terms of his theory Haeff makes a large number of special assumptions. Of these the assumptions that the current density at "the surface of the Sun" is about 10^{-5} amp./cm^2 and that the mean electron velocity is about 2×10^8 cm/sec. lead to an electron density near the sun's surface which is about 10^{-6} times the correct value according to Smerd.

6. ULTIMATE LIMIT OF A GROWING FLUX OF RADIATION

When the transverse perturbations become larger it is necessary to take account of the non-linear terms, depending on time, which occur in the fundamental Eq. (6).

On taking mean values in time of all terms, with the perturbations periodic in time and propagated along the x axis, this equation yields:

$$U_x(\partial\mathbf{U}_0/\partial x)+\langle u_x(\partial\mathbf{u}/\partial x)\rangle_{Av}+\nu\mathbf{U}_0 = (e/m)(\mathbf{E}_0+c^{-1}\mathbf{U}_0\times\mathbf{H}_0+\mathbf{F})-G\mathbf{i}, \quad (72)$$

where

$$\mathbf{F}=c^{-1}\langle\mathbf{u}\times\mathbf{h}\rangle_{Av}, \quad G=\tau\frac{\partial}{\partial x}\langle\log N\rangle_{Av}. \quad (73)$$

For the case (C 11) we obtain from (72) the following relation between the components along $0x$:

$$\tfrac{1}{2}\frac{\partial}{\partial x}U_x^2+\nu U_x=(e/m)(E_x+F_x)-L, \quad (74)$$

where

$$F_x=c^{-1}\langle\mathbf{u}_T\times\mathbf{h}_T\rangle_{Av}, \quad (75)$$

$$L=\tfrac{1}{2}\frac{\partial}{\partial x}\langle u_x^2\rangle_{Av}+G. \quad (76)$$

F_x arises from the transverse perturbations and L arises from the longitudinal ones.

On using (13) and (21) it is easily found that

$$F_x\doteqdot-\int_0^\infty\frac{\omega\beta}{8\pi N_0 ec}(|M|^2+1)|e_T|^2d\omega, \quad (77)$$

where

$$M=\mu+i\beta, \quad |e_T|^2=|e_y|^2+|e_z|^2.$$

Since $e<0$ it follows that for the *growing* components of the transverse perturbations (which ultimately dominate the others) we have

$$F_x>0. \quad (78)$$

From (74) and (78) we see that as the transverse perturbations grow, they impose on the electrons a notable mean force eF_x which opposes the velocity of drift U_x and so tends to reduce it.

It is interesting to note that this opposing force eF_x can also be regarded as arising from the gradient of the mean Maxwellian pressure p_{xx} due to the growing transverse perturbations. For if

$$p_{xx}=1/8\pi\langle(|e_T|^2+|h_T|^2)\rangle_{Av}, \quad (79)$$

then it can be deduced without much difficulty||| that in the situation considered here

$$N_0eF_x=-(\partial p_{xx}/\partial x). \quad (80)$$

(For small perturbations this can also be deduced from (77) and (79) combined with (13).)

With perturbations growing in the direction of $0x$ it is evident that p_{xx} increases with x and so, by (80), it follows that $F_x>0$, which confirms (78).

Thus, with large growing perturbations the radiation pressure gradient acts on the stream of electrons so as to reduce their mean velocity of drift U_x.

Similarly from the nature of the term L in (74) we see that U_x is reduced by the growth of longitudinal waves.

Hence it follows that ultimately a *kinetic steady state* in the medium is reached in which U_x is so small that, on account of the energy lost by collisions of electrons, the transverse perturbations cease to grow.

The ultimate value reached by F_x will depend on circumstances. Thus, if initially $\tau>U_x^2$ and a suitable random longitudinal perturbation did occur, this could lead to growing longitudinal perturbations and then F_x might not be able to attain a large value. On the other hand, if τ were small or if the initial perturbation were not longitudinal, then when ν is small, F_x would ultimately approximate to the reversed static electric field $-E_x$.

Thus the ultimate intensity of the growing waves could at the most be such that the effect of their radia-

[19] M. Ryle, Proc. Roy. Soc. **195**, 82 (1948).
[20] A. V. Haeff, Phys. Rev. **74**, 1532 (1948); **75**, 1546 (1949).
[21] V. A. Bailey, Phys. Rev. **75**, 1104 (1949).

||| For example, from Eqs. (6.3) and (7.6) in R. Becker's *Theorie der Elektrizität* (B. G. Teubner, Leipzig, 1933), Vol. II, pp. 34–37.

tion pressure gradient on the electrons approximately balances that of the static electric field.

We may also consider the situation in which some or all of the electrons are ejected with an initial drift velocity U_1 and the static electric field is zero. Then we can readily deduce that, with ν small, the initial drift kinetic energy of the electrons is ultimately converted into oscillatory kinetic energy and radiation of transverse wave energy. This sets an upper limit to the intensity of the growing transverse waves.

ACKNOWLEDGMENTS

I am indebted to Mr. G. F. Cawsey for computing and drawing the curves in Figs. 2 to 5, to Mr. R. F. Mullaly for checking some of the theory and to Mr. J. A. Roberts for his careful checking and helpful criticism of the whole of the theory as well as for a suggestion relating it to eclipse observations.

I am also indebted to Dr. J. L. Pawsey for putting me in quick touch with much of the available observational work on solar noise and for freely giving me the benefit of his wide knowledge of this subject. Lastly I wish to thank Dr. E. J. Bowen, Chief of the Radio-Physics Division of the Council for Scientific and Industrial Research, for his permission to mention the unpublished work of Messrs. Christiansen, Yabsley, and Mills.

The assistance of Messrs. Roberts and Mullaly has been made possible by Australian Commonwealth Grants for Research Students.

APPENDIX 1

In a frame of reference which is at rest relative to the positive ions and with the axis $0x$ in the direction of the drift velocity $\mathbf{U}$, the dispersion equation in the relativistic E.M.I. theory, for a wave of the form $A\exp[i(\omega t-Llx-Lmy)]$ turns out to have either of the following forms:

$$XY^2-(\beta^2\Omega_x^2+\Omega_T^2)\beta RZY+(\beta^2S\Omega_x+Lm\Omega_y)^2Z(c^2p_0^2+\tau Z)=0; \quad (1A)$$

$$X[Y^2-(\beta^2\Omega_x^2+\Omega_T^2)Z^2]-[\beta^2(S\Omega_y-Lm\Omega_x)^2+c^{-2}(Z+\beta^2R^2)\Omega_x^2]Z(c^2p_0^2+\tau Z)=0, \quad (2A)$$

where

$$X=\beta^2R^2-\tau c^{-2}(Z+\beta^2R^2)-p_0^2-i\beta^2\nu R,$$
$$Y=\beta R(Z+p_0^2)-i\beta\nu Z,$$
$$Z=c^2L^2-\omega^2,$$
$$\beta=(1-U^2/c^2)^{-\frac{1}{2}},$$
$$R=\omega-Ull,$$
$$S=Ll-\omega U/c^2,$$

$(l, m, 0)$ = direction cosines of the direction of propagation,
$\mathbf{\Omega}=(-e/\beta m_0c)\mathbf{H}_0$, $\Omega_T^2=\Omega_y^2+\Omega_z^2$,
$p_0^2=4\pi N_0e^2/m_0$,
m_0 = the rest-mass of an electron,
N_0 = the rest-density of the electrons.

When $|U|$ approximates to the velocity of light, (1A) approximates to

$$\{R^2(1-\tau c^{-2})-i\nu R\}\{R(Z+p_0^2)-i\nu Z\}^2=0,$$

which does not yield growing waves.

When $U^2\ll c^2$, $\tau\ll c^2$ and the frame of reference is changed by rotation about $0z$ until $0x$ is parallel to the direction of wave propagation, (1A) is transformed to the following approximation for the equation of dispersion of a wave of the form $A\exp[i(\omega t-Lx)]$:

$$XY^2-\Omega^2RZY+(L\Omega_x-c^{-2}\omega\mathbf{U}\cdot\mathbf{\Omega})^2Z(c^2p_0^2+\tau Z)=0, \quad (3A)$$

where

$$X=R^2-\tau L^2-p_0^2-i\nu R,$$
$$Y=R(Z+p_0^2)-i\nu Z,$$
$$Z=c^2L^2-\omega^2,$$
$$R=\omega-U_xL,$$
$$\mathbf{\Omega}=(-e/m_0c)\mathbf{H}_0,$$
$$p_0^2=4\pi N_0e^2/m_0.$$

Equation (3A) differs from Eq. (12), in Section 1, only by quantities which are of the second or higher orders of smallness in $\mathbf{U}$ and τ.

In the case (C11), when

$$\Omega_x=\Omega, \quad \Omega_y=0, \quad \Omega_z=0, \quad l=1, \quad m=0,$$

(2A) becomes

$$X(Y^2-\beta^2\Omega^2Z^2)=0.$$

This yields the approximate Eqs. (17) and (18) when $U^2\ll c^2$ and $\tau\ll c^2$.

The detailed derivation of the formulas (1A), (2A) and (3A) will be given in another publication.

APPENDIX 2

The use of the terms ordinary and extraordinary, which is current in the magneto-ionic theory of wave propagation, is not in *general* feasible in the electro-magneto-ionic theory.

As the literature of solar noise often contains these terms we shall here show how, nevertheless, they can be related to the E_1 and E_2 waves defined in our present special case (C11).

The ordinary wave as usually defined, with $V=0$, is that which is the less affected by the magnetic field; since

$$M^2=1-\xi/(1-k_n\eta)$$

the ordinary wave therefore corresponds to $k_n\eta<0$. Hence by (20) the ordinary and extraordinary waves correspond to our E_2 and E_1 waves respectively when $V=0$. These identifications may be retained when $V\neq0$.

Crystal Statistics of a Two-Dimensional Ising Lattice

G. F. NEWELL
University of Illinois, Urbana, Illinois
(Received January 27, 1950)

The partition function Z of a two-dimensional Ising lattice is evaluated by expressing it in the form $Z=\sum_i \lambda_i^{nm}$ where λ_i are the eigenvalues of a 2^n-dimensional matrix $\mathbf{M}$, n is the number of rows and m the number of columns of the lattice. $\mathbf{M}$ is a generalization of the V-shaped matrix studied by Kramers and Wannier in connection with the same problem. It is shown that $\mathbf{M}$ can be expressed in terms of 2^n-dimensional representations of $2n$-dimensional orthogonal matrices. The eigenvalues of $\mathbf{M}$ are determined for n large by making use of the known relations between the eigenvalues of a $2n$-dimensional orthogonal matrix and the eigenvalues of its 2^n-dimensional representative.

The lattice considered differs only slightly from that treated by Onsager and Kaufman. In the lattice considered here, the boundary effects are eliminated by introducing an interaction between the last lattice point of each row and the first point of the next row. The matrix $\mathbf{V}$ considered by Onsager and Kaufman is, except for the boundary effects, equivalent to the matrix $\mathbf{M}^n$. Z is shown to differ from the partition function calculated by Onsager and Kaufman only in order n^{-2}.

1. INTRODUCTION

THE partition function Z of a two-dimensional Ising lattice has been evaluated exactly by Onsager[1] and Kaufman.[2] The method used by them was to diagonalize a matrix $\mathbf{V}$ which represents the contribution to Z of a single *row* of lattice points. Kramers and Wannier[3] have shown that by a suitable choice of boundary conditions the partition function can also be expressed in terms of a matrix $\mathbf{M}$ which represents the contribution to Z of a single *point* of the lattice. This paper deals with the evaluation of Z according to the latter scheme. The two solutions will be shown to be equivalent in the limit of large crystals.

The model considered is a rigid two-dimensional rectangular lattice of m rows and n columns. To each lattice point is associated an "internal" coordinate μ_i which may assume the values $+1$ or -1 with equal *a priori* probabilities. The points of the lattice are numbered from 1 to $n\times m$ starting with the n points of the first row.[3] An interaction energy between a point and its nearest neighbor in a row is taken to be

$$-J\mu_j\mu_{j+1},$$

while that between a point and its nearest neighbor in a column is taken as

$$-J'\mu_j\mu_{j+n}.$$

The partition function for this model is:

$$Z=\sum_{\mu_i=\pm 1}[\exp(J/kT\sum_{j=1}^{nm}\mu_j\mu_{j+1}+J'/kT\sum_{j=1}^{nm}\mu_j\mu_{j+1})]. \quad (1)$$

Included in this expression is a row type interaction $-J\mu_{in}\mu_{in+1}$ between the last point of one row and the first point of the next row; also a column interaction between the points of the mth row and those of the first row if

$$\mu_{nm+j}\equiv\mu_j.$$

[1] L. Onsager, Phys. Rev. **65**, 117 (1944).
[2] B. Kaufman, Phys. Rev. **76**, 1232 (1949).
[3] H. A. Kramers and G. H. Wannier, Phys. Rev. **60**, 252 (1941).

2. THE EIGENVALUE PROBLEM

A matrix $\mathbf{M}$ is defined by

$$M_{\mu_n'\mu_{n-1}'\cdots\mu_1',\,\mu_n\mu_{n-1}\cdots\mu_1}$$
$$\equiv\exp(H'\mu_n'\mu_n)\exp(H\mu_n'\mu_1)\prod_{j=1}^{n-1}\delta(\mu_j'-\mu_{j+1}), \quad (2)$$

where

$$H\equiv J/kT \quad H'\equiv J'/kT. \quad (3)$$

The index $\mu_n\mu_{n-1}\cdots\mu_1$ numbers the 2^n possible values of the coordinates $\mu_n, \mu_{n-1}, \cdots, \mu_1$.

Z is expressed in terms of this matrix as follows:

$$\left.\begin{aligned} Z=\sum_{\mu_i=\pm 1}\prod_{i=1}^{nm}M_{\mu_{n+1}\cdots\mu_{i+1},\,\mu_{n+i-1}\cdots\mu_i} \\ =\text{trace } M^{nm}=\sum_{i=1}^{2^n}\lambda_i^{nm}\end{aligned}\right\}, \quad (4)$$

where λ_i are the 2^n eigenvalues of the matrix M.

The problem of evaluating Z is thus reduced to finding the eigenvalues of $\mathbf{M}$, the largest eigenvalues being particularly significant for large values of the product nm.

To simplify the notation, it is convenient to consider $\mathbf{M}$ as an operator operating on an orthogonal set of basis vectors $\psi(\mu_n\cdots\mu_1)$. To each state of the system with coordinates $\mu_n\cdots\mu_1$ is associated a state vector $\psi(\mu_n\cdots\mu_1)$. The operator $\mathbf{M}$ represented by the matrix (2) is defined by:

$$\mathbf{M}\psi(\mu_n,\cdots,\mu_1)$$
$$\equiv\sum_{\mu_i'=\pm 1}M_{\mu_n'\cdots\mu_1',\,\mu_n\cdots\mu_1}\psi(\mu_n',\cdots,\mu_1'). \quad (5)$$

It will be shown that $\mathbf{M}$ can be written in the form

$$\mathbf{M}=\exp(H'\mathbf{s}_n\mathbf{s}_{n-1})(e^H+e^{-H}\mathbf{C}_n)\mathbf{R}, \quad (6)$$

where

$$\left.\begin{aligned}&\mathbf{R}\psi(\mu_n,\mu_{n-1},\cdots,\mu_1)=\psi(\mu_1,\mu_n,\mu_{n-1},\cdots,\mu_2)\\&\mathbf{C}_j\psi(\mu_n,\cdots,\mu_j,\cdots,\mu_1)=\psi(\mu_n,\cdots,-\mu_j,\cdots,\mu_1)\\&\mathbf{s}_j\psi(\mu_n,\cdots,\mu_j,\cdots,\mu_1)=\mu_j\psi(\mu_n,\cdots,\mu_j,\cdots,\mu_1)\end{aligned}\right\}\quad(7)$$

$$\mathbf{M}\psi(\mu_n\cdots\mu_1)=\exp(H'\mu_1\mu_n)e^{H}\psi(\mu_1,\mu_n,\cdots,\mu_2)+\exp(-H'\mu_1\mu_n)e^{-H}\psi(-\mu_1,\mu_n,\cdots,\mu_2)$$

$$\begin{aligned}M_{\mu_n'\cdots\mu_1',\,\mu_n\cdots\mu_1}&=\exp(H'\mu_1\mu_n)e^{H}\delta(\mu_n'-\mu_1)\prod_{j=1}^{n-1}\delta(\mu_j'-\mu_{j+1})\\&\quad+\exp(-H'\mu_1\mu_n)e^{-H}\delta(\mu_n'+\mu_1)\prod_{j=1}^{n-1}\delta(\mu_j'-\mu_{j+1})\\&=\exp(H'\mu_n\mu_n')\exp(H\mu_n'\mu_1)\prod_{j=1}^{n-1}\delta(\mu_j'-\mu_{j+1}),\end{aligned}$$

which agrees with the definition (2).

Making the additional substitution of H^* defined by

$$e^{-2H}\equiv\tanh H^* \tag{8}$$

$\mathbf{M}$ takes the form

$$\mathbf{M}=(2\sinh 2H)^{\frac{1}{2}}\exp(H'\mathbf{s}_n\mathbf{s}_{n-1})\exp(H^*\mathbf{C}_n)\mathbf{R}. \tag{9}$$

The abstract properties of the operators (7) are as follows:

$$\left.\begin{aligned}&\mathbf{C}_j\mathbf{s}_k=\mathbf{s}_k\mathbf{C}_j\quad j\neq k\\&\mathbf{C}_j\mathbf{s}_j=-\mathbf{s}_j\mathbf{C}_j\\&\mathbf{C}_j\mathbf{C}_k=\mathbf{C}_k\mathbf{C}_j\\&\mathbf{s}_j\mathbf{s}_k=\mathbf{s}_k\mathbf{s}_j\\&\mathbf{C}_j^2=1,\ \mathbf{s}_j^2=1,\ \mathbf{R}^n=1\end{aligned}\right.\quad\text{with}\quad\left.\begin{aligned}&\mathbf{s}_j\mathbf{R}=\mathbf{R}\mathbf{s}_{j+1}\\&\mathbf{C}_j\mathbf{R}=\mathbf{R}\mathbf{C}_{j+1}\\&\mathbf{s}_{n+j}\equiv\mathbf{s}_j\\&\mathbf{C}_{n+j}\equiv\mathbf{C}_j\end{aligned}\right\}. \tag{10}$$

3. SPINOR REPRESENTATIVES OF THE ORTHOGONAL GROUP

Following a procedure similar to that used by Kaufman,[2] it will be shown that $\mathbf{M}$ can be written in terms of spinor representatives of the $2n$-dimensional orthogonal group. To do this we introduce a set of operators $\mathbf{\Gamma}_k$ satisfying the commutation rules

$$\mathbf{\Gamma}_k^2=1\quad\mathbf{\Gamma}_k\mathbf{\Gamma}_l=-\mathbf{\Gamma}_l\mathbf{\Gamma}_k\quad 1\leq k,l\leq 2n. \tag{11}$$

A possible realization of these is given by[4]

$$\left.\begin{aligned}\mathbf{\Gamma}_{2r-1}&\equiv\mathbf{C}_1\mathbf{C}_2\cdots\mathbf{C}_{r-1}\mathbf{s}_r\equiv\mathbf{P}_r\\\mathbf{\Gamma}_{2r}&\equiv i\mathbf{C}_1\mathbf{C}_2\cdots\mathbf{C}_{r-1}\mathbf{C}_r\mathbf{s}_r\equiv\mathbf{Q}_r\end{aligned}\right\}. \tag{12}$$

In terms of these operators we have:

$$\left.\begin{aligned}&\mathbf{C}_r=i\mathbf{P}_r\mathbf{Q}_r\quad\mathbf{s}_1\mathbf{s}_n=i\mathbf{P}_1\mathbf{Q}_n\mathbf{U}\\&\mathbf{s}_{r+1}\mathbf{s}_r=-i\mathbf{P}_{r+1}\mathbf{Q}_r,\quad 1\leq r\leq n-1\\&\mathbf{U}\equiv\mathbf{C}_1\mathbf{C}_2\cdots\mathbf{C}_n\end{aligned}\right\}. \tag{13}$$

In order that some operator $\mathbf{S}(o)$ be a spin representative of a rotation in the $2n$-dimensional space whose basis vectors are the $2n$ $\mathbf{\Gamma}_k$'s, $\mathbf{S}(o)$ must satisfy the relation

$$\mathbf{S}(o)\mathbf{\Gamma}_k\mathbf{S}(o)^{-1}=\sum_{j=1}^{2n}o_{kj}\mathbf{\Gamma}_j\equiv\mathbf{\Gamma}_k^*\quad 1\leq k\leq 2n, \tag{14}$$

where o_{kj} is a (not necessarily real) orthogonal $2n$-dimensional matrix.

The correspondence between the orthogonal group o and the transformations $\mathbf{S}(o)$ is not one-to-one. If $\mathbf{S}(o)$ satisfies (14) so does $\rho\mathbf{S}(o)$ where ρ is any complex number. The arbitrariness of ρ can be partially removed by restricting $\mathbf{S}(o)$ to satisfy the additional conditions,[5]

$$\left.\begin{aligned}&\mathbf{N}^{-1}\mathbf{S}(o)\mathbf{N}=[\mathbf{S}^{-1}(o)]'\\&\text{where}\qquad\mathbf{N}\equiv\mathbf{P}_1\mathbf{P}_2\cdots\mathbf{P}_n\quad\text{for } n \text{ even}\\&\qquad\qquad\equiv\mathbf{Q}_1\mathbf{Q}_2\cdots\mathbf{Q}_n\quad\text{for } n \text{ odd}\end{aligned}\right\}. \tag{15}$$

A prime denotes the transposed matrix. The index ρ may still assume the values ± 1 giving a two-to-one correspondence $\pm\mathbf{S}(o)\leftrightarrow o$.

It can be shown[2] that if o has the $2n$-eigenvalues

$$e^{\pm i\theta_1},\ e^{\pm i\theta_2},\ \cdots,\ e^{\pm i\theta_n}; \tag{16}$$

then $\mathbf{S}(o)$ has the eigenvalues

$$(\pm)e^{i/2(\pm\theta_1\pm\theta_2\pm\cdots\pm\theta_n)}. \tag{17}$$

The 2^n-eigenvalues of $\mathbf{S}(o)$ are obtained by taking all possible combinations of plus and minus signs in the exponent and *one* of the two possible signs $(\pm)$ in front. One of the signs $(\pm)$ belongs to $\mathbf{S}(o)$, the other to $-\mathbf{S}(o)$. The knowledge that $\mathbf{S}$ is a representative of o having eigenvalues (16) is not in itself sufficient to determine the sign of (17).

The operators $\exp(H'\mathbf{s}_n\mathbf{s}_{n-1})=\exp(-iH'\mathbf{P}_n\mathbf{Q}_{n-1})$ and $\exp(H^*\mathbf{C}_n)=\exp(iH^*\mathbf{P}_n\mathbf{Q}_n)$ are examples of spin representatives since

$$\left.\begin{aligned}&\exp(\theta/2\mathbf{\Gamma}_k\mathbf{\Gamma}_l)\mathbf{\Gamma}_k\exp(-\theta/2\mathbf{\Gamma}_k\mathbf{\Gamma}_l)=\cos\theta\mathbf{\Gamma}_k-\sin\theta\mathbf{\Gamma}_l\\&\exp(\theta/2\mathbf{\Gamma}_k\mathbf{\Gamma}_l)\mathbf{\Gamma}_l\exp(-\theta/2\mathbf{\Gamma}_k\mathbf{\Gamma}_l)=\sin\theta\mathbf{\Gamma}_k+\cos\theta\mathbf{\Gamma}_l\\&\exp(\theta/2\mathbf{\Gamma}_k\mathbf{\Gamma}_l)\mathbf{\Gamma}_j\exp(-\theta/2\mathbf{\Gamma}_k\mathbf{\Gamma}_l)=\mathbf{\Gamma}_j\quad\mathbf{\Gamma}_j\neq\mathbf{\Gamma}_k\mathbf{\Gamma}_l,\end{aligned}\right\}. \tag{18}$$

$\mathbf{R}$ itself is not, however, such an operator. The $\mathbf{\Gamma}_k$ transform under $\mathbf{R}$ according to the following:

$$\left.\begin{aligned}&\mathbf{R}\mathbf{P}_r\mathbf{R}^{-1}=\mathbf{C}_n\mathbf{P}_{r-1}=i\mathbf{P}_n\mathbf{Q}_n\mathbf{P}_{r-1}\\&\mathbf{R}\mathbf{Q}_r\mathbf{R}^{-1}=\mathbf{C}_n\mathbf{Q}_{r-1}=i\mathbf{P}_n\mathbf{Q}_n\mathbf{Q}_{r-1}\end{aligned}\right\}2\leq r\leq n\Bigg\},\quad\left.\begin{aligned}&\mathbf{R}\mathbf{P}_1\mathbf{R}^{-1}=\mathbf{C}_n\mathbf{U}\mathbf{P}_n,\quad\mathbf{R}\mathbf{Q}_1\mathbf{R}^{-1}=\mathbf{C}_n\mathbf{U}\mathbf{Q}_n\end{aligned}\right\}, \tag{19}$$

whereas the product of two $\mathbf{\Gamma}_k$'s transform according to

$$\left.\begin{aligned}&\mathbf{R}\mathbf{P}_r\mathbf{Q}_r\mathbf{R}^{-1}=\mathbf{P}_{r-1}\mathbf{Q}_{r-1}\quad 1\leq r\leq n\\&\mathbf{R}\mathbf{P}_{r+1}\mathbf{Q}_r\mathbf{R}^{-1}=\mathbf{P}_r\mathbf{Q}_{r-1}\quad 2\leq r\leq n-1\\&\mathbf{R}\mathbf{P}_1\mathbf{Q}_n\mathbf{R}^{-1}=-\mathbf{U}\mathbf{P}_n\mathbf{Q}_{n-1},\quad\mathbf{R}\mathbf{P}_2\mathbf{Q}_1\mathbf{R}^{-1}=-\mathbf{U}\mathbf{P}_1\mathbf{Q}_n\end{aligned}\right\}. \tag{20}$$

The operators $\mathbf{\Gamma}_k$ belong to the group of operators which anticommute with $\mathbf{U}$ while $\mathbf{\Gamma}_j\mathbf{\Gamma}_k$ belong to the group of operators which commute with $\mathbf{U}$. $\mathbf{U}$ has the

[4] The product of two operators $\mathbf{AB}$ is used here to denote the result of operating first with $\mathbf{B}$ and then with $\mathbf{A}$. The product of the corresponding matrices is then $(AB)_{ac}=\sum_b A_{ab}B_{bc}$. This is apparently not the same convention as used by Kaufman.

[5] See R. Brauer and H. Weyl, Am. J. Math. **57**, 425 (1935); also F. D. Murnaghan, *The Theory of Group Representations* (The Johns Hopkins Press, Baltimore, 1938), Chapter 10.

eigenvalues $+1$ and -1 corresponding to the "even" and "odd" eigenfunctions

$$\left.\begin{aligned} &2^{-\frac{1}{2}}[\psi(\mu_n\cdots\mu_1)+\psi(-\mu_n,-\mu_{n-1},\cdots,-\mu_1)]\\ &\text{and}\\ &2^{-\frac{1}{2}}[\psi(\mu_n\cdots\mu_1)-\psi(-\mu_n,-\mu_{n-1},\cdots,-\mu_1)]\end{aligned}\right\}, \quad (21)$$

respectively.

In the space of even and odd functions, $\mathbf{U}$ has the form

$$\mathbf{U}=\begin{pmatrix} I & 0\\ 0 & -I\end{pmatrix}, \quad (22)$$

where I stands for the 2^{n-1}-dimensional unit matrix. Since $\mathbf{P}_r\mathbf{Q}_r$, $\mathbf{P}_{r+1}\mathbf{Q}_r$ and $\mathbf{R}$ commute with $\mathbf{U}$, they must be of the form

$$\begin{pmatrix} x_+ & 0\\ 0 & x_-\end{pmatrix}. \quad (23)$$

The last two equations of (20) may be written

$$\mathbf{R}\mathbf{P}_1\mathbf{Q}_n\mathbf{R}^{-1}=\mp\mathbf{P}_n\mathbf{Q}_{n-1}, \quad \mathbf{R}\mathbf{P}_2\mathbf{Q}_1\mathbf{R}^{-1}=\mp\mathbf{P}_1\mathbf{Q}_n, \quad (20a)$$

where the upper sign applies in the space of even functions, and the lower sign in the space of odd functions.

Despite the fact that $\mathbf{R}$ is not a spin representative, we consider the spin representatives $\mathbf{A}_+$ and $\mathbf{A}_-$ defined by the relations

$$\left.\begin{aligned} &\mathbf{A}_\pm\mathbf{P}_r\mathbf{A}_\pm^{-1}=\mathbf{P}_{r-1}\\ &\mathbf{A}_\pm\mathbf{Q}_r\mathbf{A}_\pm^{-1}=\mathbf{Q}_{r-1}\end{aligned}\right\} 2\le r\le n \qquad \left.\begin{aligned} &\mathbf{A}_\pm\mathbf{P}_1\mathbf{A}_\pm^{-1}=\mp\mathbf{P}_n,\\ &\mathbf{A}_\pm\mathbf{Q}_1\mathbf{A}_\pm^{-1}=\mp\mathbf{Q}_n\end{aligned}\right\}. \quad (24)$$

$\mathbf{A}_+$ and $\mathbf{A}_-$ also commute the $\mathbf{U}$ and so can be represented in the block form (23).

We note that $\mathbf{A}_+^{-1}\mathbf{R}$ commutes with all elements of the form $\mathbf{P}_r\mathbf{Q}_r$, $\mathbf{P}_{r+1}\mathbf{Q}_r$ (or equivalently $\mathbf{C}_r$, $\mathbf{s}_r\mathbf{s}_{r+1}$) in the 2^{n-1}-dimensional space of even functions while $\mathbf{A}_-^{-1}\mathbf{R}$ commutes with these elements in the space of odd functions.

The operators $\mathbf{C}_r$, $\mathbf{s}_{r+1}\mathbf{s}_r$ with $\mathbf{U}=1$ generate a group having but one faithful irreducible representation,[1] namely the 2^{n-1}-dimensional representation corresponding to the upper block of (23). Since $\mathbf{A}_+^{-1}\mathbf{R}$ commutes with every element of the group, it must be a multiple of the 2^{n-1}-dimensional unit matrix (in the space of even functions). By the same argument $\mathbf{A}_-^{-1}\mathbf{R}$ must be a multiple of the unit matrix in the space of odd functions. It follows that

$$\begin{aligned} &[c_+^{-1}\tfrac{1}{2}(1+\mathbf{U})\mathbf{A}_+^{-1}+c_-^{-1}\tfrac{1}{2}(1-\mathbf{U})\mathbf{A}_-^{-1}]\mathbf{R}=I\\ &\mathbf{R}=c_+\tfrac{1}{2}(1+\mathbf{U})\mathbf{A}_++c_-\tfrac{1}{2}(1-\mathbf{U})\mathbf{A}_-\end{aligned} \quad (25)$$

c_+ and c_- are constants. The operators $\frac{1}{2}(1+\mathbf{U})$ and $\frac{1}{2}(1-\mathbf{U})$ are projection operators into the space of even and odd functions, respectively.

c_+ and c_- can be determined only if $\mathbf{A}_\pm$ are uniquely defined. If $\mathbf{A}_+$ and $\mathbf{A}_-$ are restricted to satisfy condition (15) in addition to (24) then

$$\begin{aligned} &c_+=\pm i, \quad c_-=\pm 1 \quad \text{for } n \text{ odd}\\ &c_+=\pm 1, \quad c_-=\pm i \quad \text{for } n \text{ even.}\end{aligned}$$

$\mathbf{R}$ is uniquely defined by (7) whereas $\mathbf{A}_\pm$ is defined only to a sign by (24) and (15); therefore Eq. (25) can be used, in conjunction with (15) and (24), to define $\mathbf{A}_\pm$ uniquely by requiring that

$$\left.\begin{aligned} &c_+=-i, \quad c_-=1 \quad \text{for } n \text{ odd}\\ &c_+=1, \quad c_-=-i \quad \text{for } n \text{ even}\end{aligned}\right\}. \quad (26)$$

The operator $\mathbf{M}$ may now be written in the form

$$\left.\begin{aligned} &\mathbf{M}=(2\sinh 2H)^{\frac{1}{2}}[\tfrac{1}{2}(1+\mathbf{U})c_+\mathbf{M}_++\tfrac{1}{2}(1-\mathbf{U})c_-\mathbf{M}_-]\\ &\mathbf{M}_+\equiv\exp(-iH'\mathbf{P}_n\mathbf{Q}_{n-1})\exp(iH^*\mathbf{P}_n\mathbf{Q}_n)\mathbf{A}_+\\ &\mathbf{M}_-\equiv\exp(-iH'\mathbf{P}_n\mathbf{Q}_{n-1})\exp(iH^*\mathbf{P}_n\mathbf{Q}_n)\mathbf{A}_-\end{aligned}\right\}. \quad (27)$$

$\mathbf{M}_+$ and $\mathbf{M}_-$ are spin representatives of $2n$-dimensional orthogonal matrices. The eigenvalues of $\mathbf{M}$ can be found by selecting the eigenvalues of $\mathbf{M}_+$ belonging to the even space and the eigenvalues of $\mathbf{M}_-$ belonging to the odd space. The V-shaped matrix of Kramers and Wannier[3] corresponds to the first term of (27) with $H=H'$.

4. EIGENVALUES FOR M

According to the convention of multiplying operators and matrices (see reference 4), $\mathbf{S}(o)$ is to be associated with the matrix o' since

$$\mathbf{S}(o^*)\mathbf{S}(o)\boldsymbol{\Gamma}_k\mathbf{S}^{-1}(o)\mathbf{S}^{-1}(o^*)=\sum_{j,m=1}^{2n} o_{kj}o_{jm}{}^*\boldsymbol{\Gamma}_m=\sum_m (o^{*\prime}o')_{km}{}'\boldsymbol{\Gamma}_m. \quad (28)$$

The $2n$-dimensional transposed matrices $\mathfrak{M}_\pm$ to be associated with $\mathbf{M}_\pm$ are the products of the three transposed matrices

$$\begin{pmatrix} 1&0&0&\cdot&\cdot&\cdot&\cdot&&&\\ 0&1&0&\cdot&\cdot&\cdot&\cdot&&&\\ 0&0&1&\cdot&\cdot&\cdot&\cdot&&&\\ \cdot&\cdot&\cdot&\cdot&\cdot&\cdot&\cdot&&&\\ &&&1&0&0&0\\ &&&0&\cosh 2H'&i\sinh 2H'&0\\ &&&0&-i\sinh 2H'&\cosh 2H'&0\\ &&&0&0&0&1\end{pmatrix},$$

$$\begin{pmatrix} 1&0&0&\cdot&\cdot&\cdot&\cdot&&&\\ 0&1&0&\cdot&\cdot&\cdot&\cdot&&&\\ 0&0&1&\cdot&\cdot&\cdot&\cdot&&&\\ \cdot&\cdot&\cdot&\cdot&\cdot&\cdot&\cdot&&&\\ &&&&&&&1&0&0\\ &&&&&&&0&\cosh 2H^*&i\sinh 2H^*\\ &&&&&&&0&-i\sinh 2H^*&\cosh 2H^*\end{pmatrix}$$

and

$$\begin{pmatrix} 0&0&1&0&0&\cdot&\cdot&&&&&\\ 0&0&0&1&0&\cdot&\cdot&&&&&\\ 0&0&0&0&1&\cdot&\cdot&&&&&\\ \cdot&\cdot&\cdot&\cdot&\cdot&\cdot&\cdot&&&&&\\ 0&0&0&\cdot&\cdot&\cdot&\cdot&\cdot&0&1&0\\ 0&0&0&\cdot&\cdot&\cdot&\cdot&\cdot&0&0&1\\ \mp1&0&0&\cdot&\cdot&\cdot&\cdot&\cdot&0&0&0\\ 0&\mp1&0&\cdot&\cdot&\cdot&\cdot&\cdot&0&0&0\end{pmatrix}$$

corresponding, respectively, to the operators

$$\exp(-iH'\mathbf{P}_n\mathbf{Q}_{n-1}),\quad \exp(iH^*\mathbf{P}_n\mathbf{Q}_n)$$

and $\mathbf{A}_\pm$.

$$\mathfrak{M}_\pm=\begin{pmatrix}
0&0&1&0&0&\cdot&\cdot&\cdot&\cdot&\\
0&0&0&1&0&\cdot&\cdot&\cdot&\cdot&\\
0&0&0&0&1&\cdot&\cdot&\cdot&\cdot&\\
\cdot&\cdot&\cdot&\cdot&\cdot&\cdot&\cdot&\cdot&\cdot&\\
0&0&0&\cdot&\cdot&\cdot&\cdot&1&0&0\\
0&0&0&\cdot&\cdot&\cdot&\cdot&0&1&0\\
a&b&o&\cdot&\cdot&\cdot&\cdot&0&0&g\\
c&d&o&\cdot&\cdot&\cdot&\cdot&0&0&h\\
e&f&o&\cdot&\cdot&\cdot&\cdot&0&0&0
\end{pmatrix}, \tag{29}$$

where

$$\left.\begin{array}{ll}
a=\mp i\sinh 2H'\cosh 2H^* & e=\pm i\sinh 2H^*\\
b=\pm\sinh 2H'\sinh 2H^* & f=\mp\cosh 2H^*\\
c=\mp\cosh 2H'\cosh 2H^* & g=\cosh 2H'\\
d=\mp i\cosh 2H'\sinh 2H^* & h=-i\sinh 2H'
\end{array}\right\}. \tag{30}$$

Owing to the simplicity of the matrices $\mathfrak{M}_\pm$, the eigenvalues $m_\pm$ can be found for arbitrary n by solving the determinantal equation

$$D=\det(\mathfrak{M}_\pm-m_\pm I)=0.$$

I is the $2n$-dimensional identity. The result is

$$D=(m_\pm)^{2n}-b(m_\pm)^{n+1}-2c(m_\pm)^n-b(m_\pm)^{n-1}+1=0.$$

The substitution

$$m_\pm=e^z \tag{31}$$

gives the (complex) equation

$$\cosh nz=c+b\cosh z=\mp(\cosh 2H'\cosh 2H^*-\sinh 2H'\sinh 2H^*\cosh z). \tag{32}$$

For $z=x+iy$, this is equivalent to the two real equations

$$\cosh nx\cos ny=\mp(\cosh 2H'\cosh 2H^*-\sinh 2H'\sinh 2H^*\cosh x\cos y), \tag{32a}$$

$$\sinh nx\sin ny=\pm\sinh 2H'\sinh 2H^*\sinh x\sin y. \tag{32b}$$

For $n\gg 1$, it is possible to find z explicitly in the form of an expansion in powers of n^{-1}. In particular, if $n\to\infty$, the solution can be found as follows:

$$\sinh x/\sinh nx\to 0 \text{ thus } \sin ny\to 0$$
$$ny_j\to j\pi,\ j \text{ an integer} \tag{33}$$

(32a) then gives:

$$(-1)^j\cosh nx_j\to\mp(\cosh 2H'\cosh 2H^*-\sinh 2H'\sinh 2H^*\cos j\pi/n).$$

The factor $\cosh x$ has been replaced by 1 because this equation shows that nx_j is bounded as $n\to\infty$, therefore $x\to 0$. For a given choice of sign on the right, not all values of j are allowed. The function $\cosh nx$ is always positive as is the quantity in parentheses, therefore for the upper sign j must be odd, for the lower sign j must be even.

The $2n$-eigenvalues of $\mathfrak{M}_+$ and $\mathfrak{M}_-$ for $n\to\infty$ are:

$$\left.\begin{array}{l}
m_+=\exp[\pm(x_{2r+1}+i(2r+1)\pi/n)];\quad m_-=\exp[\pm(x_{2r}+i2r\pi/n)]\\
0\le r\le n-1,\quad r=\text{integer}\\
\cos nx_j=\cosh 2H'\cosh 2H^*-\sinh 2H'\sinh 2H^*\cos j\pi/n
\end{array}\right\}. \tag{34}$$

For arbitrary n, (32a,b) shows that if $z=x+iy$ is a solution then so are $\pm(x\pm iy)$. Also $y_0=0$ is a solution for $\mathfrak{M}_-$ and $y_n=\pi$ is a solution for $\mathfrak{M}_+$ if n is odd or for $\mathfrak{M}_-$ if n is even. In view of this we adopt the following convention for ordering the value of z:

$$\left.\begin{array}{l}
\pm z_{2r+1}=\pm(x_{2r+1}+iy_{2r+1}) \text{ belong to } \mathfrak{M}_+\\
\pm z_{2r}=\pm(x_{2r}+iy_{2r}) \text{ belong to } \mathfrak{M}_-
\end{array}\right\} 0\le r\le n-1$$
$$\left.\begin{array}{l}
x_j=x_{2n-j},\quad y_j=-y_{2n-1}\\
-\pi<y_j\le\pi,\quad 0=y_0<y_1<y_2\cdots<y_n=\pi
\end{array}\right\}. \tag{35}$$

We also take x_j to be the positive solution of (32a,b) except in the case x_0 which will be considered in more detail later.

By (16) and (17), the eigenvalues of $\mathbf{M}_+$ are

$$(\pm)\exp[\tfrac{1}{2}(\pm z_1\pm z_3\pm z_5\pm\cdots\pm z_{2n-1})], \tag{36a}$$

and those of $\mathbf{M}_-$ are

$$(\pm)\exp[\tfrac{1}{2}(\pm z_0\pm z_2\pm z_4\pm\cdots\pm z_{2n-2})]. \tag{36b}$$

To complete the solution of the eigenvalue problem, it is necessary to select the eigenvalues of $\mathbf{M}_+$ belonging to even eigenfunctions, those of $\mathbf{M}_-$ belonging to odd eigenfunctions and to determine the correct sign $(\pm)$ of (36a,b).

In the expressions (36a,b), those eigenvalues with an even number of minus signs in the exponent belong to one of the two subspaces and those with an odd number of minus belong to the other subspace.[6] It is possible to determine from $\mathfrak{M}_\pm$ which subspace goes with the even number of minus signs and which goes with the odd number of minus signs. The procedure is to determine explicitly an orthogonal transformation which carries $\mathfrak{M}$ into its canonical form. Knowing the spin representative associated with the canonical form and whether the orthogonal transformation has determinant $+1$ or -1, one can decide which sign combinations to select in the exponent of (36a,b). Though one can easily find an orthogonal transformation of desired type, the evaluation of its determinant presents difficulties. It is possible, however, to determine uniquely the eigenvalues of $\mathbf{M}$ by a less direct approach.

Equation (2) shows that in that representation $\mathbf{M}$ has all real, non-negative elements. If $\mathbf{M}$ is transformed to the space of even and odd functions, that part of $\mathbf{M}$ belonging to even functions also has non-negative elements. Frobenius[7] and Oldenburger[8] have shown that

[6] See reference 2, pp. 1238, 1239.
[7] S. B. Frobenius, Preuss. Akad. Wiss. 514 (1909).
[8] R. Oldenburger, Duke Math. J. 6, 357 (1940).

if the elements of a matrix are real and non-negative, then the characteristic value with maximum absolute value is real and non-negative.

If we assume that the eigenvalues (36a) with an even number of minus signs belong to the space of even eigenfunctions, then the eigenvalue of $\mathbf{M}$ with the largest absolute value in this space is

$$\max\lambda_+ = (\pm)(2\sinh 2H)^{\frac{1}{2}} c_+ \exp[\tfrac{1}{2}(z_1+z_3+\cdots z_{2n-1})].$$

The value $y_n=\pi$ yields a solution of (32a,b) if n is odd. All other solutions of (32a,b) occur in complex conjugate pairs with $\pm y$ in the range (35). Thus

$$\max\lambda_+ = (\pm)(2\sinh 2H)^{\frac{1}{2}} \times \exp[\tfrac{1}{2}(x_1+x_3+\cdots x_{2n-1})]. \quad (37)$$

We see that Frobenius' theorem is satisfied for the plus sign and the assumption that an even number of minus signs in the exponent gives the desired set of eigenvalues from (36a).

The alternative assumption, that the eigenvalues of (36a) with an odd number of minus signs belong to the space of even functions, leads to a contradiction. Under this assumption, the largest eigenvalue is obtained by choosing all the signs in (36a) positive except the one before the smallest x. By (32a), the smallest x is obtained by taking $|y|$ small. The value $y=0$ is not, however, a solution in the space of even functions, therefore the largest eigenvalue will not be real contrary to Frobenius' theorem.

A similar argument can be applied to the space of odd functions. Though some of the elements of $\mathbf{M}$ are negative in the space of odd basis vectors considered previously, the elements of $\mathbf{M}$ are all non-negative when referred to the system of odd and even basis vectors which are the eigenfunctions of $\mathbf{C}_j$ provided $H'\geq 0$ and $H\geq 0$. With this restriction, Frobenius' theorem can be applied to the odd space. The same arguments as before lead to

$$\max\lambda_- = (\pm)(2\sinh 2H)^{\frac{1}{2}} \times \exp[\tfrac{1}{2}(\pm x_0+x_2+x_4+\cdots+x_{2n-2})]. \quad (38)$$

The proper sign in front is the plus sign. In this case, however, one does not succeed in ruling out either of the possible assumptions regarding the distribution of signs in the exponent of (36b) because $z_0=x_0$ is real. Changing the sign of z_0 does not effect the agreement with Frobenius theorem.

The quantity x_0 is unique in that it is the only x_j that can be zero for finite n. We have $x_0=0$ for $H'=H^*$. The absolute value of dx_0/dT at $H'=H^*$ is not zero; thus if x_0 does not change sign at this point $d(\max\lambda_-)/dT$ will have a discontinuity. A calculation of Z from (4) assuming $x_0\geq 0$ for all T leads to a function which for finite n and m is not analytic in T at the point $H'=H^*$. This is contrary to the definition (1). We define the sign of x_0 by

$$x_0=|x_0| \text{ for } H'>H^*, \quad x_0=-|x_0| \text{ for } H'<H^*. \quad (39)$$

Finally, to select the correct sign before x_0 in (38) one can calculate Z in the limit H', $H\gg 1$. In this limit, $nx_j\to 2H'$ for all j and n. In order that Z calculated from (4) approach the correct limit of (1), namely $Z\to 2e^{nm(H+H')}$, it is necessary that $\max\lambda_+\to\max\lambda_-$. The correct sign in (38) is the upper one.

The eigenvalues of $\mathbf{M}$ are now uniquely determined as

$$\left.\begin{aligned}&(2\sinh 2H)^{\frac{1}{2}} c_+ \exp[\tfrac{1}{2}(\pm z_1\pm z_3\pm\cdots\pm z_{2n-1})]\\ \text{and}\\ &(2\sinh 2H)^{\frac{1}{2}} c_- \exp[\tfrac{1}{2}(\pm z_0\pm z_2\pm\cdots\pm z_{2n-2})]\end{aligned}\right\}, \quad (40)$$

where each expression may have only an even number of minus signs in the exponent.

5. DISCUSSION OF RESULTS

The calculations considered here differ from those of Onsager and Kaufman in two respects. Aside from the fact that the boundary conditions assumed in each case are not the same, the matrix $\mathbf{V}$ of Onsager and Kaufman is that associated with a complete row of the lattice whereas the $\mathbf{M}$ used here is associated with a single point of the lattice. To compare the results of the two calculations one should compare $\mathbf{M}^n$ of this paper with their $\mathbf{V}$. λ^n of this paper corresponds to their λ, which we will refer to here as λ' to avoid confusion. Equation (34) shows that nx_j is equal to γ_j of Onsager and Kaufman in the limit $n\to\infty$. Furthermore, they differ for large n only in order n^{-2}. The nth power of the two largest eigenvalues (37), (38), which contains only x_j, thus differ from the two largest λ' only in order n^{-2}.

A comparison of eigenvalues other than these two is complicated slightly by the fact that most of the λ^n are complex whereas the λ' are real. In general, the λ^n, which occur in complex conjugate pairs, differ from the λ' in absolute value only in order n^{-2}.

The value of the partition function Z for large n and m is accurately expressed in terms of the largest eigenvalues of $\mathbf{M}$. For large temperatures $H'<H^*$, $\max\lambda_+$ is non-degenerate, whereas for $H'>H^*$, $\max\lambda_-$ as $n\to\infty$ and one has a twofold degeneracy of the largest eigenvalues. In neither case do the other eigenvalues give an appreciable contribution to Z. Only in the immediate vicinity of the transition point $H'=H^*$ need they be considered. Here one sees from (32a,b) that if $|y_j|\ll 1$ then $nx_j\ll 1$. At $H'=H^*$ one can, by making n large enough, obtain solutions x_s arbitrarily small. The eigenvalues (37), (38) approach a degeneracy with those eigenvalues in which the sign of an even number of such x_j are changed. As $n\to\infty$, these eigenvalues form a dense sequence of values with $\max\lambda_+$ as their limit.

To complete the comparison of these calculations with those of Onsager and Kaufman, it is necessary only to compare those eigenvalues λ^n, λ' which contribute to Z near the transition point. The complex phase of such λ^{nm} is of order m/n^2. The sum of λ^{nm} and its complex conjugate differ from the corresponding two terms of Onsager and Kaufman only in order m^2/n^4 and in order n^{-2}. If m and n are of comparable size, the par-

tition function of this paper and that of Onsager and Kaufman differ in order n^{-2} at most for all values of T.

Because of the smallness of the discrepancy between the two calculations for $n \gg 1$, a detailed study of these differences would seem of little value. The thermodynamic properties and investigations of order in the lattice have been studied in some detail by Onsager and Kaufman.

A two-dimensional system in which the jth point interacts with the $j+m-1$th in addition to the $j+1$th and $j+n$th can also be treated by the methods given here. In such a model each point interacts with six neighbors. The thermodynamic properties of such a system are now being studied.

The author is indebted to Professor A. Nordsieck for suggesting the problem and giving helpful advice. Thanks are also due to the AEC for a predoctoral fellowship grant.

PHYSICAL REVIEW VOLUME 78, NUMBER 4 MAY 15, 1950

Ferromagnetic Resonance Absorption in Magnetite Single Crystals*†

L. R. BICKFORD, JR.‡
Laboratory for Insulation Research, Massachusetts Institute of Technology, Cambridge, Massachusetts
(Received December 16, 1949)

The microwave resonance absorption technique, at both 1.25 and 3.3 cm wave-lengths, was used to study the ferromagnetic crystalline anisotropy characteristics and g-factor of magnetite Fe_3O_4. The experiments were performed on single crystals, both synthetic and natural, from room temperature to −195°C. Depending upon the temperature, magnetite single crystals were found to have magnetic anisotropy characteristics similar to those of single crystals of the three ferromagnetic elements. From room temperature to −143°C, they behave like nickel; between −143° and the transition which magnetite is known to undergo at *ca.* −160°C, like iron; and below the transition, somewhat like cobalt. At room temperature, values of $g=2.12$ and K_1 (first-order anisotropy constant) $=-1.10\times10^4$ joule/m³ (-1.10×10^5 erg/cm³) were obtained. It was found that below about −90°C the absolute value of K_1 decreases with decreasing temperature, reaching zero at *ca.* −143°C. Between −143° and the transition K_1 is positive and increases with decreasing temperature. The vanishing of crystalline anisotropy at −143°C accounts for the peak in initial permeability found near this temperature. The g-value was found to decrease gradually and monotonically with decreasing temperature. The behavior of magnetite in the resonance experiments below the transition seems to indicate that the magnetic symmetry is uniaxial in this temperature region. This conclusion is consistent with the findings of other investigators. Below the transition the magnetic axis is that [100] direction most nearly parallel to a strong magnetic field applied to the crystal as it is cooled through the transition. At temperatures not far below the transition it is possible to change the magnetic axis from one [100] direction to another by means of a strong magnetic field.

I. INTRODUCTION

THE investigation reported here was part of a program initiated at the Laboratory for Insulation Research to study the fundamental properties of magnetite, as the first step in a longer-range plan to investigate the properties of ferromagnetic semiconductors. Its object was to study magnetite by the microwave resonance technique from room temperature to liquid nitrogen temperature. As will be seen, the microwave resonance absorption experiment is capable of yielding information concerning ferromagnetic crystalline anisotropy. Specifically, it provides one with sufficient information to calculate the anisotropy constants appearing in the energy expression of a ferromagnetic crystal. In addition, it gives a value of the spectroscopic splitting factor, or g-factor, for the material.

II. PROPERTIES OF MAGNETITE

It has been established by Verwey and co-workers[1–3] that magnetite possesses the cubic inverse spinel structure. The explanation proposed[1] for the high electrical conductivity of magnetite at room temperature (10^{-2} ohm cm) is that the distribution of ferrous and ferric ions among the octahedral cation lattice sites is random and fluctuating. That is, one can think of all 16 of these positions as being occupied by ferric ions, with 8 electrons continually changing their position from one site to another.

In a wide range around room temperature, the magnetic properties of magnetite are quite similar to those of nickel. Its saturation magnetization (4.6×10^5 amp/m or 460 c.g.s/cm³) is about the same as for nickel, and, like nickel, its direction of easy magnetization is the body diagonal [111].

Millar[4] determined the specific heat as a function of temperature, and found an anomalous peak *ca.* 10° wide

* This work was sponsored jointly by the ONR, the Army Signal Corps, and the Air Force under ONR Contract N5ori-07801.

† From a thesis submitted in partial fulfillment of the requirements for the degree of Doctor of Philosophy in Physics at the Massachusetts Institute of Technology.

‡ Now at Alfred University, Alfred, New York.

[1] E. J. W. Verwey and J. H. de Boer, Rec. trav. chim. 55, 531 (1936).

[2] E. J. W. Verwey and P. W. Haayman, Physica 8, 979 (1941).

[3] Verwey, Haayman, and Romeijn, J. Chem. Phys. 15, 181 (1947).

[4] R. W. Millar, J. Am. Chem. Soc. 51, 215 (1929).

centered at *ca.* −160°C. Although the magnetization in weak fields drops sharply, the saturation magnetization does not change in cooling through this temperature region, in which magnetite undergoes a transition of some sort.[5] Li[6] showed by the results of torque measurements that the magnetic symmetry changes from cubic above the transition to some form of uniaxial below. He reported that if a single crystal had been cooled through the transition in a strong magnetic field, the direction along which this field had been applied became the direction of easy magnetization, or symmetry axis, below the transition. It is interesting to note that the torque curves made at −155°C (just above the transition) show that the crystal is most easily magnetized along the [100] direction. Li apparently failed to notice this fact.

Okamura[7] showed that the electrical resistivity increases abruptly upon cooling through the transition region. In studying this effect, Verwey and Haayman[2] made extensive measurements on a series of sintered samples of varying composition. They discovered that both the transition temperature and the magnitude of the discontinuity in resistivity varied uniformly with the ratio Fe_2O_3/FeO. From this behavior of the electrical resistivity Verwey concluded that the distribution of ferrous and ferric ions among the octahedral lattice sites became ordered at the transition. Such an ordering implies that electronic interchange becomes more difficult, and the resistivity, together with its activation energy, would be expected to increase. According to this picture the transition is an electronic order-disorder phenomen. Verwey[3] further pointed out that the ordered structure could no longer have cubic symmetry, and suggested that the most probable structure was a tetragonal** arrangement of the cations in their normal positions. Referring to Li's experiments[6] with cooling magnetite through the transition in a magnetic field, Verwey suggested that the tetragonal axis of his ordered structure would be the cube edge most nearly parallel to the applied magnetic field.

An anomalous peak in initial permeability found by Weiss and Renger[8] at −138°C and by Snoek[9] at −130°C seems to have been regarded as another direct manifestation of the transition, even though it occurs 20° or so higher than the transition.

III. THEORY OF THE RESONANCE EXPERIMENT

The resonance process can be pictured as a "coupling in" of a microwave field with the Larmor precession of electron spins. As a result, energy is absorbed from the microwave field by the spins. The Larmor precession frequency ν_L of free electron spins in an external magnetic field is given by the relation††

$$\nu_L = g(e/4\pi m)B, \tag{1}$$

where B is the applied magnetic induction, g the spectroscopic splitting factor, e the electron charge, and m the electron mass. For free electrons, $g=2.00$, and the Larmor frequency is 2.80 megacycles per 10^{-4} weber/m^2, or one gauss, of magnetic induction.

In a ferromagnetic material, the electrons participating in the resonance process are the 3*d*-shell electrons which are responsible for the ferromagnetism. Because of the influence of demagnetizing effects and effects of ferromagnetic crystalline anisotropy, the magnetic induction governing the spin precession is not the externally applied induction.

As a consequence of ferromagnetic crystalline anisotropy, the energy of a crystal depends upon the relative orientation of the magnetization. For magnetite, as for other cubic ferromagnetic crystals, the anisotropy energy can be written

$$E = K_1(\alpha_1^2\alpha_2^2 + \alpha_2^2\alpha_3^2 + \alpha_3^2\alpha_1^2) + K_2(\alpha_1^2\alpha_2^2\alpha_3^2) + \cdots, \tag{2}$$

where K_1 and K_2 are the first- and second-order anisotropy constants, and α_1, α_2, α_3 are the direction cosines of the magnetization with respect to the crystallographic axes. For most purposes only the first term of this expression need be used, and the crystalline anisotropy is characterized by a single constant K_1.

Kittel[10] has derived equations governing the resonance condition for ferromagnetic materials by solving classically the equations of motion of the bulk magnetization. For an ellipsoid with principal axes parallel to the x, y, z co-ordinate axes, and demagnetizing factors designated by N_x, N_y, and N_z, the resonance condition is

$$\nu_0 = \frac{\gamma}{2\pi}\mu_0\{[H_x + (N_y + N_y^e - N_z)M_z] \times [H_x + (N_x + N_x^e - N_z)M_z]\}^{\frac{1}{2}}, \tag{3}$$

where ν_0 is the microwave frequency, γ is the gyromagnetic ratio equal to $ge/2m$, μ_0 is the magnetic permittivity of free space, H_z is the static magnetic field, and M_z is the z-component of the magnetization. The microwave magnetic field is along the x-direction.

The dependence of the resonance condition upon crystal orientation is contained in the factors N_x^e and N_y^e, which express the effect of crystalline anisotropy, and must be calculated for individual cases. The general expressions for N_x^e and N_y^e, in case the xy-plane (containing both the static and r-f magnetic field) is the (100) plane of a cubic crystal, have been given by Kittel. In corrected form[11] they are, considering only the first-order anisotropy term,

$$\mu_0 N_x^e = (2K_1/M_z^2)\cos 4\theta, \tag{4}$$

$$\mu_0 N_y^e = (\tfrac{3}{2} + \tfrac{1}{2}\cos 4\theta)K_1/M_z^2, \tag{5}$$

[5] P. Weiss and R. Forrer, Ann. de physique [10] **12**, 279 (1929).
[6] C. H. Li, Phys. Rev. **40**, 1002 (1932).
[7] T. Okamura, Science Repts. Tôhoku Imp. Univ. [1] **21**, 231 (1932).
** The proposed structure, which Verwey calls tetragonal, is actually orthorhombic, belonging to the Imm crystal class.
[8] P. Weiss and K. Renger, Archiv f. Elektrotechnik **2**, 406 (1914).
[9] J. L. Snoek, *New Developments in Ferromagnetic Materials* (Elsevier Publishing Company, Inc., New York, 1947).
†† Rationalized MKS units are used in this presentation.
[10] C. Kittel, Phys. Rev. **73**, 155 (1948).
[11] C. Kittel, Phys. Rev. **76**, 743 (1949).

where θ is the angle between the manetization and a [100] crystal direction.

Corresponding expressions for the (110) plane of a cubic crystal are[12]

$$\mu_0 N_x^e = (2-\sin^2\theta-3\sin^2 2\theta)K_1/M_s^2, \quad (6)$$

$$\mu_0 N_y^e = 2(1-2\sin^2\theta-\tfrac{3}{8}\sin^2 2\theta)K_1/M_s^2, \quad (7)$$

where θ is the angle between the static magnetization and a [100] crystal direction.

Equation (3), together with expressions for N_x^e and N_y^e in terms of crystalline anisotropy, specifies the resonance condition in ferromagnetic single crystals. It was assumed in the derivations that the crystal is magnetized to saturation and the static magnetization is along the z-direction. Accordingly, M_z can be replaced by M_s, the saturation magnetization. It has been verified[13] by resonance experiments on an iron single crystal that Eq. (3) correctly describes the effect of crystal anisotropy on the resonance process.

IV. EXPERIMENTAL PROCEDURE

The procedure employed in measuring the resonance absorption is essentially that described by Arnold and Kip.[14] The sample is mounted in a rectangular resonant cavity, driven in the $T\dot{E}_{102}$ mode; this cavity forms one arm of a wave guide magic T bridge. The opposite arm of the bridge is terminated by a matched load. In the other two arms are a klystron oscillator and a crystal detector. To a good approximation, the power reflected from the cavity on resonance, P_r, is related to the unloaded Q of the cavity Q_0 by

$$P_r/P_i = \left\{\frac{Q_e/Q_0-1}{Q_e/Q_0+1}\right\}^2, \quad (8)$$

where Q_e is the external Q of the cavity, which is unaffected by the magnetostatic field, and P_i is the power incident on the cavity, maintained constant during the experiment. The magnetic loss in the cavity is proportional to $1/Q_0$, since the sample is located in a region of maximum magnetic and minimum electric field. Therefore, by measuring P_r/P_i as H_z increases, and applying Eq. (8), one obtains the relative magnetic absorption as a function of H_z.

Two microwave frequencies were used in these experiments; one in the X band (*ca.* 9000 mc/sec.), and the other in the K band (*ca.* 24,000 mc/sec.). The same type of experimental arrangement was used at both frequencies. An electromagnet provided the static field, which was applied normal to the wide face of the wave guide, orthogonal to the r-f magnetic field.

Figure 1 shows a detailed view of the cavity. In order to allow a change in its orientation with respect to the magnetic field, the sample, in the form of a thin circular disk, is mounted on a rotatable cylinder which forms a section of the cavity end-wall. At the other end of the cylinder is a pointer to indicate the orientation of the crystal relative to a graduated arc on the cavity body. By means of a screw, the cylinder is forced into close contact with a tapered phosphor-bronze "iris" in the cavity end-wall, thus providing good electrical contact and a continuous flat end-wall. The disk, on one side of which a thin layer of copper has been electroplated, is soft-soldered to the cylinder.

The cavity is thermally insulated from the rest of the wave guide system in order that measurements can be carried out continuously from room temperature to liquid nitrogen temperature. This insulation is provided by a short section of wave guide made of Bakelite, on the inside walls of which has been evaporated a thin layer of silver. The cavity, located below the Bakelite thermal junction, is surrounded by a cylindrical copper container. A nichrome resistance wire heater, wound around a mica form, surrounds the cavity inside the copper container. The container is immersed in liquid nitrogen in a Dewar flask between the magnet poles. By controlling the heater current, the sample temperature can be maintained constant within ± 0.5°C during the experiment, from *ca.* -100° to -195°C.

Resonance absorption experiments were made on both natural and synthetic magnetite crystals. To permit measurements to be made along all principal crystallographic directions, disks were cut in two different crystal planes, (100) and (110). Each experiment was made on at least two different samples.

The disk thickness is about 0.005 to 0.008 cm, and the diameter ranges from about 0.28 cm for X band to about 0.18 cm for K band. The ratio of diameter to thickness averages about 25, so the demagnetizing factors in the plane of the sample are small. Formulas given by Osborn[15] were used for the calculation of N_x, N_y, and N_z, with the disks considered as oblate spheroids.

The natural single crystals were from Chester, Vermont. Their Fe_2O_3/FeO ratio could not be determined by chemical analysis because of the presence of small inclusions of pyrite and other foreign materials. Comparison of the transition temperature (-163°C) for these materials with the transition temperatures of a series of samples of varying oxygen content published by Verwey and Haayman[2] indicates that the ratio Fe_2O_3/FeO must be about 1.05.

The synthetic crystals were grown by Smiltens and Fryklund[16] of this Laboratory. They were grown from a melt into the form of cylinders 0.6 cm in diameter and *ca.* 5 cm long. Since the orientation of the crystal axis with respect to the cylinder axis was random, it was necessary to orient the crystal, for cutting, by means of x-rays. The probable error in cutting the disks to the proper plane was ± 1.0 degrees of arc. Smiltens has found

[12] L. R. Bickford, Jr., Tech. Rept. XXIII, ONR contract N5ori-07801, Lab. Ins. Res., M.I.T., (October, 1949).
[13] A. F. Kip and R. D. Arnold, Phys. Rev. **75**, 1556 (1949).
[14] R. D. Arnold and A. F. Kip, Phys. Rev. **75**, 1199 (1949).
[15] J. A. Osborn, Phys. Rev. **67**, 351 (1945).
[16] J. Smiltens and D. H. Fryklund, Lab. Ins. Res., M.I.T. (to be published in the near future).

the synthetic crystals to be essentially stoichiometric with respect to the ratio of iron oxides (Fe_2O_3/FeO) $=0.998$). This is consistent with the fact that the transition temperature is about -155°C. Domenicali's[17] values of saturation magnetization, obtained from pendulum magnetometer measurements, were used for M_s.

V. RESULTS

The results obtained from the resonance experiments and subsequent discussion thereof will be presented in three sections, corresponding to different temperature ranges: (A) Above the transition (from room temperature to -153°C for synthetic crystals and to -160°C for natural crystals); (B) in the transition region (-154° to -157°C for synthetic, -163° to -168°C for natural crystals); and (C) below the transition (-158° to -195°C for synthetic crystals). No detailed experiments were made below the transition with natural crystals.

A. Above the Transition

Figure 2 shows a typical room temperature resonance at 1.25 cm wave-length. The line is very broad, as is the case for most ferromagnetic materials. A minimum of absorption can be seen at about 0.3 weber/m² (3000 gauss). This minimum is predicted by theory if a relaxation term is introduced into the equations of motion as has been shown by Yager.[18]

Equation (3), together with expressions for N_x^e and N_y^e in terms of crystal orientation and anisotropy, contains two unknowns: g and K_1. Therefore, results

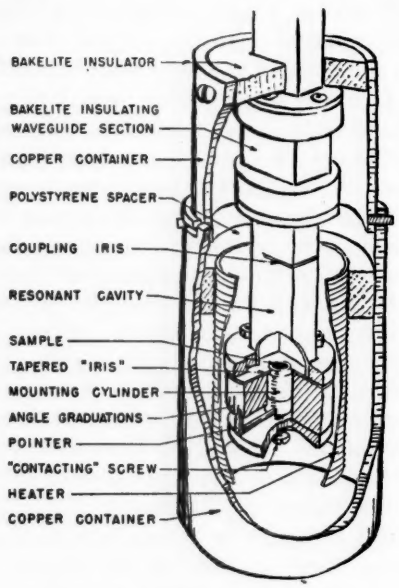

FIG. 1. Details of resonant cavity.

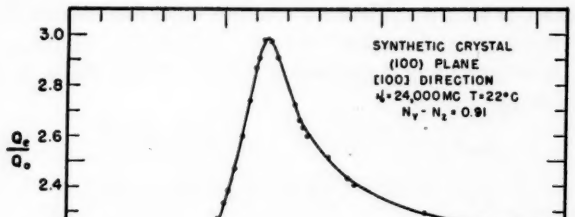

FIG. 2. Typical K-band absorption curve.

obtained from two different crystal orientations are sufficient to determine these quantities. In the case of samples cut from the (100) crystal plane, measurements made with the [100] and [110] directions parallel to the static field were used for this purpose. For (110) plane samples, [100] and [111] direction measurements were used.

Table I gives average values of g and K_1 obtained at room temperature. The number of different samples used, including both (100) and (110) planes, is indicated.

An additional uncertainty is introduced because the values of M_s have a probable error of ± 2 percent.

Figure 3 shows theoretical and experimental values of resonance induction (applied magnetic induction corresponding to the maximum of absorption) as a function of crystal orientation. It represents experiments made at 1.25 cm with a (100) plane sample of a synthetic crystal. The theoretical curve, given by the solid line, was obtained in the following manner. From experimental data for [100] and [110] parallel to the static field ($\theta=0$, 45°), g and K_1 were calculated. These values of g and K_1 were introduced into (4) and (5) to obtain $\mu_0 N_x^e$ and $\mu_0 N_y^e$ as a function of θ. Finally, these effective demagnetizing factors were used in Eq. (3) to obtain $\mu_0 H_z$ as a function of crystal orientation. The circles represent the experimentally observed values of $\mu_0 H_z$.

Figure 4 shows resonance induction *vs.* crystal orientation for the (110) plane of a synthetic crystal, at room temperature and 1.25 cm wave-length. The theoretical curve was calculated using Eqs. (6) and (7).

From Figs. 3 and 4 it can be seen that the crystal orientation with respect to the static field direction can be accurately obtained by the resonance experiment,

TABLE I. Room temperature values of g and K_1.

Wave-length	3.3 cm		1.25 cm
Type of crystal	natural	synthetic	synthetic
No. of samples	2	4	7
$10^{-4} K_1$ (joule/m³) / $10^{-5} K_1$ (erg/cm³)	-1.15 ± 0.04	-1.10 ± 0.08	-1.12 ± 0.10
g	2.13 ± 0.04	2.12 ± 0.04	2.09 ± 0.04

[17] C. A. Domenicali, Tech. Rept. XXV, ONR contract N5ori-07801, Lab. Ins. Res., M.I.T. (October, 1949); Phys. Rev. 78, 458 (1950).

[18] W. A. Yager, Phys. Rev. 75, 316 (1949).

once the crystal plane has been established. It is to be noted that the resonance induction is lowest in any crystal plane when the static field is near the direction of easy magnetization, and is highest near the direction of most difficult magnetization.

Essentially the same information as that given in Figs. 3 and 4 is plotted as a function of temperature in Fig. 5. Here the resonance induction at 3.3 cm is plotted for three directions in a (100) plane synthetic crystal from room temperature to the transition. Corresponding curves for (110) plane samples have a similar appearance. All the curves cross at −143°C, indicating that at this temperature the resonance field is independent of crystal orientation. In other words the crystal is magnetically isotropic at this temperature, the anisotropy constant K_1 vanishing. It is interesting to note that this "isotropy point," or temperature at which the anisotropy vanishes, is the same for both natural and synthetic crystals, whereas the transition temperature is different for the two types of crystal. Below −143°, the minimum resonance induction is along [100], indicating that this is the direction of easy magnetization.

Values of K_1 and g obtained from data such as that plotted in Fig. 5 are given in Table II. K_1 is plotted as a function of temperature in Fig. 6. It is seen that K_1 changes rapidly below −90°C, changing sign at −143°C. The g-factor decreases monotonically with temperature.

The absorption line width decreases with decreasing temperature, with a corresponding increase in intensity at the maximum. Very roughly, the line-width is halved and the maximum absorption intensity is doubled between room temperature and the transition.

B. In the Transition Region

In the original experiments at X band the surprising discovery was made that the resonance absorption dropped off rapidly and completely disappeared in the transition region without any significant change in resonance induction. This disappearance was especially disturbing since it was found that the line-width did not change during the process, thus ruling out the most likely explanation for the phenomenon, namely, that some frictional forces present during the transition caused the line to broaden to such an extent that it was no longer observable.

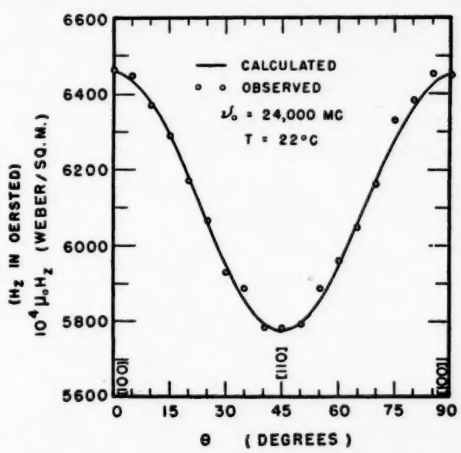

FIG. 3. Resonance induction *vs.* crystal orientation in (100) plane of synthetic crystal at K band. Solid line is theoretical curve for $g=2.07$; $K_1=-1.10\times10^4$ joule/m³; $M=4.72\times10^5$ amp./m; and $N_y-N_z=0.91$.

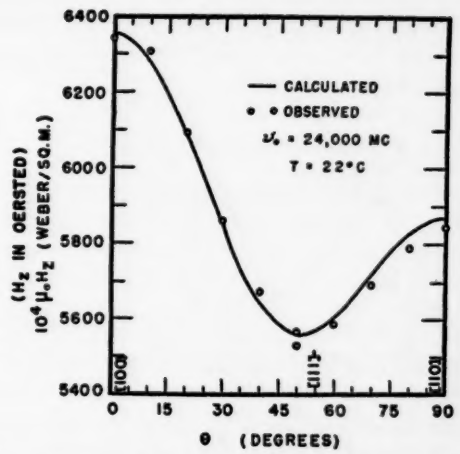

FIG. 4. Resonance induction *vs.* crystal orientation in (110) plane of synthetic crystal at K band. Solid line is theoretical curve for $g=2.10$; $K_1=-1.12\times10^4$ joule/m³; $M=4.72\times10^5$ amp./m; and $N_y-N_z=0.91$.

The initial experiments were performed with oblate ellipsoids having a thickness exceeding the skin depth of the microwave field. With these samples it was observed that the disappearance of resonant absorption was accompanied by a large increase in non-resonant absorption, that is, by absorption which was more or less independent of magnetic field strength. This was interpreted as being due to a large increase in eddy current skin depth in the sample as the electrical resistivity increased by a large factor in the transition region. Thus a greater volume of the sample was exposed to the microwave field, leading to an increased absorption not necessarily of magnetic origin. This effect was not observed in samples whose thickness was roughly equal to the microwave skin depth at room temperature.

When the resonance experiments were repeated at K band, it was found that as the absorption line disappeared in passing through the transition, an additional double peak appeared at low values of magnetic induction. Figure 7 shows this effect. There was no gradual shift in resonance induction. Above the transition (curve A) one line was present, while below the transition (curve C) the other was present. In the transition region (curve B), one line grew as the other diminished in such a manner that the total absorption remained more or less constant.

The duration of the transition region, as reflected in the resonance experiments, is *ca.* 5°C for the natural crystals and *ca.* 3°C for the synthetic crystals. This fact was determined by observing the absorption at

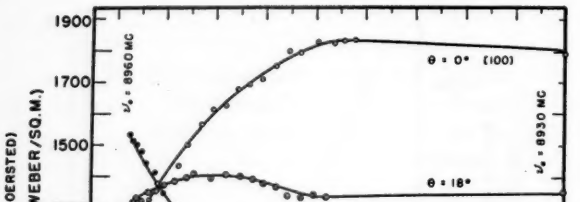

FIG. 5. Resonance induction *vs.* temperature in (100) plane of synthetic crystal at *X* band. $N_y - N_z = 0.935$.

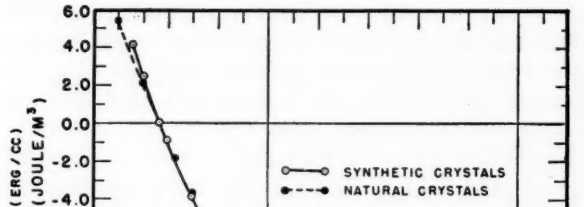

FIG. 6. Anisotropy constant K_1 as a function of temperature (from *X*-band data).

zero applied induction as the temperature slowly changed through the transition region. As can be seen from Fig. 7, at *K* band there is an increased absorption below the transition at zero static field.

C. Below the Transition

Experiments were made below the transition in both (100) and (110) planes along the principal crystallographic directions [100], [110], and [111]. The results obtained support the interpretation that the magnetic symmetry below the transition is tetragonal (or some other uniaxial symmetry in which the crystal is difficult to magnetize in the plane orthogonal to the axis), and that the magnetic axis can be selected from among the equivalent [100] directions of the original cubic crystal by cooling the magnetite through its transition in a strong magnetic field. In particular, it seems that the axis, or direction of easy magnetization, becomes the [100] direction most nearly parallel to the biasing magnetic field.*

For example, one of two different absorption curves can be obtained along the [100] direction of a (100) plane sample, depending upon magnetic treatment through the transition, as is shown in Fig. 8. Both curves of Fig. 8 were obtained with the measuring field along the same [100] direction of the crystal at −190°C. For curve *A* the biasing and measuring fields were parallel, and for curve *B* they were orthogonal.** In the former case the measuring field is along the direction of easy magnetization, and the resonance induction is low; whereas in the latter case the measuring field is along a [100] direction in the plane perpendicular to the magnetic axis, hence along a direction of difficult magnetization, and the resonance induction is high. Curve *A* results if the biasing field is applied within 45° of the [100] direction of the measuring field, and curve *B*, if the biasing field is applied within 45° of the perpendicular [100]. Similar results were obtained for other combinations of measuring and biasing field orientations, consistent with the picture of uniaxial magnetic symmetry below the transition.

Resonance absorption was observed at 3.3 cm wavelength for the three combinations of biasing and measuring field orientation which led to *K* band resonance at high induction; namely, along the [100] direction in (100) plane, and along both [100] and [110] directions in the (110) plane when the biasing field had established the magnetic axis orthogonal to these directions. Otherwise, resonance absorption was not detectable below the transition at *X* band.

In those cases where the resonance occurred at high applied induction at 1.25 cm, it was found that the position of the maximum changed quite rapidly with temperature. An even more interesting effect which depends upon the temperature is the following. At temperatures less than 20° or so below the transition, the application of a strong magnetic field (1.5 weber/m² or 15,000 gauss) appeared to change the direction of the magnetic axis. For example, suppose that in a (100) plane crystal the biasing field had established the mag-

TABLE II. g and K_1 as a function of temperature.

Temperature	$10^{-3} M_s$†	Synthetic crystal g	Synthetic crystal $10^{-4} K_1$*	Natural crystal g	Natural crystal $10^{-4} K_1$*
(°C)	(amp/m)		(joule/m³)		(joule/m³)
22	472	2.12	−1.08	2.17	−1.10
−100	491	2.08	−0.97	2.13	−0.98
−120	494	2.08	−0.64	2.12	−0.63
−130	496	2.07	−0.39	2.10	−0.37
−140	497	2.05	−0.08	2.08	−0.08
−143	497	2.05	0.00	2.08	0.00
−150	499	2.03	0.26	2.06	0.22
−153	499	2.02	0.42		
−160	500			2.06	0.54

* $10^{-3} K_1$ (erg/cm³). † M_s (c.g.s.).

* In order to simplify the discussion we shall denote by *biasing field* that magnetic field, applied to the crystal as it cools through the transition, which establishes the direction of the magnetic axis. In general, the biasing field is removed and the crystal demagnetized before it is rotated into position for making the absorption measurement. The field which is used in the resonance experiment we shall call the *measuring field*.

** Experimentally this is easily accomplished by rotating the entire cavity about its axis for cooling through the transition, then rotating it back to the normal position for making the measurement. In this way the biasing field can be applied along any crystal direction *in the plane of the sample*.

netic axis along the same [100] direction as the measuring field. Suppose further that at −170°C the cavity was rotated 90° about its axis and an induction of 1.5 weber/m² applied for a short time along the perpendicular [100] direction. If the cavity were then returned to its normal position and the resonance experiment performed rapidly, the resulting absorption curve would be the same as one which would be obtained after the biasing field had been applied along the perpendicular [100]. In other words, the magnetic axis had been rotated by the strong magnetic field. It can be seen from this behavior that the measuring field itself acts as a biasing field at temperatures close to the transition, making it difficult to observe the resonance at these temperatures along crystal directions normal to the magnetic axis.

Figure 9 shows the biasing effect of a measuring field along the [100] direction of a (100) plane sample. Curve *A* was made after the biasing field had established the magnetic axis along the perpendicular [100] direction. Continued application of 1.5 weber/m² along the measuring field direction at temperatures below *ca.* −187°C did not change the appearance of this curve. Curves *B*, *C*, and *D* were made in succession as the crystal warmed from −186° to −180°C. It can be seen that the measuring field for each curve produced a change in the succeeding curve. At temperatures between −155° and −170°C a curve like curve *A* of Fig. 9 could be observed only if the experiment were performed rapidly, and could not be reproduced unless the crystal were again subjected to a perpendicular biasing field. The shifting of the axis takes place gradually, as though in intermediate curves (*B* and *C*) the axes were along different [100] directions in different domains, or regions of the crystal. Figure 9 also shows the dependence of resonance induction upon temperature for the high field peak.

For the very low field peak of curve *D* of Fig. 9, and for similar peaks occurring in other crystal orientations, it was found that the absorption as a function of applied induction increased discontinuously. This effect was strongly suggestive of the Barkhausen effect which can be observed during the magnetization of ferromagnetic materials.

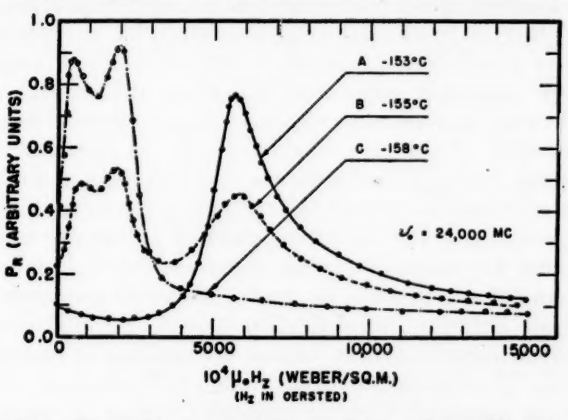

FIG. 7. Absorption curves in the transition region at *K* band. (100) plane; [100] direction; $N_y - N_z = 0.905$.

VI. DISCUSSION OF RESULTS

Above the Transition

The values of first-order anisotropy constant obtained from our resonance experiments are in agreement with the small amount of information about magnetite's crystalline anisotropy given in the literature. Our value of $K_1 = -1.10 \times 10^4$ joule/m³ at room temperature agrees with -1.07×10^4 joule/m³ calculated from the results of Quittner's torque experiments.[19] Similar calculations from Li's results[6] at −155°C give $K_1 = 0.43 \times 10^4$ joule/m³, which should be compared with our value of 0.40×10^4 joule/m³ at the same temperature.

The vanishing of crystalline anisotropy at −143°C explains the maximum in initial permeability which was reported by various observers[8,9] to occur 20° or 30° above the transition. The two parameters of major importance in determining initial permeability are crystalline anisotropy and magnetostrictive energy. According to elementary domain theory,[20] the surface energy of domains varies as the square root of these quantities, and the initial permeability is large when this surface energy is small. The development of mixed ferrites of high initial permeability is accomplished by reducing both the crystalline anisotropy and the magnetostriction to very low values.[9] Domenicali's[17] curves of magnetostriction *vs.* temperature for a magnetite single crystal show no anomalous behavior in the vicinity of −145°C. Therefore the initial permeability should be affected by variations in the absolute magnitude of the crystalline anisotropy in such a way that it increases as this quantity decreases with temperature, and *vice versa*. Accordingly, a peak in initial permeability is to be expected near the temperature at which the crystalline anisotropy vanishes.

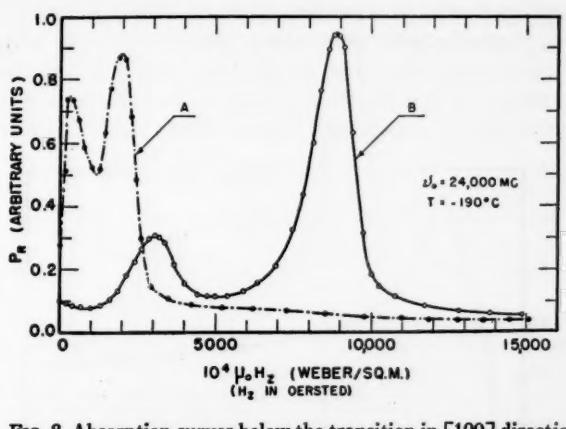

FIG. 8. Absorption curves below the transition in [100] direction of (100) plane, showing effect of magnetic prehistory. For curve *A*, biasing and measuring fields were parallel; for *B*, they were perpendicular. $N_y - N_z = 0.910$.

[19] V. Quittner, Ann. d. Physik [4] 30, 289 (1909).

[20] See, for example, R. Becker and W. Döring, *Ferromagnetismus* (Verlag. Julius Springer, Berlin, 1939).

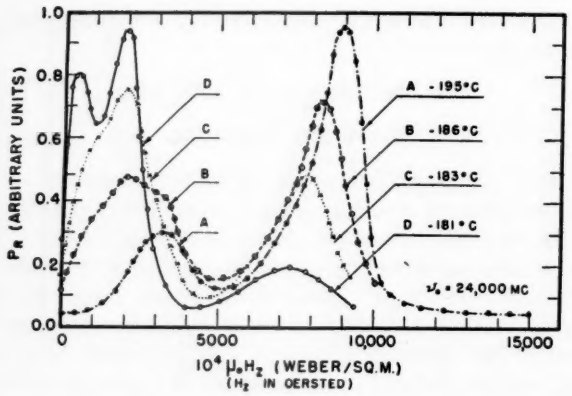

FIG. 9. Absorption curves below the transition, showing effect of temperature and strong magnetic field. (100) plane; [100] direction; $N_y - N_z = 0.910$.

Figure 10 shows the behavior of initial permeability κ_i as a function of temperature for the same natural single crystals of magnetite used in the resonance experiments. It can be seen that the maximum of this curve lies within a few degrees of the isotropy point, −143°C. Figure 10 also shows that κ_i drops off sharply in the transition region. The previous interpretation[9] of the initial permeability peak as a direct manifestation of the transition appears to be incorrect.

In the Transition Region

The complete disappearance of resonance absorption in the transition region in the initial X band experiments can be explained by the following considerations. Equation (3) shows that resonance absorption is to be expected for a particular microwave frequency even at zero static magnetic field. Using tentative values of anisotropy constants for magnetite below the transition (obtained from the resonance experiments) it was calculated that, at zero applied induction, resonance absorption would be observed at about 16,000 mc/sec. if the magnetization were along the direction of easy magnetization. In other words, the Larmor precession frequency of the electron spins even in the absence of an applied static magnetic field is 16,000 mc/sec., which exceeds the frequency of 3.3 cm microwaves. Addition of a static field increases the precession frequency. Consequently, resonance absorption below the transition is undetectable at 9000 mc/sec. unless the magnetization is along a direction of difficult magnetization, that is, in the plane perpendicular to the magnetic axis.

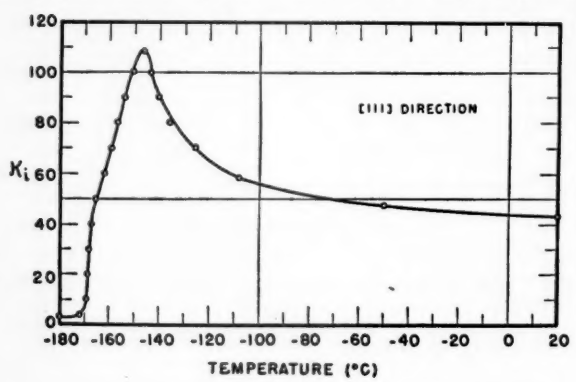

FIG. 10. Initial permeability of natural single crystal of magnetite.

The simultaneous existence in the transition region of absorption peaks characteristic of both cubic and uniaxial magnetic symmetry indicates that the transition of the entire crystal from one type of symmetry to the other does not occur simultaneously. On the other hand, the absence of a gradual shift in resonance induction with decreasing temperature shows that the transition does not produce a gradual distortion of magnetic symmetry, with the uniaxial anisotropy increasing continuously to its value below the transition. Rather, it is concluded that in a given small region of the crystal the symmetry changes discontinuously from cubic to uniaxial, and that as the temperature decreases through the transition region more and more of these small regions of the crystal change to the lower form of magnetic symmetry. The temperature range over which this process occurs is narrower for the synthetic crystals (3°C) than for the natural (5°C).

Below the Transition

From the results of some of our resonance experiments, anisotropy constants were calculated[12] for magnetite below the transition, assuming tetragonal magnetic symmetry. Predictions concerning resonance induction in other experiments, using these constants, were verified only qualitatively. It was not felt that sufficient experimental data were obtained in this investigation to warrant a distinction between the different types of uniaxial symmetry. For this purpose, it would be especially informative to investigate in detail the dependence of resonance induction upon orientation in the plane perpendicular to the magnetic axis. Such an investigation would require that the biasing magnetic field be applied normal to the plane of a (100) plane sample. This condition could not be fulfilled with our experimental arrangement.

Domenicali[17] has investigated the magnetization *vs.* applied magnetic field characteristics for magnetite after it had been subjected to different kinds of magnetic treatment while cooling through the transition. The area between magnetization curves for two different directions of a single crystal represents the difference in energy of magnetization for the two directions, and can be expressed in terms of the crystalline anisotropy constants. Using the tentative values of anisotropy constants for magnetite below the transition calculated from our experiments, we made predictions concerning areas between magnetization curves for different crystal directions after various orientations of biasing field. The agreement between our predicted areas and those measured from Domenicali's curves is within about 30 percent. Domenicali has offered an alternative

interpretation of magnetic effects at the transition in terms of a freezing-in of the domain pattern by internal stresses as the crystal cools through the transition.

We can only speculate as to the cause of the change in magnetic symmetry at the transition. Verwey's picture[1-3] of an ordering of the electronic structure at the transition, leading to a tetragonal (or orthorhombic) lattice symmetry, seems to give a reasonable explanation for the observed electrical effects. Domenicali's[17] results of thermal expansion measurements with magnetite single crystals would seem to indicate that the crystal structure is no longer cubic below the transition, although the change in structure is so small that it cannot be detected readily by x-rays. It is probable that the magnetic symmetry follows the crystal symmetry. In determining the magnetic axis, the biasing magnetic field may act through magnetostrictive effects which lead to a condition of minimum energy with the axis along the [100] direction most nearly parallel to the biasing field.

The ability of a strong magnetic field to change the direction of the magnetic axis below the transition calls to mind an analogous effect in ferroelectric barium titanate reported by Matthias and von Hippel.[21] Above its Curie point (120°C) barium titanate is cubic; below it, tetragonal, the tetragonality increasing with decreasing temperature. One of the [100] crystal directions is the tetragonal axis. If an electric field is applied to the crystal, the axis becomes the [100] direction most nearly parallel to the field. Thus it is possible to establish the direction of the axis by cooling the crystal through its Curie point in an electric field, or to change the direction of the axis below the Curie point by the application of a field.

Finally, a few remarks will be made concerning the double resonance peaks observed below the transition. Double peaks were observed in X band experiments with iron single crystals by Kip and Arnold,[13] and also in our early experiments with magnetite above the transition. The explanation offered by Kip and Arnold is that in weak fields the magnetization is not completely aligned by the field. When this fact was accounted for in the resonance equation, it was found that a second and very broad peak was predicted at low field strengths. According to this explanation no double peak would be expected along the direction of easy magnetization. Experimentally, only single peaks were observed at K band, where the resonance induction was much larger than that required to saturate the material magnetically.

Figure 8 shows two very well-defined peaks in a resonance curve obtained below the transition with the measuring field along the magnetic axis, or direction of easy magnetization. In some cases, the low field peak was sharper and stronger than the high field peak. Both of these observations are difficult to explain on the basis of incomplete magnetic saturation.

A critical experiment would be to repeat the measurements at a higher microwave frequency ($K/2$ band), where the resonance would occur at higher values of applied induction. If the double peaks should still appear in these experiments, an explanation for them would have to be found on grounds other than lack of magnetic saturation.

The author is grateful to Professor A. von Hippel for making the facilities of the Laboratory for Insulation Research available to him, and also for continued encouragement and helpful advice during the course of this work. Thanks are also due many members of the Laboratory for their cooperation, in particular C. A. Domenicali and S. Lawrence. In addition, the author wishes to thank Dr. C. Kittel, of the Bell Telephone Laboratories, for some illuminating discussions of his results.

[21] B. Matthias and A. von Hippel, Phys. Rev. 73, 1378 (1948).

Magnetic and Electric Properties of Natural and Synthetic Single Crystals of Magnetite*†

C. A. DOMENICALI‡
Laboratory for Insulation Research, Massachusetts Institute of Technology, Cambridge, Massachusetts
(Received December 16, 1949)

When a crystal of magnetite has been cooled through the low temperature transition (near −164°C) in a demagnetized state, the magnetization undergoes a large and abrupt increase in the three principal crystallographic directions [100], [110], and [111] upon warming. The behavior of the magnetization upon cooling in a magnetic field is influenced by crystallographic orientation as well as by the strength of the applied field. The form of the magnetization curve at temperatures below the transition depends on the crystallographic direction and on the magnetic treatment of the specimen while cooling through the transition. Barkhausen experiments lead to tentative ideas concerning domain orientation. Significant information concerning the nature of the transition was also obtained from measurements of thermal expansion and saturation magnetostriction.

The magnetic effects in the low temperature transition region appear to be influenced by the establishment of internal stresses which cause a "freezing-in" of preferential domain directions below the transition region. The stress and domain pattern resulting appears to depend on the magnetic treatment of the crystal during its passage through the transition region.

The temperature dependence of the electrical resistivity is in agreement with the results of Verwey and de Boer for sintered magnetite. Some preliminary observations are reported on the effects of magnetic fields on the resistivity.

1. INTRODUCTION

MAGNETITE (Fe_3O_4) is a ferromagnetic semiconductor crystallizing in the so-called inverse spinel lattice.[1] In the vicinity of −160°C it exhibits a second-order transition at which its physical properties change rather abruptly.[2–8] A brief survey of early work on magnetite is given by Bickford.[9]

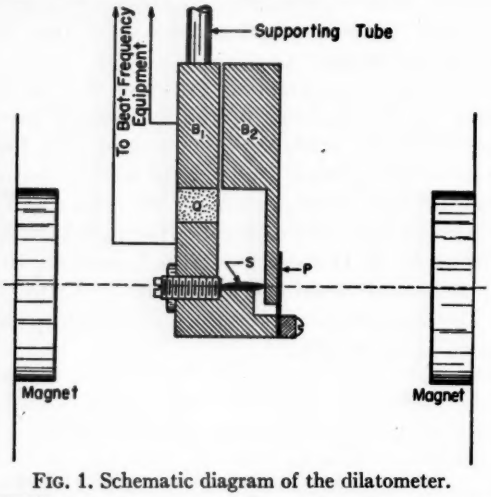

FIG. 1. Schematic diagram of the dilatometer.

The purpose of the present study was to investigate the magnetic and electric properties of magnetite single crystals in static fields, the dependence of these properties on temperature, and in particular the behavior in the vicinity of the low temperature transition. It became apparent during the work that helpful information might be obtained by also investigating the Barkhausen effect, the longitudinal saturation magnetostriction, and the thermal expansion of magnetite single crystals. Such measurements were therefore performed and are also reported.

2. SPECIMENS AND MEASUREMENTS TECHNIQUES

Measurements were made on both natural and synthetic single crystals of magnetite. The natural crystals were analyzed by J. Smiltens of this Laboratory; their composition appeared to be very nearly stoichiometric, although some ambiguity arises from the presence of impurities, mostly iron pyrite. The synthetic single crystals were grown by J. Smiltens[10] from a melt in the form of cylinders *ca.* 5 mm diam. and 20–40 mm long. Their chemical composition corresponded to the stoichiometric ratio within limits of error (Nos. 3 and 4). Some measurements were also made on a polycrystalline specimen (No. 5, composition, Fe_2O_3: FeO = 1.074).

In order to allow magnetic as well as electric measurements to be made on a single specimen, the shape chosen was that of an oblate spheroid (*ca.* 5 mm diam., 1 mm thickness). The specimens were cut with a diamond wheel and ground to shape with emery cloth. The only synthetic crystals available at the time of this investigation appeared to have rather large internal stresses, and to be cracked along the scratches drawn on the specimen for purposes of orientation (No. 3 cracked along [110], No. 4 along [100]). The magnetic measurements indicated greater hysteresis than for the natural single crystals, especially at temperatures below the transition. The crystallographic planes of the

* Sponsored by the ONR, the Army Signal Corps, and the Air Force under ONR Contract N5ori-07801.

† From a thesis submitted in partial fulfillment of the requirements for the degree of Doctor of Philosophy in Physics at the Massachusetts Institute of Technology.

‡ Now at Alfred University, Alfred, New York.

[1] E. J. W. Verwey and E. L. Heilman, J. Chem. Phys. **15**, 174 (1947).
[2] P. Weiss, thesis, Paris (1896).
[3] P. Weiss and K. Renger, Archiv f. Elektrotechnik **2**, 406 (1914).
[4] R. W. Millar, J. Am. Chem. Soc. **51**, 215 (1929).
[5] P. Weiss and R. Forrer, Ann. de Physique [10], **12**, 279 (1929).
[6] C. H. Li, Phys. Rev. **40**, 1002 (1932).
[7] T. Okamura, Science Repts. Tôhoku Imp. Univ. **21**, 231 (1932); T. Okamura and S. Ogawa, Proc. Phys.-Math. Soc. Japan **23**, 363 (1941).
[8] E. J. W. Verwey and J. H. de Boer, Rec. trav. chim. **55**, 531 (1936).
[9] L. R. Bickford, Tech. Rept. XXIII, ONR Contract N5ori-07801, Lab. Ins. Res., M.I.T. (October, 1949).
[10] J. Smiltens, Lab. Ins. Res., M.I.T. (to be published).

specimen disks No. 1, 2, and 3 were (110); No. 4, (100). The place of origin of the natural single crystals was Chester, Vermont.

The resistivity of the specimens was obtained in the usual manner by measuring the difference in potential between two probes in contact with the specimen for a known current traversing the specimen. No attempt was made to determine accurately the absolute value of the resistivity since the current density was not uniform throughout the specimen, and because the temperature coefficient of resistivity is in our case the parameter of interest.

The magnetization was measured with a new type of pendulum magnetometer[11] in which the specimen is surrounded by a "null-coil" through which a current is passed in such a sense as to cancel the magnetic moment of the specimen. In this manner one avoids the necessity of measuring directly the magnetic field gradient and the force acting on the specimen in the inhomogeneous field.

The Barkhausen effect in the spheroidal specimens was observed by means of a small search coil with *ca.* 150 turns of No. 42 enameled copper wire wound closely around the specimen on a thin paper form. The pick-up coil was connected to the input of a wide-band, high gain amplifier the output of which was connected to the vertical plates of an oscilloscope. The Barkhausen pips, on the average, were 5 to 10 times higher than the background noise.

The dilatometer for measuring the magnetostriction and thermal expansion of the spheroidal magnetite specimens is shown in schematic form in Fig. 1. The basic idea of the device is that, as the diameter of the specimen S changes, the inner faces of the brass blocks B_1 and B_2 alter their separation; if these two faces are used as condenser plates the corresponding variation in capacity can be used to calculate the change in dimensions of the specimen.[12] A positive pivot-action is furnished by the phosphor-bronze ribbon P; the Bakelite block Q isolates the two condenser plates electrically. The change in capacity was measured with a beat-frequency equipment developed in this Laboratory for the measurement of the dielectric constant of gases.[13] The instrument was calibrated with a fused quartz specimen.

Besides ease of construction, the holder showed very good stability as a result of the "pinching" action exerted by the phosphor-bronze ribbon. By placing the

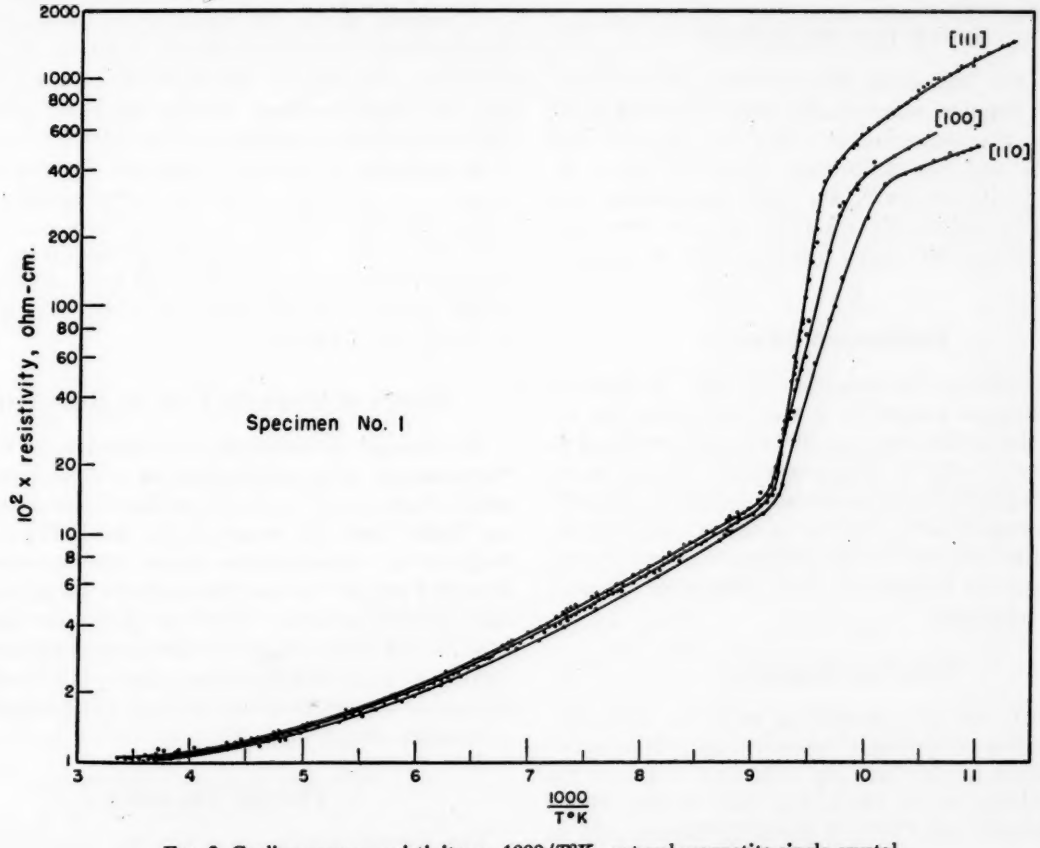

FIG. 2. Cooling curves, resistivity *vs.* 1000/T°K; natural magnetite single crystal.

[11] C. A. Domenicali, Tech. Rept. XXIV, ONR Contract N5ori07801, Lab. Ins. Res., M.I.T. (October, 1949); Rev. Sci. Inst. **21**, 327 (1950).
[12] C. W. Heaps and A. B. Bryan, Phys. Rev. **36**, 326 (1930).
[13] J. G. Jelatis, J. App. Phys. **19**, 419 (1948).

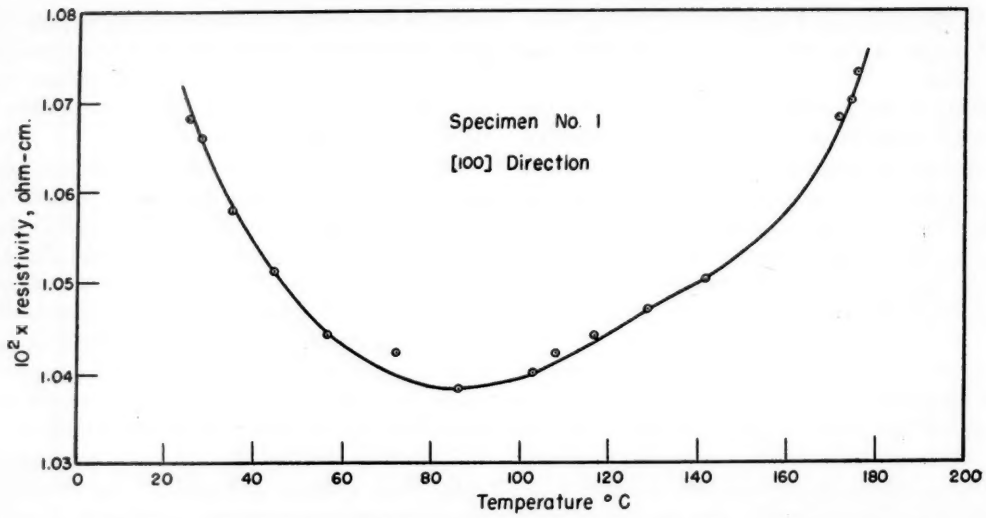

FIG. 3. Warming curve, resistivity *vs.* temperature, natural magnetite single crystal, showing maximum.

specimen horizontally the magnetostriction for a selected direction in the plane of the disk could be measured in magnetic fields applied parallel to this or to any other direction in the plane of the disk.

3. MAGNETIC AND ELECTRIC BEHAVIOR ABOVE THE TRANSITION

Above the transition temperature (*ca.* −164°C) magnetite behaves magnetically much like nickel; its saturation magnetization is 4.45×10^5 amp./m (445 c.g.s./cm³) and its anisotropy constant $K=-10^4$ joule/m³ (-10^5 erg/cm³). Its Curie temperature lies at *ca.* 570°C, and in polycrystalline form at room temperature it has an initial permeability of approximately 17.

Barkhausen Effect

In the present investigation of the Barkhausen effect of natural magnetite it was found that the activity on the oscilloscope vanishes almost completely in the vicinity of −143°C. This is in accord with the recent work of Bickford,[14] who determined, from ferromagnetic resonance experiments, that the anisotropy constant K_1 of magnetite vanishes at this temperature but increases rapidly again in magnitude as the transition temperature is approached.

Electrical Properties

Magnetite exhibits interesting electrical properties above the low temperature transition as well as below. A discussion of the striking difference between the electrical behavior of Fe_3O_4 and that of the related lattices Mn_3O_4 and Co_3O_4 is given by Verwey and de Boer[8] based on experiments with sintered bars of these materials. In Fig. 2 are shown the results of our measurements of the resistivity of natural magnetite single crystals for the three principal crystallographic directions. These measurements were made while the crystal was cooled very slowly in a demagnetized state.

Of interest above the transition is the behavior of the resistivity in the vicinity of +100°C, as already pointed out by Verwey and de Boer; in order to bring out the situation more clearly we have plotted in Fig. 3 resistivity *vs.* temperature for the [100] direction of a specimen of natural magnetite. It appears that magnetite is another of the few investigated cases of substances for which the conductivity traverses a maximum value at a reasonably low temperature. Another interesting example of this type of behavior is silicon carbide, which has been thoroughly investigated by Busch and Labhart.[15]

Effects of Magnetic Field on Resistivity

The change in resistivity of magnetite at ordinary temperatures upon application of a strong magnetic field is quite small (*ca.* 0.1 percent). For example, it was found that the resistivity in the [110] direction *decreases* at temperatures above the transition by about 0.1 percent upon application of a strong magnetic field parallel to either [110] or [111]. On the other hand, if the strong magnetic field is applied parallel to [100] at these temperatures, the [110] resistivity *increases* a few tenths of one percent. These observations were made on specimen No. 1.

Thermal Expansion

The thermal expansion of natural single crystals of magnetite has apparently been investigated only by Okamura.[7] He gives the results of measurements on

[14] L. R. Bickford, Jr., Phys. Rev. **76**, 137 (1949); Tech. Rept. XXIII, ONR Contract N5ori-07801, Lab. Ins. Res., M.I.T. (October, 1949).

[15] G. Busch and H. Labhart, Helv. Phys. Acta **19**, 463 (1946).

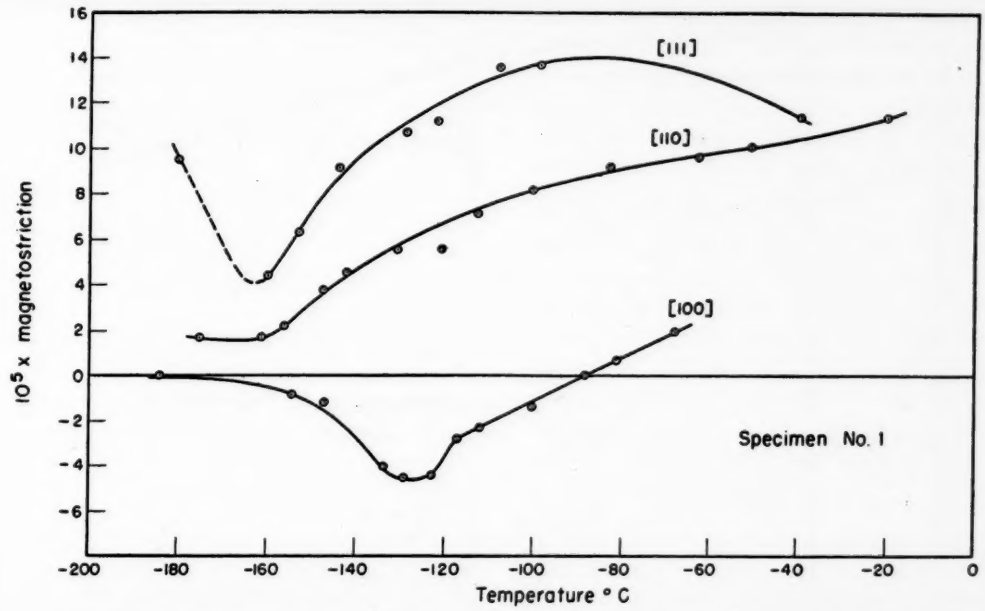

FIG. 4. Longitudinal saturation magnetostriction *vs.* temperature, natural magnetite single crystal.

one rod cut from a single crystal, but does not indicate the crystallographic orientation of the axis of the rod.

The present measurements were made on one of the oblate spheroids cut from a natural single crystal. For a temperature interval of 50°, i.e., from −150° to −100°C, the thermal expansion coefficients for the three principal crystallographic directions were found to be as follows: [100], 4.66×10^{-6}/°C; [110], 7.16×10^{-6}/°C; [111], 11.3×10^{-6}/°C±*ca.* 5 percent.

Magnetostriction

At temperatures above the transition, the longitudinal saturation magnetostriction ($\Delta L/L$ measured parallel to applied magnetic field) proved to be positive for the [110] and [111] directions; the [100] direction has a positive value at temperatures above −88°C and is negative below this temperature (Fig. 4). Because of the so-called "form effect" (specimen No. 1 is an oblate spheroid) the values of magnetostriction given in Fig. 4 are too large by possibly as much as a factor of 2. No accurate estimate of this factor can be made, since the elastic constants of magnetite are not known. By using long, thin rods the influence of the specific form of the specimen can be eliminated, but the present data are still useful in showing the temperature dependence of the magnetostriction and the relative values for the three principal crystallographic directions.

4. EFFECTS IN THE VICINITY OF THE TRANSITION

Magnetization

As the temperature of a magnetite specimen is lowered the magnetization, measured by the steady state method, increases in a manner depending not only on the applied magnetic field but also on the crystallographic direction along which the field is applied. This behavior as such is, of course, not unusual, but the effects occurring when the transition region of magnetite is reached are quite so.

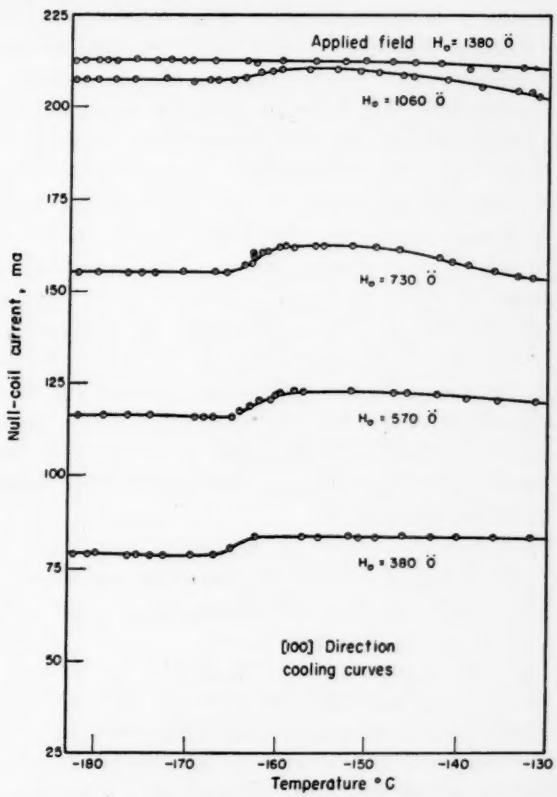

FIG. 5. Cooling curves, magnetization (arbitrary units) parallel to [100] *vs.* temperature, natural magnetite single crystal. Curves are for various values of fixed external magnetic field.

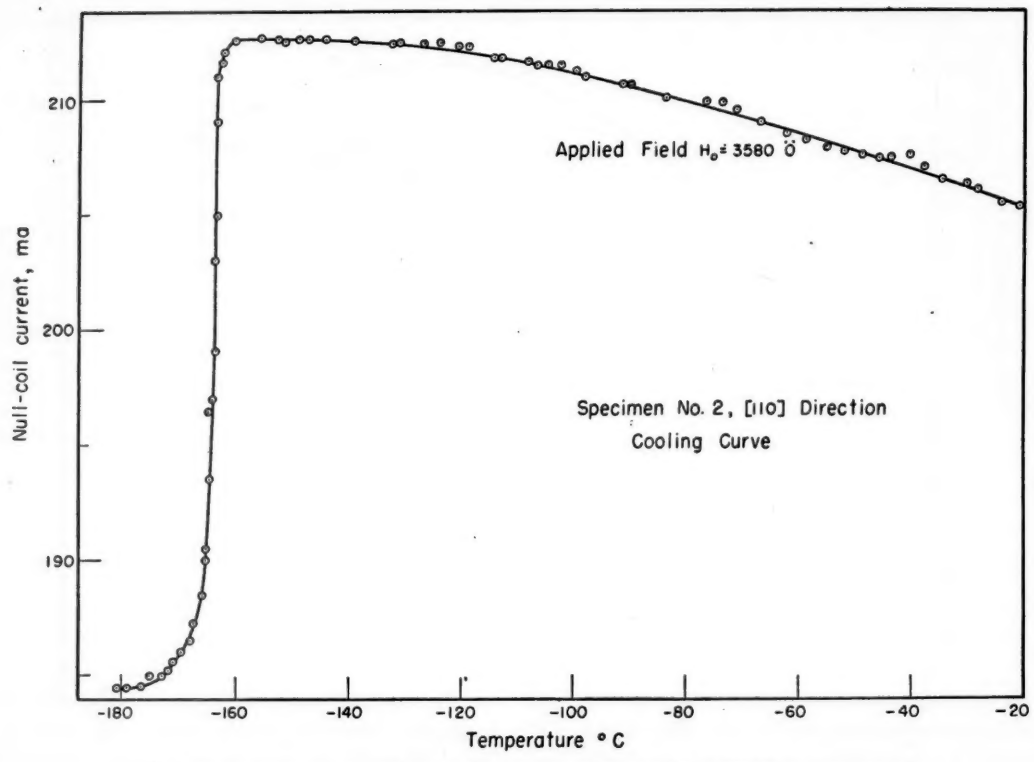

FIG. 6. Cooling curve, magnetization (arbitrary units) parallel to [110] *vs.* temperature, natural magnetite single crystal.

Figure 5 shows measurements on specimen No. 2; the ordinate gives the values of the magnetometer null-coil current, which is proportional to the magnetization of the specimen. The field was applied in this case along the [100] direction, and the various curves correspond to fixed values of the external magnetic field. If the field is applied along the [111] direction the results are very similar to those for the [100] direction. Repeated with the magnetic field along the [110] direction, the outcome of this experiment is quite different (Fig. 6). Even for large fields one observes in this orientation upon cooling a large and rapid decrease in magnetization. In the [100] and [111] directions on the other hand, only a slight diminution in magnetization occurs if weak fields are applied, while in strong fields one observes a slow monotonically increasing magnetization with falling temperature.

This behavior might be interpreted as indicating that the abrupt change in magnetization is primarily a characteristic of the [110] direction of magnetite. However, if one demagnetizes the specimen carefully while the temperature is still above the transition, cools then through the transition in zero field, and measures again in successive experiments the magnetization along the three principal crystallographic directions while the temperature rises through the transition, one finds the results shown in Fig. 7. These data refer to specimen No. 1, but the same situation was found to hold for No. 2, for several samples cut parallel to other

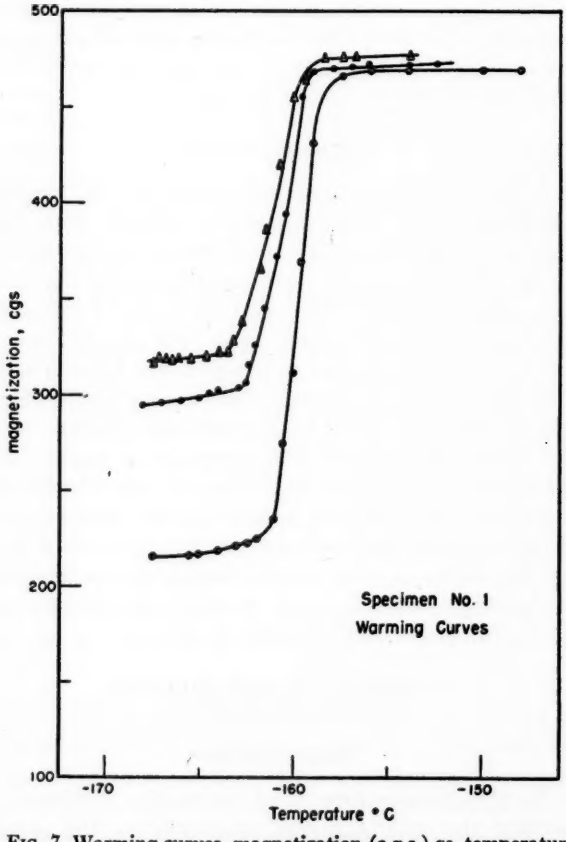

FIG. 7. Warming curves, magnetization (c.g.s.) *vs.* temperature, parallel to the three principal crystallographic directions, natural magnetite single crystal.

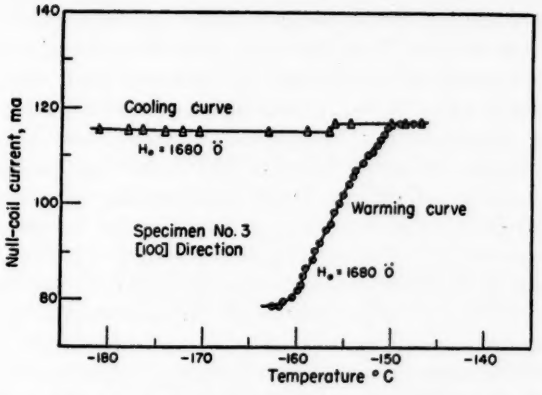

FIG. 8. Magnetization (arbitrary units) *vs.* temperature, synthetic magnetite single crystals. Specimen No. 3, [100] direction.

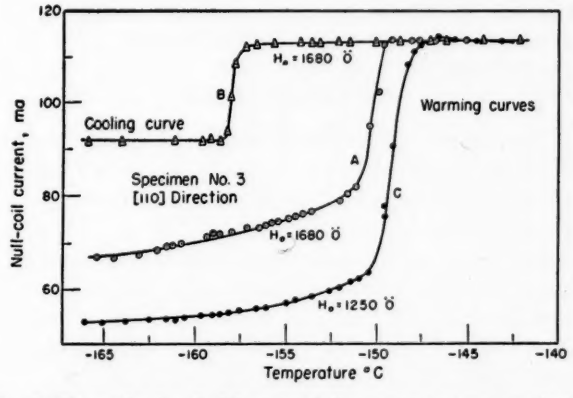

FIG. 9. Magnetization (arbitrary units) *vs.* temperature, synthetic magnetite single crystals. Specimen No. 3, [110] direction.

crystallographic planes, and also for synthetic single crystals.

Comparing Figs. 5, 6, and 7 we see that the temperature dependence of the magnetization is different for the three principal crystallographic directions, and is determined by the magnetic prehistory of the specimen. Cooled through the transition in zero field, the crystal upon warming undergoes a large abrupt increase in magnetization in all three crystallographic directions. During cooling through the transition in intermediate and large fields, the magnetization undergoes a large abrupt decrease for the [110] direction but not for the [100] nor [111] directions. In weak fields all three directions exhibit during cooling a complicated behavior, but always an over-all decrease in magnetization occurs as the temperature is lowered through the transition.

Although the same general behavior was found for the two synthetic single crystals,[16] these latter specimens showed several additional features of interest which were not found in the natural crystals. The warming curve (Fig. 8) of specimen No. 3, for example, shows that the magnetization in the [100] direction increases gradually over a 10° interval with an increase in magnetization of about 45 percent for an applied induction of 0.168 weber/sq. m (1680 oersteds). The center of this magnetic transition (for the [100] direction) is at a slightly higher temperature (−155°C) than that of the natural crystals (−161°C; see Fig. 6). On the other hand, the [110] direction of this specimen behaves quite differently (Fig. 9). The change in magnetization is rapid for both cooling and warming through the transition region, but the temperatures at which the abrupt changes in magnetization take place for the same external induction (0.168 weber/sq. m), differ in curves *A* and *B* by 8°C. Warming in a weaker field, after cooling through the transition region in zero external field, caused a rapid change in magnetization at an even higher temperature than −150°C (curve *C*, Fig. 9).

Specimen No. 4 gave similar results (Figs. 10 and 11), except that the temperature difference between the transitions for warming and cooling was even larger, namely 20°C. Furthermore, whereas for specimen No. 3 the warming curve in the region below the transition for the [110] direction (Fig. 9) shows a gradual increase in magnetization, specimen No. 4 in its corre-

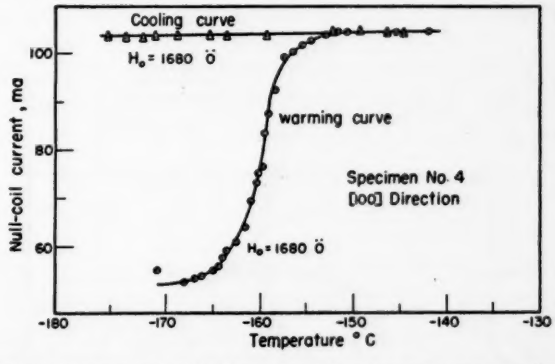

FIG. 10. Magnetization (arbitrary units) *vs.* temperature, synthetic magnetite single crystals. Specimen No. 4, [100] direction.

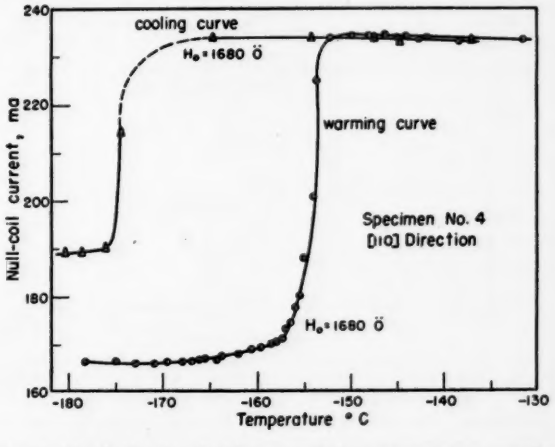

FIG. 11. Magnetization (arbitrary units) *vs.* tempeature, synthetic magnetite single crystals. Specimen No. 4, [110] direction.

[16] Specimen Nos. 3 and 4 cracked in the grinding process; measurements were nevertheless made on these specimens after cementing the pieces together, because no other synthetic single crystals were available at that time.

sponding temperature range shows (warming curve, Fig. 11) a constant value of magnetization in this same crystallographic direction. The center of the [100] warming curve (specimen No. 3) in Fig. 8 lies at a temperature (−155°C) between the [110] "warming transition" and "cooling transition" (−150° and −158°C) of Fig. 9; the same is true for specimen No. 4 (Figs. 10 and 11).

Specimen No. 5, the synthetic polycrystalline specimen of non-stoichiometric composition, was found to give in the transition region a small decrease in magnetization upon cooling in an applied induction of 0.168 weber/sq. m, but after cooling in zero field showed a large and rapid increase in the vicinity of −180°C upon warming (Fig. 12).

Next, the shape of the magnetization curves (M *vs.* H) for the three principal directions at temperatures just above and below the transition was investigated[17] (Fig. 13). The curves corresponding to −180°C were each taken after the specimen (No. 1) had been demagnetized above the transition and then cooled directly to −180°C in zero field. It is seen that below the transition, after cooling in zero field, the crystal is much more difficult to magnetize than at temperatures above this region.

If, on cooling through the transition, a "freezing in" of some unit occurs, either on an atomic or on a domain scale, the magnetization curves below the transition might differ after cooling in fields of various strengths. This is actually the case, as shown for the magnetization parallel to [100] in specimen No. 2 (Fig. 14). The specimen was demagnetized above the transition, the indicated field H_0 applied and held constant while cooling through the transition, and the specimen demagnetized again below the transition temperature before the corresponding magnetization curve was taken. Similar experiments for the [111] direction gave the same kind of curves, except that cooling in a given field H_0 parallel to [111] did not raise the magnetization curve quite as much as for cooling in a field of the same strength oriented parallel to [100]. In contrast, the [110] direction remained difficult to magnetize even after cooling through the transition region at applied inductions of several tenths of a weber/sq. m (several thousands of oersteds) oriented parallel to [110]. This difference between the three principal crystallographic directions makes less surprising the behavior of the magnetization upon cooling in the transition region as shown in Figs. 5 and 6.

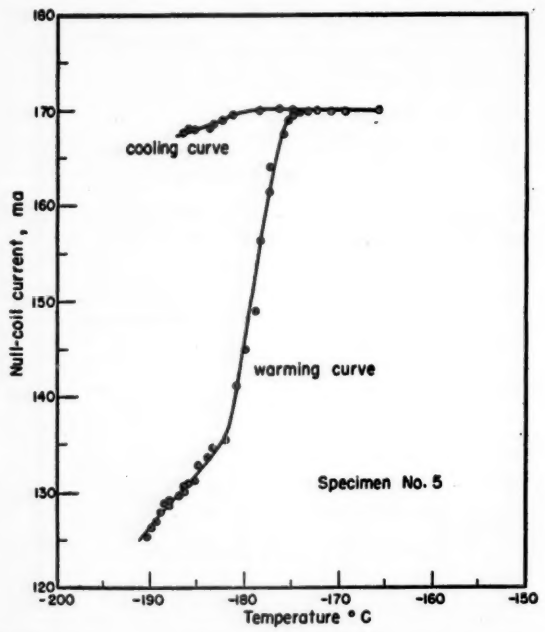

FIG. 12. Magnetization (arbitrary units) *vs.* temperature, synthetic polycrystalline non-stoichiometric magnetite.

[17] Okamura and Ogawa (reference 7) apparently failed to observe the important differences between the magnetization curves below the transition for cooling in finite and in zero fields.

Barkhausen Effect

The magnetic behavior of magnetite in the vicinity of the transition might be the result of oriented internal stresses resulting from a rapid change of the magnetostriction and the lattice dimensions in the transition region. If this results in a "freezing in" of ferromagnetic domains by the internal stresses, an investigation of the Barkhausen effect in the vicinity of the transition should give significant information. The following observations were made on specimen No. 2.

(a) After careful demagnetization and cooling through the transition in zero field, observation of the Barkhausen effect with slowly increasing applied field indicated that only about 75 to 85 percent of the magnetization results from irreversible wall displacements, as indicated by strong pips on the cathode-ray screen; the remainder, not visible on the screen, may be due to domain rotations. A similar experiment performed at

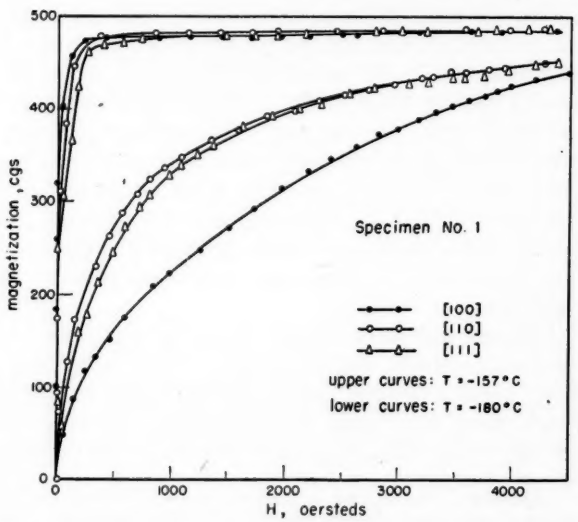

FIG. 13. Magnetization *vs.* H, natural magnetite single crystal. Upper curves for $T=-157$°C; lower curves for $T=-180$°C.

room temperature indicated that more than 95 percent of the technical saturation magnetization is the result of irreversible wall displacements; this observation is in accord with the well-known interpretation of the magnetization process in ferromagnetic single crystals.

(b) We have seen that the [100] direction is very easy to magnetize after cooling through the transition in a strong field parallel to [100] and careful demagnetization. After such treatment, the crystal showed during slow magnetization a Barkhausen noise over practically the whole extent of the [100] magnetization curve.

(c) When the crystal is cooled through the transition in a strong field parallel to [100] and subsequently carefully demagnetized, the domains might be expected to align themselves with their magnetization vectors parallel to that particular [100] axis along which the external field had been applied. If then a weak or medium field is applied parallel to this [100] edge and its direction made to oscillate slightly, the domains would rotate to follow the applied field and little or no Barkhausen noise should be observed. On the other hand, if the same demagnetized crystal, after cooling in a strong field parallel to [100], were exposed to a medium field, slowly changing in direction by a few degrees about [110] (that is, normal to the [100] direction in the (110) plane) the domain walls might be displaced irreversibly and in very great numbers since the sign of the [100] component of the bulk magnetization M tends to reverse. In this case one would expect to observe a strong Barkhausen noise. Such experiments were performed and this picture was verified. This interpretation might be the basis of an explanation of the "magnetic memory" first observed by Li.[2]

(d) A supposition that irreversible domain reorientations might occur upon simply cooling or warming the demagnetized crystal through the transition did not prove to be true. No Barkhausen noise was observed when the crystal was treated this way. However, when the specimen was warmed through the transition in a weak field, after having been cooled in a demagnetized condition, a very definite display of Barkhausen pips was seen on the oscilloscope screen during the passage through a temperature interval of approximately 5°C, beginning at about −166°C. This effect probably results from the decrease of the inner magnetic field, upon warming through the transition, which in turn results in an increase in the demagnetizing field.

(e) If a magnetic field is suddenly applied to a ferromagnetic crystal the magnetization will of course require some finite time to acquire the value corresponding to the applied field. A rough estimate of this time interval can be obtained by observing the duration of the Barkhausen noise immediately after the sudden application of a magnetic field. It was found that the time lag in the magnetization, by irreversible wall displacements, of magnetite at temperatures below the transition depends upon the magnetic treatment during cooling. After cooling in zero field, the lag is approximately one second for all three principal crystallographic directions. After cooling in a strong field parallel to [100], however, the lag corresponding to the same field is approximately 2 sec. for the field suddenly applied parallel to [110], but is less than $\frac{1}{4}$ sec. for the field applied parallel to either [100] or [111]. It would be of interest to investigate the low frequency complex permeability of magnetite at low temperatures and its dependence on magnetic treatment while cooling through the transition.

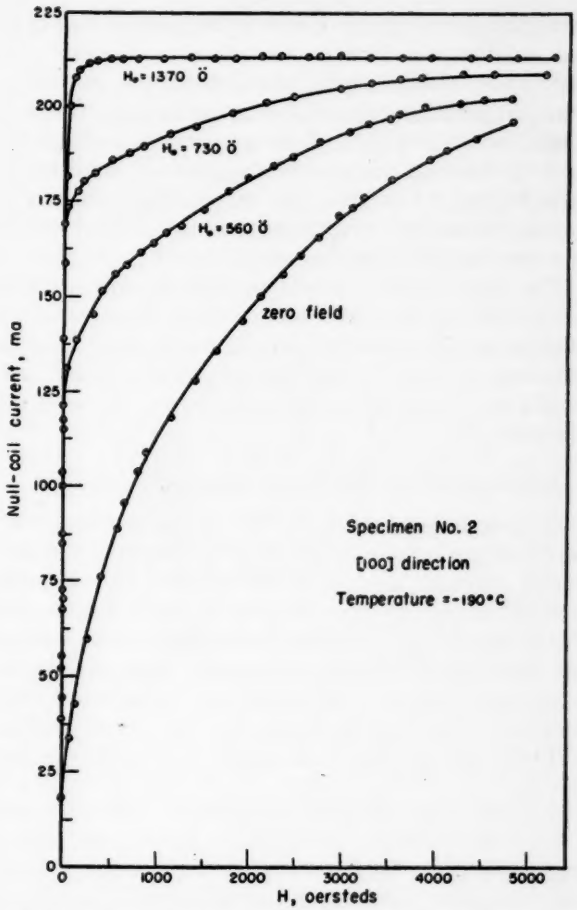

FIG. 14. Magnetization *vs.* H, natural magnetite single crystal. $T = -180$°C. Curves are for various values of external "annealing field" H_0 applied during passage through transition region.

Resistivity

In agreement with the results of Okamura[7] and of Verwey,[8] the single crystal specimens of magnetite showed a large and rapid increase in resistivity as the temperature was lowered through the transition region (Fig. 2). The resistivity at temperatures below the transition depends markedly upon crystallographic direction and the values of this parameter for the three principal directions are in the approximate ratios $(\rho)_{[111]}:(\rho)_{[100]}:(\rho)_{[110]} = 5:3:2$. Furthermore, although the magnitude of the rapid change in the transition interval is approximately the same for all three direc-

tions, the rate of change is seen to be greatest for [111] and smallest for [110]. According to Verwey and Haayman[18] the resistivity of stoichiometric magnetite changes approximately 100-fold in the transition region; specimen No. 1 (Fig. 2) gives an increase of about 30-fold. A chemical analysis of this sample indicated a ratio Fe_2O_3: FeO of 0.967, but this chemical analysis is probably somewhat meaningless because of the presence of a small amount of iron pyrite.

The polycrystalline specimen (No. 5), with a ratio Fe_2O_3: FeO = 1.074, gave only a small change in resistivity at its transition, which occurred at a lower temperature than that of the natural crystals. These results are also in agreement with those of Verwey and Haayman.[18]

Influence of the Magnetic Field on Resistivity

In general, the fractional change in resistivity at temperatures below the transition upon application of a strong magnetic field is of the order of one percent, that is, somewhat larger than above the transition. As stated previously, for temperatures above the transition the application of a strong magnetic field parallel to either the [110] or [111] direction caused the [110] resistivity to *decrease ca.* 0.1 percent; for a field parallel to [100] the resistivity *increased* a few tenths of one percent. Below the transition the application of a strong magnetic field in any of the three principal crystallographic directions caused the [110] resistivity to *decrease* by a few percent.

Thermal Expansion

When warmed through its transition magnetite shows a rapid increase in dimensions in the transition region, as shown in Fig. 15. The [111] and [110] directions have positive expansion coefficients both above and below this region; [100] below the transition shows an anomalous contraction upon warming, and apparently undergoes a change in sign of the expansion coefficient at approximately −152°C, becoming normal or positive above this latter temperature. The coefficient of thermal expansion for the [111] direction within the transition region itself is very large, having approximately the value 150×10^{-6}/°C (see the slope of the [111] curve at −164°C in Fig. 15), or about ten times that of copper at ordinary temperatures. The rate of expansion of the crystal (No. 1) in the [110] direction appears from Fig. 15 to be even larger, but obviously the data within the transition region for this direction are too scanty to permit definite quantitative conclusions. On the other hand, the [100] curve indicates a less radical change of dimension parallel to this

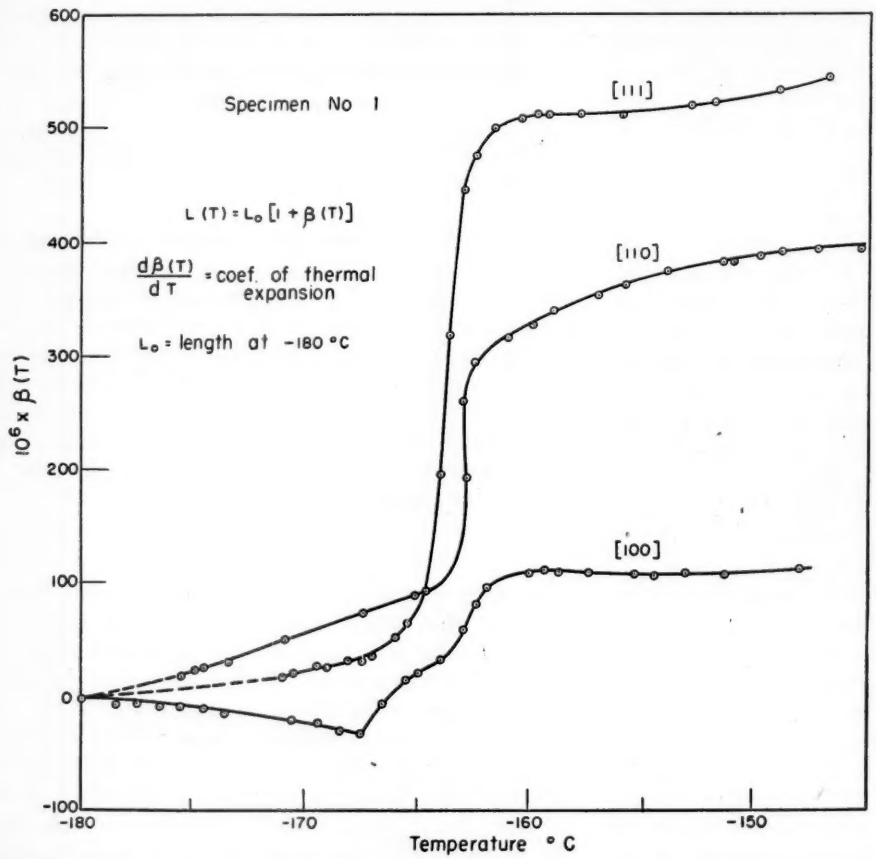

FIG. 15. Change of dimension *vs.* temperature, for the three principal crystallographic directions, natural magnetite single crystal. Coefficient of thermal expansion is slope of the curves shown.

[18] E. J. W. Verwey, Nature 144, 327 (1939); E. J. W. Verwey and P. W. Haayman, Physica 8, 979 (1941).

direction. The rapid changes in the [111] and [110] directions are seen to take place within a 1° or 2°C interval around −164°C, the same temperature at which the magnetization changes most rapidly (e.g., see Fig. 6).

Magnetostriction

The longitudinal saturation magnetostriction of specimen No. 1 is shown as a function of temperature in Fig. 4. The values were taken while the specimen was cooling; those at temperatures below the transition were found after cooling the crystal through the transition in a demagnetized state. As previously mentioned, the values given have not been corrected for the "form effect" which depends[19] on the demagnetization coefficient, the magnetization, and several unknown elasticity parameters. Nevertheless, the magnetostriction below the transition is seen to be negative and small in the [100] direction, positive and approximately five times larger parallel to [111] than [110].

5. CONCLUSIONS

We may summarize the principal electric and magnetic properties of magnetite single crystals as follows.

(1) The resistivity increases rapidly within the transition region upon cooling; the magnitude and the temperature of the "resistivity transition" depend on composition.

(2) The resistivity at temperatures below the transition is markedly influenced by the presence and orientation of a magnetic field applied during cooling through the transition.

(3) There is a minimum in the resistivity of magnetite at a temperature of approximately +100°C.

(4) The magnetic properties of magnetite below the transition temperature depend on its magnetic state while cooling through the transition region. The crystal is magnetically hard in all three principal crystallographic directions if cooled in a demagnetized state. Certain crystallographic directions can be made magnetically soft below the transition by a "magnetic annealing" process, that is, by cooling the crystal through the transition with a strong magnetic field applied in these directions.

(5) Barkhausen experiments seem to indicate that this magnetic annealling establishes preferred directions for domain alignment.

(6) In a narrow temperature region centered about 20°C above the low temperature transition, there is little or no Barkhausen activity.

(7) Upon warming through the transition region magnetite undergoes an abnormal expansion which is anisotropic.

(8) The longitudinal saturation magnetostriction at temperatures below the transition is strongly anisotropic, positive for the [111] and [110] directions, negative for the [100] direction. The magnetostriction in the [100] direction changes sign at −88°C, being negative below this temperature and positive above; the values for the [111] and [110] directions remain positive up to room temperature.

The behavior of the resistivity of magnetite in the vicinity of the low temperature transition has been attributed by Verwey and de Boer[8] to an ordering of the conduction electrons, and in a more recent paper Verwey, Haayman, and Romeijn[20] suggest a pattern of order. According to their model the tetragonal axis of of the "electron lattice" (at temperatures below the transition) can be established by the application of a magnetic field while the crystal is cooled through the transition; the tetragonal axis is that [100] axis of the high temperature crystal which makes the smallest angle with the applied magnetic field. This model of Verwey *et al.* has been used recently by Bickford[9] to explain the magnetic effects exhibited by magnetite in the low temperature transition region, and is discussed in the accompanying paper.[21] An alternative explanation is as follows. As the crystal is cooled through the transition, there occurs a rapid anisotropic contraction of the lattice which, together with the finite magnetostriction, gives rise to a peculiarly oriented stress pattern. This stress pattern, as might be expected from elementary ferromagnetic domain theory, could give rise to energetically preferred crystallographic directions parallel to which the domains would become aligned. One might expect that the nature of the low temperature stress pattern (and consequently of the domain pattern) would depend upon the orientation of the domains as the crystal cools through the transition region, and this orientation depends, of course, upon the magnitude and direction of the applied magnetic field. We have thus a tentative picture of the magnetic annealling process and of the magnetic memory of magnetite. It is clear, however, that a satisfactory detailed explanation of the low temperature transition of magnetite is not yet at hand.

The author wishes to express his appreciation for the cooperation and encouragement he received during this research from Professor A. R. von Hippel under whose direction it was undertaken, to Dr. L. R. Bickford, Jr., for helpful discussions, and to the Cyclotron Laboratory, M.I.T., for the loan of the wide-band amplifier used in this work.

[19] R. Becker and W. Döring, *Ferromagnetismus* (Verlag. Julius Springer, Berlin, 1939).

[20] Verwey, Haayman, and Romeijn, J. Chem. Phys. **15**, 181 (1947).

[21] L. R. Bickford, Jr., Phys. Rev. **78**, 449 (1950).

A New Criterion for the Occurrence of Slip in Thin Single Crystals

T. L. Wu* AND R. Smoluchowski
Metals Research Laboratory, Carnegie Institute of Technology, Pittsburgh, Pennsylvania
(Received January 16, 1950)

It has been found that in thin crystals of aluminum slip does not occur in the plane or direction which corresponds to the maximum resolved shear. Instead, slip directions are favored which correspond to a short path of slip across the crystal. A formula is derived which permits one to predict the behavior of thin single crystals in tension.

IN the course of preparation of thin, single crystal specimens of aluminum for the study of internal friction as a function of elongation, it was found that the slip did not occur according to the usual rules governing the maximum resolved shear. This being a serious deviation from the generally accepted behavior, a systematic investigation of this phenomenon has been undertaken.

By using the method of carefully controlled strain-anneal, single crystals of aluminum 10 to 20 cm long and a few centimeters wide were obtained in a sheet 0.03 cm thick. Since the samples were to be used for the study of internal friction, they had to be cut out in such a manner as to avoid any straining. This was achieved by covering a single crystal with an asphalt lacquer and etching[1] along an outline from which the lacquer was removed prior to its complete hardening. The specimens were then electrolytically polished[2] to the desired thickness and shape. The final size was 2 cm length, 2 mm width and around 0.2 mm thickness, with somewhat larger butts at the ends for clamping in a tensile device. The stretching was performed under continuous microscopic observation which indicated a uniform appearance of slip lines along the length of the specimen.

Orientation of the crystallographic axes of the crystal with respect to the direction of tension was determined by means of x-rays or by optical methods. A face-centered cubic lattice slips on a (111)-type plane in a [110]-type direction. The actual index of the active slip plane is easily determined from the measurement of the inclination of the slip lines to the direction of tension as observed on the surface of the sample. Inasmuch as the samples were very small it was found advantageous to determine the direction of slip by comparing the Laue x-ray spots of planes perpendicular to the various possible directions of slip.[3] The spot corresponding to the active direction of slip was much broader than those of the other, inactive, directions in the same slip plane.

According to the usual criterion,[4] the first slip should occur on a slip system which corresponds to the maximum resolved shear. The latter is given by

$$S=(F/A)\cos\theta\sin\theta\cos\eta=(F/A)\cos\theta\cos\lambda, \quad (1)$$

where F/A is the tension per unit cross section of the sample, θ is the angle between the direction of tension and the normal to the slip plane, λ is the angle between the direction of tension and the direction of slip and η is the angle between the slip direction and the projection of the direction of tension on the slip plane. Assuming $F=A$, the relative resolved shear S was computed for all possible slip systems; the maximum value should correspond to the system which is first to become active. A comparison with experiments showed a complete lack of agreement.

It is difficult to imagine any "macroscopic" reason why formula (1) would not apply. Thus attention was directed to the actual mechanism of slip, according to which for a slip to occur a dislocation has to form at or near the surface and cross the specimen. There it undergoes reflection and retraces its path producing additional slip and so on until it is stopped by an obstruction. If we compare a dislocation moving across the thickness (0.2 mm) of the sample with a dislocation moving across the width (2 mm) of the sample we see that in the first case the area on which a dislocation can

TABLE I. Observed slip systems and calculated values of S and S' for four crystals. Only those having high values of S or S' and the active ones are shown.

Crystal	Slip plane	Slip direction	S	S'	Observed slip
#7	$\bar{1}11$	$0\bar{1}1$	0.245	0.179	2nd
		$10\bar{1}$	0.365	0.066	
	$11\bar{1}$	$\bar{1}10$	*0.469*	0.125	
		$0\bar{1}1$	0.301	0.192	
	$1\bar{1}1$	$\bar{1}01$	0.230	0.227	1st
#8	$11\bar{1}$	$\bar{1}01$	*0.442*	*0.348*	1st
		$0\bar{1}1$	0.418	0.214	
	$\bar{1}11$	011	0.373	0.313	2nd
#9	$\bar{1}11$	011	0.361	0.289	2nd
		$10\bar{1}$	*0.472*	0.136	
	$11\bar{1}$	$\bar{1}01$	0.372	*0.342*	1st
#10	$\bar{1}11$	101	0.383	0.152	
		011	0.338	*0.322*	—simult.
	$11\bar{1}$	$\bar{1}01$	*0.438*	*0.326*	
		$0\bar{1}1$	0.400	0.113	

* Now at Syracuse University, Syracuse, New York.
[1] Edwards, Frary, and Jeffries, *The Aluminum Industry* (McGraw-Hill Book Company, Inc., New York, 1930), p. 469.
[2] R. B. Mason, U. S. Patent No. 2108603.
[3] Turner, Wu, and Smoluchowski, Rev. Sci. Inst. (to be published).
[4] W. Boas and E. Schmid, *Kristallplastizität* (Verlag. Julius Springer, Berlin, 1935), p. 111.

form, and thus the probability of its occurrence, is much bigger. Also, in that case the path is shorter and thus the probability, per unit length of a dislocation, that a dislocation will be stopped in its run by an obstacle (a mosaic boundary, etc.) is smaller. It appears, therefore, that the resolved shear as computed from formula (1) should be multiplied by some factor P which takes into account these additional geometrical considerations which favor a short path. We assume this factor to be inversely proportional to the length of the path of the dislocation, which is given by

$$L_1=\frac{t\sin\delta}{\sin\Phi\cos\theta} \quad \text{or} \quad L_2=\frac{w\sin\delta}{\cos\Phi-\cos\lambda\cos\delta}, \qquad (2)$$

whichever is the smaller. Thus, depending on whether the path is limited by the thickness t or by the width w of the sample the factor P is given by c/L_1 or c/L_2 where c is a proportionality constant. The angle Φ is the angle between the direction of slip and the trace of the plane of slip on that surface of the sample which is perpendicular to the thickness t, while δ is the angle between that trace and the direction of tension. In our case the samples were quite thin ($w=10t$) and so in all cases the limiting factor was due to the thickness of the sample. Thus

$$S'=(PF/A)\cos\theta\cos\lambda=(cF/L_1A)\cos\theta\cos\lambda$$

$$=\frac{c}{t}\frac{F}{A}\frac{\cos^2\theta\cos\lambda\sin\Phi}{\sin\delta} \qquad (3)$$

and the corresponding relative values were computed assuming $cF=tA$. The values obtained from formulae (1) and (3) are given in Table I, for several crystals together with the actually observed first and second slip systems. For these and all other samples, observations agree with the new formula (3) and not with formula (1) except in one case (crystal #8) where both formulas gave the same result. It is important to note that in general the two formulas indicate not only different directions of slip but also different planes of slip. If the average distance between the obstacles in the metal is much smaller than the dimensions of the sample and the sample itself is approximately square or round in cross section then the usual formula (1) is applicable. It should be noted that a similar preference for slip in the direction of shortest path was observed by Smekal[5] in his experiments on the tensile deformation of rock-salt crystals at room temperature.

Whenever the rotation of the crystal during the operation of the first slip system is small, the relative values of S' do not change much and then, as expected, the second slip occurs in a slip system which has the next highest S' in a new plane. An interesting case was Sample No. 10 for which two slip-systems had almost identical values of S' while the corresponding values of S differed by 30 percent: the first slip occurred on both systems at once (so-called duplex slip) in agreement with formula (3). It is interesting to note that this crystal was extremely ductile. A measurement of the actual shear stresses is planned.

Slip systems in crystals in relation to the orientation of the tensile direction are conveniently described by means of a diagram used by Schmid and Boas.[6] In our case, however, the slip system depends also on the dimensions of the sample and on the orientation of the various surfaces. For that reason no similar general diagram can be constructed. It should be noted, however, that the second slip system was always a conjugate[7] of the primary slip system.

[5] A. Smekal, Zeits. f. Physik **93**, 166 (1934).
[6] Reference 4, p. 93.
[7] "Conjugate" in the sense used by Professor C. H. Mathewson (see, for instance, Maddin, Mathewson, and Hibbard, Jr., J. Metals, **1**, 527 (1949)), to whom the authors wish to express their appreciation for stimulating discussion concerning the results here reported.

Letters to the Editor

PUBLICATION of brief reports of important discoveries in physics may be secured by addressing them to this department. The closing date for this department is five weeks prior to the date of issue. No proof will be sent to the authors. The Board of Editors does not hold itself responsible for the opinions expressed by the correspondents. Communications should not exceed 600 words in length.

Angular Dependence of Crystalline Nuclear Resonance Absorption

E. F. CARR AND C. KIKUCHI
Department of Physics and Astronomy, Michigan State College, East Lansing, Michigan
April 3, 1950

IN a series of brief notes, Pound[1] has reported his observations on the absorption spectrum of Al^{27} and Li^{7} nuclei in crystals. His experiments prompted us to investigate the radiofrequency absorption for nuclei of spin I and of electric quadrupole moment Q, as a function of the orientation of the steady magnetic field with respect to the crystalline electric field. In particular, we have investigated the consequences of assuming that the nuclei are subject to the interactions of the nuclear magnetic moment with the external magnetic field and of the quadrupole moment with the static crystalline electric field of tetragonal symmetry.

Let θ represent the angle which the steady magnetic field makes with the tetragonal axis (z axis), and for convenience choose the x axis so that it lies in the plane determined by the tetragonal axis and the external field vector, H_0. It follows then from group-theoretical considerations, that the wave functions which diagonalize the magnetic energy, are given by[2]

$$\Psi_m=(a\xi+b\eta)^{I+m}(-b\xi+a\eta)^{I-m}/((I+m)!(I-m)!)^{\frac{1}{2}}$$

where $a=\cos\theta/2$, $b=\sin\theta/2$, and ξ and η determine the nuclear spin functions χ_m, given by

$$\chi_m=\xi^{I+m}\eta^{I-m}/((I+m)!(I-m)!)^{\frac{1}{2}}$$

whose axis of quantization coincides with the tetragonal axis. The advantage of the above representation of the spin functions lies in the fact that the matrix elements are easily evaluated.

The quadrupole energy operator is known to be[3] $DQ(3I_z^2-I^2)$, where $D=(\partial^2V/\partial Z^2)[e/4I(2I-1)]$. Therefore, to carry out the perturbation calculation, the matrix elements

$$(m|I_z^2|m)=\tfrac{1}{2}m^2(3\cos^2\theta-1)+\tfrac{1}{2}I(I+1)\sin^2\theta,$$

$$(m\pm1|I_z^2|m)=\mp\tfrac{1}{2}\sin\theta\cos\theta(\pm2m+1)((I\mp m)(I\pm m+1))^{\frac{1}{2}}$$

and

$$(m\pm2|I_z^2|m)=\tfrac{1}{4}\sin^2\theta((I\mp m)(I\pm m-1)(I\pm m+1)(I\pm m+2))^{\frac{1}{2}}$$

are needed, The first-order perturbation calculation then gives

$$E_m=-m\mu_N g_N H_0+DQ[\tfrac{1}{2}m^2(3\cos^2\theta-1)+\tfrac{3}{4}I(I+1)\sin^2\theta-I(I+1)].$$

Since the allowed transitions in a perpendicular radiofrequency field are those for which $\Delta m=\pm1$, the absorption spectrum consists of the components

$$h\nu(m\rightarrow m\pm1)=\pm g_N\mu_N H_0\mp3mDQ(3\cos^2\theta-1)-\tfrac{3}{2}DQ(3\cos^2\theta-1)$$

with the intensities proportional to $(I(I+1)-m(m\pm1))$. The upper sign is to be taken for positive g_N and the lower sign for negative g_N. It is readily seen that the absorption spectrum consists of $2I$ components all equally spaced, having separations between adjacent components given by $3DQ(3\cos^2\theta-1)$. Furthermore, the component separations $\Delta\nu_{\parallel}$ and $\Delta\nu_{\perp}$ for the steady field parallel and perpendicular respectively to the tetragonal axis are in the ratio of 2 to 1, and the spectrum coalesces into a single line when the external magnetic field is inclined at $\theta=\cos^{-1}(3)^{-\frac{1}{2}}$ with respect to the tetragonal axis. The term values to the second approximation can also be readily calculated by means of the off-diagonal matrix elements given above. According to Pound, it appears that second or even higher approximations are necessary in calculating the Al^{27} spectrum.

We are also investigating the angular dependence of the hyperfine structure of the paramagnetic absorption spectrum reported by Penrose *et al.*[4]

[1] R. V. Pound, Phys. Rev. **73**, 1247 (1948); **76**, 1410 (1949); Proc. Phys. Soc. London **61**, 576 (1948).
[2] E. Wigner, *Gruppentheorie* (Edwards Brothers, Inc., Ann Arbor, Michigan), p. 175.
[3] C. Kikuchi, Phys. Rev. **77**, 746(A) (1950).
[4] Penrose, Abragam, and Pryce, Nature **163**, 992 (1949); for further references, see C. Kikuchi and R. D. Spence, Am. J. Phys. **18**, 167 (1950).

The Schmidt Model and Odd-Even Staggering of the Isotopic Shift

G. BREIT
Yale University, New Haven, Connecticut*
April 4, 1950

CENTROIDS of the hyperfine structure patterns of isotopes with odd A and even Z usually fall between the lines of isotopes with even N and closer to those of the lighter even isotope. This phenomenon is referred to as the odd-even staggering. An explanation of it has been proposed[1] in terms of nuclear polarization. This explanation involves assumptions about nuclear wave functions and leaves room for the consideration of other effects, with which it might combine.

Schmidt's model[2] appears to have a bearing on the phenomenon. Schmidt accounts for features of nuclear magnetic moments on the single nucleon+core picture. The nucleon is supposed to have the same spin magnetic moment as in its free condition. The orbital magnetic moment of the proton is used as though the proton were free.

If the success[3] of Schmidt's model is not accidental then the unpaired nucleon must be mostly outside the core. Nuclear reactions suggest strong and intimate binding of nucleons with nuclear matter and the formation of compound states. While the nucleon is in the core it would be expected to affect the state of the nuclear matter as a whole and the effective value of the nucleon's charge and magnetic moment can be expected to be affected by correlated motions of the nuclear matter.

When two neutrons are added to a nucleus with even Z the spin and magnetic moment are often practically unchanged. On Schmidt's model this situation is easily explained provided the neutron pair is supposed to form part of the core. An odd neutron, however, has to be pictured as mostly outside. The addition of a neutron pair to the interior will result in an expansion of the positive charge distribution. The odd neutron, remaining mostly outside the positive charge, would cause only secondary expansion effects accounting for odd-even staggering. Such a view is not at variance with general features of shell structure of nuclei.[4]

Considerations related to the virial theorem appear at first sight to indicate an abnormally large nuclear volume for the odd isotopes. But the current hypothesis[5] of strong spin-orbit coupling makes such reasoning inapplicable. The weaker binding of odd neutron need not be connected with an anomalous expansion of the nucleus, therefore.

* Assisted by the joint program of the ONR and AEC.
[1] Breit, Arfken, and Clendenin, Phys. Rev. **77**, 569 (1950). A longer paper on the same subject by the same authors is in press.
[2] T. Schmidt, Zeits. f. Physik **106**, 358 (1937); H. Schueler, Zeits. f. Physik **107**, 12 (1937); F. Hund, Physik. Zeits. **38**, 929 (1937).
[3] Aage Bohr and V. F. Weisskopf, Phys. Rev. **77**, 94 (1950).
[4] W. Elsasser, J. de phys. et rad. **5**, 625 (1934); A. Berthelot, J. de phys. et rad. **3**, 17, 52 (1942); Maria Goeppert Mayer, Phys. Rev. **74**, 235 (1948); **75**, 1969 (1949); Eugene Feenberg and Kenyon C. Hammack, Phys. Rev. **75**, 1877, 1968 (1949); L. W. Nordheim, Phys. Rev. **75**, 1894 (1949).
[5] Papers by M. G. Mayer in preceding footnote.

On the Magnetic Moments of Xe^{129}, Bi^{209}, Sc^{45}, Sb^{121}, and Sb^{123}*

W. G. PROCTOR AND F. C. YU
Department of Physics, Stanford University, Stanford, California
March 30, 1950

THE nuclear magnetic resonances of Xe^{129}, Bi^{209}, Sc^{45}, Sb^{121}, and Sb^{123} have been observed by use of the nuclear induction spectrometer described earlier.[1] The magnetic moments listed in column two of Table I have been computed directly from our measured frequency ratios and the value of the magnetic moment of the nucleus used as a standard. Diamagnetic corrections were not applied; they are listed separately in column three, and have been determined by linear interpolation from the values for specific atoms given by Lamb, using Hartree fields.[2] These corrections are to be applied in a direction such as to increase the magnitude of the listed magnetic moments.

As a monatomic gas, Xe presented certain difficulty with regard to a suitable mechanism for establishing thermal equilibrium. An admixture of O_2 could be used as paramagnetic catalyst,[3,4] but it would require rather excessive pressures to obtain the full signal magnitude. Instead, we followed a suggestion by Professor Bloch, filling a test tube packed with powdered Fe_2O_3 to a pressure of about 12 atmos. of xenon for a sample. The kinetic motion of the Xe atoms about the paramagnetic Fe_2O_3 particles successfully shortened the longitudinal relaxation time by providing time-varying magnetic fields at the Xe nuclei. Samples made without paramagnetic powders present, and samples using $CuCl_2$ or $K_3Fe(CN)_6$, gave no signals. The resonance was located near 7.7 Mc, using a magnetic field of 6600 gauss. Comparing this frequency with that from Na^{23}, we found

$$\nu(Xe^{129})/\nu(Na^{23})=1.0456\pm0.0001$$

leading to the magnetic moment listed in Table I. This is in good agreement with the spectroscopic[5] value, $\mu(Xe^{129})=-0.9\mu_N$. The negative sign has been confirmed.

Using an aqueous solution of 0.69M $Bi(NO_3)_3$, the resonance of Bi^{209} was found in the neighborhood of 7.0 Mc, with a magnetic field near 10,000 gauss. Comparing the resonance frequency with that from D^2, we found

$$\nu(Bi^{209})/\nu(D^2)=1.0468\pm0.0001.$$

The magnetic moment was found to be positive and it is in good agreement with the h.f.s. value[6] of $3.45\mu_N$.

The Sc^{45} resonance was observed with a magnetic field of 7400 gauss, near 7.6 Mc, using a sample of Sc_2O_3 in HNO_3. We found

$$\nu(Sc^{45})/\nu(Na^{23})=0.9183\pm0.0001$$

which leads to a value in excellent agreement with the h.f.s.[7] value $\mu(Sc^{45})=4.8\mu_N$. The positive sign was verified.

The antimony resonances were observed using a sample of $NaSbF_6$ in weak HF. The absorption lines of both the Sb^{121} and the Sb^{123} resonances manifested a structure inasmuch as they were each composed of five lines, approximately 2 gauss apart. The structure can be understood qualitatively, and will be reported upon in detail elsewhere. It appears most likely that it is due to the additional field, acting on the Sb nucleus, which originates from the magnetic moments of the six surrounding fluorine nuclei in the $(SbF_6)^-$ ion; the analysis shows that the central line suffers no displacement from this cause. Measurements then gave

$$\nu(Sb^{121})/\nu(Na^{23})=0.9048\pm0.0001,$$

$$\nu(Sb^{123})/\nu(D^2)=0.8442\pm0.0001.$$

These frequency ratios lead to values of the magnetic moments which are in good agreement with the spectroscopic values $\mu(Sb^{121})=3.7\mu_N$, $\mu(Sb^{123})=2.8\mu_N$, and their ratio,[8] $\mu(Sb^{121})/\mu(Sb^{123})=1.32$.

No attempt was made to check spin values for the above nuclei, and the spectroscopically determined values have been used in computing the magnetic moments listed[9] in Table I. In view of the observed dependence of nuclear magnetic resonance frequencies on chemical compound,[10,11] we wish to emphasize that the moments listed in Table I are without corrections of any kind. At the time of this writing none of the nuclei reported upon here has been observed in compounds other than those given.

TABLE I. Magnetic moments and diamagnetic corrections.

Nucleus	Nuclear moment in nuclear magnetons	Diamagnetic correction in percent
Xe^{129}	-0.7726 ± 0.0001	0.56
Bi^{209}	$+4.0400\pm0.0005$	1.04
Sc^{45}	$+4.7497\pm0.0008$	0.15
Sb^{121}	$+3.3427\pm0.0005$	0.52
Sb^{123}	$+2.5341\pm0.0003$	0.52

The magnetic moment of Na^{23} has been computed by taking

$$\mu(H^1)=(2.7935\pm0.0003)\mu_N;^{12}$$

and

$$\nu(Na^{23})/\nu(H^1)=0.26450\pm0.00003;^{13}$$

the magnetic moment of D^2 was similarly computed using $\mu(D^2)/\mu(H^1)=0.307013$.[14]

We should like to express here our gratitude to Professor F. Bloch for many helpful consultations during the course of this work.

* Assisted by the joint program of the AEC and ONR.
[1] W. G. Proctor, Phys. Rev. 75, 522 (1949).
[2] W. E. Lamb, Jr., Phys. Rev. 60, 817 (1941).
[3] F. Bloch, Phys. Rev. 70, 460 (1946).
[4] H. L. Anderson, Phys. Rev. 76, 1460 (1949).
[5] H. Kopfermann and E. Rindal, Zeits. f. Physik 87, 460 (1934).
[6] H. Wittke, Zeits. f. Physik 116, 547 (1940).
[7] H. Kopfermann and H. Wittke, Zeits. f. Physik 105, 16 (1937).
[8] M. F. Crawford and S. Bateson, Can. J. Research 10, 693 (1934).
[9] See "Properties of Atomic Nuclei," Publication BNL 26 (T-10), Brookhaven National Laboratory, Upton, New York (October 1, 1949).
[10] W. G. Proctor and F. C. Yu, Phys. Rev. 77, 717 (1950).
[11] W. C. Dickinson, Phys. Rev. 77, 736 (1950).
[12] H. Taub and P. Kusch, Phys. Rev. 75, 1481 (1949).
[13] F. Bitter, Phys. Rev. 75, 1326 (1949).
[14] This figure is that given by Bloch, Levinthal, and Packard, Phys. Rev. 72, 1125 (1947), rounded to six places.

Magnetic Suspension Balance*

J. W. BEAMS
University of Virginia, Charlottesville, Virginia
March 31, 1950

MAGNETIC suspension balances, in which the material to be weighed is freely suspended, have been designed and operated successfully by Holmes[1] and by Clark,[2] but these balances lacked the sensitivity and stability necessary for some types of measurement. In a recent paper[3] a magnetic suspension for high speed rotors was described which also proved to be an excellent magnetic suspension balance. This magnetic balance has now been modified and improved to a point where its sensitivity is limited only by the natural fluctuations or "Brownian motion" of the system.

The material to be weighed is attached to a cylindrical ferromagnetic body (iron, steel, or Permalloy) which is supported freely by the vertical axial magnetic field of a solenoid. The ferromagnetic body is positioned in the edge of a horizontal light beam so that it scatters or reflects light into a photo-electron multiplier cell. The signal from the cell actuates an electronic circuit which in turn regulates the current in the solenoid in such a way as to maintain the suspended ferromagnetic body at the desired height. By proper adjustment of the circuits and of the vertical gradient of the light intensity, where the suspended body is positioned in the light beam, the apparatus can be made very sensitive to slight changes in vertical force on the suspended body. If the dimensions of the suspended ferromagnetic cylinder are small in comparison to its distance below the solenoid, the upward force F on the rotor is approximately MdH/dX where H is the magnetic field, X is a

distance along the axis of the field, and M is the magnetic moment induced in the ferromagnetic cyclinder by the field H. If M is roughly proportional to μH, where μ is the permeability of the cylinder, then $F \propto \mu H dH/dX$. Consequently, it is possible to adjust H and dH/dX so that F varies very slowly with height. This has been done by proper shaping of the field of the solenoid and by supporting the ferromagnetic cylinder well below the solenoid. Also in some experiments an additional solenoid with a constant current was used to support a portion of the weight of the suspended body.

When the apparatus is properly adjusted, the suspended body shows no motion, as viewed through a microscope focused on scratches on the suspended cylinder except when a vertical force is applied to the suspended cylinder. Consequently, the elevation of the suspended cylinder in the field of view of the microscope is a measure of the applied force. However, it is preferable in practice to measure the change in the current or voltage in the circuit as a function of the vertical force on the suspended cylinder. With a suspended steel cylinder 10 mils in diameter and 50 mils long, changes in force on the cylinder of the order of 10^{-9} gram weight could be observed. The balance was calibrated by suspending the cylinder in a glass chamber which could be evacuated and then determining the change in buoyancy of the air on the suspended body when the air pressure around the body was varied.

The above magnetic suspension balance may be used in almost any experiment where small changes in mass or force are to be determined. It is especially suited to experiments where the weighing must be carried out in an evacuated or enclosed chamber, under a transparent liquid, etc., where no mechanical connections to the outside are possible. Also the same apparatus may be used to support and weigh over a wide range of masses or forces.

* This work was supported by Navy Bureau of Ordnance Contract NOrd-7873.

[1] F. T. Holmes, Rev. Sci. Inst. 8, 444 (1937).
[2] J. W. Clark, Rev. Sci. Inst. 18, 915 (1948).
[3] J. W. Beams, Rev. Sci. Inst. 21, 182 (1950), Wash. Acad. Sci. 37, 221 (1947).

Preparation of Transplutonium Isotopes by Neutron Irradiation

A. GHIORSO, R. A. JAMES,* L. O. MORGAN,† AND G. T. SEABORG
Radiation Laboratory and Department of Chemistry, University of California, Berkeley, California
March 27, 1950

THE first production of isotopes of the transplutonium elements americium (atomic number 95) and curium (atomic number 96) was reported[1] by the present authors in a preliminary way in 1945 and more recently[2] in a more complete fashion. In these communications it was pointed out that a number of americium isotopes can be formed in cyclotron bombardments with various charged particles, and in particular that the ~500-yr. Am^{241} can be produced with approximately 40-Mev helium ions according to the reactions $U^{238}(\alpha,n)Pu^{241} \xrightarrow{\beta^-\ (10\ \text{yr.})} Am^{241}$. It was also reported that a number of curium isotopes can be formed by cyclotron bombardments with charged particles and in particular that the ~150-day Cm^{242} can be prepared by the 40-Mev helium ion bombardment of Pu^{239} according to the reaction $Pu^{239}(\alpha,n)Cm^{242}$. In addition it was stated that Cm^{242} can be formed by neutron irradiation of Am^{241} according to the reactions $Am^{241}(n,\gamma)Am^{242} \xrightarrow{\beta^-} Cm^{242}$ where Am^{242} exists in two isomeric states with half-lives for beta-emission given as 17 hr. and some 10^2 to 10^3 yr.

The purpose of the present note is to point out that the isotope Am^{241} can also be formed by neutron irradiation, according to the following reactions $Pu^{239}(n,\gamma)Pu^{240}(n,\gamma)Pu^{241} \xrightarrow{\beta^-\ (10\ \text{yr.})} Am^{241}$. This method of production was first observed by the authors late in 1944, and the use of the chain reacting piles as a source of neutrons makes it the best for the production of weighable amounts of Am^{241}. (The first evidence for the reaction $Pu^{239}(n,\gamma)Pu^{240}$ was that of Chamberlain, Farwell, and Segrè.[3]) In fact, the intense irradiation of large quantities of plutonium leads to the production of *milligram amounts* of Am^{241}. The cross section of Am^{241} for the n,γ-reaction is such that it is possible with long irradiations at high neutron fluxes to transmute a substantial fraction of it to Cm^{242}.

The fact that the elements americium and curium, as represented by their isotopes Am^{241} and Cm^{242}, can be prepared in substantial quantity in this manner by pile neutron irradiations makes it possible to investigate rather completely the chemical properties of these elements by use of weighable amounts. The existence of these reactions makes it quite likely that even higher mass isotopes can be prepared by n,γ-reactions, and in fact further work at this laboratory, to be published soon, indicates that this is indeed the case.

This work was performed at the wartime Metallurgical Laboratory, University of Chicago, Chicago, Illinois (now the Argonne National Laboratory) under the auspices of the Manhattan District, and at the Radiation Laboratory and Department of Chemistry, University of California, Berkeley, under the auspices of the Manhattan District and the AEC.

* Now at the Department of Chemistry, University of California at Los Angeles.
† Now at the Department of Chemistry, University of Texas, Austin, Texas.

[1] G. T. Seaborg, Chem. Eng. News 23, 2190 (1945).
[2] Seaborg, James, and Morgan, National Nuclear Energy Series, Plutonium Project Record, Vol. 14B, *The Transuranium Elements: Research Papers* (McGraw-Hill Book Company, Inc., New York, 1949), Paper No. 22.1 "The new element americium (atomic number 95)": Seaborg, James, and Ghiorso, Paper No. 22.2 "The new element curium (atomic number 96)."
[3] Chamberlain, Farwell, and Segrè (private communication, September, 1944).

The Elastic and Photoelastic Constants of Fused Quartz

K. VEDAM
Department of Physics, Indian Institute of Science, Bangalore, India
March 27, 1950

EVEN though numerous investigations have been carried out on the various physical properties of fused quartz, the only known work on its photoelastic properties is that of Heymans and Williams,[1] who have determined the value of $(p-q)$ from bending experiments on a bar of fused silica, p and q being Neumann's strain-optical constants. In the present investigation the absolute values of p and q have been determined, and the results obtained are given below. The details of the method adopted will be published elsewhere.[2] The specimen studied was obtained from the Thermal Syndicate Ltd., England, and was in the form of a rectangular block of dimensions $2.7 \times 1.6 \times 0.85$ cm.

The elastic constants of fused quartz were determined by Hiedemann's method;[3] i.e., by observing the diffraction patterns produced by standing ultrasonic waves in the medium itself. Mueller[4] has shown that this method, with slight modifications, can be used to determine the value of p/q for isotropic substances. Using incident light polarized at 45° to the sound wave front, the light diffracted by the longitudinal waves is viewed through an analyzer. Then the analyzer is rotated through an angle θ, from the initial crossed position, to get the extinction of the first-order longitudinal pattern. By plotting the angle θ against the sound amplitude and extrapolating, it is possible to obtain "θ_{max}" corresponding to zero amplitude, which is given by the relation [Eq. (25) of reference 4]

$$\tan(\theta_{max}+45°) = p/q.$$

By this method the value of p/q for fused quartz was determined by the author and was found to be 2.85.

The value of $(p-q)$ was also determined by the well-known compression method[5] using a lever arrangement and a Fuess-Babinet compensator. The value of $(p-q)$ obtained by the author is equal to 0.135. This is about 50 percent too large, as compared with the value obtained by Heymans and Williams. However, repeated measurements have yielded consistently the same result within the limits of experimental error. As the original paper of Heymans and Williams dealing with this measurement was not available to the author, it is not possible to explain this discrepancy between the results. It is possible that the discrepancy may be due to the different natures of the specimens used.

The values of the Pockels' elasto-optic and piezo-optic constants of fused quartz calculated from the measured values of p/q, $(p-q)$, and the elastic constants are listed in Table I. All of the measurements were carried out using λ5893A.

TABLE I. Constants of fused quartz.

Density = 2.213 g/cc, $n_D = 1.4585$		
Young's modulus = 7.445×10^{11} dynes/cm²		
Modulus of rigidity = 3.195×10^{11} dynes/cm²		
$p = 0.208$	$p_{11} = 0.100$	$q_{11} = 0.078 \times 10^{-13}$
$q = 0.073$	$p_{12} = 0.285$	$q_{12} = 2.98 \times 10^{-13}$

(a pressure of 1 dyne/cm² is taken as the unit of stress)

It is seen on comparison with the corresponding values for the various silicate glasses,[2] that the values of p/q and $(p-q)$ are maximum for the vitreous silica. The addition of metallic oxides has the effect of reducing the value of $(p-q)$ and thus the birefringence produced by any fixed stress.

In conclusion the author wishes to express his indebtedness to Professor R. S. Krishnan for his kind interest and guidance during the progress of the above work.

[1] Heymans and Williams, J. Math. Phys. Mass. Inst. Tech. 2, 216 (1923).
[2] Vedam, Proc. Ind. Acad. Sci. (to be published).
[3] Heidemann, Naturwiss. 24, 60 (1936).
[4] Mueller, Zeits. f. Krist. (A) 99, 122 (1938).
[5] Pockels, Ann. d. Physik (4) 7, 745 (1902).

A Square-Wave Modulation Method for Microwave Spectra

T. R. HARTZ AND A. VAN DER ZIEL
University of British Columbia, Vancouver, Canada
March 31, 1950

THE double modulation method employed in microwave spectroscopy by Gordy and Kessler,[1] Watts and Williams[2] and others, usually consists in applying a radiofrequency modulation voltage to the reflector of a klystron in addition to the low frequency saw-tooth voltage. The modulated microwave output power is allowed to pass through a wave guide section containing the absorbing gas and is then fed to a receiver tuned at the frequency used for modulation. We have replaced the radiofrequency sine wave with a 50 kc square wave voltage, applied this along with the low frequency saw-tooth voltage to the klystron repeller, and proceeded as usual. The square-wave voltages used are of the order of 10 volts, but higher values may be used quite satisfactorily.

Several disdvantages of the old system of double modulation are apparent. The absorption line observed on the cathode-ray oscilloscope has a differentiated line shape, making for a possible error in the location of the center of the line. Perhaps more serious is the fact that there is considerable distortion in the observed pattern for large modulation voltages, such as would be required for increased sensitivity. Our method of detection gives immediately the true line shape when viewed on the oscilloscope. Due to the large square-wave signal there is also better sensitivity with very little distortion. However, each absorption line appears double; that is, a signal is obtained when the tops of the square-wave sweep over an absorption and another when the bottoms sweep over the same line. These appear on the screen as two lines, separated by an amount depending on the magnitude of the square-wave voltage. The use of lock-in detection inverts one of these lines with respect to the other, so that there is never any possibility of confusion.

We subsequently introduced a feature which removes one of these lines entirely. Instead of applying the square-wave and the saw-tooth modulations separately to the klystron repeller, the square-wave modulation is applied with a saw-tooth envelope. In this way only one absorption line is obtained from our detector since the bottoms of the square-wave remain fixed at the same level and hence contribute no signal.

This work was made possible by a grant from the Defence Research Board of Canada and by the award of a studentship from the National Research Council to one of us (T.R.H.).

[1] W. Gordy and M. Kessler, Phys. Rev. 72, 644 (1947).
[2] R. J. Watt and D. Williams, Phys. Rev. 72, 1122 (1947).

Stars and Showers at Balloon Altitudes*

A. M. THORNDIKE AND A. W. WOTRING
Brookhaven National Laboratory, Upton, Long Island, New York
February 27, 1950

EVENTS have been observed in a cloud chamber flown to approximately 95,000 ft. from Camp Ripley, Minnesota (magnetic latitude 55°N).[1] It contained four plates; the top plate was 3.5 g/cm² of carbon, followed by 7.2 g/cm² of lead, 14.4 g/cm² of lead, and 14.4 g/cm² of lead.[2] About 1 g/cm² of material of low atomic weight was present above the cloud chamber in addition to about 14 g/cm² of the atmosphere.

The term "star" will be used to denote an event in which two or more heavily ionizing tracks appear to diverge from a common point, while "shower" will be used to denote one in which three or more lightly ionizing tracks do so. Tracks estimated to have a density of ionization one to three times minimum are classed as "light," those of four times minimum or more as "heavy." At high altitudes events with both light and heavy tracks are common. The term "shower-star" will be used when both two or more heavy tracks and three or more light tracks are present.

Events observed in 313 random expansions at altitude are given in Table I. Of a total of 66 events nine are shower-stars with three

TABLE I. Frequency of multiple events with various numbers of light and heavy tracks.

Number of heavy tracks	0	1	2	3–4	5–6
Number of light tracks			(Stars)		
0–2	—	—	4	6	2
	(Showers)			(Shower-Stars)	
3–4	18	1	3	3	1
5–9	15	6	0	1	1
10–19	3	0	0	0	0
20–30	2	0	0	0	0

or more lightly ionizing particles. In eight of the nine shower-stars the lightly ionizing particles are fairly well collimated in a downward direction. Our results are consistent with the assumption[3] that the majority of lightly ionizing tracks from shower-stars are mesons. Of a total of 38 lightly ionizing prongs from shower-stars there are 11 which apparently stop in the next plate, 10 that penetrate without visible secondaries, one which appears to produce a small shower, and 16 whose behavior is uncertain, mainly because of leaving the illuminated region. Protons would have greater penetration and electrons greater multiplication than is observed. If the particles are mainly mesons, the results are understandable, since a meson ionizing one to three times minimum has a minimum range of 2 g/cm² of lead and some could well stop in the plates. Kaplon, Peters, and Bradt have interpreted multi-

plication in a very large shower-star as evidence for photons from the decay of neutral mesons whose number was comparable with the number of charged mesons.[3] Our shower-stars do not show such striking multiplication, perhaps because the energies involved are lower. Some of the shower particles from stars may be electrons produced in the plates by photons from neutral mesons

In Table I 45 showers are listed which do not have two or more heavy tracks. Some of these are probably immediate products of nuclear explosions which have only one or no slow fragments emerging from the plate, but since some show the typical form of small electron cascades it is unlikely that all are formed in this way. We estimate that about 16 of these showers originate at the point of a nuclear explosion and about 29 do not. If these showers were caused by a primary electronic component, which was even 10 percent as numerous as the proton component,[4] the number of energetic showers observed in our cloud chamber would be approximately equal to the number of nuclear explosions caused by protons. There are actually about 25 of the latter (including "showers" which we estimated to have unobserved heavy tracks concealed in the plates) and one or two energetic electron showers. We conclude that primary electrons are rare, or non-existent, as is generally considered to be the case, and that the small showers observed must arise in some way from the nuclear interactions of the primary protons. One expansion showed two small showers coming from the second plate which project back to a common point in the first (carbon) plate, the angle between them being 40°, a type of event which suggests the neutral meson hypothesis.

* Work performed at Brookhaven National Laboratory under the auspices of the AEC.

[1] Flights were made by General Mills, Inc., Project Skyhook, sponsored by the ONR.

[2] The cloud chamber has been described by Shutt, Johnson, and Thorndike, Rev. Sci. Inst. 20, 398 (1949).

[3] Camerini, Coor, Davies, Fowler, Lock, Muirhead, and Tobin, Phil. Mag. 40, 1073 (1949). Kaplon, Peters, and Bradt, Phys. Rev. 76, 1735 (1949). P. Freier and E. P. Ney, Phys. Rev. 77, 337 (1950).

[4] Janossy, Rossi, and Hulsizer, Nature 163, 246 (1949).

Erratum: X-Ray and Gamma-Ray Reflection Properties from 500 X Units to Nine X Units of Unstressed and of Bent Quartz Plates

[Phys. Rev. 77, 475 (1950)]

D. A. LIND, W. J. WEST, AND J. W. M. DUMOND
California Institute of Technology, Pasadena, California

ON p. 482, column 1 of the text the statement is made that $t=w_1=w_4$. This should read: $t=w_1=w_2$. The text material is otherwise correct.

Equation (18), p. 485, is not complete as it stands. It should read:

$$\exp[\mu_0 l_0/\gamma_0]R'=r_0 d_H(|F_H|/V)\lambda/2\cos\theta_B \cdot\left[\frac{1+\cos^2 2\theta_B+2l_0^2(1+\cos^4 2\theta_B)}{1+\cos 2\theta_B+l_0^2(1+\cos^2 2\theta_B)}\right]. \quad (18)$$

On p. 485, bottom of column 1, the words *electron vector* should read *electric vector*.

In Fig. 3, the boxes represent the *maximum* spread in the experimental data, and not the probable errors as stated in the text.

The Thermal Rayleigh Disk in Liquid He II*

JOHN R. PELLAM
National Bureau of Standards, Washington, D. C.
AND
PHILIP M. MORSE
Massachusetts Institute of Technology, Cambridge, Massachusetts

March 30, 1950

DURING early discussions regarding the validity of formulas for radiation pressure[1] and associated properties of second sound, it became apparent that a Rayleigh disk[2] experiment might constitute an additional crucial test of the two-fluid hypothesis[3-5] for liquid He II. Measurements of this nature are being conducted at the Cryogenics Laboratory of the National Bureau of Standards and the positive effects observed thus far have been in full conformity with the currrent concepts[3,4] of the second sound mechanism. In addition to allowing a more detailed examination of the quantum hydrodynamics of liquid He II, the Rayleigh disk method provides an absolute measure of second sound intensity, dependent only upon such fundamentals as the kinetic energy and the geometry.

The singular feature of second sound in liquid He II is of course the basically thermal nature of the propagation. Ordinary acoustical sources cannot generate second sound waves, nor can ordinary microphones detect them; thermal methods are customarily employed instead.[6] This situation may be rationalized on the basis of the current two-fluid hypothesis for He II. Whereas the oppositely directed momenta (and particle velocities) of the component fluids logically constitute zero net momentum,[4,5] the internal mass transport establishes a net heat flow with an associated temperature fluctuation.

Although detectors of the microphone class (either pressure or velocity type) cannot recognize this process, the mechanical device known as the Rayleigh disk can and does resolve the existent internal convection. This disk can detect second sound as well as ordinary (sound) because it responds to particle velocity squared, rather than to mere particle velocity. The disk accordingly recognizes the existence of a kinetic energy density within the second sound as pictured on the two-fluid basis.

A thin circular mirror (½-in. diam.) has been suspended vertically within the second sound field by a thin torsion wire. The mirror orientation was adjusted for equilibrium conditions (in the absence of second sound) to make a 45° angle with the axis of wave propagation. The second sound field was then set up within a horizontally oriented cavity, and the mirror deflections observed for conditions of resonance. The sharp response of the mirror disk (and deflection of a reflected light beam) as the system was tuned through resonance verifies the internal mass flow and its associated kinetic energy density.

The wave velocity determined in this manner from critical resonance frequencies (half-wave-length fixed) is in essential agreement as a function of temperature with the results of earlier purely thermal methods.[6,7] Measurements can be extended quite close to the λ-point where velocities of less than 1 m/sec. have been observed.

The maximum torque set up at resonance can be measured directly, knowing the torsion constant of the system (from the observed period of free oscillation). Since, furthermore, the resonance response is regular and symmetrical, band width determinations are practicable. The associated reinforcement factor Q combined with the known periodic heating rate (introduced uniformly over one end-wall of the cavity) leads to an estimate of the actual heat flow density at the location of the disk.

By comparison of the observed dependence of the torque on the temperature with theoretical predictions based on modifications of the classical Rayleigh formula,[2] the individual roles of normal fluid and superfluid in deflecting the disk can be examined. Space does not permit giving expressions for the separate torques, but should *both* fluids contribute it can be shown that the resultant torque τ would be

$$\tau=(4/3)a^3\rho(\rho_n/\rho_s)[\dot{H}^2/(\rho ST)^2]. \quad (1)$$

Here a is the radius of the disk. The properties of liquid He II enter through the entropy S and total density ρ; also ρ_n is the density of the normal fluid, ρ_s that of the superfluid. T denotes the ambient absolute temperature and $\dot{H}$ the heat flow density. A similar expression holds for the contributions by each individual fluid component.

Thus far Eq. (1) has been checked only near the λ-point, but there the agreement seems complete. The significance of this verification however is that *superfluid is providing the predominant*

torque in this temperature region [since near the λ-point $\rho_s \ll \rho_n$, making the superfluid particle velocity (squared) relatively large]. Whether the normal fluid is contributing its share awaits extension of the measurements to the lower temperature range where the condition $\rho_n < \rho_s$ holds.

Otherwise stated, the results thus far substantiate a form of the Bernoulli equation now generalized to suit the quantum hydrodynamics of He II

$$\tfrac{1}{2}\rho(\rho_n/\rho_s)[\dot{H}^2/(\rho ST)^2]+\tfrac{1}{2}\rho V^2+\rho gh+p=\text{const.} \qquad (2)$$

Here the additional first term represents the contribution of pressure due to heat flow density $\dot{H}$. The derivation of (2) will be given more completely in a later discussion.

The technical assistance of Mr. W. Hanson of the National Bureau of Standards Cryogenics Laboratory has been invaluable in conducting this research and is gratefully acknowledged.

* Supported by the ONR, Contract Na-onr-12-48.

[1] J. Pellam, Phys. Rev. **76**, 872 (1949).
[2] Lord Rayleigh, *The Theory of Sound* (Dover Publications, New York, 1945), Vol. II, p. 44.
[3] F. London, Nature **141**, 643 (1938); Phys. Rev. **54**, 947 (1938).
[4] L. Tisza, J. de phys. et rad. **1**, 165, 350 (1940); Phys. Rev. **72**, 838 (1947).
[5] L. Landau, J. Phys. U.S.S.R. **5**, 71 (1941); also **8**, 1 (1944).
[6] V. Peshkov, J. Phys. **10**, 389 (1946); also **8**, 381 (1944).
[7] J. Pellam, Phys. Rev. **74**, 841 (1948); also **75**, 1183 (1949).

Extension of Alpha- and Beta-Decay Systematics of Protactinium Isotopes*

W. W. MEINKE† AND G. T. SEABORG
Radiation Laboratory and Department of Chemistry, University of California, Berkeley, California
March 31, 1950

AS part of our program for obtaining data to extend the scope of the systematics of alpha-radioactivity[1] and to obtain more data pertaining to the energy surface in the heavy region of elements, we have made some pertinent new measurements on protactinium isotopes.

The heaviest isotope of protactinium hitherto reported is that of mass 234 and hence it would be of interest to know the beta-emission properties of heavier isotopes in order to tie them in with the known radioactive data in this general region. Since low energy deuteron bombardment of U^{238} might be expected to lead to Pa^{235} and Pa^{236} by $(d,\alpha n)$ and (d,α) reactions and proton bombardment to Pa^{235} by the (p,α) reaction, these irradiations were made in the 60-in. cyclotron at energies of 19 and 9.5 Mev, respectively.

The protactinium was chemically separated following the bombardment of natural uranium by a procedure which involved a number of manganese dioxide cycles coupled with extractions of protactinium from aqueous into organic solvents. The manganese dioxide cycles consisted in precipitating this compound from the solution of uranium in nitric acid, followed by centrifugation, dissolution of the solid with hydroxylamine solution, dilution, and reprecipitation. The dissolved precipitate from the last cycle was acidified, salted with ammonium nitrate, and the protactinium extracted with diisopropyl ketone, several washings with salted solutions being made to insure good separation from fission products. The protactinium was then washed back into a low acidity aqueous solution and after acidification was extracted into a benzene solution of thenoyltrifluoroacetone which forms a complex ion with the protactinium. This solution was then evaporated to dryness on a platinum counting plate leaving a weightless deposit of protactinium.

The protactinium from the 19-Mev deuteron bombardment contained 23.7±0.5 min. and 27-day beta-particle emitters. The cross section for the formation of the former is about 2×10^{-27} cm² on the assumption that it is formed from U^{238} while that for the latter is about 4×10^{-27} cm² on the assumption that it is due to Pa^{233} produced in the reaction $U^{235}(d,\alpha)Pa^{233}$. Small amounts of two intermediate periods were present but these most probably can be attributed to a small amount of zirconium and niobium fission product contaminants. The 23.7-min. activity was also found in the protactinium fraction from the bombardment of U^{238} ($U^{238}/U^{235}=2300$) with 9.5-Mev protons in a yield corresponding to a cross section of about 3×10^{-29} cm². These observations are consistent with the assignment of the 23.7-min. activity to Pa^{235}, produced in the reactions $U^{238}(d,\alpha n)Pa^{235}$ and $U^{238}(p,\alpha)Pa^{235}$.

An aluminum absorption curve taken on this 23.7-min. activity shows that the beta-particles have a range of about 600 mg corresponding to an energy of about 1.4 Mev according to the Feather relationship.[2] Gamma-rays are either absent or are present in amounts too small to be detected by absorption experiments.

If one closes a decay cycle involving Pu^{239}, Np^{239}, Pa^{235}, and U^{235} using the values 0.7 Mev for the beta-disintegration energy[3] of Np^{239}, 5.24 Mev for the alpha-disintegration energy[3] of Pu^{239}, and 4.6 Mev for the estimated alpha-disintegration energy[1] of Np^{239}, a beta-disintegration energy of 1.34 Mev is obtained for Pa^{235}. This measurement, therefore, gives added weight to the somewhat uncertain measured beta- and estimated alpha-disintegration energies of Np^{239}, and hence adds to the reliability of the data needed for the construction of the energy surface in this region.

We also were interested in determining the partial half-life of Pa^{230} for alpha-disintegration. A half-life of some hundreds to thousands of years would be predicted from the alpha-systematics by obtaining the alpha-disintegration energy from mass number *versus* energy plots (5.5 Mev) and taking into account the prohibition introduced by the presence of two odd nucleons in determining its alpha-disintegration rate.[1] In this experiment the alpha-particles of the Pa^{230} were not measured directly but its half-life for alpha-disintegration was inferred by measuring the equilibrium amount of its alpha-disintegration product, the beta-particle emitting 29-hr. Ac^{226}, on the assumption that the predicted negligible branching decay of Ac^{226} by electron capture is correct. (The half-life of Ac^{226}, originally reported as 22 hr.,[3] has been more recently determined to be 29 hr.[4])

The actinium was chemically separated from a sample containing a large amount of Pa^{230} and the Ac^{226} was identified and the amount measured through an alpha-pulse analysis in which the alpha-particles of its daughters, 30-min. Th^{226} and daughters, were measured. In a bombardment of a thick thorium target with 60-Mev deuterons for 10μa-hr. in the 184-in. cyclotron a sample of Pa^{230} corresponding to 1.3×10^{6} negative beta-disintegrations/min. (as determined by alpha-pulse analysis of the daughter U^{230} decay chain) was chemically isolated as described above. The actinium was chemically separated from this protactinium fraction by carrying it on lanthanum and cerium fluorides which were redissolved and reprecipitated several times and further purified after dissolution by removing thorium through repeated zirconium phosphate precipitations. At the end of the procedure, the cerium (III) was oxidized to cerium (IV) with sodium bismuthate, the cerium (IV) removed on a zirconium phosphate precipitate, and the actinium activity precipitated with a small amount of lanthanum fluoride. After dissolution in hydrochloric acid, the soluble chloride of the carrier when evaporated on platinum gave a thin plate suitable for alpha-pulse analysis.

The actinium fraction from the protactinium containing 1.3×10^{6} beta-disintegrations/min. of Pa^{230} contained 300 alpha-disintegrations/min. of Th^{226} which decayed with the 29-hr. half-life of its beta-emitting Ac^{226} parent. Correcting for chemical yield (as determined by 10.0-day Ac^{225} tracer) and taking into account the fact that Pa^{230} has a half-life of 17 days[5] and also decays by electron capture in a ratio of 10 as compared to its decay by negative beta-particle emission,[6] these data lead to a partial half-life for alpha-emission of about 1400 yr.±20 percent. This corresponds, as in the case[1] of the analogous nucleus Pa^{228}, to a prohibition by a factor of about 100 in the alpha-decay, presumably due to the presence of two odd nucleons.

It is a pleasure to acknowledge the assistance of A. Ghiorso in a number of the measurements. We also wish to express our appre-

ciation to Dr. J. G. Hamilton, B. Rossi, T. M. Putnam, Jr., and the 60-in. cyclotron crew as well as J. Vale and the other members of the 184-in. cyclotron operating group for making the irradiations.

* This work was performed under the auspices of the AEC.
† Now at the University of Michigan, Ann Arbor, Michigan.
[1] Perlman, Ghiorso, and Seaborg, Phys. Rev. 77, 26 (1950).
[2] N. Feather, Proc. Camb. Phil. Soc. 34, 599 (1938).
[3] G. T. Seaborg and I. Perlman, Rev. Mod. Phys. 20, 585 (1948).
[4] K. Street, Jr. (private communication).
[5] M. H. Studier and E. K. Hyde, Phys. Rev. 74, 591 (1948).
[6] M. H. Studier and R. J. Bruehlman (private communication).

On the Structural Absorption of Ultrasonic Waves in Ethyl Alcohol

D. SETTE
Istituto Nazionale di Ultracustica, Roma, Italy
March 14, 1950

AN interpretation of the difference between the experimental ultrasonic absorption coefficient in water and the value of the same coefficient to be expected from viscosity and heat conductivity data has been given by Hall.[1] Water can be considered as a mixture of two structures: an open one (ice-like) and a compact one (close-packed); the elastic waves alter the equilibrium between the two structures and the rearrangement of the molecules takes place with a certain time lag. For this reason a relaxation phenomenon occurs and the absorption increases.

Hall has also suggested that a similar structural absorption could explain the excess of the absorption coefficient in other associated or hydrogen-bonded liquids of low viscosity.

It seems worth while giving the conclusions we have reached in considering the absorption of ethyl alcohol, in which the parameter α/f^2 expected on the classical theory is, at 20°C, about 25×10^{-17} sec.^{2} cm^{-1}, whereas the experimental value is about 50×10^{-17} sec.^{2} cm^{-1} (α=amplitude of the absorption coefficient; f=frequency).

The values of the interaction energy for the case of two alcohol molecules and for that of four molecules, differently arranged,[2] show that the potential energy of two molecules is a minimum when the two dipole moments lie antiparallel, whereas the stability of four molecules is a maximum when they are arranged in a chain.

We can therefore assume that two states are possible for the alcohol molecules: (1) molecules bonded to one another in chains; (2) molecules arranged in pairs with antiparallel dipole moments. The energy is lower in the first state. A compression during wave propagation will produce an increase in the number of the molecules in state (2).

We have applied Hall's treatment working on the same hypothesis and furthermore assuming that, as a first approximation, the molecules of ethyl alcohol at rest, are mainly bonded in chains of four molecules.

As Hall's treatment requires numerical values of any two of the three quantities: (1) the instantaneous compressibility β_∞, (2) the relative change in volume $\Delta V/V$ involved in the transition 1–2, and, (3) the free energy difference of the two states ΔF, we have calculated ΔF and $\Delta V/V$.

The free energy difference per mole is $\Delta F=0.68$ kcal. and the relaxation time calculated from it is, at 20°C, $\tau\sim9\times10^{-12}$ sec.

We evaluated ΔV approximately from alcohol-carbon tetracloride mixtures, assuming that in very dilute solutions the alcohol molecules are mostly in pairs, and, moreover, that the volume of the carbon tetrachloride molecules is not altered by the presence of the alcohol molecules. The volume calculated in this way for the alcohol molecules in the state (2) is only a little lower than that for the state (1), so that $\Delta V/V$ is very small.

In consequence of this, the value of α/f^2 computed for the structural absorption in this way is much smaller than the difference between the experimental value and that obtained using classical theory.

The assumptions made in the calculation, especially as regards ΔV, are indoubtedly very rough ones. Nevertheless, it would appear from this treatment that if we wish to maintain the simple notion of a liquid as a mixture of two structures, while the parameter $\Delta V/V$ is applicable to the case of water where the molecules can pass from a very open structure to a closed one, it does not lend itself to the cases of liquids whose molecules have a large volume and which can pass under the action of ultrasounds from one energy state to another without a large volume difference between the corresponding configurations.

[1] L. Hall, Phys. Rev. 73, 775 (1948).
[2] P. Maladière and M. Magat, Comptes Rendus 225, 676 (1947).

A Thermodynamic Temperature of 1.5 Millidegrees Absolute

D. DE KLERK, M. J. STEENLAND, AND C. J. GORTER
Kamerlingh Onnes Laboratory, Leiden, Netherlands
April 3, 1950

TWO years ago[1] we announced that we had measured very low thermodynamic temperatures obtained by adiabatic demagnetization of a large crystal of chromium potassium alum. These temperatures were determined by straightforward application of the second law of thermodynamics. Coherent results were obtained with three different thermometric parameters and two different ways of heat supply.

At a molar magnetic entropy of $-1.0\ R$ (relative to high temperatures) the magnetic susceptibility has a maximum and a small magnetic hysteresis appears.[2] This was found to occur at a thermodynamic temperature of 4.0 millidegrees absolute, while the lowest temperature measured was about 3 millidegrees at a molar magnetic entropy of $-1.1\ R$.

Since then we have been measuring thermodynamic temperatures in several other substances.[3] Quite recently we studied powdered mixed crystals of chromium alum and aluminium alum containing 1 part of Cr on about 20 parts of Al, a substance similar to that with which de Haas and Wiersma[4] obtained very high susceptibilities in 1935. Even with a molar entropy as low as $-1.1\ R$, no maximum of the susceptibility was found. Thermodynamic temperatures between 1.5 and 20 millidegrees were measured by using the susceptibility as a thermometric parameter and by heating with an oscillating magnetic field at 225 c.p.s. The accuracy of the temperature measurements is not better than 10 to 20 percent.

[1] de Klerk, Steenland, and Gorter, Nature 161, 678 (1948); Physica, 's-Grav. 15, 649 (1949); Leiden Commun. 278c; Steenland, de Klerk, and Gorter, Physica, 's-Grav. 15, 711 (1949); Leiden Commun. 278d.
[2] Kürti, Laîné, and F. Simon, Comptes Rendus 204, 675 (1937).
[3] Steenland, v. d. Marel, de Klerk, and Gorter, Physica, 's-Grav. 15, 906 (1949); Leiden Commun. 279c.
[4] W. J. de Haas and E. C. Wiersma, Physica, 's-Grav. 2, 335 (1935); Leiden Commun. 236b.

The Nuclear Magnetic Moment of Niobium[93]

ROBERT E. SHERIFF,* WILLIAM H. CHAMBERS, AND DUDLEY WILLIAMS
Ohio State University, Columbus, Ohio
March 27, 1950

THE nuclear magnetic resonance absorption peak for niobium (columbium)[93] has been located in a field of approximately 6300 gauss with a solution of Nb_2O_5 in HF. By super-regenerative oscillator techniques similar to those described in earlier reports,[1,2] the niobium resonance peak was compared with the B^{11} peak observed simultaneously in the same magnetic field. The tentative value of the ratio of the Nb^{93} resonant frequency to the B^{11} resonance frequency is

$$\nu(Nb^{93})/\nu(B^{11})=0.76187\pm0.00040.$$

Assuming a value[2] of 0.32080 for the ratio $\nu(B^{11})/\nu(H^1)$, one obtains

$$\nu(Nb^{93})/\nu(H^1)=0.24441\pm0.00013.$$

This value should be increased by a Lamb[3] correction of 0.38 percent because of the diamagnetic effects of the atomic electrons. Use of this correction and of the value 5.58504 for the g-factor of the proton[4] leads to the following value for the nuclear g-factor of Nb^{93}:

$$g(Nb^{93})=1.3702\pm0.0007.$$

Since the spin of Nb^{93} is known from hyperfine structure data[5] to be 9/2, the nuclear magnetic moment of Nb^{93} is

$$\mu(Nb^{93})=6.1659\pm0.0032 \text{ nuclear magnetons.}$$

These values are to be compared with the earlier values $g=1.18$ and $\mu=5.31$ obtained by Meeks and Fisher[6] from hyperfine structure studies. The value obtained in the present work lies close to the upper Schmidt limit value of $+6.79$ for a $g_{9/2}$ odd proton, which Nb^{93} has according to Mayer's[7] theory.

We wish to express our appreciation to the Ohio State University Development Fund and Research Foundation for grants that made this work possible.

* AEC Research Fellow.
[1] J. R. Zimmerman and D. Williams, Phys. Rev. **76**, 350 (1949).
[2] W. H. Chambers and D. Williams, Phys. Rev. **76**, 638 (1949).
[3] W. E. Lamb, Phys. Rev. **60**, 817 (1941).
[4] J. E. Mack, Rev. Mod. Phys. **22**, 64 (1950).
[5] S. S. Ballard, Phys. Rev. **46**, 806 (1934).
[6] W. W. Meeks and R. A. Fisher, Phys. Rev. **72**, 451 (1947).
[7] M. Mayer, Phys. Rev. **75**, 1969 (1949).

Isotope Effect in the Superconductivity of Mercury*

EMANUEL MAXWELL
National Bureau of Standards, Washington, D. C.
March 24, 1950

THE existence of a small quantity of Hg^{198} at the National Bureau of Standards[1] prompted us to investigate its properties as a superconductor.[2] The sample available to us had a high degree of isotopic separation and was approximately 98 percent pure Hg^{198}. The average atomic weight[3] of natural mercury is 200.6. The mercury had been produced by the transmutation of gold and had been prepared by distilling it off the bombarded gold foil.

Preliminary results are now available on the critical field behavior and transition temperature. The destruction of superconductivity was detected magnetically by a ballistic galvanometer method and the zero-field transition temperature determined by extrapolation of the critical field curve to zero field. (Further details of the experimental method will appear elsewhere.) Tests were made with natural mercury and with two specimens of Hg^{198} about 400 mg each (both derived from the original sample). The natural mercury was prepared by our Chemistry Division and is presumed to contain less than 0.001 percent impurity. The specimens of Hg^{198} were separately redistilled in vacuum (following the original distillation from the gold foil) and were enclosed in Pyrex capillaries which were evacuated and sealed off. Temperatures were measured with a helium vapor pressure thermometer using the tables prepared at the Royal Society Mond Laboratory (June 4, 1949) for reducing the pressures to degrees Kelvin.

The results are indicated in Fig. 1 which is a plot of current in the Helmholtz coils (at critical field) *vs.* the absolute temperature for both the natural mercury and Hg^{198}. Any small difference in slope is not significant since the demagnetization factors of the samples and the exact disposition in the field may have been different. The intercepts are significant and give the transition temperatures as 4.156°K for natural mercury and 4.177°K for Hg^{198}.

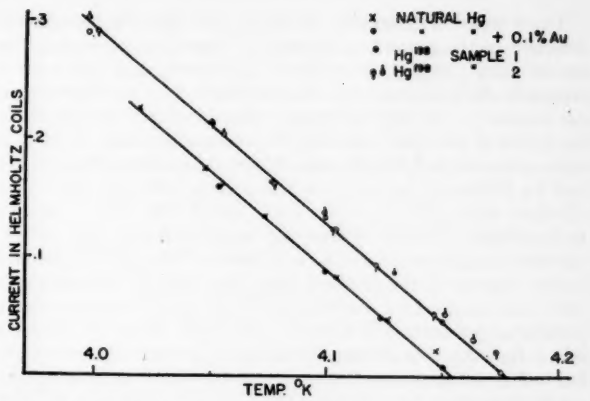

FIG. 1. Current in the Helmholtz coils at the critical field *vs.* the absolute temperature.

Many pains were taken to exclude the possibility of secondary effects. The earth's field was compensated to within 10^{-4} gauss. The distillation apparatus and capillaries were carefully cleaned. The clean appearance of the mercury was good evidence of the absence of base metal impurities in excess of 0.001 percent but there was some possibility that the Hg^{198} might have contained a gold impurity, derived from the original foil which would not have shown up in the form of surface sum. Spectrochemical analysis of the Hg^{198} was not feasible, so a sample of natural mercury with 0.1 percent gold was prepared and tested. (A saturated solution of gold in mercury will contain about 0.15 percent.) The results are given by the black dots and show that even this large amount of gold impurity is unimportant.

From these results one may infer that the transition temperature of a superconductor is a function of the nuclear mass, the lighter the mass the higher the transition temperature. At the ONR conference in Atlanta, March 20–21, it was reported that Serin and Reynolds[4] at Rutgers University had undertaken a similar investigation independently and simultaneously with our own. They found that the transition temperatures of Hg^{199}, Hg^{202}, and Hg^{204} were also a function of the atomic mass, with the lighter isotopes having higher transition temperatures. It is gratifying to find that our results are mutually consistent and complementary. Taken together they definitely establish a dependence of transition temperature on mass number.

* Supported by the ONR Contract NA-onr 12-48.
[1] We are indebted to Dr. W. F. Meggers for making this sample available to us.
[2] The suggestion of examining a pure isotope was also made to us independently by Professor K. F. Herzfeld.
[3] A. O. Nier, Phys. Rev. **52**, 933 (1937).
[4] Reynolds, Serin, Wright, and Nesbitt, Phys. Rev. **78**, 487 (1950).

Magic Numbers and Elements with No Stable Isotopes

LEW KOWARSKI
Laboratoire du Fort de Châhillon, Paris, France
March 20, 1950

THAT the abnormal instability of *all* isotopes of $_{43}Tc$ and $_{61}Pm$ may have something to do with the occurrence, close by, of magic neutron numbers 50 and 82, is an obvious enough suggestion. It becomes even more plausible if we consider that only the absence of odd-mass isotopes requires a special explanation (even-mass isotopes are, for $Z=43$ and 61, excluded by parity rules). Two other elements, A and Ce, then appear to share the same anomaly and in both the latter cases the connection with the magic neutron numbers (20 and 82, respectively) is even more evident.[1,2]

UNIVERSITY OF MICHIGAN LIBRARIES

These cases of abnormal instability can also be seen as an anomaly in the pattern of stability of the adjacent nuclei. The stable pairs Cl^{37}/K^{39}, Mo^{97}/Ru^{99}, La^{139}/Pr^{141}, and Nd^{145}/Sm^{147} represent the transition from an odd-valued A to $A+2$ by adding *two protons* (a "*pp* step" for short). The occurrence of such steps, for nuclei of odd mass, however, is incompatible with the simple assumptions underlying the semi-empirical formulas of Weizsäcker and his followers,[3] according to which there exists for each A an idealized value of Z (or of $I=N-Z$) which "should" correspond to maximum stability so that the isotopic number I_{nat} of any naturally stable nucleus of an odd mass A "should" be the odd integer nearest to the *idealized* value $I_{id}=f(A)$. If this picture is true, then on an $A-I$ diagram all odd-A nuclei lie on successive horizontal segments which begin and end at those abscissae for which I_{id} is an even integer. For example, between A corresponding to $I_{id}=4$ and that corresponding to $I_{id}=6$, all stable odd-mass nuclei must have $I_{nat}=5$. Since the $I_{id}=f(A)$ function is steadily rising, two successive odd-mass nuclei can differ either by one nucleon of each kind (an "*np* step," or a step along the horizontal), or by two neutrons (an "*nn* step," or a step leading from the end of a horizontal to the beginning of the next one). There must be no backsliding into a lower valued horizontal; that is, no "*pp* steps."

Figure 1 shows all stable odd-mass nuclei from $A=71$ to 171, together with the $I_{id}=f(A)$ curve according to reference 3 (one of its original constants, however, has been adjusted in order to improve the fit). The scale of I is exaggerated in order to emphasize the transitions between horizontals. We see that at the *beginning* of each horizontal there is a surfeit of neutrons; it is there that any perturbing factors, favoring the addition of protons, are most likely to produce a *pp* step instead of a normal *np* one.

In the case of the magic number $N=20$ the nature of the disturbance is clear. The first odd-mass nucleus which contains exactly 20 neutrons, that is Cl^{37}, also happens to be the first on the horizontal $I=3$. Since the 21st neutron is supposed to be bound very weakly, the competition of a *pp* step, always strong at the beginning of a horizontal, becomes overwhelming and we find the next odd-mass nucleus, K^{39}, back on the horizontal 1, in contradiction to the normal Weizsäcker picture.[1]

This step brings back the condition of neutron deficiency, as it exists at the end of a horizontal; the next step should be *nn*, or possibly an *np* if the binding of the 22nd neutron as well is abnormally weak (since both competing steps contain the 21st neutron, the weakness of the latter's binding is irrelevant). No such continued abnormality seems to exist, since with K^{41} the horizontal 3 is resumed, and hereafter no further deviations are observed until the completion of the next neutron shell. We may conclude that, after the closing of the shell $N=20$, only one neutron is bound weakly enough to cause visible perturbation.

In the case of the shell $N=82$, the completion takes place at La^{139}. Since this nucleus is the *second* on its horizontal ($I=25$), and not the first, as in the previous case, the competition of a *pp* step is less pronounced. The binding of the 83rd neutron is, however, weak enough to make an *np* step unable to stand even this competition. Accordingly, we find the next odd-mass nucleus, Pr^{141}, on the horizontal 23. One more step is taken *along* this lower horizontal, leading to Nd^{143}, which shows that the abnormal weakness of binding extends to at least one more open-shell neutron.

The completion of the shell $N=50$ looks, however, quite different. Here the odd-mass nucleus concerned (Y^{89}) happens to be the fifth on its horizontal ($I=11$), in a region of neutron deficiency (below the I_{id} line) rather than surfeit as in the previous cases. The chances of a *pp* step toward a still lower horizontal appear to be nil, but the weakness of the binding of the open-shell neutrons (51st, 52nd, etc.) favor *np* steps against *nn*. Accordingly, the horizontal 11 is abnormally long and leads into a region of an abnormally pronounced neutron deficiency. An *nn* step leading to Mo^{97} ($I=13$) relieves this deficiency almost completely, but before the horizontal 13 asserts itself, we have, with Ru^{99}, a last

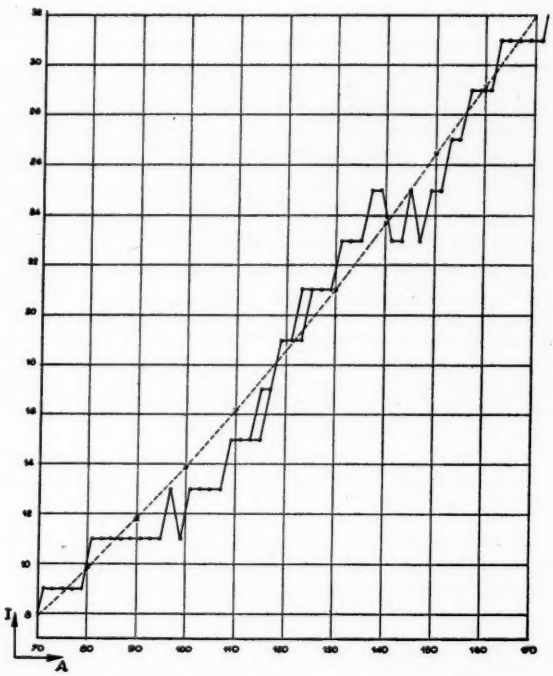

FIG. 1. Dotted line: $I_{id}=A(A^{\frac{1}{3}}-0.7)/(A^{\frac{1}{3}}+128)$.

reappearance of the horizontal 11. To explain this abnormal step (which is responsible for the instability of Tc), we have no longer the resource of postulating a very weakly bound neutron (56th, which would be analogous to the 21st in the argon case) sandwiched between two more strongly bound ones: the 55th neutron does *not* close a shell. And yet it seems tempting to look for some property of open-shell neutrons (this description should cover half a dozen, or so, neutrons attached after the completion of the shell $N=50$) which would be responsible for this anomaly.

Short of devising waves or kinks in the sequence of binding energies for open-shell neutrons, we suggest one *ad hoc* hypothesis. The usual parity rules make no distinction of principle between odd-Z and odd-N nuclei; if we start, for example, from an odd-N nucleus, then an *np* step, which pairs off the neutrons and introduces an odd proton, is no more and no less likely, from the point of view of these rules, than an *nn* or a *pp* step which do not change parity at all. We suggest that in the region of open-shell neutrons, this equivalence does not hold: for these loosely bound neutrons, the pairing-off does *not* bring the full normal benefit in binding energy and therefore *cannot* be balanced against the pairing-off of protons. Starting from an odd-N nucleus, the competition of *both nn* and *pp* steps is strengthened; and as the competition is strongest, respectively, at the end and at the beginning of a horizontal, we must expect it to become operative at the transition between horizontals. In other words, if a horizontal begins in a region of open-shell neutrons, we may expect to find there a tendency toward the elimination of stable isotopes of odd Z. By the time the end of the next horizontal is reached, the next neutron shell is built far enough to allow the resumption of normal parity rules.

The natural instability of Tc and Pm thus gives us a glimpse of the conditions governing the binding of open-shell neutrons (comparable in a way to the open-shell electrons of strongly metallic chemical elements). Other glimpses can be derived from:

(1) The asymmetric fission of uranium. The rule already mentioned by M. G. Mayer[4] can be conveniently formulated as follows: "the most probable modes of fission are those which lead to a minimum number of open-shell neutrons," this number being obtained by adding such neutrons from *both* fragments.

(2) The general trend of capture cross sections for slow neutrons. There seems to be little doubt that these cross sections are, in the aggregate, noticeably lower in the regions of open-shell neutrons (say, $A=88$ to 100 and 138 to 148) than in the regions starting with Rh and Sm. One would say that the addition of neutrons is "inhibited" in the weak-binding region, and then "stimulated" by the accumulated lag behind the rising trend of the idealized Weizsäcker curve. Such crude considerations may help in finding the way to reconcile the droplet and the shell concepts.

I am indebted to Dr. B. T. Feld and Professor J. A. Wheeler for valuable discussions.

[1] H. Bethe and R. Bacher, Rev. Mod. Phys. **8**, 177 (1936).
[2] N. Popelka and W. D. Harkins, Phys. Rev. **77**, 756 (1950).
[3] H. Bethe and R. Bacher, reference 1, p. 166.
[4] M. G. Mayer, Phys. Rev. **74**, 235 (1948).

General Operator Field Equations Derived from A Variation Principle. Construction of "Divergence-Less" Four-Vector Operator

CHRISTOPHER GREGORY
University of Hawaii, Honolulu, Hawaii
April 3, 1950

IT was shown in a recent report[1] that commutator equations for fields, in particular Maxwell's field equations in vacuum, could be derived from a variation principle. The Lagrangian was constructed by replacing the classical space-time derivatives of the field variables by $i/\hbar$ multiplied into the respective commutators of the displacement operators and the field variables. The operator field equations resulted when the first variation of the *trace* of the Lagrangian with respect to the matrix elements of the field variables was made to vanish. It is of interest to generalize this procedure to general invariant functions constructed from four displacement operators p_μ and any number of field operators f_A, $A=1, 2, \cdots$, without putting emphasis upon the replacement of partial derivatives by corresponding commutators.

The arbitrary invariant function of the p_μ and f_A will be denoted by $L(p_\mu, f_A)$ and its trace by G, with

$$G=Tr[L(p_\mu, f_A)]. \tag{1}$$

Now the complete first variation of G is

$$\delta G=[\partial G/\partial(p_\mu)_{mn}]\delta(p_\mu)_{nm}+[\partial G/\partial(f_A)_{mn}]\delta(f_A)_{nm} \tag{2}$$

$$=(N^\mu)_{mn}\delta(p_\mu)_{nm}+(F^A)_{mn}\delta(f_A)_{nm}, \tag{3}$$

where N^μ and F^A are accordingly defined. It is well known, however, that the trace of a matrix, say M, is invariant under transformations of type

$$M'=e^{iS}Me^{-iS}. \tag{4}$$

Consequently, if one subjects L in (1) to a transformation of type (4) and takes S to be an arbitrary infinitesimal operator of the first order, then we have to the desired order

$$\delta(p_\mu)=i[S, p_\mu], \quad \delta(f_A)=i[S, f_A], \tag{5}$$

so that,

$$\begin{aligned}\delta G&=i(N^\mu)_{mn}[S, p_\mu]_{nm}+i(F^A)_{mn}[S, f^A]_{nm}\\&=i[P_\mu, N^\mu]_{mn}S_{nm}+i[F_A, f^A]_{mn}S_{nm}.\end{aligned} \tag{6}$$

But the field equations are

$$F^A=0, \tag{7}$$

and the transformation (4) was such that $\delta G=0$. One concludes then that

$$[p_\mu, N^\mu]=0. \tag{8}$$

As a summary, we have shown that a field theory based on the traces of an arbitrary invariant function of the four displacement operators p_μ and any number of field operators f_A, $A=1, 2, \cdots$, has associated with it the four-vector operator N^μ, defined in (3), which satisfies the "continuity" equation, (8).

As an example, let us consider the field equations for a scalar field U based on the Lagrangians L_+ or L_- defined by

$$L_\pm=\tfrac{1}{2}[p_\mu, U]_\pm[p^\mu, U]_\pm,$$

where $[p_\mu, U]_+$ denotes the anti-commutator expression and $[p_\mu, U]_-$ the usual commutator expression:

$$[p_\mu, U]_\pm\equiv[p_\mu U\pm Up_\mu].$$

From (2) and (3), the field equations are

$$[p_\mu, [p^\mu, U]_\pm]_\pm=0,$$

and the 4-vector operators are

$$N_\pm{}^\mu=[U, [U, p^\mu]_\pm]_\pm.$$

It can be shown that $[p_\mu, N_\pm{}^\mu]\equiv 0$. Preliminary investigations indicate that N^μ has the character of a 4-current "particle" density operator. Similar expressions can be calculated for fields based upon Lagrangians of types resembling those in current use. There are no classical analogs, however, for fields based on Lagrangians which contain anti-commutator expressions or, more generally, for those fields based on Lagrangians which have the p_μ entering in an arbitrary way.

[1] C. Gregory, Phys. Rev. **78**, 67 (1950).

Masses of Pd^{104}, Pd^{108}, Pt^{195}, and Cu^{65} *

HENRY E. DUCKWORTH, KARL S. WOODCOCK,† AND RICHARD S. PRESTON
Scott Laboratory, Wesleyan University, Middletown, Connecticut
March 16, 1950

A DOUBLE-FOCUSING mass spectrograph has been used to photograph a number of doublets formed by singly charged hydrocarbon molecules and multiply charged palladium and platinum atoms. These photographs have been used to obtain precise values for the masses of Pd^{104}, Pd^{108}, and Pt^{195}.

Masses of Pd^{104} and Pd^{108}.—A high frequency spark between two palladium electrodes served as the source of palladium ions. The quadruply charged Pd^{104} and Pd^{108} atoms formed wide doublets at mass numbers 26 and 27 with singly charged C_2H_2 and C_2H_3. The hydrocarbons were secured in the manner described previously.[1] From fourteen photographs of the $C_2H_2-Pd^{104}$ doublet, the difference in packing fraction between C_2H_2 and Pd^{104} was found to be $\Delta f=15.34\pm0.04$, with extreme values of 15.05 and 15.60. From seventeen photographs of the $C_2H_3-Pd^{108}$ doublet, the packing fraction difference was found to be $\Delta f=17.74\pm0.03$, with extreme values of 17.48 and 17.97. The spacing between the two hydrocarbons was used as the mass scale in these measurements. Using K. T. Bainbridge's recommended mass values[2] for H^1 and C^{12}, the packing fractions of C_2H_2 and C_2H_3 are found to be $f=9.218\pm0.017$ and $f=11.887\pm0.018$, respectively. These values, combined with the above packing fraction differences, give for Pd^{104}, $f=-6.12\pm0.05$, and for Pd^{108}, $f=-5.85\pm0.04$.

It was planned to check these values by photographing the $Pd^{104}-Cr^{52}$ and $Pd^{108}-Fe^{54}$ doublets at mass numbers 52 and 54, and combining the results with the Cr^{52} and Fe^{54} masses reported previously.[1] From nine photographs, the $Pd^{104}-Cr^{52}$ packing fraction difference was found to be $\Delta f=2.31\pm0.04$, with extreme values of 2.08 and 2.46. These doublets were very unsymmetrical, the Cr^{52} line being very much the heavier. From twelve photographs of the well-matched $Pd^{108}-Fe^{54}$ doublet, $\Delta f=2.25\pm0.02$, with extreme values of 2.16 and 2.37. On eight of these photographs, well-matched $Pd^{106}-Cr^{53}$ and $Pd^{110}-Mn^{55}$

UNIVERSITY OF MICHIGAN LIBRARIES

doublets were photographed, the measured packing fraction differences being 1.99±0.03 and 2.70±0.05.

It has been necessary to revise the reported values[1] for Cr^{50}, Cr^{52}, and Fe^{54} to correct for a recently observed small inhomogeneity in the magnetic field of the mass spectrograph. These values, calculated using hydrocarbon spacings for the mass scale, rather than the mass scales previously described, are as follows: Cr^{50}, $f=-7.96\pm0.05$ (formerly -7.92); Cr^{52}, $f=-8.25\pm0.05$ (formerly -8.19); and Fe^{54}, $f=-8.03\pm0.05$ (unchanged).

These revised values, when used with the above packing fraction differences, give for Pd^{104}, $f=-5.94\pm0.07$ (cf. $f=-6.12\pm0.05$ by $C_2H_2-Pd^{104}$ comparison), and for Pd^{108}, $f=-5.78\pm0.06$ (cf. $f=-5.85\pm0.04$ by $C_3H_3-Pd^{108}$ comparison). The lack of agreement between the two Pd^{104} values is attributed largely to the unsatisfactory $Pd^{104}-Cr^{52}$ doublets. The agreement between the two Pd^{108} values is gratifying.

Mass of Pt^{195}:—The $C_3H_3-Pt^{195}$ doublet was photographed at mass 39, the quintuply charged platinum ions being obtained from a spark between two platinum electrodes. From thirteen photographs of this well-matched doublet, $\Delta f=7.86\pm0.03$, with extreme values of 7.71 and 8.05. The $Pt^{195}-Pt^{196}$ separation, assumed to be integral, served as the mass scale. Assuming the packing fraction of C_3H_3 to be 9.219±0.017, that of Pt^{195} is calculated to be $+1.36\pm0.04$.

Mass of Cu^{65}:—Measurements of the $Pt^{195}-Cu^{65}$ packing fraction difference, recently made in in this laboratory,[3] have given $\Delta f=9.23\pm0.03$. Using the above value for the packing fraction of Pt^{195}, that of Cu^{65} is found to be -7.87 ± 0.05.

These results are summarized in Table I.

TABLE I. Packing fractions and masses.

Nuclide	Packing fraction ×10⁴	Mass
Cr^{50}	−7.96±0.05	49.96020±0.00025
Cr^{52}	−8.25±0.05	51.95710±0.00026
Fe^{54}	−8.03±0.05	53.95664±0.00027
Cu^{65}	−7.87±0.05	64.94884±0.00032
Pd^{104}	−6.12±0.05	103.93635±0.00052
Pd^{108}	−5.85±0.04	107.93682±0.00043
Pt^{195}	+1.36±0.04	195.02652±0.00078

In these experiments the authors have been assisted by Mr. Howard A. Johnson, Mr. Clifford Geiselbreth, and Dr. Henry B. Duckworth. They are grateful to Professor Carl Stearns for the use of the comparator.

* This letter is based on work done at Wesleyan University under Contract AT(30-1)-451 with the AEC.

† On leave from Bates College, Lewiston, Maine.

[1] H. E. Duckworth and H. A. Johnson, Phys. Rev. **78**, 179 (1950).
[2] K. T. Bainbridge, "Isotopic weights of the fundamental isotopes," Preliminary Report No. 1, National Research Council (June, 1948).
[3] Duckworth, Johnson, Preston, and Woodcock, Phys. Rev. **78**, 386 (1950).

Revision of the Hyperfine Structure of the Spectrum of Mercury

K. MURAKAWA
Institute of Science and Technology, Komaba, Meguro-ku, Tokyo, Japan
February 10, 1950

DURING the last twenty years numerous photographs of the hyperfine structure of the mercury spectrum have been taken in this laboratory with the aid of a Lummer plate crossed with another one, or with a Fabry-Pérot etalon. As the light source, a Geissler tube, a hollow-cathode discharge tube and a specially constructed arc lamp were used. From the measured structure of the lines λ3654 ($6^3P_2-6^3D_3$), λ4047 ($6^3P_0-7^3S_1$), λ4359 ($6^3P_1-7^3S_1$), λ4916 ($6^1P_1-8^1S_0$), λ5461 ($6^3P_2-7^3S_1$) and λ5790 ($6^1P_1-6^1D_2$), the hyperfine separations of the terms $6s6p_{3/2}{}^3P_2$, $^1P_1$ and $6s7s^3S_1$ were deduced, and are listed in Table I. Separations of the term 7^3S_1 are in substantial agreement with the results of previous observers.[1] In Table I the values of the constants A and B calculated by the use of the usual formula $\nu=A_0+(A/2)C+BC(C+1)$, $C=F(F+1)-I(I+1)-J(J+1)$ are also listed. The value of A^{199}/A^{201} which was calculated from the result of the nuclear absorption experiment published by Proctor and Yu[2] is shown in the last row. From the table it is evident that the value of the ratio A^{199}/A^{201} obtained spectroscopically is not only different from that obtained by the nuclear absorption method, but is also different for different terms. This situation is somewhat similar to the case of rubidium ($A(Rb^{85})/A(Rb^{87})$) which was studied by Bitter[3] and by Millman and Kusch,[4] but in that case no dependency on electronic configuration was noticed.

TABLE I. Hyperfine structure of the terms of Hg I.

Term	Hg^{199} ($I=1/2$)	Separations in unit of 10^{-3} cm^{-1} Hg^{201} ($I=3/2$)	A^{199}	A^{201}	B^{201}	A^{199}/A^{201}
7^3S_1	1077.2	−398, −664	718.1	−265.4	0.02	−2.705 ±0.0006
6^3P_2	759	−179.5, −287, −380	303.4	−111.9	0.26	−2.713 ±0.004
6^1P_1	−182.3	113, 51	−121.5	42.4	0.7₀	−2.86 ±0.05
Nuclear absorption value (reference 2)						−2 703₃

The term $6s6p_{3/2}{}^1P_1$ of Hg I is anomalous, but is far enough away from other terms of the same parity to make it very unreasonable to ascribe the anomaly to a perturbation.

A dependency of $A(Sb^{121})/A(Sb^{123})$ on electronic configuration has also been detected in the spectrum of antimony, and details will be published in the near future.

It is well known that the components due to the even isotopes show displacement effects in the hyperfine structure of numerous lines of mercury. The ratio of the distances $Hg^{204}-Hg^{202}$:$Hg^{202}-Hg^{200}$:$Hg^{200}-Hg^{198}$ in the lines λλ4047, 4078, 4359, 6072, 6123, and 6716 was measured and was found to be constant for all lines within experimental error and equal to 1:0.993:0.880. Such a regularity was also found in the hyperfine structure of Pb I, Pb II, and Pb III, and the ratio of the distances $Pb^{208}-Pb^{206}$:$Pb^{206}-Pb^{204}$ was measured to be 1:0.93. Also the hyperfine structure of the spectrum of Os I which was measured by Kawada[5] obeys this regularity and gives the ratio $Os^{192}-Os^{190}$:$Os^{190}-Os^{188}$:$Os^{188}-Os^{186}$=1:0.98:0.96. In all of the above mentioned elements the ratio decreases toward the lighter isotope, and this regularity will be important in the theoretical explanation of the isotope shift in the spectra of heavy elements.

[1] For example, K. Murakawa, Proc. Phys. Math. Soc. Japan **17**, 14 (1935); H. Schüler and T. Schmidt, Zeits. f. Physik **98**, 239 (1935).
[2] W. G. Proctor and F. C. Yu, Phys. Rev. **76**, 1728 (1949).
[3] F. Bitter, Phys. Rev. **75**, 1326; **76**, 150 (1949).
[4] S. Millman and P. Kusch, Phys. Rev. **58**, 438 (1940).
[5] T. Kawada, Proc. Phys. Math. Soc. Japan **20**, 653 (1938).

Microwave Spectra of Asymmetric Top Molecules*

W. J. PIETENPOL,** J. D. ROGERS, AND DUDLEY WILLIAMS
Ohio State University, Columbus, Ohio
March 27, 1950

SIX spectral lines have been observed for the monomeric form of HCOOH at 22,370, 22,470, 23,200, 24,566, 27,810, and 31,000 Mc/sec. The Stark patterns of these lines follow a second-order law and the Stark coefficient is relatively small. The most intense line at 22,470 Mc/sec. arises from a high J-value whereas the other three appear to arise from lower J-levels. The Stark patterns have not been completely resolved for these lines. At high vacuum some intensity is sacrificed in favor of better line definition and at low vaccum intensity also appears to decrease because of both dimmer formation and pressure broadening. The work of Bauer and Badger,[1] who assumed a planar structure for the

molecule, permits a rough calculation of several transitions in the above indicated region.

The $J=2$ to $J=3$ transitions for nitrosyl chloride have been observed in the region from 33,130 to 33,950 Mc/sec. as predicted from previous data.[2] This spectrum is complicated by the isotopic shift between $NOCl^{35}$ and $NOCl^{37}$, the slight asymmetry of these molecules, and the nuclear quadrupole effects of the chlorine and nitrogen nuclei. The theory, excluding the nitrogen quadrupole interaction, predicts five sets of lines for each isotopic molecule with hyperfine structure giving a total of thirty-three lines per molecule. More accurate frequency measurements are being made and a detailed analysis of both spectra is in progress.

* This work was done in connection with a contract between The Geophysical Research Directorate, Cambridge Laboratory, AMC, U. S. Air Force, and The Ohio State University Research Foundation. It is published for technical information only and does not represent recommendations or conclusions of the sponsoring agency.

** Present address: Bell Telephone Research Laboratories, Murray Hill, New Jersey.

[1] S. H. Bauer and R. M. Badger, J. Chem. Phys. 5, 852 (1937).
[2] Pietenpol, Rogers, and Williams, Phys. Rev. 77, 741 (1950).

Transitions to the Ground States in Nuclei Excited by Slow Neutron Capture

B. B. KINSEY, G. A. BARTHOLOMEW, AND W. H. WALKER
Division of Atomic Energy, National Research Council of Canada, Chalk River, Ontario, Canada

March 20, 1950

THE γ-radiations produced by the capture of slow neutrons in various elements have been studied with the aid of a pair spectrometer. A brief description of the method of energy measurement and the results for Be, C, N, and Pb and Bi have been given in a previous communication.[1] The present note concerns the intensities of the γ-radiations resulting from transitions from the capturing states to the ground states of the product nuclei. For brevity, these radiations will be called "ground-state" radiations. The intensities are determined by correcting the peak coincidence counting rate for the pair formation cross section and its angular distribution.

TABLE I. Ground-state radiations.

Capturing nucleus[a]	Spin of capturing nucleus	Spin of product nucleus: Excited state	Spin of product nucleus: Ground state[a]	Minimum spin radiated	Neutron binding energy in product nucleus (Mev)
		Class A: Predominant			
Be^{9}	3/2	1, 2	0	1, 2	6.797 ±0.008
C^{13}	0	1/2	1/2	1	4.947 ±0.010
Al^{27}	5/2	2, 3	2 ?	1	7.72 ±0.02
Mn^{55}	5/2	2, 3			7.25 ±0.03
Fe^{54} ?	0	1/2			9.28 ±0.03
Fe^{56}	0	1/2			7.63 ±0.01
Ni^{58}	0	1/2			9.01 ±0.03
Ni^{60}	0	1/2			8.55 ±0.03
Cu^{63}	3/2	1, 2	1 ?	1	7.91 ±0.01
Pb^{206}	0	1/2	1/2	1	6.67 ±0.02
Pb^{207}	1/2	1	0	1	7.37 ±0.02
		Class B: Weak			
N^{14}	1	1/2, 3/2	1/2	1, 2	10.823 ±0.012
F^{19}	1/2	0, 1	2 ?	1, 2	6.63 ±0.03
S^{32}[b]	0	1/2	3/2	1	8.66 ±0.02
Cl^{35}	3/2	1, 2	2	1	8.56 ±0.03
Cl^{37}	3/2	1, 2	2	1	6.11 ±0.03
K^{39}	3/2	1, 2	4	2, 3	7.76 ±0.03
K^{41}	3/2	1, 2	2	1	7.39 ±0.03
V^{51}	7/2	3, 4			7.30 ±0.03
Co^{59}	7/2	3, 4	6 ?	2, 3	7.73 ±0.04
		Class C: Very weak or not detected			
Si^{28}	0	1/2	1/2	1	8.38 ±0.10
Si^{29}	1/2	0, 1	0	1	11.00 ±0.30
Na^{23}	3/2	1, 2	4 ?	2, 3	(7.0)
Mg^{24}	0	1/2	5/2	2	(7.3)
Mg^{25}	5/2	2, 3	0	2, 3	(12.0)
P^{31}	1/2	0, 1	2 ?	1, 2	(8.2)

[a] A question mark in column 1 indicates an uncertain isotope assignment, in column 4, a doubtful spin value.
[b] Assignment doubtful.

The results are summarized in Table I. With Be and C and with Pb no radiations other than the ground-state radiations were observed. All other elements studied give some radiations producing excited states. From some elements (e.g., Fe and Ni), there are relatively few radiations; from others, there is a copious emission, for example, seventeen different γ-rays have been separately detected in the Al spectrum with a resolution of 2 percent. In most of the heavier elements, such as Cr, Zn, Sr, In, Cd, Sn, W, Ta, and Au, the complexity of the spectrum or lack of knowledge of the binding energies do not permit classification in the table. With the exception of Cr, these elements produce a few homogeneous γ-rays superposed on a continuous spectrum of unresolved radiations.

In Table I, the capturing nuclei are classified according to the intensities of the ground-state radiations relative to those leading to excited states. In Class A, the intensity of the ground-state radiation predominates over that of all other radiations; in Class B, it has an intensity comparable to, or weaker than those of transitions to excited states; in Class C, it is less than 5 percent of the intensity of the strongest γ-ray emitted by the excited nucleus, or it is not detected. The first column of Table I indicates the capturing nucleus; the second, its spin; the third, the spin of the capturing state of the product nucleus and the fourth, the spin of its ground state. The minimum angular momentum ra liated in the ground-state transition is given in the fifth column and the energy of this radiation, as measured in the present experiments, in the sixth. In Class C the energies in parentheses have not been measured directly because the ground state transitions have not been observed and they refer to the energies calculated from the energy balance of (d,p) reactions and the binding energy of the deuteron, or from other sources.

The interpretation of the spectra obtained is difficult because little is known about the parities of the ground states of the nuclei of the target material or their products. Even in circumstances where the parity can be inferred from other evidence, it is not possible to account unambiguously for the intensities of the ground-state transitions. Nuclei such as N^{15} and K^{39}, which contain a closed shell of neutrons, possess magnetic moments in good agreement with those deduced from the Schmidt formula on the basis of a single unmixed state. For these nuclei the parity is determined by the proton which must be added to complete the proton shell. From this and from the shell structure theory of Feenberg and Hammack,[3] it follows that the parity of N^{15} in its ground state should be odd and the parities of K^{39} and K^{41} should be even. Similarly, the parity of N^{14} should be even and the parities of K^{40} and K^{42} should be odd, a conclusion which is supported by the β-decay[3] of K^{42}.

If these parity assignments are correct the ground-state radiation of N^{15} is of the electric dipole type since the spin of the capturing state must be $\frac{1}{2}$ or $\frac{3}{2}$. Our measurements show that it is weak compared to the radiation emitted to the excited state at 5.3 Mev. Further, the ground-state radiation from K^{40} should be electric octupole or magnetic quadrupole because the minimum angular momentum radiated in this transition is two units. It is surprising that a radiation of this type should compete successfully with the numerous radiations emitted by the capturing state (its intensity is about one-fifth of that producing an excited state at 2 Mev).

The low intensity or absence of the ground-state transitions of the Mg, P, and Si isotopes presents further difficulties. Since Mg^{24} and Mg^{26} are even-even nuclei the ground-state transitions in Mg^{25} and Mg^{26} are of the same type where parities are concerned: if there is a parity change in the one nucleus there is a parity change in the other. If there is no change, as the shell model would seem to indicate, the ground-state transition in Mg^{25} is electric quadrupole and it is difficult to understand why it is not detected, although that of Mg^{26} may be forbidden if capture in Mg^{25} takes place in a state with a spin of three units. If there is change in parity, the radiation is magnetic quadrupole and capture in Mg^{24} should fall into the same intensity class as K^{39}. A similar difficulty

UNIVERSITY OF MICHIGAN LIBRARIES

occurs in the understanding of the low intensity of the ground-state transition in P^{32}. Furthermore, the very weak intensities for the ground-state radiations in Si^{29} and Si^{30} are hard to reconcile with the single unit of angular momentum which must be radiated in these transitions if the spin of $\frac{1}{2}$ recently suggested for Si^{29} is correct.[4]

It is clear that the familiar selection rules concerning differences in parity and spin are not sufficient to account for the relative intensities of ground-state transitions. The experimental data, therefore, indicate the existence of additional parameters which determine the relative intensities of nuclear radiations. We wish to thank Dr. L. G. Elliott for helpful discussions.

[1] Kinsey, Bartholomew, and Walker, Phys. Rev. **77**, 723 (1950); **78**, 77 (1950).
[2] E. Feenberg and K. C. Hammack, Phys. Rev. **75**, 1877 (1949).
[3] F. B. Shull and E. Feenberg, Phys. Rev. **75**, 1768 (1949).
[4] Townes, Mays, and Dailey, Phys. Rev. **76**, 700 (1949).

The Viscosity of Liquid He^3

R. A. BUCKINGHAM
University College, London, England
AND
H. N. V. TEMPERLEY,
King's College, Cambridge, England
March 6, 1950

SOME recently announced results by Weinstock *et al.*[1] show that the vuscosity of liquid He^3 increases smoothly from a value of 22 micropoise at 2.8°K to 30 micropoise at 1.05°K. The curve is everywhere convex to the temperature axis and shows no sign of a discontinuity anywhere in this range. Such a variation of viscosity is similar to that of an ordinary liquid, but it does not seem possible to explain it in the conventional way by assuming that the atoms moving through the liquid have potential barriers to surmount. Liquid He^4 (above the λ-point) already shows a viscosity increasing with temperature in much the same way as does that of a gas. The density of liquid He^3 is only just over half that of liquid He^4, and the effective height of any potential barrier is therefore correspondingly smaller. The fact that an opposite trend of viscosity is observed in liquid He^3 therefore points to an increase in mean free path as the temperature falls, which may be explained in one of two ways: (a) by a decrease in the effective cross-section at low velocities of impact of helium atoms (Ramsauer effect); (b) by a decrease in the effective cross section at low temperatures due to the scattered states being already occupied. The existence of such an effect in a Fermi gas was first pointed out by Tomonaga,[2] and a similar point has recently been made by Singwi and Kothari.[3]

We have examined the consequences of effect (a) alone, by extending to He^3 the calculations of the viscosity of He^4 gas made by Massey and Mohr,[4] and by Buckingham, Hamilton, and Massey.[5] Two models have been used, the rigid sphere model (with a diameter of 2.1A for a helium atom[4]), and another using an interaction potential formed from repulsive exponential and van der Waals attractive terms. This second potential is one called "potential *C*" by the second group of authors. Although the attractive part of potential *C* is too weak to represent the interaction of He atoms correctly, it happens that the adjustment to the correct magnitude is very nearly compensated by the smaller mass of He^3. Consequently the results of previous calculations are readily adapted to give values of viscosity which are probably a good approximation for He^3.

TABLE I. Theoretical values of η (in micropoise) as a function of T.

T (°K)	Rigid sphere ↑↓ (1)	Rigid sphere ↑↑ (2)	Rigid sphere Mixture (3)	Potential *C* ↑↓ (4)	Potential *C* ↑↑ (5)	Potential *C* Mixture (6)	Classical (7)	Complete degeneracy (8)	Observed (9)
0.25				3.6	5.3	4.7	3.6	—	
0.5	1.1	32	3.6	8.0	5.2	5.5	6.3	—	
0.75	1.6	19.5	4.7	6.0	4.8	5.0	8.7	41	
1.0	1.8	14.7	5.3	4.8	6.3	5.8	10.8	23	30.5
1.25	2.3	13.2	5.9	4.4	8.5	6.8	12.3	14.5	
1.5	2.7	12.2	6.4	4.4	11.0	8.0	13.5	10.2	
2.0	3.7	11.1	7.4	4.9	14.8	9.8	15.4	5.8	
2.5	4.7	10.8	8.2	5.7	15.9	11.0	17.0	3.8	22 at
3.0	5.8	11.0	9.0	6.7	15.4	11.6	18.5	2.5	2.80°K

In Table I, columns 1 and 2 refer to the rigid sphere model, and assume that the nuclear spins of each colliding pair of atoms are respectively antiparallel and parallel, whereas column 3 represents the consequences of assuming a 3:1 mixture of these two types of collision. Columns 4, 5, and 6 give corresponding results for the interaction potential *C*. Column 7 gives the viscosity of a classical gas of atoms of diameter 2.1A, while column 8 refers to the formula

$$\eta=(1/15\pi^3)\cdot(2mE_0^5)^{\frac{1}{2}}/(kT)^2\cdot(1/Q),$$

obtained by Tomonaga for an almost completely degenerate gas. (His actual expression refers to a mixture of two types of Fermi particle, so we have divided it by 2. The scattering cross section, *Q*, has been taken to be πr^2, *r* being taken as 1.05A, the gas-kinetic radius.) Since E_0, for the observed density (~0.07 g/cm³) of liquid He^3, corresponds to a Fermi degeneracy temperature of the order of 5°K, the Tomonaga formula is only the limiting form at very low temperatures.

Though it might seem that model 2 (rigid spheres with parallel spins) has at least the correct trend to interpret the observed results, it appears nevertheless that the Ramsauer effect is insufficient by itself to explain them: first, because model 5 shows that alteration of the interaction to a more correct form lowers the predicted viscosity at temperatures below 1.5°K considerably; secondly, because the effect of many-body collisions, neglected in models 1 to 7, can only shorten the mean free path; and thirdly, because models 2 and 5 seem to be practically ruled out by the observation of Sydoriak and Hammel[6] that liquid He^3 is not ferromagnetic within the range of temperatures considered.

We thus seem forced to conclude that the observed rise in viscosity as the temperature falls is due, at least in part, to the effect of the exclusion principle in reducing the probability of scattering.

[1] Weinstock, Osborne, and Abraham, conference on "Very Low Temperatures," Massachusetts Institute of Technology, 1949.
[2] S. Tomonaga, Zeits. f. Physik 110, 573 (1938).
[3] K. S. Singwi and L. S. Kothari, Phys. Rev. **76**, 305 (1949).
[4] H. S. W. Massey and C. B. O. Mohr, Proc. Roy. Soc. **A141**, 434 (1934).
[5] Buckingham, Hamilton, and Massey, Proc. Roy. Soc. **A179**, 103 (1941).
[6] S. G. Sydoriak and E. F. Hammel, conference on "Very Low Temperatures," Massachusetts Institute of Technology, 1949.

The Nuclear Magnetic Moment of Praseodymium[141]

WILLIAM H. CHAMBERS, ROBERT E. SHERIFF,* AND DUDLEY WILLIAMS
Ohio State University, Columbus, Ohio
March 13, 1950

BY means of super-regenerative oscillator techniques similar to those previously described,[1,2] a nuclear magnetic resonance absorption peak for Pr^{141} has been located. By comparison of the resonance peak with the sodium resonance peak observed simultaneously in the same magnetic field, the following tentative value for the ratio of the resonance frequency of Pr^{141} to the resonance frequency of Na^{23} in sodium borate in the same applied field was obtained:

$$\nu(Pr^{141})/\nu(Na^{23})=1.2362\pm0.0006.$$

Using Pound's value for the ratio of the resonance frequency of Na^{23} to the resonance frequency of the proton in the same field,[3] one obtains the following value for the ratio of the resonance frequency of Pr^{141} to that of the proton:

$$\nu(Pr^{141})/\nu(H^1)=0.32698\pm0.00016.$$

On the basis of an interpolated value of 0.62 percent for the correction due to the diamagnetism of the atomic electrons as given by Lamb[4] for Hartree fields, and the value of the magnetic moment of the proton given by Mack,[5] the value of the nuclear g factor is:

$$g(\mathrm{Pr}^{141}) = 1.8375 \pm 0.0009.$$

The spin of praseodymium is known from hyperfine structure measurements[6] to be 5/2. Thus the magnetic moment is

$$\mu(\mathrm{Pr}^{141}) = 4.5938 \pm 0.0023 \text{ nuclear magnetons.}$$

The praseodymium resonance absorption was found in a saturated solution of praseodymium nitrate in water.

This value for the magnetic moment is in agreement with predictions made on the basis of Mayer's[7] theory of nuclear shell structure. According to this theory, praseodymium with 59 protons and 82 neutrons has one extra $4d$-proton in addition to the completed $5g$-proton sub-shell and $6h_{11/2}$ neutron shell. The calculated magnetic moment due to such a $4d$ proton is $+4.79$ nuclear magnetons. The sign of the magnetic moment cannot be determined from the present experimental results, but White's data[6] indicate definitely a positive value for the magnetic moment.[8]

We wish to express our appreciation to The Ohio State University Development Fund and Research Foundation for grants which made this work possible.

* AEC Fellow.
[1] J. R. Zimmerman and D. Williams, Phys. Rev. **76**, 350 (1949).
[2] W. H. Chambers and D. Williams, Phys. Rev. **76**, 638 (1949).
[3] R. V. Pound, Phys. Rev. **73**, 1112 (1948).
[4] W. E. Lamb, Jr., Phys. Rev. **60**, 817 (1941).
[5] J. W. Mack, Rev. Mod. Phys. **22**, 64 (1950).
[6] H. E. White, Phys. Rev. **34**, 1397 (1929).
[7] M. G. Mayer, Phys. Rev. **75**, 1969 (1949).
[8] Rosen, Harrison, and McNally, Phys. Rev. **60**, 722 (1941).

Cosmic-Ray Bursts in Ionization Chambers of Different Materials*

HAROLD W. LEWIS
Department of Physics, Duke University, Durham, North Carolina
March 7, 1950

MEASUREMENTS have been made of the cosmic-ray bursts in three cylindrical ionization chambers of different wall materials. The characteristics of the chambers and the burst sizes measured were such that nearly all the events were caused by nuclear disintegrations in the walls of the chambers.[1] Hence a comparison of the counting rates permits an approximate calculation of the relative cross sections for star production in the three materials, aluminum, copper, and lead.

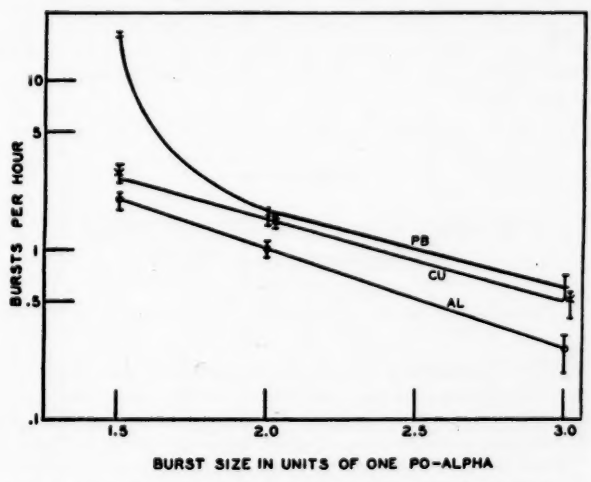

FIG. 1. Integral burst size distribution for three ionization chambers of different wall materials.

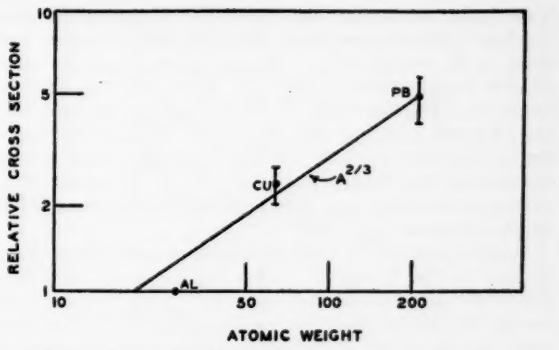

FIG. 2. Relative cross sections for star production calculated from ionization bursts larger than 2 Po-α.

The chambers were as nearly identical as possible, consisting of a cathode of $2\frac{1}{2}''$ outside diameter and 18" length, with a 0.030" collector wire. The wall thickness of the aluminum and copper chambers was $\frac{1}{16}''$ and of the lead $\frac{1}{8}''$. Because of the danger of porosity and the difficulty of soldering aluminum and lead, each chamber was enclosed in a larger brass case, the latter withstanding the high pressure. The case was 20 inches long and $3\frac{3}{4}''$ in diameter, with a $\frac{1}{16}''$ wall. The cathode was supported on insulators inside the case to permit the former to be operated at 1500 volts negative and the case and collector near ground. The active cylinder was equipped with end caps with clearance holes for the passage of the collector to Kovar glass seals on the ends of the case. Electron collection was used. Each chamber was filled with argon to a pressure of seven atmospheres and the gas purified by circulation through a hot calcium purifier. After purification, saturation occurred at about 1000 volts.

The pulse amplifiers were of the type designed by Jordan and Bell.[1] A rise time of 0.7 μsec. and RC clipping time of 40 μsec. were used. A multi-channel pulse height discriminator was used to obtain several points on an integral-bias curve simultaneously. Pulse shapes were not photographed. Calibration of the system was effected by a retractable polonium source rod mounted in the side of the chamber. The size of pulse produced by a polonium alpha-particle, corresponding to 5.3 Mev, is used as the unit for measuring burst size.

Measurements were made at Durham (elevation 400 feet) and on Mt. Mitchell (at an elevation of 6240 feet), the higher station giving four times the counting rate of the lower. Results obtained at Mt. Mitchell are shown in Fig. 1. Bursts smaller than 1.5 Po-α were not measured because of radioactive contamination of the chambers, nor above 3 Po-α because of the low counting rates at the altitudes used. An estimate of the number of bursts produced by electron showers was obtained by the use of a tray of counters directly below the chamber. The counter axes were perpendicular to the chamber axis, and alternate counters were connected in parallel, the two groups being connected in threefold coincidence with the chamber discriminator pulse. Bursts coincident with the discharge of at least one counter in each group indicated either a dense air shower or an event in the chamber itself in which two or more particles emerge and discharge counters. Such coincidences constituted 3 percent of the events in the aluminum and copper chambers and 15 percent of the events in lead. In the analysis below it is assumed that such coincidences are due to showers. The results in Fig. 1 represent the counting rates corrected for showers in this manner. The rapid rise in counting rate for lead below 2 Po-α is probably caused by long range contamination alpha-particles. The altitude variation in the bias curves, however, bears out the conclusion that the bursts above 2 Po-α are caused by nuclear disintegrations only.

The calculation of the relative star-production cross sections from the chamber counting rates can be only approximate, since the number of energy distribution of the nuclear fragments, protons and alpha-particles, is not known. The rough assumption

UNIVERSITY OF MICHIGAN LIBRARIES

is made that the number-size distribution of stars is the same for the three materials measured. The cross section is then proportional to the product of the counting rate in the chamber and the relative atomic stopping power, S, of the wall material for the fragments. Using the values of 1.45, 2.3, and 4.4 for S and 1.0, 1.5, and 1.6 for the measured counting rates at 2 Po-α, the cross sections are in the ratio 1:2.4:4.9. Since the integral bias curves are exponential with nearly equal slopes for the three chambers, the relative cross sections are quite insensitive to the choice of bias at which calculations are made.

A logarithmic plot of these cross sections against atomic weight is given in Fig. 2, together with a line of slope $\frac{2}{3}$ to indicate a power-law variation with that exponent. The relative cross sections for the two heavier materials are consistent, within the limits of error, with an $A^{\frac{2}{3}}$ law. If the somewhat low value of the aluminum cross section is real, it may be due to a smaller average star size in aluminum, resulting in fewer bursts above a given bias than for the heavier elements. The values of the relative atomic stopping power used in the above calculations are those for alpha-particles from radioactive materials.[2] If one uses the recent values of Teasdale[3] for 12-Mev protons, the copper and lead cross sections are closely consistent with $A^{\frac{2}{3}}$, but the aluminum cross section deviates even more from this power law. We conclude that the results are not inconsistent with a cross section proportional to the $\frac{2}{3}$ power of the atomic weight. Several experiments[4-6] with nuclear emulsions under various absorbers have indicated that the absorption cross section for the star-producing radiation is proportional to the nuclear geometrical cross section. The emulsion tracks and stars were used as indicators of the star-producing radiation. Our results, based on measurements of nuclear-type bursts, are consistent with this conclusion.

* This investigation was supported by the ONR.
[1] Bridge, Hazen, Rossi, and Williams, Phys. Rev. **74**, 1083 (1948).
[2] Madame P. Curie, *Radioactivité* (Hermann et Cie, Paris, 1935), p. 223.
[3] J. G. Teasdale, ONR Technical Report No. 3, University of California at Los Angeles, December, 1949.
[4] E. P. George, Nature **162**, 333 (1948).
[5] E. P. George and A. C. Jason, Proc. Phys. Soc. London **A62**, 243 (1949).
[6] Bernardini, Cortini, and Manfredini, Phys. Rev. **74**, 1878 (1948).

A Correction to Be Applied to the Activity of Neutron-Activated Cadmium-Covered Indium Foils

JOHN W. KUNSTADTER
Brookhaven National Laboratory, Upton, New York
March 27, 1950

ONE common method of measuring a slow neutron flux involves the use of foils of some material having a high neutron activation cross section in the resonance region. A necessary part of the technique is the activation by neutrons of one known energy. This is most easily done by the use of cadmium covers on the foils, since cadmium is transparent to neutrons in the resonance region above the 1 ev, and is effectively black in the 1/v region below about 0.4 ev (Table I). The low energy end of the resonances of some elements, notably indium, extends below the cadmium cut-off,[1] and a correction depending on the cadmium thickness used must be applied to the calculated activity to account for those neutrons normally captured by the resonance, but which are absorbed by the cadmium.

TABLE I. Correction factors on indium activity and other data as a function of the thickness of the cadmium cover.

Cadmium thickness—in.	Correction factor	99% black region—ev	% absorption at 0.6 ev	% absorption at 1.0 ev
0.010	0.90[a]	0.11–0.23	11	0.2
0.020	1.072	<0.26	21	0.5
0.030	1.111	<0.28	30	0.7
0.040	1.150	<0.30	38	0.9
0.050	1.191	<0.32	45	1.2
0.060[b]	1.236	<0.34	51	1.4
0.070	1.28	<0.35	56	1.6
0.080	1.32	<0.36	61	1.9
0.100	1.42	<0.38	69	2.3

[a] Calculated from curve.
[b] Equation (1) is probably not valid at greater thicknesses because of abrupt changes in the shape of the cross-section curves in the energy region above about 0.6 ev. Correction factors given for greater thicknesses are therefore only approximations.

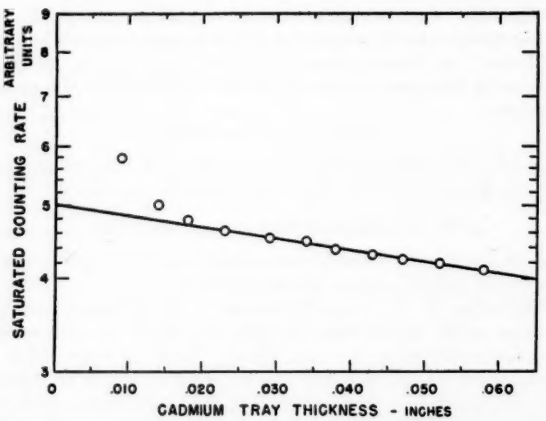

FIG. 1. The saturated activities of neutron-activated indium foils surrounded by cadmium is shown as a function of the cadmium thickness. The errors are less than the size of the circles.

An investigation of this correction as applied to indium was made in a constant and well-known flux or graphite moderated neutrons from a 1g Ra-Be source. The foils were irradiated at a point about 20 inches from the source, where there is a mixture of neutrons of varying energies. The foils used were made from high purity indium, measured 4.00×6.35 cm, and weighed 2.4000±0.0030 g. Cadmium plates the size of the foils were made in about 5, 10, and 30-mil thicknesses, and trays were made in 10 and 30-mil thicknesses. A particular thickness was made up of a sandwich of appropriate plates and tray. The actual thicknesses ran from 0.009″ to 0.058″ in about 0.005″ steps. The points obtained for those thicknesses which were black to thermals lie in a straight line on a logarithmic plot (Fig. 1). A least-squares fit gives an equation of the form

$$C' = Ce^{3.507t}, \tag{1}$$

where C is the observed activity, C' is the true activity, and t is the thickness of cadmium in inches. A tabulation of correction factors for various thicknesses and other data is given in Table I.

The errors involved in all measured quantities were less than 1 percent, with the exception of the cadmium thicknesses, where the error was ±0.0005″. Because of the exponential form of Eq. (1), however, the error in the correction factors given in Table I is estimated at less than 0.5 percent for the thicknesses between 20 and 60 mils.

[1] Goldsmith, Ibser, and Feld, Rev. Mod. Phys. **19**, 259–297 (1947).

The Intensity of Primary Heavy Nuclei in the Stratosphere at Night*

J. J. LORD AND MARCEL SCHEIN
Department of Physics, University of Chicago, Chicago, Illinois
March 28, 1950

FREE balloon flights in the stratosphere have been conducted in order to investigate the flux of primary heavy nuclei and the rate of production of nuclear disintegrations during the night. The elevation and duration of these flights are given in Table I.

Ilford G-5 type photographic emulsion plates, 200μ in thickness, were arranged with emulsions in contact and the plane surfaces parallel to the zenith direction. The total matter per sq. cm. of the

TABLE I. Data on balloon flights.

Time of launching Day	Hour	Average ceiling elevation in cm of Hg pressure	Time at average ceiling elevation
July 22, 1949	5:30 A.M.	1.0	6.2 hr.
August 3, 1949	5:36 A.M.	3.5	5.0 hr.
October 31, 1949	10:17 P.M.	3.3	7.8 hr.
November 30, 1949	10:08 P.M.	6.4	6.9 hr.

upper hemisphere of the gondola covering the plates was in all cases negligible compared to the mass of the atmosphere directly above the plates.

The plates were carefully examined for heavy nuclei tracks and cosmic-ray stars. The intensity of cosmic-ray stars is given in Fig. 1 for the day flight of August 7 and the night flight of October 31. The rate of production of stars with more than n prongs is given in units of the number of stars per cc per day.

In order to be sure that the lower temperature of the plates at night did not affect the interpretation of this experiment the grain density as a function of ionization energy-loss was determined on the plates used during the night flights and those used during the day. For corresponding energy-losses the grain densities were reduced by less than 10 percent by the lower temperatures during the night, which would make a negligible difference in the intensity of delta-rays between day and night.

The number of delta-rays extending 1.1μ from the center of the heavy nuclei tracks was measured in each case, and the tracks grouped according to their intensity of delta-rays per 100μ (Fig. 2). The relationship between the delta-ray intensity of primary heavy nuclei tracks and the type and velocity of the particles has been shown by previous investigations.[1,2]

Since the night balloon flight of October 31 leveled off at a slightly lower elevation than did the day flight, and in order to correct for the contribution of heavy nuclei during the time of rise and fall, it is necessary to know the altitude dependence of the heavy nuclei tracks.

For the investigations reported in this paper it is sufficient to know the variation of all tracks, with a given number of delta-rays per 100μ, with the altitude. This is shown in Fig. 3, where the number of tracks with more than 12 delta-rays per 100μ is given as a function of the pressure-altitude.

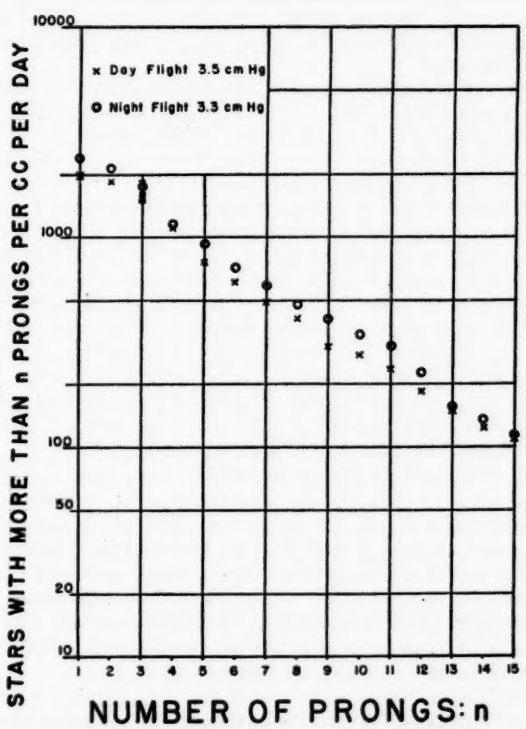

FIG. 1. Distribution of stars with respect to the number of their prongs.

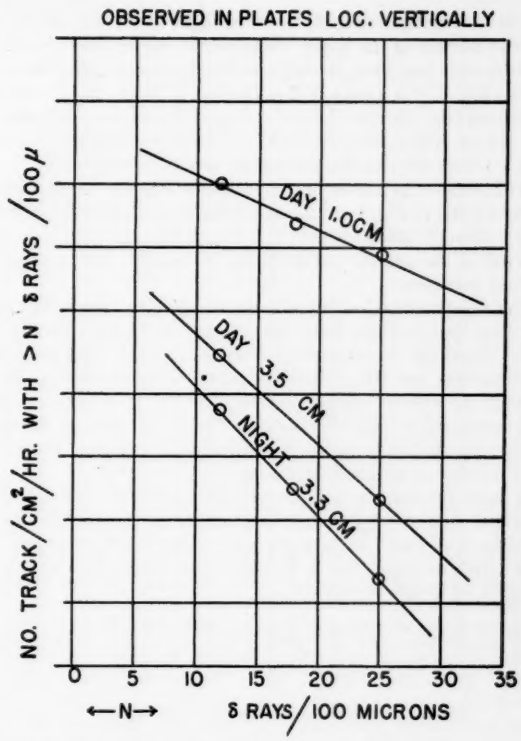

FIG. 2. Distribution of delta-rays on the heavy particle tracks. (The ordinate scale is the same as that for Fig. 3.)

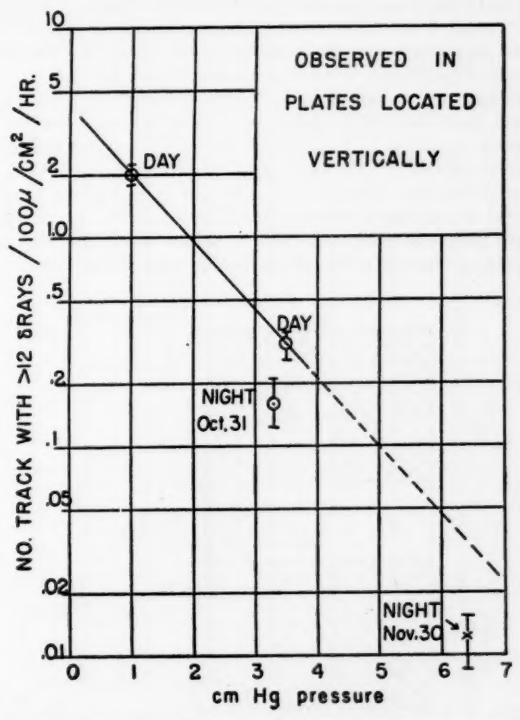

FIG. 3. The number of tracks with more than 12 delta-rays per 100μ as a function of the altitude.

It is to be noticed (Fig. 3) from the flight of October 31 that the ratio of the flux of the heavy nuclei tracks, which have more than 12 delta-rays per 100μ, during the day to those during the night is 2.1±0.6. If it is assumed that the flux of heavy nuclei tracks is an exponential function of the atmospheric pressure between 1.0 and 6.4 cm of Hg, then the flight of November 30 gives a ratio of 3.0±1.1 between the flux during the day to that at night.

Within experimental error of five percent the rates of production of stars given in Fig. 1 are the same during the day and the night, which strongly indicates that the proton and alpha-particle components of the cosmic radiation do not exhibit any appreciable diurnal variation.

The experimental evidence presented here indicates that there is a large change in the intensity of heavy nuclei between day and night. Since the measurements refer to tracks having more than 12 delta-rays per 100μ, the data refers to nuclei having, on the average, an atomic number greater than 10. It is not clear from this investigation whether or not this large diurnal variation applies only to heavy nuclei of relatively low energies. They could then possibly originate from the sun.

A more detailed study of the diurnal variation of heavy nuclei with the time of day and as a function of the energies of the particles may lead to a new approach regarding their origin.

We wish to thank Mr. J. Litwin for assistance in scanning the plates used in this experiment.

* Assisted by the joint program of the ONR and AEC.
[1] Freier, Lofgren, Ney, and Oppenheimer, Phys. Rev. **74**, 1818 (1948).
[2] H. L. Bradt and B. Peters, Phys. Rev. **74**, 1828 (1948).

Detection of the π-μ-Decay with a Scintillation Crystal†

W. L. KRAUSHAAR,* J. E. THOMAS, JR.,** AND V. P. HENRI*
Department of Physics and Laboratory for Nuclear Science and Engineering, Massachusetts Institute of Technology, Cambridge, Massachusetts
March 28, 1950

THIS letter summarizes the preliminary results of an experiment from which it is hoped to obtain an accurate and direct measurement of the mean life of the π^+-meson. The experimental arrangement is shown schematically in Fig. 1.

Mesons are produced in a carbon or beryllium target T by γ-rays from the M.I.T. synchrotron. Some of the π-mesons pass through an absorber A_1 ($\frac{1}{4}$ in.-Pb+$\frac{1}{4}$ in.-Al) traverse a 2 g/cm^{-2} stilbene crystal X_1 (facing a 1P21 photo-multiplier, PM$_1$), a 2 g/cm^{-2} bakelite absorber A_2, and stop in a 1 g/cm^{-2} stilbene crystal X_2 (facing a 5819 photo-multiplier, PM$_2$). Practically all of the μ-mesons (range 0.1 g/cm^{-2}) arising from the decay of the stopped π^+-mesons come to rest in the same crystal X_2 and subsequently decay, giving rise to positrons. The arrival of the π^+ meson, the disintegration of the π^+-meson, and the disintegration of the μ^+-meson produce light flashes that are detected by the photo-multiplier PM$_2$. The resulting pulses are amplified by a distributed constant amplifier, delayed 10^{-7} seconds by a coaxial cable, and displayed on a high writing-speed oscilloscope. The over-all resolution of the crystal and electronic equipment is sufficient to measure the time between arrival and decay of π^+ mesons when this time is $3\cdot10^{-8}$ seconds or greater. The pulses from PM$_2$ are also presented on a second slower oscilloscope for the purpose of observing the decay electron from the μ-meson. The sweeps of the two oscilloscopes are triggered simultaneously by coincidences between PM$_1$ and PM$_2$. The two oscilloscopes are photographed with the same camera on a continuously moving film.

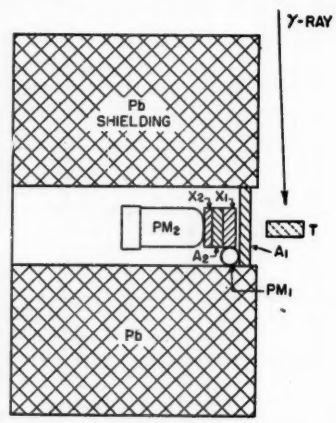

FIG. 1. Experimental arrangement for detecting the π-μ-e-decay.

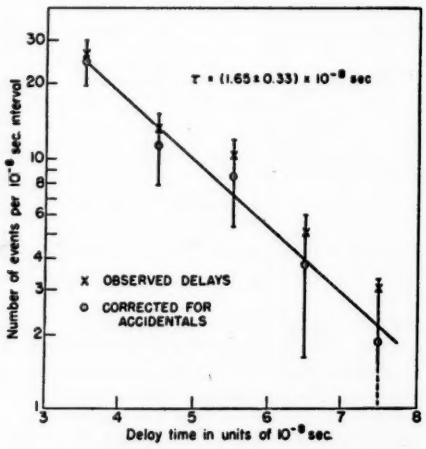
τ = (1.65±0.33) × 10⁻⁸ sec
Number of events per 10⁻⁸ sec. interval
x OBSERVED DELAYS
o CORRECTED FOR ACCIDENTALS
Delay time in units of 10⁻⁸ sec.

FIG. 2. Distribution of delayed events. The standard errors indicated are those for the data corrected for accidentals.

The synchrotron was operated at 315 Mev at a repetition rate of 2 pulses per second. Each pulse was about 100μsec. long, and produced an ionization of 0.025 roentgens in a Victoreen thimble r-meter surrounded by $\frac{1}{4}$ in.-Pb and placed in the beam 3 meters from the target.

In about 12 hours of operation some 25,000 pictures were taken, among which about 100 showed closely spaced double pulses. We selected a group of 57 satisfying the following criteria:

(1) time separation between 3 and $8\cdot10^{-8}$ sec.; (2) first pulse greater than $\frac{3}{4}$ and second pulse greater than $\frac{1}{2}$ of the average pulse produced by a minimum ionizing particle traversing 1 g/cm^{-2} of the crystal; (3) an additional pulse occurring within 5.7 μsec. which could be interpreted as being due to the electron from the decay of a μ-meson. The time distribution of these 57 double pulses is shown by the crosses in Fig. 2, in which the abscissa is the delay and the ordinate is the number of events per 10^{-8} sec. interval. We interpret these 57 events as being due mostly to π^+-decay processes. The following arguments confirm our interpretation:

(a) the time distribution (corrected for accidentals) of the additional pulses occurring within 5.7 μsec. is consistent with the known mean life of 2.15 μsec. for the μ-meson;

(b) events such as these plotted on Fig. 2 may occur by chance. However, the computed number of chance events over the period of observation is only 1.5 per 10^{-8} sec. interval. Measurements between $8\cdot10^{-8}$ sec. and $20\cdot10^{-8}$ sec. indicated the existence of a background of this magnitude. Sixteen events satisfying criteria (1) and (2) above, but not (3), (i.e., events *unaccompanied* by a third pulse) show a distribution of delays consistent with the hypothesis that most of these events are accidental. The absolute number is also consistent with this hypothesis.

(c) Delayed pulses might conceivably be produced by unexpected fluctuations in the light emission of the crystal or by some short-lived induced radioactivity. This, however, is ruled out by

the observation that 70 percent of the closely spaced double pulses are followed by a third pulse interpretable as a μ-decay while only 30 percent of all the sweeps show a second pulse.

(d) By extrapolation of the decay curve of Fig. 2 back to zero time, we conclude that about 1.5 π^+-mesons were stopped in each gram of crystal per hour. A Kodak NTB nuclear emulsion placed near the crystal indicated that about 1.2 π^+-mesons were stopped in each gram of emulsion per hour.

The circled points in Fig. 2 show the number of delayed pulses corrected for accidentals. By fitting an exponential curve to these points[1] one finds for the mean life of π^+-mesons the value $\tau=(1.65\pm0.33)\times10^{-8}$ sec. Within the rather large statistical errors involved, this value of the mean life agrees with the value $\left(1.97^{+0.14}_{-0.17}\right)\times10^{-8}$ sec. obtained by Martinelli and Panofsky[2] on the decay of π^+-mesons in flight, and with the value $\left(1.11^{+0.31}_{-0.22}\right)\times10^{-8}$ sec. obtained by Richardson[3] on the decay of π^--mesons in flight.

We wish to thank the members of the M.I.T. synchrotron staff who have cooperated in making these measurements. Professors Bruno Rossi and Matthew Sands have contributed much encouragement and sound advice. We thank Mr. W. B. Smith who constructed and assisted in the testing of most of the equipment, and Mr. A. Grubman who grew the stilbene crystals.

† This work was supported in part by the joint program of the AEC and ONR.

* Physics Department and Laboratory for Nuclear Science and Engineering.
** Electrical Engineering Department and Laboratory for Nuclear Science and Engineering.

[1] R. Peierls, Proc. Roy. Soc. **A149**, 467 (1935).
[2] E. A. Martinelli and W. K. H. Panofsky, Phys. Rev. **77**, 465 (1950).
[3] J. R. Richardson, Phys. Rev. **74**, 1720 (1948).

Superconductivity of Isotopes of Mercury*

C. A. Reynolds, B. Serin, W. H. Wright, and L. B. Nesbitt
Rutgers University, New Brunswick, New Jersey
March 24, 1950

THE superconducting transition temperatures of natural lead and the lead isotope obtained from the decay of uranium have been determined from resistance measurements by Kamerlingh Onnes and Tuyn[1] and by Justi.[2] In both instances, no detectable change in transition temperature between the natural element and the isotope was found.

In the measurements to be described, critical field *vs.* temperature curves for mercury samples enriched in various isotopes were determined by susceptibility measurements. The samples were obtained from the U. S. Atomic Energy Commission, and were prepared by electromagnetic separation. The average mass numbers for the enriched samples (samples 1, 2, 4) are shown in Table I; sample 3 is natural mercury.

The samples varying in mass from 50 to 100 mg, were sealed under helium in capillaries about 0.5 mm i.d., giving samples about 3 cm long. A coil of No. 41 copper wire was wound around each capillary. The samples were placed in a Dewar vessel of liquid helium, and formed the secondary of a mutual inductance with a solenoid placed outside the shield Dewar. The solenoid was excited by a 1000 c/sec. oscillator, and produced a magnetic field at the sample of less than 0.1 oersted. The signal picked up by the sample coil was amplified and detected. The signal was balanced out with the sample superconducting, and then the detected signal

Table I. Transition temperatures.

Sample	Average mass number	T_0(°K)
1	203.4	4.126
2	202.0	4.143
3	200.7	4.150
4	199.7	4.161

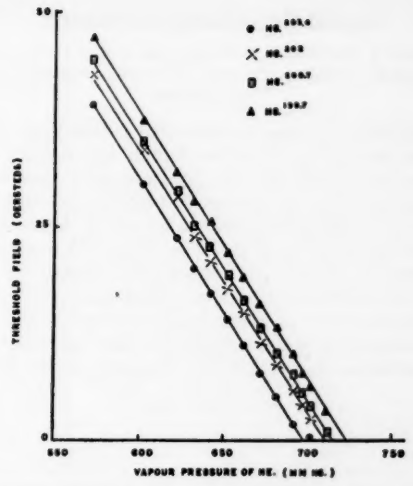

Fig. 1. The critical magnetic field as a function of the absolute temperature.

was observed as a function of the magnetic field of a large Helmholtz coil surrounding the Dewars. The earth's magnetic field was canceled to 0.3 percent. When the magnetic field reached the neighborhood of the critical value at any temperature, there was a rapid increase in detected signal. The critical field was taken to be the average value in the transition interval. Figure 1 shows the critical field curves for the four samples. It is to be noted that there is a *systematic decrease of transition temperature with increasing mass.* The transition temperatures (in zero magnetic field), T_0, of the samples are given in Table I. The slopes of these curves at zero field agree within 1.0 percent; the magnitude of the slope is -204 ± 2 oersteds/°K.

Figure 2 is a plot of transition temperature *vs.* average mass

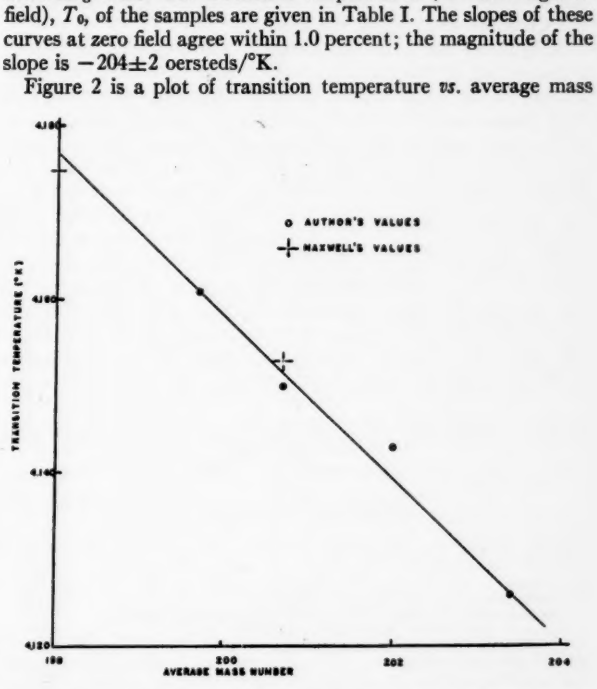

Fig. 2. The transition temperature *vs.* the average mass numbers of the isotopic mixtures.

number. The values obtained by Maxwell[3] for Hg^{198} and natural Hg are included. The slope of the line in Fig. 2 is 0.009 °K/(mass number).

* This work was supported by the ONR, by the Research Corporation, by the Rutgers University Research Council, and by the Radio Corporation of America.

[1] H. Kamerlingh Onnes and W. Tuyn, Leiden Comm. No. 160b (1922).
[2] E. Justi, Physik. Zeits. **42**, 325 (1941).
[3] E. Maxwell, Phys. Rev. **78**, 477 (1950).

UNIVERSITY OF MICHIGAN LIBRARIES

Liquid Scintillation Counters*

GEORGE T. REYNOLDS, F. B. HARRISON, AND G. SALVINI**
Palmer Physical Laboratory, Princeton University, Princeton, New Jersey
March 24, 1950

EXPERIMENTS have been initiated to investigate the scintillation properties of various liquids by studying the light flashes due to ionizing particles. Measurements have been made to date on the following solutions and liquids: (a) naphthalene in benzene; (b) naphthalene plus anthracene in benzene; (c) terphenyl[1] in benzene; (d) dibenzyl in ether; (e) anthracene plus naphthalene in xylene; (f) terphenyl in xylene, (g) benzene, (h) ether, (i) xylene, and (j) melted dibenzyl. Because of the well-known inconvenience of photo-multiplier background, particularly troublesome in measurements with poor geometry, the coincidence technique shown in Fig. 1 was used. A thin-walled glass

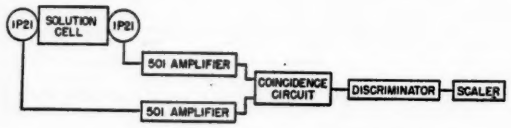

FIG. 1. Coincidence method for measurement on solutions and crystals.

cell, of inner dimensions 1 in.$\times\frac{1}{2}$ in.$\times 2\frac{3}{8}$ in. containing approximately 20 cc of solution was mounted between two 1P21 photo-multipliers. The output pulses of the 1P21's were led into model 501 amplifiers and then into a coincidence circuit with 0.5 μsec. resolving time. The coincidence circuit output was fed into a discriminator and scaler. Counting rates were taken with and without the presence of a Co^{60} source, counts thus being obtained from the Compton electrons in the solution.

A figure of merit for each solution was measured as follows: Suppose that θ Compton electrons are formed in the solution per second. As the result of the scintillation properties of the solution, each photo-multiplier counts n times per second where $n=x\theta$, $x<1$. If x is small so that on the average only a few photons reach the cathode of the photo-multiplier, then the number of coincidences per second will be given by $c=x^2\theta$. Thus the ratio $c/n=x$ is a measure of the "efficiency" of the solution for the detection of charged particles. If x is found to be large, the counts in the two photo-multipliers are not independent and c/n is not strictly an efficiency but is still useful for the purpose of comparing the various samples. The "efficiencies" for some of the solutions tried are listed in Table I. Because of the particular geometry used and the spread in energy of the Compton electrons, the results given in Table I should be taken only as an indication of relative performance and not as an attempt at establishing absolute numbers. With the measured resolving time of the coincidence circuit, the number of chance twofold coincidences is of the order of 5 per minute, whereas the observed coincidence counting rate was in all cases of the order of several thousand per minute. For the sake of comparison an efficiency was measured for a fairly good naphthalene crystal of the same dimensions as the solution, and is included in the table.

TABLE I. "Efficiencies" of various solutions (at room temperature unless otherwise noted).

Liquid or solution	"Efficiency"
Benzene	0.07
Benzene at 70°C	0.07
Ether	0.07
m-Xylene	0.08
Naphthalene (40 g) in benzene (100 cc)	0.15
Naphthalene (35 g)+anthracene (0.35 g) in benzene (90 cc)	0.36
Terphenyl (2 g) in benzene (100 cc) at 60°C	0.84
Terphenyl (0.5 g) in m-Xylene (100 cc)	0.80
Liquid dibenzyl at 60°C	0.4
Naphthalene crystal	0.87

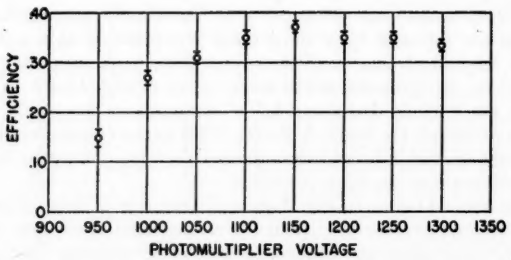

FIG. 2. Dependence of efficiency on photo-multiplier voltage for a solution of naphthalene plus anthracene in benzene.

The efficiency measured for a solution depends somewhat on the voltage applied to the photo-multipliers, in the manner shown in Fig. 2 for the case of a solution of naphthalene plus anthracene in benzene. A plateau is indicated. In Table I it is interesting to note the high efficiencies of the terphenyl solutions. The measurement on terphenyl in benzene was made at 60°C in order to get a significant amount of terphenyl into solution. The high efficiency for terphenyl in xylene was obtained at room temperature. The effect of temperature on efficiency was tested directly in the case of several solutions and the results showed that the temperature in itself had very little effect, if any.

It may be noted that the high efficiency of the terphenyl solutions is accomplished by very small quantities of terphenyl. This is consistent with the observations of Ageno, Chizzotto, and Querzoli[2] who measured the total fluorescence in solutions activated with γ-rays.

The pulses from the solutions have been observed on an oscilloscope and have been compared with the pulses from the more familiar scintillation crystals. In our experiments the rise and decay times of the pulses from dibenzyl crystals and terphenyl solutions are observed to be determined by the characteristics of the amplifiers used (rise time=0.02 μsec., decay time=0.03 μsec.). Experiments are underway to determine the response to electrons, mesons and alpha-particles with improved geometry, using end window photo-multipliers. Further investigation of the terphenyl solutions, which appear especially promising, is also under way.

Discussions with R. Hofstadter have been very helpful.

* Assisted by the joint program of the ONR and the AEC.
** On leave from the University of Milan, Italy.
[1] Hofstadter, Liebson, and Elliot, Phys. Rev. **78**, 81 (1950).
[2] Ageno, Chizzotto, and Querzoli, Atti Accad. naz. Lincei **6**, 626 (1949).

Copper 61 and 67

D. N. KUNDU AND M. L. POOL
Ohio State University, Columbus, Ohio
March 31, 1950

A COPPER activity of 56 hr. was reported[1] as a bismuth fission product and was tentatively assigned to Cu^{67} on the basis of the mode of disintegration and half-life. A similar activity of half-life 61 hr. was also produced[2] as result of the bombardment of As with 200-Mev deuterons. No definite mass assignment was made perhaps because of the large charge and mass change involved in this high energy deuteron bombardment. Though later on through a private communication, the same activity was reported as having been produced by photo-disintegration[3] of Zn, the mass number was still uncertain, first because non-enriched zinc had been used and second because no confirmation was available from cross reactions from neighboring isotopes. The disintegration characteristic was privately given[4] as the emission of negative beta-particles without any reference to gamma-rays. The purpose of this present note is a definite mass assignment to this activity made possible by the availability* of highly enriched isotopes of Ni^{64} and Zn^{67}.

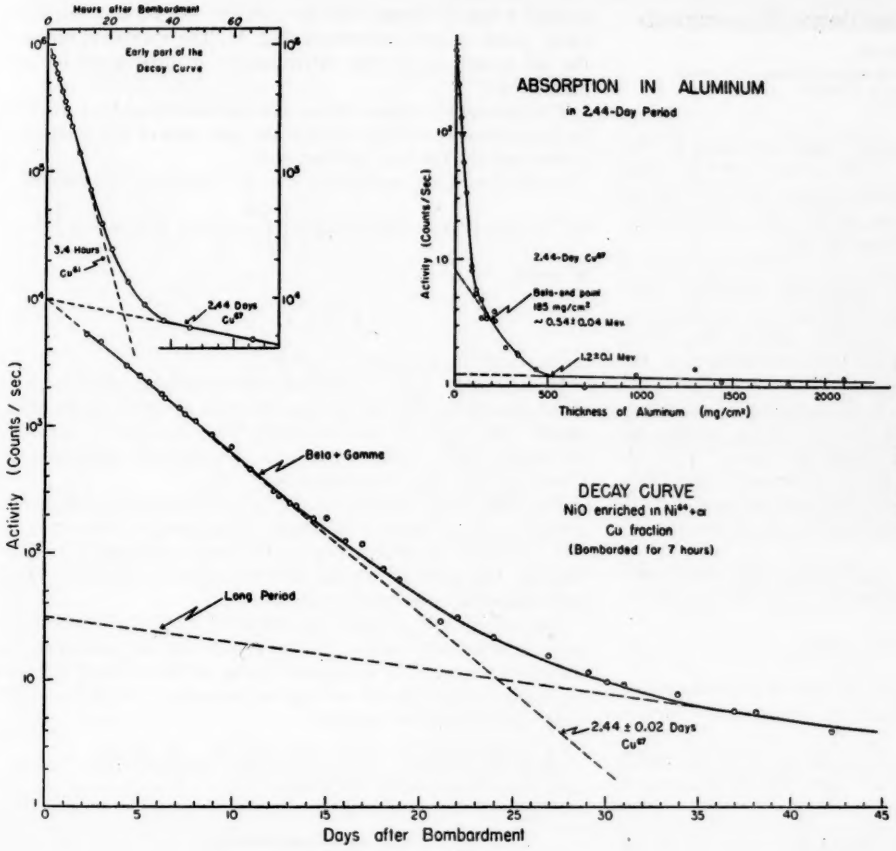

FIG. 1. Decay curve of the copper fraction from nickel oxide enriched in Ni^{64} and bombarded with 20-Mev alpha-particles showing the 2.44-day Cu^{67} activity. The inset in the left-hand corner with the expanded time-scale shows the 3.4-hr. Cu^{61} in the earlier part. In the right-hand top inset, the absorption curve with thin aluminum foils as absorbers shows the beta-end point at 0.54 Mev.

In view of the already available information,[5] the 3.4-hr. copper activity should have been clearly assigned to Cu^{64}. However, the mass number has still been regarded[6] as uncertain. Considerations of the percentage of enrichment are used here to check the assignment of this 3.4-hr. copper activity.

A sample of nickel oxide enriched in Ni^{64} to 80.6 percent from the low natural abundance of 1.16 percent in ordinary nickel was bombarded with approximately 20-Mev alpha-particles. The decay curves of the copper fraction after chemistry, followed with Geiger counters and a Wulf electrometer, showed activities (Fig. 1) of half-lives 3.4 hr. through 8 half-lives, no 12.8 hr., 2.44±0.02 days through 12 half-lives and a long period in minute amount. The 3.4-hr. copper activity is confirmed at Cu^{61} from the reaction $Ni^{58}(\alpha,p)Cu^{61}$ resulting from the 11.5 percent of Ni^{58} present in the target sample. The 2.44-day half-life must be assigned to Cu^{67} and this is produced through the reaction $Ni^{64}(\alpha,p)Cu^{67}$. This assignment is further sybstantiated by fast neutron bombardments of zinc oxide containing zinc enriched in Zn^{67} to 56.0 percent from its natural abundance of only 4.07 percent. The decay curve of the copper fraction showed the 2.44-day half-life in addition to the 12.-hr. and a long period. The 2.44-day activity clearly arises from the reaction $Zn^{67}(n,p)Cu^{67}$.

An absorption measurement with thin aluminum foils shows the beta-end point at 0.54±0.02 Mev. The second end point at 1.2 Mev is, perhaps, to be ascribed to the long period because the extrapolated zero-foil intensity approximately corresponds to the intensity of the long period at the time of the absorption. The ratio of the ionization in the ion chamber of the electrometer due to beta- and gamma-rays in the 2.44-day period was 135:1, thereby indicating the presence of one gamma-ray per beta-particle on the basis of the ionization characteristics of the chamber used.

The absence of any appreciable amount of the 12.8-hr. Cu^{64} in the Ni+α-bombardment may be due to the fact that the enriched nickel sample contained only 0.4 percent of Ni^{61} isotope. In the Zn+n bombardment, however, where Zn^{64} was present in 18.7 percent, the 12.8-hr. activity was produced due to the reaction $Zn^{64}(n,p)Cu^{64}$. Noting that there is 54 percent K-capture in the 12.8-hr. activity, the ratio of the cross sections for the two reactions was $Zn^{64}(n,p):Zn^{67}(n,p)=23:1$. This order of magnitude may be examined in the light that though Cu^{64} and Cu^{67} both emit beta-particles of about the same energy, the gamma-ray associated with Cu^{67} may put this nucleus at a much higher energy state from the ground level than is the case with Cu^{64} where the gamma is associated with K-capture. The saturation yield ratio for the (α,p) reaction from Ni^{58} and Ni^{64} was 88:1. The cross-section ratio cannot be estimated, however, because whereas the reaction $Ni^{64}(\alpha,n)$ causes no complication, the product nucleus Zn^{67} being stable, the reaction $Ni^{58}(\alpha,n)$ introduces the corresponding cross section of unknown magnitude into the computations. Because Zn^{61}, produced if any, will be radioactive, it will continually decay into Cu^{61}. In fact, the observed high yield ratio 88:1 may be taken to indicate that a short-lived isotope Zn^{61} is produced and within the time of bombardment and chemistry decays into Cu^{61}, thereby giving a high saturation intensity as calculated from the decay curves. By a rough extrapolation method,[7] the half-life of Zn^{61} would be of the order of a minute.

[1] R. H. Goeckermann and I. Perlman, Phys. Rev. 73, 1127 (1948).
[2] H. H. Hopkins, Jr. and B. B. Cunningham, Phys. Rev. 73, 1406 (1948).
[3] R. B. Duffield and J. D. Knight (private communication, 1948), quoted by G. T. Seaborg and I. Perlman, Rev. Mod. Phys. 20, 585 (1948).
[4] H. H. Hopkins, Jr. (1948) quoted by G. T. Seaborg and I. Perlman, Rev. Mod. Phys. 20, 585 (1948).
[5] Kindly supplied by the Y-12 Plant, Carbide and Carbon Chemicals Corporation, US-AEC, Oak Ridge, Tennessee.
[6] Leith, Bratenahl, and Mayes, Phys. Rev. 72, 732 (1947).
[6] G. T. Seaborg and I. Perlman, Rev. Mod. Phys. 20, 585 (1948).
[7] D. N. Kundu and M. L. Pool, Phys. Rev. 78, 488 (1950).

UNIVERSITY OF MICHIGAN LIBRARIES

Decay Constants from Coincidence Experiments

T. D. NEWTON
Chalk River Laboratories, National Research Council of Canada, Chalk River, Ontario, Canada
April 3, 1950

A HIGH speed coincidence circuit[1] has been used in this laboratory to study half-lives of the order of 10^{-9} sec.[2] This prompted a consideration of the mathematical form of delayed coincidence resolution curves. Simple methods have given results comparable to those recently published by Bay.[3]

In a typical experiment, one counter of a coincidence circuit is excited by a parent radiation from a radioactive source, the other counter by a daughter radiation whose lifetime is to be measured. Artificial delays can be inserted in either side of the circuit. Experiment relates the number of observed coincidences to the (negative or positive) artificial delay, x.

If there is no natural delay; i.e., if the daughter has a lifetime much too short to be measured by the coincidence circuit, one obtains the "prompt coincidence resolution curve," $P(x)$. If there is a measurable lifetime, the daughter emission has a probability $f(t)dt$ of occurring t sec. after the parent emission. Experiment then provides a "delayed coincidence resolution curve," $F(x)$.

If $F(x)$, $P(x)$, and $f(t)$ are all normalized as differential probability distributions, i.e., are all normalized to unit area, then

$$F(x)=\int_{-\infty}^{\infty} f(t)P(x-t)dt. \tag{1}$$

Here $P(x)$ represents the response of the circuit to simultaneous emission of particles of the same kind and energy as are used to give $F(x)$.

If only a single decay is involved, whose mean life is $\tau=1/\lambda$ then $f(t)=0$ for $t<0$, and $f(t)=\lambda e^{-\lambda t}$ for $t\geqslant 0$. With $y=x-t$, (1) then becomes

$$F(x)=\lambda e^{-\lambda x}\cdot\int_{-\infty}^{x} e^{\lambda y}P(y)dy. \tag{2}$$

Differentiation of (2) gives

$$dF(x)/dx=\lambda\{P(x)-F(x)\} \tag{3}$$

and

$$d/dx[\ln F(x)]=-\lambda\{1-P(x)[F(x)]^{-1}\}. \tag{4}$$

Equation (3) shows that the maximum of $F(x)$ occurs at its intersection with $P(x)$, and Eq. (4) shows when it is safe to fix λ by the slope of the "tail" of $F(x)$.

For short lifetimes it is preferable to use most of the experimental points. By integration of (3)

$$\lambda=\{F(A)-F(B)\}\left[\int_A^B (F(x)-P(x))dx\right]^{-1}, \tag{5}$$

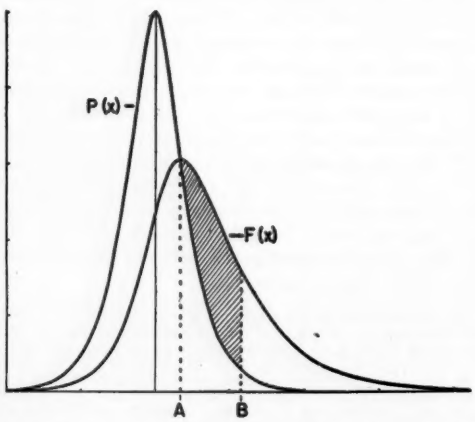

FIG. 1. By Eq. (5) λ is equal to the difference $\{F(A)-F(B)\}$ divided by the shaded area. The delayed curve $F(x)$ is calculated by relation (2) from the assumed prompt curve $P(x)$.

so that λ can be found from that section $A\leqslant x\leqslant B$ of the delay curve which is best determined (Fig. 1). The statistical errors of the tail occur only in the determination of total areas for normalization.

The parameter λ characterizes the asymmetry of $F(x)$. It could be determined from $F(x)$ alone if the true zero of the delay were known and if $P(x)$ were symmetrical.

Let $G(x)=F(-x)$ and $Q(x)=P(-x)$. Then from (5) one has

$$\lambda=\{F(A)+G(A)-F(B)-G(B)\}\left[\int_A^B (F(x)-G(x))dx-C\right]^{-1} \tag{6}$$

in which

$$C=\int_A^B [P(x)-Q(x)]dx$$

measures of the asymmetry of $P(x)$.

If the circuit itself introduces no asymmetry, $G(x)$ may be found experimentally by reversing the roles of the two sides of the circuit. This fixes the zero of delay. The correction C may still not vanish, due to asymmetries introduced by the excitation, but C will be small in a good experiment.

This discussion applies to simple decays, and experimental arrangements in which the daughter radiation is able to excite only one side of the circuit. More complicated cases can be similarly treated. The general relation between moments given by Bay[3] is an immediate consequence of (1).

The integrals in (5) and (6) should be computed numerically from experimental data. This allows a definite statement of statistical error. The arithmetic error so introduced becomes negligible if experimental settings are arranged in triples to which Simpson's rule can be applied.

[1] R. E. Bell and H. E. Petch, Phys. Rev. **76**, 1409 (1949).
[2] R. E. Bell and R. L. Graham, Phys. Rev. **78**, 490 (1950).
[3] Z. Bay, Phys. Rev. **77**, 419 (1950).

Measurement of a Second Half-Life in Yb^{170}

R. E. BELL AND R. L. GRAHAM
Atomic Energy Project, National Research Council of Canada, Chalk River, Ontario, Canada
April 3, 1950

THE half-life of the 83-kev transition in Yb^{170} has been measured as $(1.60\pm0.2)\times10^{-9}$ sec. by delayed coincidence techniques, using the coincidence apparatus of Bell and Petch.[1] The experimental data were analyzed by the methods of Newton[2] and Bay.[3]

The beta-spectrum of Tm^{170} is complex,[4] a fraction of the beta-disintegrations leading to an excited state of Yb^{170}. This state is de-excited by the emission of 83-kev gamma-rays and K, L, and M conversion electrons. A source of Tm^{170} on a backing of 1.5-mg/cm^2 Al foil was mounted in a thin-lens beta-ray spectrometer. Coincidences were observed between nuclear beta-rays incident on an anthracene-1P21 counter placed immediately behind the source, and 73-kev L-conversion electrons focused by the spectrometer on a second similar counter. The delayed-coincidence resolution curve was recorded by an automatic device which inserted lengths of cable to delay the pulses and recorded the corresponding coincidence counting rates. Counting was carried out for equal times at the different delays. The resulting curve is shown in Fig. 1.

The resolution curve for prompt coincidences was obtained by replacing the source of Tm^{170} by one of Au^{198} without otherwise changing the apparatus. The coincidences then observed were due to conversion electrons of the 411-kev excited state of Hg^{198} in the source counter, and 73-kev nuclear beta-rays of Au^{198} in the spectrometer counter. This method of comparing Tm^{170} with Au^{198} ensures that any effects on the resolution curves due to electron transit time in the spectrometer or small pulse size from the 73-kev electron counter will cancel. In order to establish the promptness of the Au^{198} coincidences, the Au^{198} beta-conversion line coin-

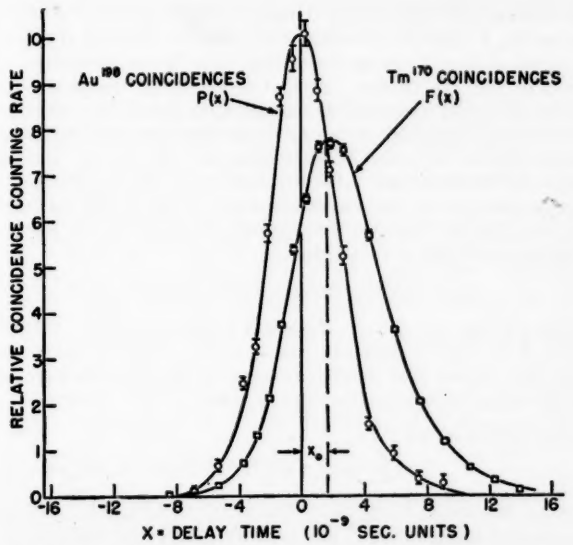

FIG. 1. Coincidence resolution curves. $P(x)$ is the prompt resolution curve obtained with an Au^{198} source and $F(x)$ is the delayed resolution curve observed with a Tm^{170} source, normalized to equal included areas. The curves intersect at $x=x_0$ where $F(x)$ is a maximum. Positive values of the delay time x correspond to delaying the pulses from the Tm^{170} beta-ray counter behind the source. The standard deviations of the points are indicated by vertical bars.

cidence resolution curve was compared in the spectrometer with the resolution curve obtained when hard beta-rays were passed through the anthracene crystals of both counters. The results showed that the half-life of the 411-kev transition in Hg^{198} does not exceed 2×10^{-10} sec.[5] The Au^{198} coincidences are thus prompt for purposes of this experiment.

Figure 1 shows the prompt resolution curve $P(x)$ observed for Au^{198} and the delayed resolution curve $F(x)$ observed for Tm^{170}, plotted to the same included area. Positive values of the delay, x, correspond to delaying the pulses from the Tm^{170} beta-ray counter behind the source. The areas were determined by numerical integration and the statistical error in equalizing the areas is less than two percent. The two curves obey the criterion[2] of intersecting at the maximum of $F(x)$.

The mean life $\tau=1/\lambda$ for the Yb^{170} transition has been evaluated from the curves of Fig. 1 in three ways. Newton's[2] Eq. (5) applied with $A=-\infty$, $B=x_0$ gives $\tau=(2.34\pm0.12)\times10^{-9}$ sec., and with $A=x_0$ and $B=\infty$ gives $\tau=(2.31\pm0.09)\times10^{-9}$ sec., the average being $\tau=(2.32\pm0.07)\times10^{-9}$ sec. Bay's[3] Eq. (4) gives $\tau=(2.28\pm0.08)\times10^{-9}$ sec. The value of τ obtained in the usual way from the slope of $\log F(x)$ at large positive delay is $(2.3\pm0.4)\times10^{-9}$ sec.

The new analyses give much improved statistical accuracy for a case such as this one, where $P(x)$ and $F(x)$ overlap to a large extent. The standard deviations quoted were obtained by carrying the standard deviations of the measured points through the numerical integrations. Averaging the above determinations of τ and making allowance for the fact that the Au^{198} coincidences are only known to be prompt within 2×10^{-10} sec., we get $\tau=(2.3\pm0.3)\times10^{-9}$ sec., or $T_{\frac{1}{2}}=(1.6\pm0.2)\times10^{-9}$ sec. for the 83-kev transition in Yb^{170}.

The new methods of analysis enable the present coincidence apparatus to set upper limits on half-lives of the order of 2×10^{-10} sec., and to measure half-lives of the order of 5×10^{-10} sec. with fair accuracy.

[1] R. E. Bell and H. E. Petch, Phys. Rev. **76**, 1409 (1949).
[2] T. D. Newton, Phys. Rev. **78**, 490 (1950).
[3] Z. Bay, Phys. Rev. **77**, 419 (1950).
[4] J. S. Fraser, Phys. Rev. **76**, 1540 (1949).
[5] Bell and Petch (reference 1) showed that this half-life was less than 2.1×10^{-9} sec. The new reduced limit was obtained with the same apparatus but using improved methods of analysis of coincidence resolution curves.

Saturation Backscattering of Positive Electrons

H. H. SELIGER
National Bureau of Standards, Washington, D. C.
April 3, 1950

THE percentage backscattering of positive electrons from a source backing thick enough to ensure complete absorption of the beta-particles (saturation thickness) has been studied under the conditions of geometry shown in Fig. 1. It was found that the backscattering of the positrons of Na^{22} under the same geometrical conditions is consistently 30 to 40 percent lower than the electron backscattering of I^{131}, RaE, and P^{32}.

As a check on the accuracy of the experimental technique, the backscattering of the negative electrons of I^{131}, Bi^{210}, and P^{32} was also investigated. In one set of experiments the weightless deposit approximately 12 mm in diameter was mounted on a thin aluminum leaf (0.22 mg/cm²) and net counting rates were measured with saturation thicknesses of Be, C, Al, Fe, Cu, Ag, and Pb backings placed directly beneath the weightless source. The net counting rate with no backing material beneath the source was assumed to be due only to forward radiation. The ratio of the net counting rate measured with a backing of atomic number Z to the net counting rate due to forward radiation will then indicate the percentage backscattering. In a different set of experiments, aliquots identical in activity and geometric size within one percent were deposited directly on polished faces of disks of saturation thickness again ranging from Be to Pb. The net counting rate in each case was plotted against the atomic number of the backing material and this curve was extrapolated to $Z=0$. The net counting rate extrapolated for $Z=0$ was assumed to be due to forward radiation only. The percentage backscattering was then calculated in the same manner as before.

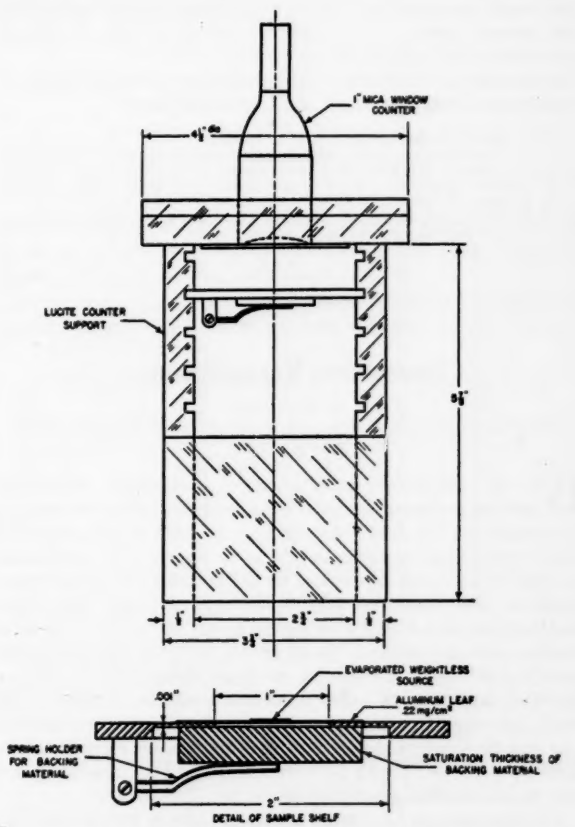
1" MICA WINDOW COUNTER
LUCITE COUNTER SUPPORT
EVAPORATED WEIGHTLESS SOURCE
ALUMINUM LEAF 22 mg/cm²
SPRING HOLDER FOR BACKING MATERIAL
SATURATION THICKNESS OF BACKING MATERIAL
DETAIL OF SAMPLE SHELF

FIG. 1. Diagram showing dimensions of counter and source used in the backscattering experiments.

UNIVERSITY OF MICHIGAN LIBRARIES

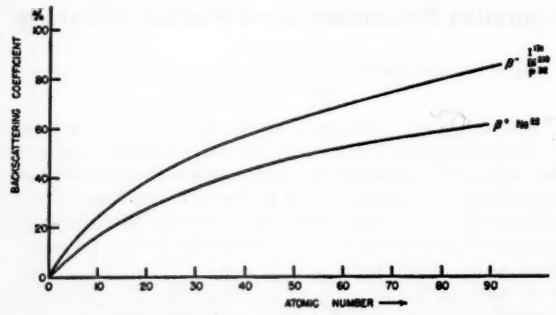

FIG. 2. Experimentally determined curves for the percentage of the backward radiation reflected into the counter as a function of the atomic number of the backing material.

The results of these experiments for I^{131}, RaE, P^{32}, and Na^{22} are shown in Fig. 2. The curve for percentage backscattering of negative electrons as a function of Z indicates that the backscattering is energy independent within the experimental accuracy, and is in good agreement with results obtained by Burtt[1] and by Engelkemeir.[2] This energy independence for negative electrons was indicated in a paper by Schonland,[3] although his quantitative results were lower, probably due to differences in geometry.

It is a little surprising to note the lower values of backscattering found for the positrons of Na^{22} as compared to the electrons of I^{131}, although the maximum energies of the β^+-particles and of the β^--particles are nearly equal.

Annihilation of positrons should account for a reduction of backscattering by only a few percent according to theoretical data.[4] However, the relativistic treatment of Coulomb scattering shows a marked increase of β^--scattering and a reduction of β^+-scattering as compared with the Rutherford formula.[5] This effect tends to explain our results, except that it ought to increase with atomic number, while the two curves in Fig. 2 indicate approximately a constant ratio.

A detailed interpretation of the present experiments seems to require additional theoretical and experimental work.

[1] B. P. Burtt, Nucleonics 5, No. 2, 28 (1949).
[2] D. W. Engelkemeir, Plutonium Project Memorandum MUC-NS 312.
[3] B. F. S. Schonland, Proc. Roy. Soc. A108, 187 (1925).
[4] W. Heitler, *Quantum Theory of Radiation* (Clarendon Press, Oxford, 1936), p. 231.
[5] N. F. Mott and H. S. W. Massey, *The Theory of Atomic Collisions* (Clarendon Press, Oxford, 1933), pp. 80–85.

Dissociative Recombination

D. R. BATES*
Department of Astronomy, Princeton University, Princeton, New Jersey
March 6, 1950

BY the successful exploitation of microwave techniques several groups of workers[1] have recently derived interesting information on the decay of ionization. In most of the gases used there could be no complications due to negative ion formation, and the decay could apparently be attributed to electron recombination. The measured rate coefficients, α, were very high, ranging from about 10^{-8} cm³/sec. to about 10^{-6} cm³/sec. for the various gases investigated. In an earlier letter[2] it was shown that atomic ions could scarcely be involved since radiative recombination, and the few other processes available to these, seem much too slow. Consideration was therefore given to molecular ions and the suggestion was made that dissociative recombination, $XY^+ + e \rightarrow X' + Y'$, might be very effective. This possibility will now be examined in greater detail.

The reaction can be treated as taking place in two stages. As a result of a radiationless transition an excited molecule, XY' is formed. If this is unstable its constituents may move apart under the influence of their mutual repulsion thereby preventing auto-ionization. A quantal expression is available for the rate at which electrons of energy ϵ enter the excited state. It can be written in terms of $f(\epsilon)$, the familiar Franck-Condon factor measuring the degree of overlap between the nuclear wave functions concerned in the initial transition, and of $t_A(\epsilon)$, the time associated with the auto-ionization process. To determine the fraction of excited molecules that dissociate, $t_S(\epsilon)$, the time for effective separation to occur, must also be introduced. From the product of the rate and the fraction the following approximate formula for the recombination coefficient is obtained:

$$\alpha(\epsilon) = \{rh^3 f(\epsilon)/8\pi(2m^3\epsilon)^{\frac{1}{2}}(t_A(\epsilon)+t_S(\epsilon))\}, \quad (1)$$

where r is the ratio of the statistical weight of XY' to that of XY^+, h is Planck's constant and m is the electronic mass. As usual $f(\epsilon)$ is such that $\int_\epsilon f(\epsilon)d\epsilon$ is unity. If the electrons have an energy distribution corresponding to a temperature T then

$$\alpha(T) = \{rh^3/2(2\pi mkT)^{\frac{1}{2}}\} \times \int_\epsilon \{\exp(-\epsilon/kT)f(\epsilon)/(t_A(\epsilon)+t_S(\epsilon))\}d\epsilon. \quad (2)$$

k being Boltzmann's constant. Numerical substitution, and the adoption of mean values t_A and t_S for $t_A(\epsilon)$ and $t_S(\epsilon)$ respectively, yields

$$\alpha(T) = 2\cdot1\times10^{-16}\{r/T^{\frac{1}{2}}(t_A+t_S)\} \times \int_\epsilon \exp(-\epsilon/kT)f(\epsilon)d\epsilon \text{ cm}^3/\text{sec}. \quad (3)$$

Accurate computations for any specific ion would be extremely difficult to perform, but by making estimates of the permissible magnitudes of the various quantities appearing in the formula some indication of the potentialities of the recombination mechanism under consideration can be obtained. Clearly r can be appreciably greater than unity; a figure as high as 10 is not impossible, especially if a number of excited states are included. It is not easy to assess t_A; for many transitions it must certainly be long, but judging from the theoretical and spectroscopic evidence available[3] it may actually be of the order of 10^{-13} sec. in some instances, and even shorter times have been reported. The value of t_S may also be of this order since the relative velocity is perhaps 10^8 cm/sec. and since a movement of less than 10^{-8} cm will often be sufficient to ensure the permanence of the neutralization.[4] The integral in (3) depends on details of the potential curves which in general are unknown; it will be very small unless $f(\epsilon)$ is appreciable for low ϵ, but in favorable circumstances it can equal the numerical value of $2kT$ when expressed in electron-volts. If these tentative estimates of the *possibilities* are accepted, and if (for the sake of definiteness) T is taken to be 250°K a recombination coefficient of some 10^{-7} cm³/sec. is obtained. As need scarcely be stressed, little significance should be attached to this figure which is given merely to demonstrate that *in certain by no means exceptional cases* dissociative recombination can be extremely rapid.

The assumption has hitherto been made that the ions studied by Brown, Holt and their associates were diatomic. This is not necessarily true. In some instances they may conceivably have been complex and the fragments may have been in part molecular. It is most important to determine the nature of the ions by means of optical or mass spectrographs. For until this is done the results obtained cannot be extrapolated to the low pressures and comparatively high temperatures that are of interest for many geophysical and astrophysical applications. In this connection it may be noted that even in the E layer the value of α found by radio-workers[5] is only 10^{-8} cm³/sec. which is more than an order smaller than the higher values obtained in the laboratory.

Finally, attention may be drawn to the fact that much might be learned from a supplementary experimental investigation of the closely analogous process of dissociative attachment (e.g., $XY + e \rightarrow X' + Y^-$) in both di- and polyatomic gases. The coefficients so far obtained are of order 10^{-10} cm³/sec. or smaller.[6] In view of effects due to the absence of an attractive Coulomb field, and to the restricted number of excited states, etc., it would be

expected that they would in general be less than those for recombination. Further data on them would be useful.

* On leave from the Department of Mathematics, University College, London.

[1] M. A. Biondi and S. C. Brown, Phys. Rev. **75**, 1700 (1949) and **76**, 1697 (1949); Holt, Richardson, Howland, and McClure, Phys. Rev. **77**, 239 (1950). I wish to take this opportunity of thanking Professors Brown and Holt and their associates for a helpful discussion of their experiments.
[2] D. R. Bates, Phys. Rev. **77**, 718 (1950).
[3] Ta-You Wu, Phys. Rev. **66**, 291 (1944); A. G. Shenstone, Phil. Trans. Roy. Soc. **A241**, 297 (1948).
[4] It is apparent that "stabilization" by the emission of radiation or by collisions of the second kind, are very inefficient by comparison. Thus the time associated with the former cannot be much less than 10^{-8} sec.: and at a pressure of, say, 25 mm Hg, that associated with the latter would still be as long as 10^{-10} sec. even if the deactivation cross section were several orders greater than the gas kinetic.
[5] S. K. Mitra, *The Upper Atmosphere* (Royal Asiatic Society of Bengal, Calcutta, 1948).
[6] H. S. W. Massey, *Negative Ions* (Cambridge University Press, London, 1938).

The Detection of Artificially Produced Photo-Mesons with Counters*

J. Steinberger and A. S. Bishop
Radiation Laboratory, Department of Physics, University of California, Berkeley, California.
March 23, 1950

DELAYED coincidences between mesons and their decay electrons, as first observed by Rasetti,[1] have been widely used in cosmic-ray research as a means of counting mesons. A closely related technique in which the delay is timed from a very short proton pulse, has been used by Alvarez *et al.*[2] in the first electronic detection of artificially produced mesons. With the synchrotron the x-ray pulses are not short enough for the use of the latter method; therefore that of Rasetti has been used, with the x-ray pulse widened to about 2 msec. in order to reduce random coincidences.

When a positive π-meson comes to rest, it disintegrates very quickly into a μ-meson, and this in turn into an electron, with the well-known 2.1×10^{-6}-sec. mean-life. The range of the μ-meson is only $\sim$0.2 g, so that when this process takes place in a scintillation crystal with linear dimensions of the order of several centimeters, a large fraction of the decay electrons will also appear in the crystal. The $\pi\rightarrow\mu$-decay is too rapid to be resolved in the electronics of the experiment; instead, the characteristic half-life of the $\mu\rightarrow e$ decay is used to identify the meson. Negative mesons coming to rest in condensed matter do not produce decay electrons and therefore are not counted.

The apparatus is sketched in Fig. 1. The 330-Mev (max.) x-ray beam is collimated to 1½ in. diameter and allowed to strike a target. The mesons produced at the target are detected in a telescope of three anthracene scintillation crystals after traversing variable amounts of aluminum absorber. The telescope can be rotated about the target in the plane of the beam. A meson is counted if it comes to rest in crystal II and its decay electron appears in the same crystal. That is, we require a pulse simultaneously in crystals I and II, but no pulse in crystal III. This coincidence starts several successive delay gates of two microsecond time width and if a pulse appears in crystal II during the gate time, it is recorded in that channel. There is an appreciable number of accidental delayed coincidences. These can be calculated from the known single counting rates, gate width, and duty cycle, and are then subtracted. The accidental rate is usually about 10 to 20 percent of the counting rate in the first channel. When the target is removed, both accidental and real coincidences are smaller by a factor of several hundred.

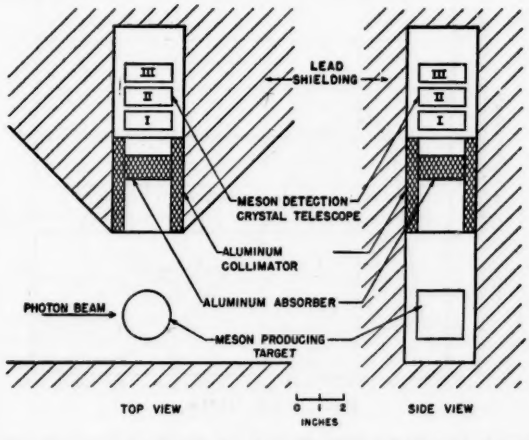

FIG. 1. Arrangement of target, absorbers, and meson detection scintillation counter telescope.

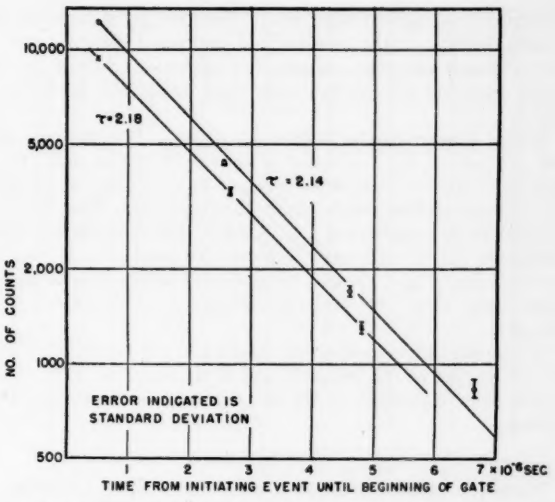

FIG. 2. Relative counting rates in the delayed channels. Two sets of data are shown because three channels were used at first, later four.

After the background subtraction the counting rates in the several delay channels should reproduce the exponential $\mu\rightarrow e$ decay. The lifetime data so far obtained are plotted in Fig. 2. When the x-ray energy is reduced below threshold no mesons are observed.

Since the crystals are proportional counting devices, the counting rates are functions of the amplitudes required for those pulses

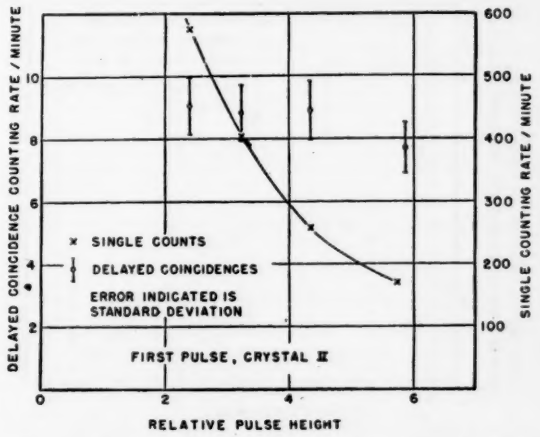

FIG. 3. Counting rate in crystal II (points without statistical error) and meson counting rate (with mean statistical error indicated) as a function of the minimum voltage required of the first pulse in crystal II.

entering into a delayed coincidence. The stability of the detecting system depends on the sensitivity of the meson counting rate to the minimum amplitudes required of the pulses. Such a plateau curve (counting rate *vs.* minimum pulse amplitude) is shown in Fig. 3.

With a synchrotron beam intensity of about 10^{10} Mev/sec. and the geometry of Fig. 1, a target of 4 g/cm² of carbon, and 1 in. of aluminum absorber, corresponding to a meson energy of 54 Mev, the meson counting rate is about 15 counts/min. This makes it possible to do experiments more quickly than with photographic emulsions. On the other hand, only positive mesons can be counted in this manner, and absolute cross-section measurements have a large error, since the detection efficiency is not known with precision.

We should like to express our thanks to Professor E. McMillan for his support of this research, and to the operating crew of the synchrotron, especially to Mr. W. Gibbins, for their able cooperation.

* This work was sponsored under the auspices of the AEC.

[1] F. Rasetti, Phys. Rev. **60**, 198 (1941).
[2] Alvarez, Longacre, Ogren, and Thomas, Phys. Rev. **77**, 752 (1950).

Preliminary Results on the Production of Mesons by Photons on Carbon and Hydrogen*

J. Steinberger and A. S. Bishop
Radiation Laboratory, Department of Physics, University of California, Berkeley, California
March 23, 1950

THE method of meson detection described in the preceding letter[1] is being applied to the study of the production of positive mesons by x-rays on hydrogen and heavier nuclei. We report here some preliminary results in which the hydrogen cross sections are obtained by subtracting the yields on carbon from those on paraffin. All the measurements reported here are being continued, and hydrogen cross section measurements with a liquid hydrogen target are in progress.

In interpreting these results it should be kept in mind that both energy and angle of production of the meson are measured, and these determine the incident x-ray energy by momentum and energy conservation in the case of production on hydrogen. This means, for instance, that a knowledge of the energy distribution of the mesons at a fixed angle of production and of the energy

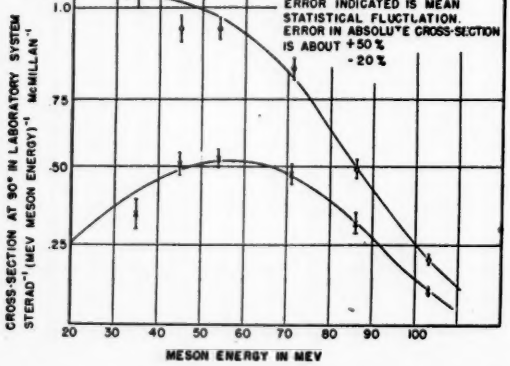
CARBON CROSS-SECTION
HYDROGEN CROSS-SECTION
ERROR INDICATED IS MEAN STATISTICAL FLUCTUATION. ERROR IN ABSOLUTE CROSS-SECTION IS ABOUT +50% -20%
CROSS-SECTION AT 90° IN LABORATORY SYSTEM STERAD⁻¹ (MEV MESON ENERGY)⁻¹ McMILLAN⁻¹
MESON ENERGY IN MEV

FIG. 1. Production of mesons by photons on carbon and hydrogen at 90°. The photons have a bremsstrahlung spectrum with a 330-Mev maximum energy. The number of McMillans in a bremsstrahlung beam is defined as the total energy in the beam divided by the maximum photon energy.

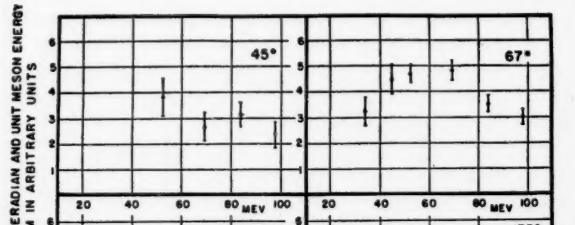

FIG. 2. The production of mesons in $C_{17}H_{14}$ at various angles as a function of the meson energy.

distribution of the incident x-ray beam allows a determination of the excitation function for photo-meson production. We feel however that the energy, angular and statistical accuracies of the data reported here do not yet warrant such an analysis.

Figure 1 shows the relative number of mesons produced by carbon atoms and hydrogen atoms at 90° in the laboratory system as a function of energy. The incident photons have a bremsstrahlung spectrum of 330-Mev maximum energy. The meson energy is determined from the energy-range relationship, and it is assumed that the nuclear absorption of mesons is zero.[2] The carbon cross sections have already been determined by photographic detection methods,[3] and the two results agree within the statistical inaccuracies. The most startling fact shown in Fig. 1 (and also in Fig. 3) is that the cross section of the six bound protons in a carbon atom is only about twice as large as that of a single free proton. It is perhaps surprising that the effects of nuclear binding are so pronounced. However, a more detailed analysis[4] shows that since the energy of the recoil nucleons is not very much greater than the Fermi energy, this inhibition of the reaction in the case of complex nuclei may be no more than a manifestation of the exclusion principle.

Figure 2 shows an attempt at obtaining similar information at several other angles. However, the statistical accuracies are not great enough to make the subtraction meaningful. So the data

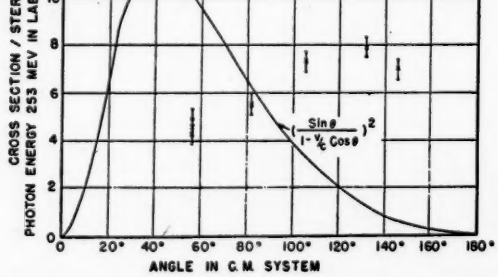

FIG. 3. The angular distribution of the mesons produced by 250-Mev (laboratory system) photons on hydrogen and carbon. The theoretical curve is that for an electric dipole photo-effect, $\{\sin\theta/[1-(v/c)\cos\theta]\}^2$.

are added, instead of subtracted, and the points represent the production by a molecule of composition $C_{17}H_{14}$. The interesting thing here is that the cross sections are fairly independent of angle. This is shown again in Fig. 3. Here the cross sections are shown for five angles. At each angle a different amount of absorber is used, so that for hydrogen the photon energy at all angles is unique, 253 Mev. For the carbon points the analysis has been carried through in the same way, although in this case the binding of the nucleons makes the momentum and energy conservation arguments invalid. The cross sections have been plotted in absolute units; however, the error in the absolute value may be quite large. The errors indicated are the statistical errors, and represent the likely errors in the relative values. The theoretical curve in Fig. 3 is a plot of the function $\{\sin\theta/[1-(v/c)\cos\theta]\}^2$, the angular distribution of a simple electric dipole photo-effect. It is also substantially the prediction of the scalar meson theory.[5] It can be seen that the actual distribution is quite incompatible with this, in fact the only theories which predict such a flat distribution are those in which the electromagnetic interaction is chiefly with the magnetic moment of the nucleons rather than the electric charge of the meson. This is so for the pseudoscalar meson theory with both types of coupling.[6] However, the same theories which, because of the tight coupling of the mesons to the magnetic moment of the nucleon, predict a flat angular distribution, also predict nuclear radii of the dimensions of the Compton wavelength of the nucleons and can therefore hardly be taken seriously. On the one hand, the theories which predict a different distribution cannot be rejected because there remains the possibility, though small, that the disagreement is caused by the fact that the calculations are incorrect because relativity and the largeness of the coupling constant are not simultaneously taken into account. On the other hand, those theories which predict the observed result disagree violently with experiment in the nuclear force problem. It seems, therefore, impossible to make a meaningful comparison of the experiment with existing theory.

We wish to thank Professor E. McMillan for his support, Professor R. Serber for theoretical discussions, and Mr. Gibbins and the synchrotron crew for their assistance.

* This work was done under the auspices of the AEC.

[1] J. Steinberger and A. S. Bishop, Phys. Rev. **78**, 494 (1950).

[2] If, instead, the nuclear mean free path of mesons in aluminum were 200 g/cm², this would mean that the 100-Mev points would be too low by about 15 percent; lower energies would have proportionately smaller errors.

[3] McMillan, Peterson, and White, Science **110**, 579 (1949).

[4] The calculations for helium targets have been made by G. Chew and H. Lewis. They show that one may easily account for a σ (free proton)/σ (bound proton) $=3$, but it is not possible to make an accurate prediction of the expected effect. We wish to express our thanks to the authors for permission to quote their results before publication.

[5] In the scalar theory this result is obtained in relativistic perturbation theory, and also rigorously without expansion in g if the nucleons are assumed to have infinite mass. We are indebted to Drs. K. M. Case and K. Watson who have independently obtained this result.

[6] The perturbation theoretical results have been obtained by H. Feshbach and M. Lax, Phys. Rev. **76**, 134 (1949) and more completely by K. Brueckner (to be published).

Proton-Proton Scattering in Charged Scalar Theory*

K. A. Brueckner and K. M. Watson
Radiation Laboratory, University of California, Berkeley, California
March 23, 1950

THE recent measurements by the Berkeley experimentalists[1] of 345-Mev proton-proton and 280-Mev neutron-proton scattering have shown a remarkable difference in the two types of scattering. The neutron-proton scattering has a cross section of 36 millibarns and is very strongly peaked at 0° and 180° in the center-of-mass system; the proton-proton scattering has a much larger differential cross section at 90 degrees and is nearly isotropic in the angular range 20 to 160 degrees.

An immediate qualitative explanation of these differences is obtained by assuming that neutron-proton scattering takes place in lowest order through the exchange of single charged mesons, while proton-proton scattering in the lowest order occurs only through the exchange of pairs of charged mesons. This is equivalent to assuming that protons are coupled directly only to positive mesons.[2] If the calculations of Watson and Lepore[3] on the radiative corrections to nuclear forces for pseudoscalar theory are considered in this hypothesis, it is found that not even rough qualitative agreement can be obtained with the experimental results. We therefore have calculated the neutron-proton and proton-proton scattering to fourth order in the meson nucleon coupling, using charged scalar theory.

It is found that the only important contributions to the fourth-order processes come from the exchange of two mesons. Terms corresponding to the polarization of the vacuum by the mesons give negligible contributions. The resulting fourth-order contribution to the S-matrix, ignoring corrections of order v^2/c^2, which are less than 10 percent, is

$$M_4(PP)=i(f/2\pi)^4(V_{PP}{}^4-\text{exchange term}), \tag{1}$$

where

$$V_{PP}{}^4=\frac{1}{M^2}\int_0^1 dx\int_0^x dy\frac{4y}{[y^2+(1-y)\rho+(1-x)(x-y)\theta]^2} \tag{2}$$

and

$$\rho=\mu^2/M^2,\quad \theta=(\mathbf{P}-\mathbf{P}')^2/M^2C^2.$$

The contribution to $N-P$ scattering in the fourth-order is very similar to that given by Eq. (1). It is apparent that since these matrix elements depend only on the momentum transfer, they can be expressed in a coordinate representation as purely static potentials. It is interesting to observe that the $P-P$ scattering given by (1) is almost exactly equivalent to that given by the Born approximation applied to the static Yukawa potential[4]

$$-(f/2\pi)^4(11.15/4\pi)(e^{-kr}/r),$$

where

$$k=2.80\mu c/\hbar=0.207\times10^{-14}\ \text{cm}^{-1}.$$

The differential cross section at 180 Mev for the $N-P$ scattering including the second-order contribution, and for the $P-P$ scattering are given in Fig. 1. Corrections of order v^2/c^2 have been included. It is apparent that the inclusion of the fourth-order $N-P$ scattering tends to reduce the asymmetry of the $N-P$ scattering about 90 degrees, and that the $P-P$ scattering is much less strongly peaked at 180 degrees than the $N-P$ scattering. These are in the direction of the effects shown by the experimental measurements. It is also apparent, however, that for $f^2/2\pi\sim\frac{1}{2}$, the contributions of the fourth-order terms are much too small. The $P-P$ total cross section is less than $\frac{1}{10}$ that for the $N-P$ scattering.

The failure of the scalar theory to give a better qualitative

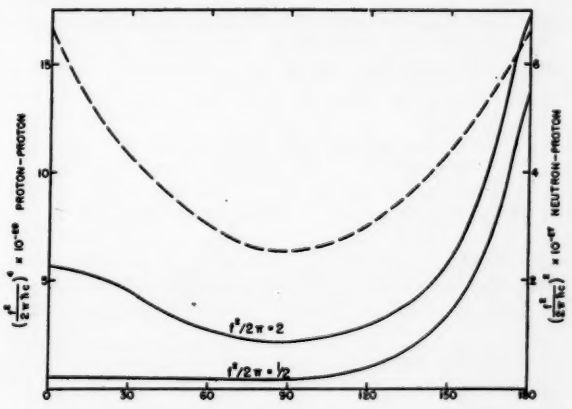

FIG. 1. N–P scattering (solid curves) and P–P scattering (dashed curve) at 180 Mev for the charged scalar theory.

UNIVERSITY OF MICHIGAN LIBRARIES

explanation of the experimental observations is due to the smallness of the fourth-order contributions. It actually appears that the weak coupling approximation can be applied to scalar theory with considerable justification. However, couplings which are strong enough to predict sufficiently large $P-P$ scattering in fourth-order would at the same time invalidate the neglect of processes of even higher order. Inclusion of such processes would tend to remove the asymmetry in the $N-P$ and $P-P$ scattering which exists for a charged theory only if the lowest few orders in which the process can take place are considered.

There does not appear at present to be any simple way of applying meson theory in even a very qualitative way to the processes of high energy nucleon-nucleon scattering. Both the weak and strong coupling approximations seem to be invalidated by comparison of such calculations with experiment. It is not impossible, however, that in the region of intermediate coupling some of the asymmetry in the $N-P$ and $P-P$ scattering might be retained, while at the same time the correct magnitude of the forces be predicted.

* This work was sponsored by the AEC.
[1] R. Christian, Phys. Rev. **78**, 82 (1950).
[2] Experimental observations at Berkeley on meson production have not yet indicated conclusively that neutral mesons are coupled directly to protons.
[3] K. Watson and J. Lepore, Phys. Rev. **76**, 1157 (1949).
[4] The range of this potential is too short to agree with measurements of low energy $P-P$ scattering.

Production Cross Sections for π^+ and π^- Mesons by 345-Mev Protons on Carbon at 90° to the Beam*, **

C. RICHMAN AND H. A. WILCOX
Radiation Laboratory, Department of Physics, University of California, Berkeley, California
February 14, 1950

WE have developed a method for measuring the absolute production cross sections for π^+ and π^- mesons when various kinds of nuclei are bombarded with high energy charged particles from the Berkeley 184-inch synchro-cyclotron. In this method the external beam from the cyclotron is allowed to pass through the target to be studied. It is then received in a Faraday cup and is integrated by conventional methods. The π^+ and π^- mesons produced by the beam leave the target with various energies, E, and at various angles, θ, to the beam. Large absorber blocks are arranged so that mesons leaving the target at any angle are stopped in these blocks at depths determined by their initial energies. Nuclear emulsions are embedded in the absorbers to sample the population of stopped mesons.

The developed emulsions are scanned under high magnification. The ends of the meson tracks are distinguished from the "background tracks" caused by other charged particles by their characteristic scattering and rapid change in grain density. An observed meson is identified as a π^+ if it gives rise to a μ-meson,[1] and as a π^- if it produces a nuclear star.[2] The true number of π^- mesons is 1.37 times the star producing mesons.[3]

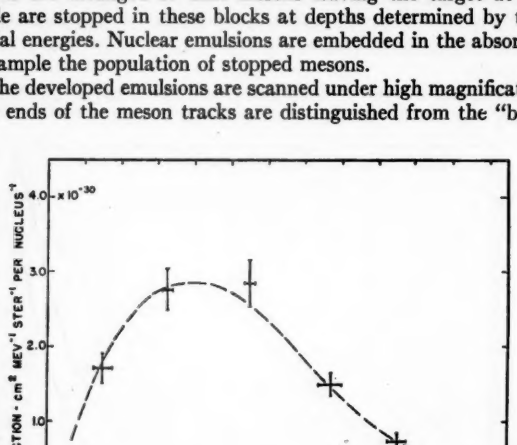

FIG. 1. Differential cross section for the production of π^+ mesons in carbon by 345-Mev protons. Angle of observation $=90°\pm12°$ to beam direction.

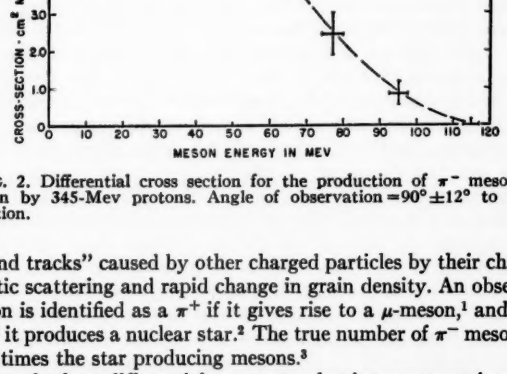

FIG. 2. Differential cross section for the production of π^- mesons in carbon by 345-Mev protons. Angle of observation $=90°\pm12°$ to beam direction.

The absolute differential meson production cross sections are calculated from the geometry, the number of mesons observed per unit volume of emulsion, and the stopping powers of the emulsion and the absorbers. The results are subject to a number of systematic errors. For this reason we assign the usual statistical probable errors to our relative cross sections, whereas to the absolute values we assign an additional ±15 percent.

As a first application of the method we have studied the mesons production by protons on carbon. The beam current was $\sim10^{-11}$ amperes and the energy was 345 Mev with a spread of about 2 Mev. Thin graphite targets were used. A preliminary study of the energy and angular distribution of mesons and of the other charged particles coming from the carbon target showed that the simple method described above is entirely satisfactory for observations at angles from about 60° to nearly 180° from the direction of the beam. For the forward angles on the other hand, the background on the plates due to the protons scattered by carbon makes scanning very difficult. Our first work has been done at $\theta=90°\pm12°$.

Figure 1 shows the differential cross section $\sigma_+(E, 90°)$ for the production of π^+ mesons in carbon by 345-Mev protons as a function of the energy of the mesons. This curve is based on 205 observed $\pi-\mu$-events. The probable errors shown on the graph are purely statistical in origin and are valid for the relative values of the plotted curves. To these errors must be added the above mentioned ±15 percent to take account of possible systematic errors in the absolute values of the cross sections. Figure 2 is a similar curve for the π^- mesons. It is based on 48 observed meson-initiated stars. The integral of the σ_- curve over meson energy is $(4.0\pm1.6)\cdot10^{-29}$ cm² ster.$^{-1}$ nucleus^{-1}, and the similar integral of the σ_+ curve is $(2.0\pm0.5)\cdot10^{-28}$ cm² ster.$^{-1}$ nucleus^{-1}. The ratio of these integrals is 0.2 ± 0.1. The negative to positive ratio, σ_-/σ_+, at each meson energy is limited in accuracy by the scarcity of π^- mesons, but there is some evidence to indicate that it drops off at the very high meson energies.

We wish to thank Professors E. O. Lawrence, L. W. Alvarez, and R. L. Thornton for their interest and encouragement during the whole course of this work. We also wish to thank Mr. J. Vale and the cyclotron crew for making the bombardments.

* A preliminary account of this work was presented at the Physical Society meeting at Stanford University in December, 1949.
** This work was done under the auspices of the AEC.
[1] Lattes, Muirhead, Occhialini, and Powell, Nature **159**, 694 (1947); Lattes, Occhialini, and Powell, Nature **160**, 453, 486 (1947); Burfening, Gardner, and Lattes, Phys. Rev. **75**, 382 (1949).
[2] D. H. Perkins, Nature **159**, 126 (1947); G. P. S. Occhialini and C. F. Powell, Nature **162**, 168 (1948); E. Gardner and C. M. G. Lattes, Science **107**, 270 (1948).
[3] F. L. Adelman and S. B. Jones, Phys. Rev. **75**, 1468(A) (1949).

The Positive-Negative Ratio for π-Mesons Produced Singly in Collisions of Nucleons with Complex Nuclei

GEOFFREY F. CHEW AND JACK L. STEINBERGER
Department of Physics, University of California, Berkeley, California
February 23, 1950

THE primary purpose of this note is to point out that because of the Pauli principle the positive-negative ratio for π-mesons produced singly in collisions of nucleons with complex nuclei may be completely different from that due to collisions with an equal number of free nucleons. One must therefore be cautious in interpreting the meaning of this ratio when complex nuclei are used as targets for the neutron or proton beams from existing accelerators. A secondary purpose is to show that the exclusion principle leads one to predict a variation of the positive-negative ratio with meson and nucleon energies, the direction of the variation (but not the magnitude) being independent of detailed properties of the π-meson, which are still unknown.

Because of the Pauli principle, a kind of short-range order must exist in all complex nuclei: Near any given proton there are more neutrons than protons and vice versa. This notion finds its extreme expression in the alpha-particle model of nuclei, which pictures the nucleons as being grouped in clusters of four, two neutrons and two protons, with a relatively large distance between clusters. This model is not to be taken too seriously, but it may be used to show the direction of the exclusion principle effect. Consider the final configuration of the five nucleons which are close together when an incoming proton collides with one of the bound nucleons to produce a single π-meson. If a positive meson is created, one proton must be transformed into a neutron and as a result there are two protons and three neutrons. This is one more neutron than can be accommodated in a single unit cell of phase space, so at least one of these neutrons must have a high momentum. If a negative meson is produced, the final situation is that of one neutron and four protons, a situation which is obviously more strongly inhibited by the Pauli principle than the former, since two of the final particles must now have high momenta. Qualitatively, therefore, we see that the production of positives is favored when protons are incident, and vice versa with incident neutrons.

The order of magnitude of the effect depends on the energy available, after the meson is produced, to the two nucleons which actually collide. According to the uncertainty principle the momentum space which is densely occupied in a nuclear cluster corresponds to a maximum kinetic energy of about 25 Mev. If one of the nucleons which directly participates in the meson production happens to end up with the same spin as a nucleon which does not, then the former is required, roughly speaking, to have a kinetic energy greater than about 25 Mev or the transition is forbidden. It is not difficult to show that such a requirement fractionally reduces the available phase space by approximately 25 Mev divided by the total energy available to the two outgoing nucleons. If *both* outgoing nucleons are subject to this restriction, the reduction is approximately 50 Mev divided by the available energy. These rough estimates have been confirmed by detailed calculations using nuclear wave functions whose Fourier analysis is more realistic than the "square" assumed above.

The effect can obviously be big, according to our estimate, if the available energy is less than about 100 Mev. For example, if the available energy is 75 Mev, the positive-negative ratio might be altered in the approximate ratio

$$\left(1-\frac{25\text{ Mev}}{75\text{ Mev}}\right)\Big/\left(1-\frac{50\text{ Mev}}{75\text{ Mev}}\right)=2.$$

This would correspond, for instance, to mesons of 100-Mev kinetic energy produced by 340-Mev incident protons. Obviously the detailed nature of the meson-nucleon coupling affects the final orientation of the nucleonic spins, but it seems improbable that the exclusion effect could be washed out completely by a peculiar spin dependence of the reaction.

Because the effect depends inversely on the energy left to the nucleons, two predictions can be made: (1) for a fixed incident proton energy, the positive-negative ratio should increase with meson energy, approaching infinity at the upper limit of the meson spectrum; (2) for a fixed meson energy, the positive-negative ratio should increase as the proton energy is decreased, approaching infinity at the threshold for that particular meson energy. Both statements apply to the negative-positive ratio when neutrons are the incident particles. In testing these predictions experimentally, mesons of very low kinetic energy must be avoided because they may be affected by the Coulomb barrier.

Three separate pieces of existing information tend to confirm the influence of the exclusion principle. Richman and Wilcox[1] find 24 positives and no negatives when looking at 115-Mev mesons at 90° from a carbon target placed in a 345-Mev proton beam. The *average* positive-negative ratio for the entire meson spectrum at this angle, on the other hand, is 4.5 ± 1. Using a lead target in the same geometry, Weissbluth[2] finds a systematic increase of the positive-negative ratio with meson energy, only part of which seems attributable to a Coulomb effect. Finally Bradner[3] and co-workers find that the negative-positive ratio for 50-Mev mesons at 90° produced by a 280-Mev neutron beam incident on carbon is 12.6 ± 1.5, whereas the positive-negative ratio for the same source in the 345-Mev proton beam[4] is only 4.8 ± 0.5. The difference might be attributed to the exclusion principle because of the lower incident energy in the neutron case.

[1] C. Richman and H. Wilcox, Phys. Rev. **78**, 496 (1950).
[2] M. Weissbluth, private communication.
[3] Bradner, O'Connell, and Rankin, private communication.
[4] H. Bradner and S. B. Jones, Phys. Rev. **78**, 90(A) (1950).

Fine Structure of N_2O near 4.06μ in the Solar Spectrum*

J. H. SHAW, M. L. OXHOLM, AND R. M. CHAPMAN
Mendenhall Laboratory of Physics, Ohio State University, Columbus, Ohio
March 24, 1950

THE solar spectrum in the region 3.0 to 4.2μ has been investigated recently with a prism-grating spectrometer of the Pfund type, equipped with a 7200 line per inch echelette, replica grating and a Perkin-Elmer 13-cycle per second thermocouple-amplifier system.

During this mapping program, several spectrograms showing clearly the fine structure of the N_2O band at 4.06μ have been obtained.

The existence of N_2O in the solar spectrum was first reported by Adel[1] in 1939 and later verified by Migeotte[2] and Shaw, Sutherland, and Wormell[3] in 1948. It is interesting to note that the envelopes of the 3.9μ band, the 4.06μ band, and part of the 4.5μ band of N_2O stand out clearly in the solar spectra taken by Langley[4] in 1900.

The identification of the 4.06μ band was first reported by one of us,[3] but only a faint band envelope was observed.

In the present work, over 70 rotation lines in this band have been observed with the absorption of the strongest lines not more than 10 percent.

The position of the band center has been compared with laboratory data taken on the same spectrometer and has been located at 2461.8 cm^{-1}(vac.), on both laboratory and solar spectra.

* This work was supported in part by Contract No. AF19(122)65 between the U. S. Air Force and The Ohio State University Research Foundation, through sponsorship of the Geophysical Research Directorate, Air Materiel Command.
[1] A. Adel, Astrophys. J. **90**, 627 (1939).
[2] M. V. Migeotte, Astronomical J. **54**, 45 (1948).
[3] Shaw, Sutherland, and Wormell, Phys. Rev. **74**, 978 (1948).
[4] S. P. Langley, Ann. Ap. Obs., Smithsonian Inst. **1**, 1 (1900).

UNIVERSITY OF MICHIGAN LIBRARIES

Disintegration Scheme of In^{116}

HILDING SLÄTIS, STEFAN J. DU TOIT,* AND KAI SIEGBAHN
Nobel Institute of Physics, Stockholm, Sweden
March 16, 1950

SLOW neutrons produce two β-active isomers in indium with mass number 116 and half-lives of 13 sec. and 54 min. Especially the last isomer has been investigated several times and by different methods.[1] Spectrometric measurements[2] have indicated a complex γ-spectrum of energies 0.423, 1.12, 1.31, 2.32 Mev. The existence of an additional 1.8-Mev γ-ray found by cloud-chamber measurements[3] was confirmed by the photo-neutron reaction[4] on Be, giving rise to two groups of neutrons of comparable intensity. Cloud-chamber results[3] indicated still other γ-rays. The end point of the β-spectrum was determined to be 0.85 ± 0.10 Mev by means of a β-spectrometer.[5]

We have studied this isomer recently and the results enable us to give a rather complete description of the disintegration scheme. The following γ-rays exist: 0.137; 0.406; 1.085; 1.274; 1.487; 2.090 Mev (error <0.5 percent; for 0.137 Mev $\lesssim 1$ percent).

We have not found any γ-ray around 1.8 Mev (if existent less than 3 percent) or any other γ-lines, which could give rise to photo-disintegration in Be (i.e., $E_\gamma > 1.63$ Mev) except the one at 2.090 Mev. This is consistent with the previous spectrometric results by Deutsch *et al.* The β-spectrum is complex, having the components: 1.00; 0.87; 0.60 Mev with relative intensities 51, 28 and 21 percent. Six percent of the total β-radiation deviates above the last straight Fermi line at energies <250 kev. Since, however, there is no γ-component, which could take care of a possible soft β-component of this energy, we believe that the slight surplus of low energy electrons is due to other causes. From the photo-electron spectrum it was possible to determine the relative intensities of some of the γ-lines. A disintegration scheme which satisfies all energetic and intensity data is presented in Fig. 1.

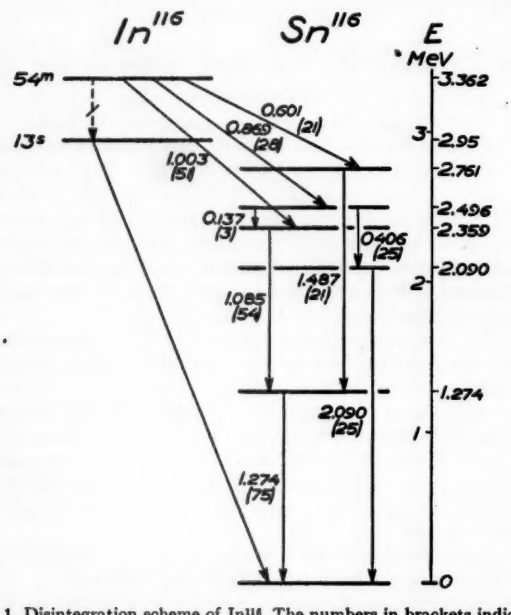

FIG. 1. Disintegration scheme of In^{116}. The numbers in brackets indicate the approximate number of β-particles or γ-quanta per 100 disintegrations.

The β-γ-coincidence effect was $C_{\beta-\gamma}/N_\beta = 1.86\pm0.10\times10^{-3}$. With the calibrated gold γ-tube used one would expect $C_{\beta-\gamma}/N_\beta$ to be 1.80×10^{-3} according to the scheme. We have been able to determine the small conversion coefficients for the 1.085 and 1.274 γ-lines. They are $\alpha_{1.085}=8.4\times10^{-4}$ and $\alpha_{1.274}=5.7\times10^{-4}$, respectively. The theoretical values[6] for electric quadrupole lines are 9.62×10^{-4} and 6.79×10^{-4}. Electric dipoles give 4.20×10^{-4} and 3.06×10^{-4} and magnetic dipoles 13.2×10^{-4} and 8.40×10^{-4}. Within the experimental errors the results for the two lines are well consistent with electric quadrupoles.

In the same way the conversion coefficient for the 0.406-Mev γ-ray indicates a quadrupole transition.

According to the scheme the fourth excited level in Sn can be de-excited by the competitive emission of two different γ-lines at 0.137 Mev and 0.406 Mev (or 2.090 Mev). Considerations regarding the transition probabilities for different spin changes at different energies afford rather strong theoretical arguments for concluding that, (1) the γ-ray at 0.406 Mev is emitted *before* the 2.090-Mev γ-ray; and (2) both the 0.406-Mev γ-ray and the 0.137-Mev γ-ray are quadrupole lines.

The 0.137-Mev transition is almost certainly a quadrupole line for the following reason. The *ft*-values for the various β-transitions show that all β-transitions belong to the symmetry forbidden class with no change in parity. The 0.137-Mev transition thus occurs between levels of equal parity and according to the γ-selection rules the transition cannot be electric dipole but electric quadrupole ($\Delta J=2$) or a mixture of electric quadrupole and magnetic dipole radiation ($\Delta J=1$).

The experimental determination of the intensity of the converted 0.137-Mev line can then be used to compute the intensity of the 0.137-Mev transition from theoretically known conversion data.

The total disintegration energy is 3.36 ± 0.05 Mev. According to absorption measurements[7] the maximum energy of the 13-sec. isomeric state is 2.95 ± 0.10 Mev. We therefore conclude that the 54-min. isomeric state is due to an excited level in In^{116} situated 410 ± 150 kev above the 13-sec. ground level. We have not been able to detect any direct transition between the two isomeric states in In^{116}. The 0.137-Mev conversion line in the β-spectrum is not due to any isomeric transition since the K to L ratio is far too big. The conversion factor for this line is also too small to be responsible for any isomeric transition, which was shown by investigating the intensity of the unconverted γ-line in the secondary photo-electron spectrum from a thin lead foil.

The position of the 0.137-Mev transition in the scheme was localized by taking $e^-\beta$-coincidences in the high transmission spectrometer[8] between focused 0.137-conversion electrons and the continuous spectrum with different absorbers.

A calculation of the lifetime of the excited isomeric level in In^{116} shows that an "effective" l-value of at least 4 must be assumed. With the experimentally determined multipole orders for the different γ-transitions and the *ft*-values for the β-transitions one can use the γ- and β-selection rules to ascribe angular momenta and parity to the levels involved here. It is then conceivable that all levels have the same parity (including those of In^{116}). In order of increasing energy (starting with the Sn^{116} ground level) the angular momenta would be 0, 2, 2, 4, 3, 3, or 4 and in In^{116} 1, 4. Even though the angular momentum difference between the two isomeric levels in In^{116} would thus be only 3, the similar parity of two states makes this transition parity forbidden with an effective l-value of 4.

Details of the investigation will be given in *Arkiv für Fysik*.

One of us (S. J. du Toit) is indebted to the South African Council for Scientific and Industrial Research and the Nobel Institute for enabling him to take part in this research.

* On temporary leave from National Physical Laboratory, Pretoria, South Africa.

[1] For a complete list of references see: G. T. Seaborg and I. Perlman, Rev. Mod. Phys. 20, 585 (1948), and J. Mattauch and A. Flammersfeld, Isotopic Report, Zeits. f. Naturforschung, Tübingen (1949).
[2] Deutsch, Roberts and Elliott, Phys. Rev. 61, 389 (1942).
[3] B. R. Curtis and J. R. Richardson, Phys. Rev. 57, 1121 (1940).
[4] D. J. Hughes and C. Eggler, Phys. Rev. 72, 902 (1947).
[5] J. M. Cork and J. L. Lawson, Phys. Rev. 56, 291 (1939).
[6] Rose, Goertzel, Spinrad, Harr and Strong, Phys. Rev. 76, 1883 (1949).
[7] E. Bleuler and W. Zünti, Helv. Phys. Acta 19, 375 (1946).
[8] H. Slätis and K. Siegbahn, Ark. f. Fysik 1, No. 17, 339 (1949).